September 2015

Telomere Maintenance Using Cell Lines from Dyskeratosis Congenita Patients

A thesis submitted for the degree of Doctor of Philosophy

By

Chetana Devi Sharma

Division of Biosciences

Department of Life sciences

College of Health and Life sciences

Declaration

I hereby declare that the research presented in this thesis is my own work, except where otherwise specified, and has not been submitted for any other degree.

Chetana Devi Sharma

Abstract

Cells exposed to DNA damaging agents activate a network of mechanisms called DNA damage response, including telomere length regulation. Telomeres are specialized structures that protect chromosome ends from degrading and being fused together. Mouse-knockout experiments revealed that cell lines deficient of DNA-PKcs or Ku70/80 resulted in high amount of telomere end-to-end fusion. Numerous other studies have shown a functional interplay between DNA damage response and telomere maintenance. The aim of this project is to examine this interplay further by investigating mechanisms of DNA damage response, using cell lines from X-linked homozygous recessive form of Dyskeratosis Congenita (DC) patients, which have dysfunctional telomere maintenance. DC is a multi-system disorder characterised by abnormalities of the bone marrow, immune deficiency and a predisposition to cancer.

In this work we have shown that cells with defective *DKC1* (the gene implicated in the X-linked homozygous recessive form of DC) exhibit a defective DNA damage response by examining two types of cells: fibroblast and lymphoblastoid cell lines. By using various biomarkers (H2AX, TIF assay etc) we analysed the DNA damage response by exposing DC cell lines to ionizing radiation. Our results demonstrated that DC cell lines have an abnormal DNA damage response and as a result show radiosensitivity.

We have also knocked down the *DKC1* gene in normal cell lines using siRNA oligonucleotides and demonstrated that this knock-down causes radiosensitivity. Therefore our results conclusively show an abnormal DNA damage response in cells derived from DC patients.

Finally we used TA-65, a novel telomerase activator derived from the plant *Astragalus membranaceus* and showed radioprotective effects of this compound in normal lymphoblastoid cell lines. Taken together our results potentiate further the link between telomere maintenance and DNA damage response.

Acknowledgements

"To the Highest Supreme, the Almighty, with the blessings I am able to complete this phase of my research. Please continue to give me the courage and strength to progress further as a scientist."

It would not have been possible to write this thesis without the help and support of the kind people around me, and it is only feasible to give a particular mention to some here. This thesis would not have been possible without the patience and support of my principal supervisor, Dr Predrag Slijepcevic, and I am grateful to him for giving me the opportunity to train as a scientist. He believed in my ability, showed me the right path, to build a strong foundation. The good advice, support and with his great sense of humour, my second supervisor, Dr Christopher Parris has been there for me to provide encouragement and be ever ready to help, for which I am extremely grateful. In addition, I would like to give a special mention to Dr Sahar Al-Mahdawi, Dr Chiranjeevi Sandi, Dr Emma Bourton, Dr Terry Roberts and Dr Hemad Yasaei, for their talks and guiding me appropriately.

I would like to extend my gratitude towards my colleagues Dr Maryam Ojani, Dr Yaghoub Gozaly Chianea, Parisa, Sheila and Savneet for their never ending help and support, and for providing a friendly and humorous working atmosphere.

I want to give a special mention to my friends Dr Oeslya, Dr Madhavi, Dr Gabriele, Dr Jessica, Dr Sheba, Dr Hiba, Dr Gonul, Geema, Temi, Stephan, Hussein, Dimple, Christianah, Thea, Shrina and especially Dr Hannah, who have helped me get through this PhD course. You all have been equally amazing. Apologises if I missed anyone out who supported me and thank you from the bottom of my heart.

Finally, I want to thank my family, in particular my parents, for their constant support and encouragement for my research. They have been there throughout my PhD

providing the emotional support and without them, it would have been impossible to do this course. Therefore I dedicate this thesis to them, to my mother, Renu Bala Sharma for being my emotional support and to my father, Sutantar Kumar Sharma, who has been the constant positive force throughout my life.

Publications

Chetana Sharma, Maryam Ojani and Predrag Slijepcevic "DNA Damage Response and Telomere Maintenance using cell lines from Dyskeratosis Congenita patients" {{Manuscript in preparation}}.

Chetana Sharma and Predrag Slijepcevic (2014) "The relationship between DNA damage response and Telomere Maintenance in Dyskeratosis Congenita cell lines" National Cancer Research Institute (NCRI). Conference, Abstract published online.

http://abstracts.ncri.org.uk/abstract/the-relationship-between-dna-damage-and-telomere-maintenance-in-dyskeratosis-congenita-cell-lines-2

Accreditations

Associate Fellow – awarded by the Higher Education Academy in January 2015

24 External credits – approved by federation of the Royal Colleges of Physicians of UK for attending the 10th NCRI Cancer Conference

Abbreviations

ALT	Alternative lengthening of telomeres
ATM	Ataxia telangastia mutated protein
ATR	ATM-and Rad3-related proteins
Bp	Base pair
BSA	Bovine Serum Albumin
CCFL	Corrected Calibrated Fluorescence
cDNA	Complementary DNA
CF	Correction Factor
Cyt-B	Cytochalasion B
DDR	DNA damage response
DC	Dyskeratosis Congenita
DMEM	Dulbecco modified eagle medium
DMSO	Dimethylsulfoxide
DNA-PKcs	DNA-protein kinase catalytic-subunit
dNTP	Deoxynucleotide triphosphate
DSB	Double strand breaks
DTT	Dithiothreitol
DW	Distilled water
ECL	Enhanced chemiluminescence
EDTA	Ethylene diamine-tetra acetic acid
FBS	Fetal bovine serum
FCS	Fetal calf serum
FISH	Fluorescence in-*situ* hybridization
FITC	Fluorescein isothiocynate
gDNA	Genomic DNA
Gy	Gray
HR	Homologous recombination
H2AX	Histone H2AX phosphorylated on serine-139
IPA	Isopropyl alcohol
IQ-FISH	Interphase Q-Fish
IR	Ionising Radiation
Kb	Kilobase
KCL	Potassium Chloride
LY-R	Radioresistant mouse lymphoma cells
LY-S	Radio-sensitive mouse lymphoma cells
MgCl2	Magnesium chloride
miRNA	MicroRNA
ml	Mililiter
MN	Micronuclei
MRN	MRE11/RAD50/NSB1
NER	Nucleotide Excision Repair
NHEJ	Non-homologous end joining
PAR	Poly ADP-ribose
PBS	Phosphate buffer saline

PCR	Polymerase chain reaction
piRNA	Piwi-interacting RNA
PNA	Peptide nucleic acid
POT1	Protection of telomeres 1
PVDF	Polyvinylidene fluoride
RNA	Ribonucleic acid
RNAi	Ribonucleic acid interference
RPA	Replication protein A
RPM	Rotations per minute
RPMI	Roswell Park Memorial Institute
RT	Room Temperature
RT-PCR	Reverse transcriptase-polymerase chain reaction
SDS	Sodium dodecyl sulphate
siRNA	Short interfering ribonucleic acid
ss	Single stranded
SSB	Single strand breaks
SSC	Sodium chloride sodium citric acid
ssDNA	Single stranded DNA
TA-65	Telomerase activator.
T	Thymine
TBE	Tris-borate-EDTA
TBST	Tris-buffered saline tween-20
TEMED	Tetramethylethylenediamine
TERT	Telomerase Reverse Transcriptase
TFUs	Telomere fluorescence units
TIF	Telomere dysfunction induced foci
TIN2	TRF1-interacting factor
T-loop	Telomeric-loop
TRF1	Telomeric repeat binding factor 1
TRF2	Telomeric repeat binding factor 2
UV	Ultra violet
µl	Microlitre

Table of Contents

List of Figures

List of Tables

Chapter 1 General Introduction

1.1 General Introduction

When cells are exposed to DNA damage, a network of mechanisms called DNA damage response is activated. There is increasing evidence that this network of mechanisms includes telomeres, specialized structures at chromosome ends responsible for chromosome end protection. In this introductory chapter, we will review the biology of telomeres and their involvement in DNA damage response mechanisms. This will pave the way for discussing a genetic disease, Dyskeratosis Congenita (DC), characterized by defective telomere maintenance. The focus of research in this dissertation is to probe the efficiency of DNA damage response in DC cells in order to test further the link between telomere maintenance and DNA damage response.

1.2 Telomere Structure and Function

At the ends of most eukaryotic and all mammalian chromosomes, specialised structures called telomeres are found. The term telomere comes from Greek words "Telos" meaning *end* and "meros" meaning *part* (see figure 1.1, Oeseburg et al 2010; Boukamp and Mirancea 2007; de Lange 2009), and they were first discovered by Muller in 1938. We know today that conventional DNA polymerases cannot fully replicate telomeres, the extreme termini of linear chromosomes (Lundblad 1997). Telomeres consist of 2–20 kb of double-stranded TTAGGG repeats in human cells and contain a single-stranded overhang of 50–500 nucleotides (Diotti and Jackson 2011; de Lange 2005; Griffith et al 1999). In all vertebrates, telomeres are comprised of long TTAGGG nucleotide repeats sequences and associated proteins (Anderson et al 2012; Oeseburg et al 2010; Huffman et al 2000). The telomere macromolecular complex caps the tips of chromosomes so that the free ends of the DNA molecule are not recognized by DNA repair activities (Calado and Young 2008; Huffman et al 2000). In addition, telomeres

prevent the end-to-end chromosome fusion and subsequent breakage-fusion-bridge cycles which may lead to genomic instability (Slijepcevic 2001; de Lange 2005; Diotti and Loayza 2011). The telomeric single stranded, G-rich overhang is able to form the t-loop, in which the overhang invades the telomeric double-stranded helix, remodelling the DNA into a circle (Calado and Young 2008) (Figure 1.1).

With each mitotic cycle, telomeres become shorter to a point that DNA damage response is activated, resulting in cell cycle arrest and senescence or cell death (Bessler et al 2010; Harley et al 1990; Wright et al 1996). The reason for activation of DNA damage response is that the t-circle becomes linear leading to recognition of this linear structure as a DNA double strand break (DSB) by cellular repair mechanisms (de Lange, 2005). In most somatic cells between 50 and 200 bp of telomeric DNA sequence repeats are lost with each cell division due to end replication problem (Harley et al 1990; Callen and Surralles 2004). This problem is reflected in the fact that a small loss of nucleotides occurs on the lagging strand of the DNA double helix (Olovnikov 1996; Olovnikov 1973). However, in addition to the loss of telomeric DNA at the lagging strand which is not greater than 6-12 nucleotides (de lange 2005), a much more extensive loss occurs at both leading and lagging strands which eventually enables the formation of the long single strand overhang the size of which is 50-200 nucleotides (Diotti and Loayza 2011). This loss is entirely due to exonuclease activity which is essential for the formation of T-loop (Makarov et al 1997).

Given that the loss of telomeric DNA is extensive and that conventional DNA replication machinery is unable to cope with this loss, a specialised enzyme is required to synthesize telomeric DNA. This enzyme is a reverse transcriptase known as telomerase (Greider and Blackburn 1985; Armanios and Blackburn 2013). Telomerase targets single strand telomeric overhangs and uses its own RNA template to synthesize

telomeric DNA. Two major subunits are required for telomerase activity, TERT as the reverse transcriptase domain and TERC as the internal RNA template. Furthermore, a range of accessory factors like dyskerin, NOP10 and NHP2 are required for a fully functioning telomerase (de Lange 2009; Oeseburg et al 2010; Armanios and Blackburn 2013). Therefore, telomeres are essential for maintenance of genomic integrity by providing specialized function of chromosome end replication. It is important to note that telomerase activity is absent in most somatic cells but present in germline and stem cells (Armanios and Blackburn 2013; Scheel C et al 2001).

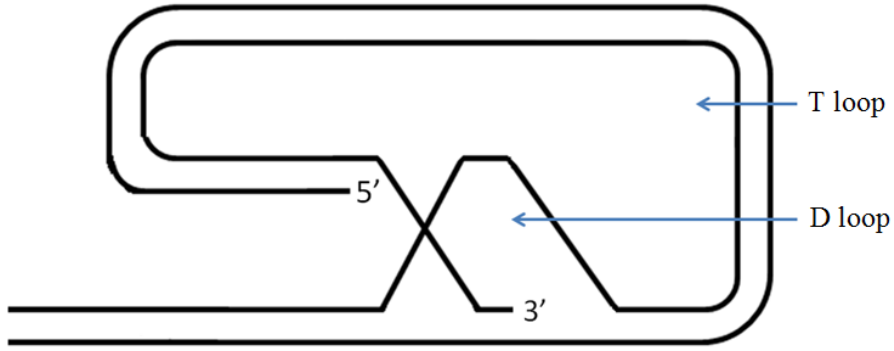

Figure.1.1 Diagram showing the T loop and D loop structures which form at the ends of telomeres, protecting them from DNA damage response machinery (Adapted from de Lange, 2009).

As a result of telomere sequence loss and the absence of telomerase telomere length declines with age in all somatic cells (Cauthon et al 1998). This loss must be prevented in germline and stem cells by telomerase which in turn prevents the activation of DNA damage response by synthesising enough telomeric DNA (Callen and Surralles, 2004). However, the telomeric DNA sequence in the form of a t-loop is not sufficient to carry out the chromosome end-protection function without specialized proteins. A protein complex termed shelterin, must bind the t-circle to facilitate the end-protection function (de lange 2005).

1.2.1 Shelterin

Shelterin, a specialised protein complex, protects the chromosomal ends from erosion and end-to-end fusion through its interaction with the t-loop (Oeseburg et al 2010). Shelterin is formed by at least six proteins called TRF1, TRF2, TPP1, POT1, TIN2, and Rap1, and some of these proteins are directly associated with telomeric DNA (see figures 1.2 and 1.3). TRF1 (telomeric repeat binding factor 1) and TRF2 proteins bind the double stranded telomeric DNA, as they recruit TPP1, POT1, TIN2, and Rap1 (Diotti and Loayza 2011, and Calado and Young 2008). TRF1 and TRF2 restrain the activity of telomerase, which functions to elongate telomere TTAGGG repeats, counteracting the process of continuous telomere elongation or shortening (Du et al 2009; Diotti and Loayza 2011). The shelterin compound TRF2 is able to remodel the telomeric DNA in a way that it folds back and forms a large duplex structure, called telomere loop or t-loop (Griffith et al 1999). POT1 protein (protection of telomeres 1) binds the single strand DNA - . the 3' overhang as this is important for the formation of the D-loop (Oeseburg et al 2010). Other shelterin components, TPP1, (Rap1) and TIN2 (TRF1 -interacting nuclear factor protein) cannot bind directly telomeric DNA but instead react with TRF1 and TRF2 (see figure 1.2, Calado and Young 2008).

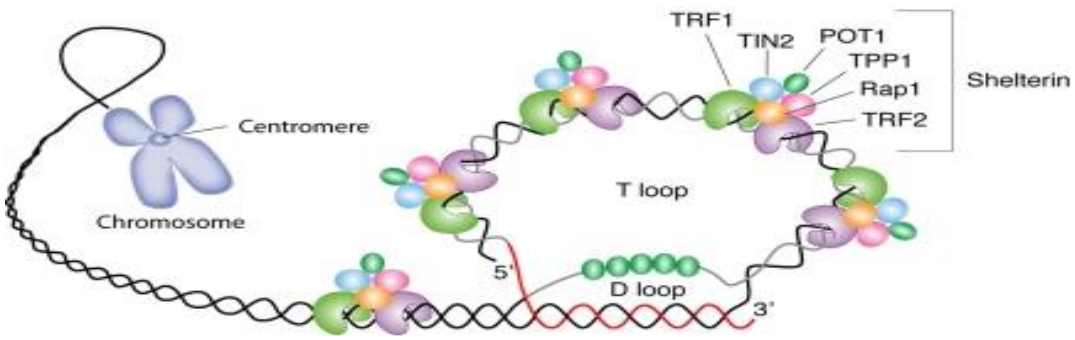

Figure 1.2 Schematic representation of telomere structure. The telomeric 3' end terminates as a single-stranded, G-rich overhang able to form the t-loop, in which the overhang invades the telomeric double helix, remodelling the DNA into a circle. Telomeres are capped by at least 6 proteins (TRF1, TRF2, TPP1, POT1, TIN2, and Rap1), collectively known as shelterin, that physically shield the DNA. (Calado and Young 2008)

The key feature of the t-loop is that the chromosome DNA terminus is tucked in (de lange 2005). The G-rich single stranded overhang invades the double-stranded telomeric repeat DNA and pairs with the CC-rich strand (Polychronopoulou and koutroumba 2004).

Shelterin also represses DNA damage responses (Diotti and Loayza 2011), and it is conceivable that t-loops are formed to protect the telomeric ends from inappropriate DNA repair, as well as to control telomere maintenance. This view has a strong experimental support. For example, telomere shortening results in destabilization of the chromosomes and an inability to recruit the proteins of the shelterin complex as shown in cells expressing a dominant negative allele of TRF2, which leads to the inhibition of wild-type TRF2, and subsequent end-to end chromosomal fusions as well as loss of the single strand overhang at an early stage (Oeseburg et al 2010; Van Steensel et al, 1998). Furthermore, the shelterin complex interacts with many DNA damage response proteins (Slijepcevic 2008). This extensive interaction process possibly reflects the role of shelterin in regulating DNA damage response. Therefore, when telomeres are critically short either physiologically (cell senescence) or as a result of genetic factors (some diseases) depletion or loss of function of shelterin components occur (Diotti and Loayza 2011) which in turn affects DNA damage response recognized by the recruitment of DNA double strand break (DSB) damage markers such as phosphorylated histone H2AX (ɣH2AX) and other factors including DNA-damage checkpoint factors (p53,ATM, p21 etc.) with the emergent cell cycle block in G1, ultimately causing cell proliferation arrest and in some cases apoptosis (Calado and Young 2008). It is important to stress that shelterin is abundant at chromosome ends but it generally does not accumulate elsewhere; it is present at telomeres throughout the cell cycle, and its function is limited to telomeres (de lange 2005). However, there is

some evidence that the component of shelterin, namely TRF2, is able to accumulate at the DNA damage sites anywhere along chromosomes following exposure of cells to DNA damage (Bradshaw et al 2005). TRF2 is involved in both telomere length regulation (Karlseder et al 2002; Smogorzewska et al 2000) and telomere end protection (de Lange 2002). The removal of this particular shelterin protein from telomeres by overexpression of a dominant-negative mutant of TRF2 caused at least 30% loss of telomere G-overhang signal and nonhomologous end joining (NHEJ)-dependent chromosome end fusions. However, this view is not as of yet widely supported by experimental evidence (Li et al 2005).

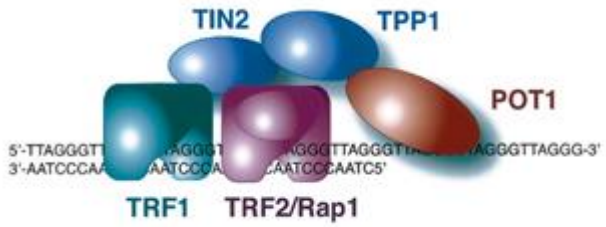

Figure 1.3 Schematic structure of shelterin and telomeric DNA. For simplicity, POT1 is only shown as binding the site closest to the duplex telomeric DNA although it can also bind to the far 3' end (taken from de lange, 2005)

1.2.2 Telomerase and Telomere maintenance

It has been said that telomeres act as a mitotic clock in human cells in order to limit the division potential in human cells (Wyatt et al 2010). However, this "end-replication problem", which was briefly addressed earlier (see above) is absent from germline cells as telomere maintenance is absolutely essential during embryonic development by telomerase activity. By contrast, the telomerase expression is suppressed within a few weeks after birth in most somatic cells (Wyatt et al 2010). However, telomerase remains active in stem cells, progenitor cells, lymphocytes, skin keratinocytes, and

cancer cells (Oeseburg et al 2010). Shcherbakova et al (2006) further clarifies that this enzyme is only active in cells capable of proliferating.

These findings had long history that started with the work of Greider and Blackburn which eventually resulted in the award of the Nobel Prize in Physiology or Medicine in 2009. In 1985 Carol Greider and Elizabeth Blackburn originally discovered telomerase in the ciliate *Tetrahymena thermophila* (Greider and Blackburn 1985). This discovery was important, but its impact was realized only when coupled with the results of telomere length measurements in human cells which showed telomere shortening with age (Oeseburg et al 2010). Furthermore, measuring telomerase activity with the original method was difficult. It was not until 1989 that telomerase activity was identified in human cells (Callen and Surralles 2004). However, the breakthrough occurred in 1994 when a PCR based method for telomerase activity measurement was invented by Kim et al (1994). This method called TRAP (Telomere Repeat Amplification Protocol) turned out to be a robust and easy to implement method which since then became the important tool for scientists interested in telomerase. Kim et al (1994) showed that telomerase is repressed in normal somatic cells but reactivated in cancer cells in which telomerase is required for indefinite proliferation (Buseman et al 2012).

The core enzyme of telomerase is a ribonucleoprotein consisting of a protein catalytic subunit, which actually acts as reverse transcriptase (Telomerase Reverse Transcriptase, TERT), and telomerase RNA subunit (TERC) also known as TR, whose short fragment (8–30 n.t. in different species) serves as a template for synthesis of telomeric repeats (Shcherbakova et al 2006). Dyskerin, is a protein that binds both TERT and TERC and increases stability of the complex (Oeseburg et al 2010). Dyskerin binds the H/ACA motif, a sequence in TERC required for its accumulation, and a

sequence present in a subset of small nucleolar RNAs (snoRNAs) involved in RNA modification (Venteicher et al 2008). TERT, TERC and dyskerin are active telomerase components and mutations in any of these can lead to human stem cell disorder Dyskeratosis congenita (DC) (Venteicher et al 2009). The best characterized mammalian telomerase accessory component is the dyskerin protein which forms a core complex with other potential components of telomerase including GAR, NHP2 and NOP10 (Venteicher et al 2009). Figure 1.4 shows the components of telomerase and how telomerase interacts with the shelterin complex. Wyatt et al (2010) discovered using mass spectrometric analysis of affinity-purified telomerase from HeLa cells, two additional proteins of telomerase, pontin/reptin and TCAB1. Venteicher et al (2009) examined the interactions between TERT and dyskerin using HeLa cells and found that TCAB1 (Telomerase cajal body protein 1) interacts specifically with dyskerin, TERT and TERC, all three known components of active telomerase. As shown in figure 1.4, the TCAB1 binds TERC (labeled TR in the figure) and regulates its trafficking. ATPases pontin and reptin are identified as essential telomerase components by the loss-in-function experiments, which established that these ATPases are essential for the accumulation of TERC and dyskerin (Venteicher et al 2008).

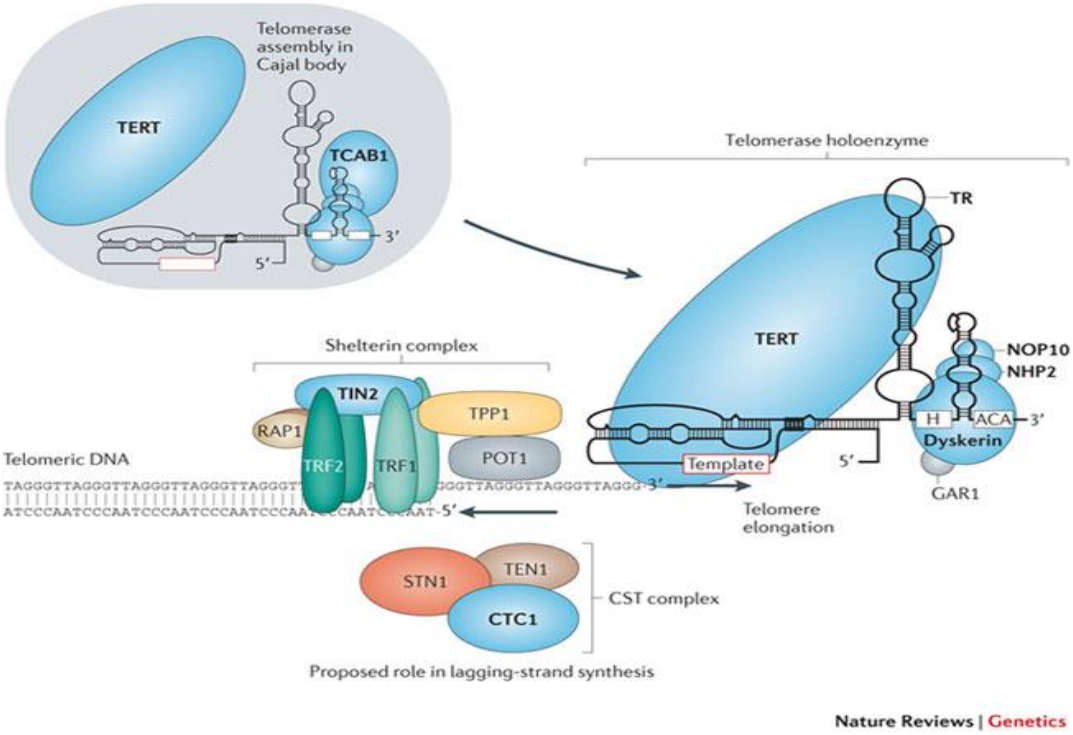

Figure 1.4 Schematic structure of Telomerase and telomere components. Components for which mutations have been identified in telomere syndromes are indicated in bold type. (Taken from Armanios and Blackburn 2013).

CST complex (shown in figure 1.4) has three components – conserved telomere protection component 1 (CTC1), suppressor of cdc thirteen 1 (STN1) and telomeric pathway with STN1 (TEN1). This complex is thought to function in part in telomere lagging – strand synthesis (Armanios and Blackburn 2013).

However, it is important to stress that telomerase is not the only mechanism for telomere maintenance. It is now clear that an alternative mechanism is operational known as alternative lengthening of telomeres (ALT) (Bryan et al 1997; Cesare and Reddel 2010).

ALT occurs in human tumors and immortalized cell lines (Cesare and Reddel 2010; Scheel et al 2001; Bryan et al 1997) but the overall presence of ALT is low in tumours. However there the ALT mechanism occurs with a high frequency in tumours of

mesenchymal origin (Cesare and Reddel 2010; Lafferty-Whyte et al 2009). A study demonstrated 15 of 35 in vitro-immortalized cell lines were negative for the telomerase activity and still showed unusually long telomeres (Bryan et al 1995). Furthermore, in 1997, Bryan published data showing four tumours (one osteosarcoma, one breast carcinoma, and two adrenocortical carcinomas (ACCs)) lacking telomerase activity and showing long telomeres by terminal restriction fragment (TRF) agarose gel analysis. TRFs of these tumours were long and irregular (Bryan et al 1997). Therefore, they concluded that telomeres were maintained by an alternative mechanism, ALT. The possible explanation for maintaining telomeres in telomerase negative cells is that these tumors may have an alteration in telomere binding proteins or their binding sites, leading to the loss of regulation of telomerase- mediated telomere lengthening, as observed in yeast (Lundblad and Blackburn 1993). Another study (Mc Eachem and Haber 2006; Grandin and Charbonneau 2009) concluded that maintenance of telomeres by ALT is based on recombination, requiring Rad52, a DNA repair protein essential for basically all types of homologous recombination (Mc Eachem and Haber 2006), where this recombination is activated by telomere shortening or disruptions in the function of telomere-binding proteins.

Given that the active ALT pathway is an indication of the altered DNA damage response (Lovejoy et al 2012), this provides another layer of evidence in support of the view that telomere maintenance and DNA damage response mechanisms are functionally related. This leads us to the next section of this overview, namely mechanisms of DNA damage response.

1.3 DNA damage response mechanisms

Damage to the structure of DNA can occur through two main mechanisms: spontaneous damage caused by sources within a cell's metabolism, and damage caused by external sources such as chemicals and radiation (Subba 2007). DNA damage will then activate cellular response known as DNA damage response (DDR) including cell cycle arrest, DNA repair, senescence and apoptosis (Huen and Chen 2008). If DNA damage is not properly repaired there will be severe consequences for cells and tissues (Henrique et al 2012). DNA damage can be repaired by more than one pathway depending on the DNA lesion. DSBs are repaired by Non-Homologous End Joining (NHEJ) or Homologous Recombination (HR), damaged bases are repaired by base excision repair, or nucleotide excision repair pathways and wrongly placed bases are repaired by mismatch repair (Roos 2012) Some of the above types of damage could be potentially lethal events for the cell, in particular DSBs and DNA lesions that prevent the replication and transcription of DNA (Roos 2012). If left unrepaired DSBs may cause apoptosis or can initiate genomic instability, ultimately leading to cancer (Bonner et al 2008). Apoptosis is a process which results in removal of cells with high degree of DNA damage from tissues (Macdonald 1997). DNA DSBs are generated by exposure to a variety of genotoxic agents such as ionising radiation and chemotherapeutics and it is one of the most dangerous lesions a cell can encounter (Doherty and Jackson 2001; Fattah et al 2010).

1.3.1 Cell cycle checkpoints and DNA damage

Cell cycle represents a series of highly orchestrated biochemical events which result in DNA duplication and cell division. It is divided in to four phases G1, S (DNA replication) G2, and M (mitosis). G1 and G2 are gap phases, the former being the first phase gap and the latter being the interphase as well as the second phase gap (Macdonald 1997). The

length of the mammalian cell cycle is approximately 16-24 hours depending on the species. DNA damage checkpoints occur towards the end of G1, during the G2 phase and at the G2 to M transition in order to monitor the completion of DNA synthesis (Macdonald 1997). The main function of these checkpoints is to monitor the integrity of the DNA sequence. Once DNA damage has occurred, the cell cycle progression is halted by a mechanism called cell-cycle checkpoint (Kastan and Bartek 2004). For example, DNA DSBs trigger ATM (ataxia telangiectasia mutated) kinase activity which is responsible for activating p53, Mdm2 and Chk2 in the G1 checkpoint, Nbs1, Brca1, FancD2 and SMC1 in S-phase arrest and Brca1 and hRad17 in the G2/M checkpoint (Bakkenist and Kastan 2003). ATR (ATM and Rad3-related) is another kinase that is activated to inhibit cell cycle progression after DNA damage that affects DNA replication-fork progression (Kastan and Bartek 2004). Additionally, upon DNA DSB induction by ionizing radiation, a DNA damage marker, H2AX, which is a histone protein, becomes phosphorylated on residue serine 139 in cells as demonstrated by Rogakou (1997) to form γH2AX (phosphorylated form) at DSB sites (d'Adda di Fagagna et al 2003). A large number of γH2AX molecules accumulate in the chromatin around the break site immediately after DSB induction (Bonner et al 2008). This phosphorylated form of H2AX is sometime called gamma-H2AX (Helt et al 2005). H2AX, a subtype of H2A, is a substrate of several phosphoinositide 3-kinase –related protein kinases (PIKKs), such as ATM, ATR, or DNA- dependent protein kinase (DNA-PK). (Podhorecka et al 2010). The relationship between γH2AX and other important DNA damage response regulating molecules will be explored next.

1.3.2 γH2AX and DNA damage response

Upon DNA DSBs, ATM, a protein kinase, is activated and signals γH2AX to become phosphorylated in a highly regulated way (Kastan and Bartek 2004). Initially, a tri-protein complex called MRN complex (MRE11-RAD50-NBS1) recognizes DNA DSBs and recruits ATM to the site of damage (figure 1.5). This MRN complex also functions to target ATM to initiate phosphorylation of H2AX to γH2AX (Podhorecka et al 2010) but also many other molecules such as MDC1, 53BP1, BRCA1 etc (Anthony and Chen 2013) responsible for the activation of cell cycle checkpoints leading to activation of DNA damage repair pathways specific to DSBs. DSBs are repaired by NHEJ usually in G1 phase of the cell cycle whereas HR is active in G2 phase of the cell cycle (Podhorecka et al 2010). Apart from H2AX, BRCA1, 53BP1, MDC1 as well as checkpoints proteins chK1 and chK2 are substrates phosphorylated by ATM.

In response to single-stranded DNA breaks and during replication stress (replication fork arrest) H2AX is also phosphorylated by ATR, and Mukerji et al 2006, demonstrated that H2AX is phosphorylated during apoptotic DNA fragmentation in mouse, Chinese hamster ovary, and human cells.

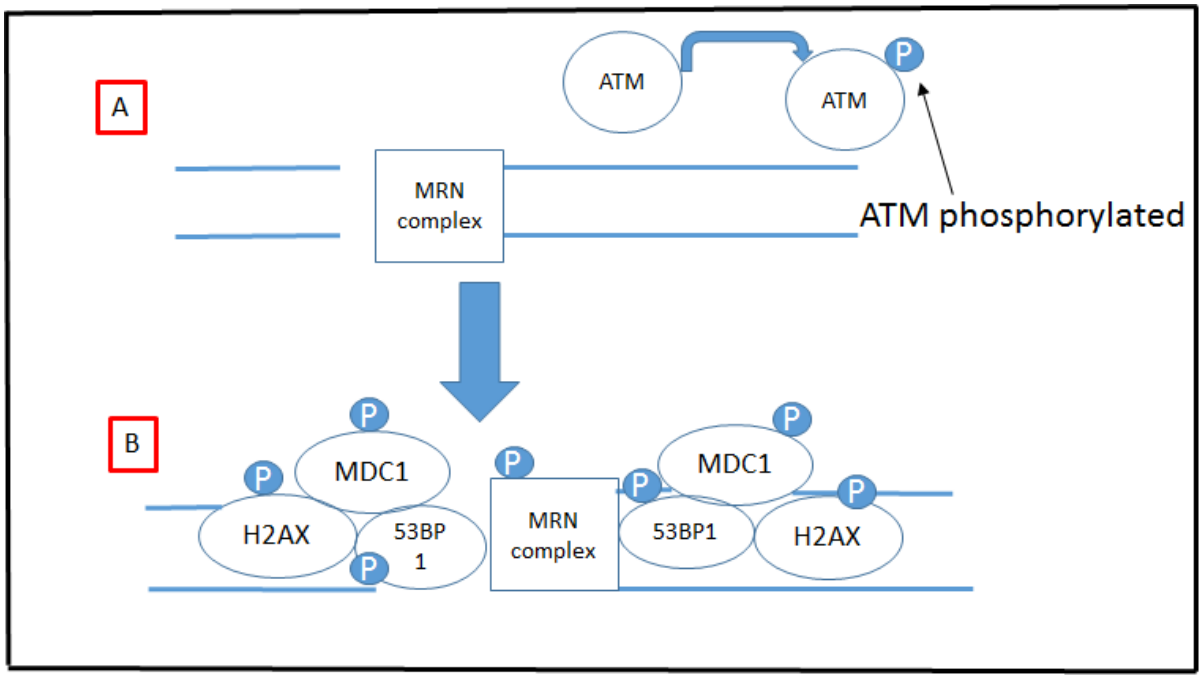

Figure 1.5 Mre11 interacts with Nbs1 and Rad50 to form the MRN complex, which activates Atm kinase (A), which participates in the DNA damage response with other Atm substrates (B).

As shown in Figure 1.5 MDC1 is a direct binder of γH2AX. Stucki et al (2005) demonstrated that mammalian MDC1 directly binds γH2AX by specifically interacting with the phosphoepitope at the γH2AX carboxyl terminus. The interaction between γH2AX and MDC1 is recognized as one of the first steps in DNA damage signaling and repair responsible for initiation of DSB repair. In the next section we will explore mechanisms behind NHEJ.

1.4 Non Homologous End Joining

Following protein molecules are known to be required for the fully functioning NHEJ pathway: ku70, ku80, the DNA dependent protein kinase catalytic subunit (DNA-PKcs), Artemis, X-ray cross complementing 4 (XRCC4), XRCC4- like factor (XLF) and DNA ligase IV (LIGIV) (Fattah et al 2010). DNA – PKcs is a multi-subunit serine/threonine kinase consisting of an approximately 470 kDa catalytic subunit (Doherty et al 2001; Haber et al 2000). Ku70 (69KDa) and ku80 (80KDa) form a heterodimer called Ku which acts as the DNA end-binding component in the NHEJ machinery when DNA has broken ends. Ku heterodimer binding to broken DNA ends is the initial step of NHEJ (Davis et al 2013). Ku heterodimer has high affinity for DNA ends without exhibiting sequence specificity and it is thought that Ku binding to DNA ends protects against nuclease digestion (Wang et al 2003). For example, it has been shown that ku70/80 localises to laser generated DNA DSBs within seconds of their creation with no sequence specificity (Mari et al, 2006). DNA-PKcs is recruited by the ku once its binds to a DNA DSB, forming a DNA dependent protein kinase complex and the assembly of this trimeric complex on the ends of double-stranded DNA activates the kinase activity of DNA PKcs (Doherty et al 2001; Löbrich and Jeggo 2007). The DNA PKcs from both ends of the DNA DSB gets connected by bridge-like domains. This leads to the phosphorylation of this kinase resulting in activating nuclease Artemis. The ligation of the broken ends are finally catalyzed by the trimeric ligase IV complex (consists of DNA LIGIV, XLF and XRCC4), whereby the scaffolding protein XRCC4 allows the ligase IV to bind DNA and ligate both DNA DSBs in order to fix the DNA damage (Doherty et al 2001; Löbrich and Jeggo 2007 see figure 1.6 and figure 1.7). The ligase IV function is enhanced by XLF. Ku heterodimer has been shown to recruit either directly or indirectly the main NHEJ factors, apart from DNA-PKcs (Mari et al 2006).

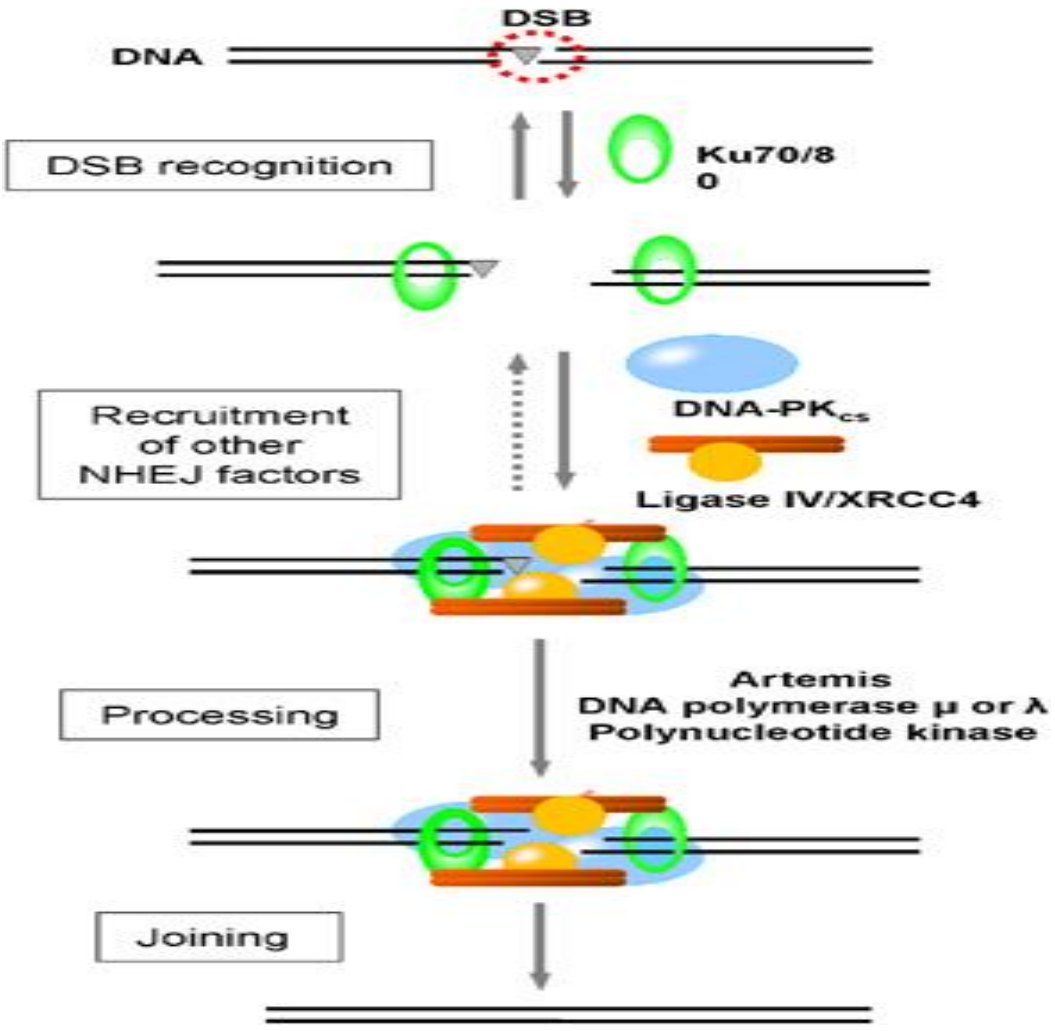

Figure 1.6 The NHEJ model. After DSB formation, the Ku70/80 heterodimer binds to the DNA ends and attracts DNA-PK$_{cs}$. This activates the DNA-PK kinase activity, which leads to autophosphorylation, which enables the subsequent processing and ligation steps. The small triangle symbolizes a DNA end that needs processing before ligation. (adapted from Van DC 2007)

The drawback of this pathway is that it is inaccurate as some deletions can occur at the site of DNA DSB. Interestingly, it has been found that some of the NHEJ proteins are found to be present at telomeres and interact with the shelterin complex (Slijepcevic 2008). Moreover, to avoid inappropriate repair by NHEJ in joining two telomeres to

create a circular or a dicentric chromosome, shelterin promotes the t-loop formation (de lange 2005). How DNA-PKcs and Ku contribute to telomere function is not fully known at present but Slijepcevic (2008) explains that ku most likely prevents telomerase from targeting DSBs. It has been shown in a series of mouse knock-out models deficient in either DNA-PKcs or Ku70/80 that a significant increase in the amount of chromosomal aberrations which includes telomere end-to-end fusion occur. This suggests that ku70, ku80 and DNA-Pkcs are needed for the telomere function discussed earlier (Bailey et al 1999).

1.5 Homologous Recombination

The HR pathway is more accurate than the NHEJ pathway as it uses an intact sister chromatid as a template for the repair in late S and G2-M phases (Barreta et al 2012; Wymana et al 2004). Many proteins are involved in HR. The most dominant HR proteins include BRCA1, BRCA2, NBS1, RAD50, RAD51, RAD52, ATM and 53BP1. These are responsible for triggering and controlling the HR repair pathway in mammalian gametes and embryos. HR also plays a prominent role in faithfully duplicating the genome by providing critical support for DNA replication, the repair of damaged replication forks and telomere maintenance, including the repair of incomplete telomeres that arise when the enzyme telomerase is non-functional (Li et al 2008; Filippo et al 2008). Rad51 is a protein that plays a crucial part in HR, where Rad51 is needed for mitotic HR events such as DSB repair and also for meiotic HR (Filippo et al 2008). Rad51 binds the single stranded DNA, which initiates HR repair pathway, and this protein is transported by BRCA2 as previous results show that RAD51 foci fail to form in BRCA2-deficient cells (Pellegrini et al 2002). This is followed by a strand

invasion creating a D‐loop and a Holliday junction which then ends with a strand extension by DNA synthesis, using the sister chromatid as a template, and the resolution of Holliday junction terminates the HR process (Pellegrini et al 2002; Filippo et al 2008; Löbrich and Jeggo 2007 see Figure 1.7)

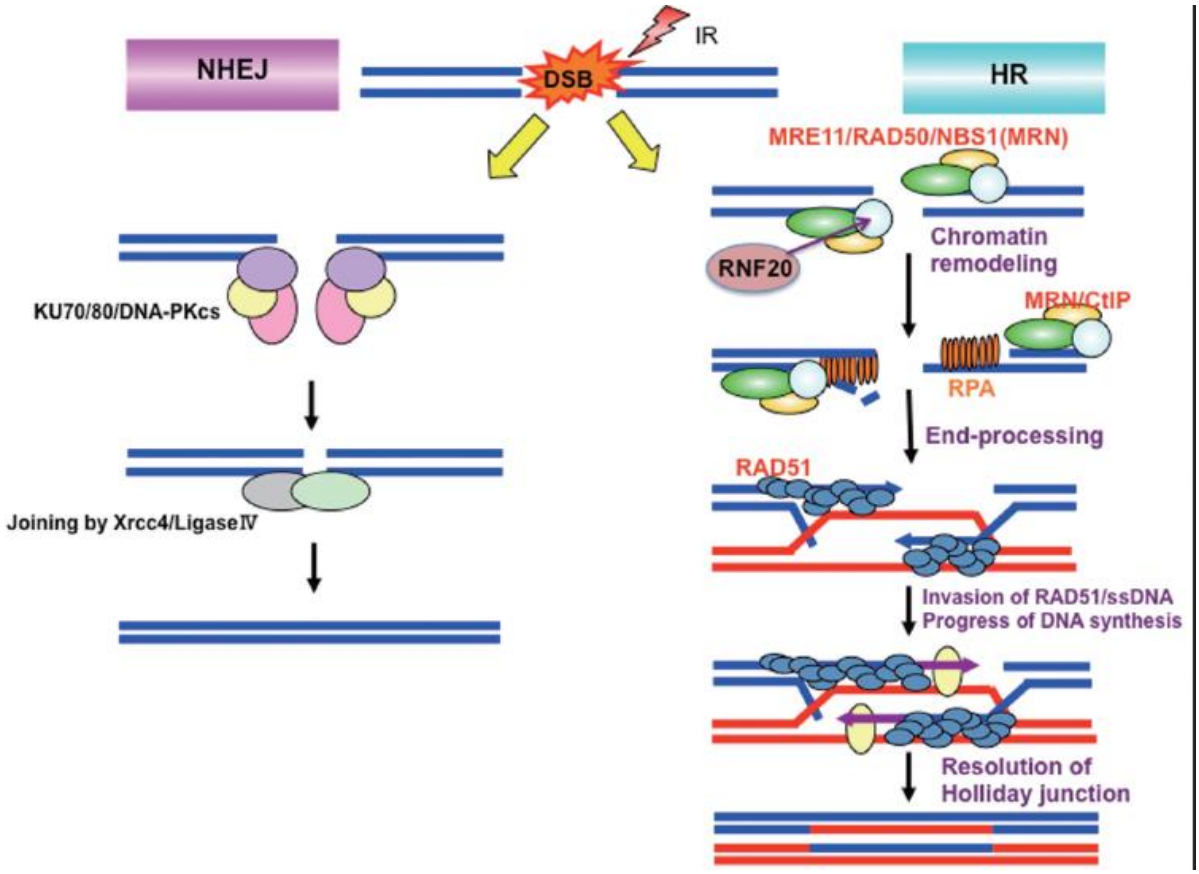

Figure 1.7 An overview of DSB repair pathways HR and NHEJ. NHEJ is the major pathway for repairing non-replication associated breaks, which represent most of those induced by ionizing radiation (IR). By contrast, DSBs arising at the replication fork and some IR‐induced DSBs in G2 are repaired by HR. (Diagram taken from Saito et al 2013). ATM is a DNA damage response protein that becomes phosphorylated when induced by IR, activating p53 (a DNA damage checkpoint factor) signalling the repair pathways (Wagner, Hans Peter 1998; Calado, RT 2008).

In the next section of this overview we will focus on the genetic disease, DC, caused by mutations in various telomere components.

1.6 Dyskeratosis Congenita (DC)

DC is a rare bone marrow disorder that arises from telomere dysfunction. DC and the genes involved in affecting telomere maintenance and DNA damage response will be discussed below.

1.6.1 Clinical presentation

DC was first described by Zinsser, 1906 (Baran et al 2010). DC is a bone marrow disorder caused by telomere dysfunction and telomeres are of much shorter length in DC patients (Baran et al 2010). It is a rare inherited disorder with a prevalence of less than one in million (Brown 2000). Patients with DC generally have the following symptoms: short stature, hypogonadism, infertility, bone marrow failure, skin defects, hematopoietic defects and premature aging (Calado and Young 2008). This could also lead to various malignancies. Oral and dental abnormalities have been reported in a few cases (Brown 2000; Baran et al 2010). Bone marrow failure and immune deficiency are the most common causes of death in up to 60-70% of patients (Nishio and Kojima 2010).

1.7 The genes involved in DC

Mutations directly implicated in causing DC have been identified in the following genes: *DKC1, TERC, TERT, NOP10, NHP2* and *TINF2* (Du et al 2008; Oeseburg et al 2010). Recently, a seventh mutated gene has been identified as *TCAB1* (Anderson et al 2012). All of these genes are implicated in telomere function (Kirwan et al 2009). *DKC1, TERC, TERT, NOP10, NHP2* and *TCAB1* belong to the telomerase holoenzyme responsible for maintaining telomere length and *TINF2* is a member of the shelterin protein complex (Anderson et al 2012).

1.7.1 DC inheritance

The first gene implicated in DC was the *DKC1* gene, (gene product, Dyskerin) located on the X chromosome (Xq28) resulting in the X-linked recessive inheritance. (Marrone et al 2005). Males are affected by x-linked recessive disorder much more frequently than females as they need a mutation to occur in both copies of the gene (Baran et al 2010). Initially, this suggested that DC is a defective pseudouridylation disorder (Marrone et al 2005). However, subsequent studies have found *TERC* mutations in some patients classified as DC suggesting a non X-linked mode of inheritance as TERC resides on chromosome 3. A frequent 821-base-pair deletion on chromosome 3q removes the 3' 74 bases of *TERC* leading to DC (Vulliamy et al 2001). This was the first clear indication that DC may be disorder of telomerase. *TERC*, located on 3q26, encodes the RNA component of telomerase whereas at that time it was not known that Dyskerin is also a component of telomerase. Another mode of inheritance was eventually detected (Marrone et al 2005). Marrone (2004) explains that a significant progress has been made in understanding the molecular basis of DC, linking it to other related bone marrow (BM) syndromes: (i) Hoyeraal-Hreidarsson (HH) syndrome, which is a multisystem disorder characterised by aplastic anaemia (AA), immunodeficiency, microcephaly, cerebellar hypoplasia and growth retardation, (ii) AA in which the BM ceases to produce sufficient numbers of blood cells, and (iii) myelodysplastic syndromes (MDS), which are a group of BM neoplastic diseases. All these findings indicate that there are 3 distinct modes of DC inheritance which will be addressed next.

1.7.2 X-linked Recessive (DKC1)

The X-linked recessive form is the most common form of DC (Marrone 2004). Investigations have shown that this mode of inheritance is associated exclusively with a mutated *DKC1* allele. This gene encodes the 514 amino acid protein, dyskerin (Heiss, et al 1998). It consists of 15 exons spanning over 15kb (Knight et al 1999). The characterisation of X-linked recessive patients has identified 41 mutations in *DKC1* (Marrone 2004). Heiss et al (1998) published data to identify mutations in *DKC1* using cDNA from five DC patients. Four of them showed missense mutations and one showed deletion of three nucleotides. Marrone (2004) and Marrone et al (2005) explain that the human dyskerin is a multifunctional pseudouridylation protein that catalyses the isomerisation of uridine to pseudouridine in certain RNA molecules and it is involved in ribosomal (r)RNA processing, ribosomal subunit assembly and/or centromere or microtubule binding. Dyskerin is a component of small nucleolar ribonucleoprotein particles (snoRNPs) and binds to small nucleolar RNA (snoRNA). Figure 1.8 shows the key domains of *DKC1*.

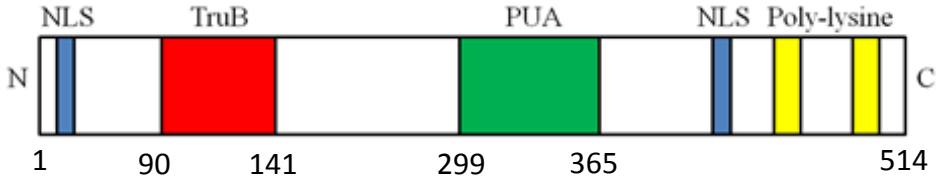

Figure 1.8. Diagram showing the key domains in the dyskerin gene. *These domains include: TruB (the catalytic domain) and the PUA (pseudouridine synthases and archaeosine-specific transglycosylases) domain. Other domains include: a NLS (nuclear localisation signal) and poly-lysine (the two lysine-rich carboxy domains) (Adapted from Dokal, 2000).*

Mutations in the *DKC1* gene almost always cause disease in males, whilst female mutation carriers rarely show disease symptoms because most tissues express normal

DKC1 alleles due to biased X-chromosome inactivation (Bessler et al 2010). A range of mutations have been found in X-linked DC patients (Bessler et al 2010). Mutations found in X-linked DC patients include a terminal deletion of 22 amino acids or an in-frame deletion of a lysine at position 37 in dyskerin (Bessler et al 2010).

In 1999, Knight et al examined 37 families with DC; 14 of these families contained 2 or more affected males and the other 23 were sporadic cases with only one affected male in the family. They detected single nucleotide mutations in 21 out of the 37 families (Knight et al 1999). This included a nucleotide substitution of cytosine with thymine at position 1058, which resulted in alanine at position 353 being changed to valine in exon 11 (Knight et al 1999). This mutation was seen in 11 families and was also seen in the 17 families studied by Dokal (2000).

Furthermore, Knight et al (1999) found two other nucleotide substitutions in exon 11. These two nucleotide substitutions resulted in a missense mutation of the same amino acid codon at position 350 (Knight et al 1999). The first nucleotide substitution is of thymine with cytosine at position 1049, resulting in methionine at position 350 being changed to threonine (Knight et al 1999). The second nucleotide substitution is of guanine with alanine at position 1050, which results in methionine at position 350 being changed to isoleucine (Knight et al 1999). Additionally, they found a missense mutation of leucine to valine at position 321 in exon 10 (Knight et al 1999). Mutations in the dyskerin gene in patients with X-linked recessive DC result in defective telomere maintenance, which cause accelerated telomere shortening, reduced telomerase activity and telomere dysfunction.

1.7.3 Autosomal Dominant (TERC)

Vulliamy et al (2008) observed that Autosomal Dominant (AD) Dyskeratosis Congenita can result from *TERC* mutations, which cause a reduction in telomerase activity and give rise to disease via haploinsufficiency. This leads researchers in the field to believe that DC is primarily the disorder of telomere maintenance. This is supported by Marrone (2004) who further elaborated that dyskerin and TERC are closely associated within the telomerase complex. At present, 18 mutations have been identified within *TERC* that contribute to DC (Marrone 2004; Marrone et al 2005). The first TERC mutation identified, was the 3'end deletion at the H/ACA domain (Marrone 2004). Most of these mutations are located in the pseudoknot domain, involving the catalytic activity and many suggest that it could reduce telomerase activity *in vivo* (Marrone 2004). Investigations found that patients with either *DKC1* or *TERC* mutations have shorter telomeres compared to age-matched controls (Marrone et al 2005) and a defective telomerase activity in vitro.

1.7.4 Other DC genes

The third form of DC inheritance has been identified as Autosomal Recessive (AR DC). Some of the newly identified DC genes are responsible for AR DC. A recent observation from small number of patients supports the notion that DC is the disorder of telomere maintenance by revealing that the disease may result from mutations in the component of shelterin,*TINF2*, which is a part of the shelterin protein complex (Vulliamy et al 2008; Calado and Young 2008). Heterozygous mutations of *TINF2* have been identified in approximately 11% of DC patients (Nishio and Kojima 2010). Gorgoulis et al (2005) also mentioned that patients with DC have in some cases reduced *TERC* levels. *NHP2* (a protein forming part of the telomerase complex) associates with *TERC*, suggesting that

telomere maintenance could also be affected through reduction of *TERC* levels in patients with biallelic *NHP2* mutations (Vulliamy et al 2008).

1.8 Telomere maintenance & DNA Damage Response

The final section of this overview is the integration of telomere maintenance mechanisms and DNA damage response mechanisms. It is becoming increasingly clear that these two sets of mechanisms are functionally related. As explained earlier, telomeres become shorter after each cell division. This eventually leads to cell senescence (Nigam 2011). d'Adda di Fagagna et al (2003) provided evidence through immunofluorescence experiments that in senescent cultures, nearly all cells had clearly detectable γH2AX and 53BP1 foci, suggesting that DNA damage response is present in senescent cells. They further demonstrated that in senescent cultures nearly all cells had γ-H2AX and 53BP1 foci following irradiation (d'Adda di Fagagna et al 2003). They then assessed whether dysfunctional telomeres directly engage with DNA damage response in senescent cells; this was carried out by studying localisation of γ-H2AX with telomeres (d'Adda di Fagagna et al 2003). Using chromatin immunoprecipitation with antibodies against γ-H2AX and whole-genome scanning approaches, it was seen that telomeres directly contribute to the DNA damage response in senescent fibroblasts and that uncapped telomeres associate directly with many DNA damage response proteins (d'Adda di Fagagna et al 2003).

These findings suggest that critically short telomeres lead to cell cycle arrest and cell senescence through activating DNA damage response. This was corroborated by a similar approach from the de Lange's laboratory (de lange 2005) in which genetic

manipulation of the shelterin component, TRF2, caused activation of DNA damage response by turning telomeres dysfunctional. These studies clearly revealed that the function of telomeres is to hide DNA termini from being recognised as DSBs by cellular DNA damage response machinery.

In line with these studies a number of papers show functional interplay between telomere maintenance and DNA damage response. These papers have been reviewed by Slijepcevic (2006). For example, a number of DSB repair proteins participate directly in telomere maintenance including Ku, DNA-Pkcs, RAD54, RAD510 and BRCA1 (Samper et al 2000; Hande et al 1999; Jaco et al 2003; Tarsounas et al 2004; McPherson 2004) . It has been shown that many DDR proteins interact with the shelterin complex (de Lange 2005). Slijepcevic (2008) stated that there are at least 17 genes involved in DDR, which if dysfunctional, can cause telomere dysfunction. Dysfunctional telomeres activate the DDR pathway and DDR machinery, which recognises telomeric ends as DSBs in DNA (Slijepcevic 2008).

Furthermore, some human genetic disorders show accelerated telomere shortening which eventually causes telomere dysfunction (Oeseburg et al 2010). Examples include Werner syndrome, Fanconi anaemia, Bloom syndrome, Nijmegen breakage syndrome and Ataxia telangiectasia (Callen and Surralles 2004). These diseases are caused by mutations in DDR genes and they all are characterized by premature aging (Oeseburg et al 2010).

The main interest of this study is to examine the possibility whether DDR will be affected when telomere dysfunction is present as a result of defects in factors that participate exclusively in telomere maintenance such as components of telomerase and shelterin. There is indirect evidence that this is possible. The examination of the TRF2 protein behaviour following induction of DNA damage suggested that TRF2 is moving to

the sites of DNA damage irrespective whether damage was at telomeres or not (Huda et al 2009; Tanaka et al 2005). Furthermore, lack of telomerase activity causes defective DNA damage response in yeast (IJpma and Greider 2003) and telomere shortening in mouse cells (Blasco et al 1997) which as a result become radiosensitive (Mcllrath et al 2001; Alexander 1961; Wlodek 1987 and Beer et al 1983).

Our approach in this study is to examine DDR in cells from DC patients. DC cells show clear telomere dysfunction as discussed above. At present it is not fully clear whether DDR is functional or not in DC cells.

Most research in DC cells focused on analysing telomere length and thus addressed DDR response only indirectly (Armanios 2013). Telomere shortening in DC was studied by Mitchell et al in 1999. Using the telomeric repeat amplification protocol (TRAP) assay and northern blot hybridisation on fibroblasts from homozygous DC patients and controls it was found that the homozygous DC cells contained lower levels of telomerase and have shorter telomeres compared to control cells (Mitchell et al 1999).

Telomere shortening was also observed by Wong and Collins (2006), who examined fibroblasts from an X-linked recessive DC patient lacking a leucine at position 37 in dyskerin and controls, including a heterozygous DC patient. They firstly used a TRAP assay on each cell line, with and without an integrated retrovirus expressing TERT, the reverse transcriptase component of telomerase (Wong and Collins 2006). The study found that control cells had greater telomerase activity than homozygous DC cells (Wong and Collins 2006). They then looked at the effect of TERT expression on telomere length by observing the cultures that expressed TERT within the first 50 post-selection population doublings (PDL) of continuous culture (Wong and Collins 2006).

They saw that telomere length remained long in the control cells but shortened in the homozygous DC cell line (Wong and Collins 2006).

Gu et al (2008) studied telomere shortening by copying a deletion mutation in dyskerin found in X-linked recessive DC patients into mice. This was a deletion of 21 amino acids from the C-terminal of the dyskerin gene (Gu et al 2008). Using Southern blot, it was seen that telomere length was significantly shorter in mutant cells compared to controls (Gu et al 2008). They therefore concluded that this 21 amino acid deletion leads to defective telomere maintenance in mutant cells (Gu et al 2008).

Zeng et al (2012) studied three X-linked recessive DC patients with the substitutions: lysine with arginine at position 314, arginine with glutamine at position 322 and alanine with valine at position 353 in dyskerin. They used a TRAP assay to restore telomerase activity in these DC and control cells; finding a reduction in telomerase activity in DC cells after forced expression of TERT (Zeng et al 2012).

However, none of these studies focus directly on DDR in DC cells. The first study that examined DDR in DC cells directly was carried out on in 1990. Radiosensitivity was observed in fibroblasts from one heterozygous and two homozygous DC patients, relative to two control fibroblast cell lines (DeBauche et al 1990). Radiosensitivity was studied by observing chromosomal damage of chromatid type after exposing cells to X-irradiation (DeBauche et al 1990). These experiments suggested that DC patients have an increased susceptibility to chromatid breaks caused by irradiation compared to control fibroblasts (DeBauche et al 1990). It is worth noting that 100% of homozygous

DC fibroblasts had chromatid breaks, whilst only 35.3% and 70.2% of control fibroblasts contained chromatid breaks (DeBauche et al 1990).

Telomere shortening has also been studied in somatic cells from chronic lymphocytic leukaemia (CLL) patients by Brugat et al (2010). CLL cells had an increased number of telomere dysfunction-induced foci containing γ-H2AX and 53BP1 (Brugat et al 2010). Finding the relationship between telomere maintenance and the DDR in X-linked recessive DC can improve our understanding of a wide range of diseases, including cancer and age-dependent disorders (Armanios 2013). This can potentially help create treatments for some diseases, which can improve the lives of sufferers of these diseases.

M'kacher et al (2003) studied fibroblasts and lymphoblasts from a 7 year old patient with Hoyeraal-Hreidarsson syndrome (HHS), a severe infantile variant of X-linked recessive DC. They found that the HHS patient had significantly shorter telomeres compared to a healthy control (M'kacher et al 2003). M'kacher et al (2003) also showed sensitivity of HHS cells to ionising radiation and other DSB inducing agents, including Bleomycin, thus suggesting further that a defective DNA damage response within these cells.

In 2011, Kirwan et al examined T lymphocytes from homozygous DC patients and controls. In their experiments they measured the levels of γ-H2AX in homozygous DC lymphocytes using flow cytometry (Kirwan et al 2011). They induced DNA damage using varying doses of a DNA damaging agent Etoposide and observed that the γ-H2AX expression is cell-cycle dependent (Kirwan et al 2011). They next labelled homozygous DC and control lymphoblasts with 53BP1, a protein known to co-localise with γ-H2AX to

sites of DNA damage (Kirwan et al 2011). It was shown that there was no difference in DNA damage response between DC and control cells (Kirwan et al 2011) thus contradicting the notion that DC cells may show radiosensitivity.

However, a study by Pereboeva et al (2013) contradicts conclusions made by Kirwan et al (2011). Pereboeva et al (2013) studied fibroblasts and lymphoblasts from autosomal dominant DC patients. These cells were exposed to DNA damaging agents such as ionising radiation, Etoposide and Paclitaxel (Pereboeva et al 2013). It was concluded by Pereboeva et al (2013) that DC lymphocytes have impaired *in vitro* cell growth and increased sensitivity to DNA damaging agents. It was also seen that DC cells can tolerate DNA damage less effectively than controls (Pereboeva et al 2013)

Manguan-Garcia et al (2014) studied fibroblasts from a heterozygous DC patient and two X-linked recessive DC patients. The cells were treated with Bleomycin for 24 hours and were incubated with antibodies against the DNA damage markers: γ-H2AX, 53BP1, p-CHK2 and ATM (Manguan-Garcia et al 2014). They found that the number of γ-H2AX foci per cell was significantly higher in cells from the homozygous DC patients than the heterozygous DC patient (Manguan-Garcia et al 2014). The same result was seen in similar experiments using the antibodies: 53BP1, CHK2 and ATM (Manguan-Garcia et al 2014). They then combined a PNA FISH probe as a telomeric marker and 53BP1 for DNA damage detection (Manguan-Garcia et al 2014). The results showed that there was a higher association of DNA damage markers with telomeres in the homozygous DC cell lines compared to the heterozygous DC cell lines (Manguan-Garcia et al 2014).
Taken together these observation point to the possibility that DDR may be defective in DC cells.

1.9 Aims and Objectives

This study will focus on analysing DDR in DC cells with a view of confirming initial studies which point to the possibility that DDR may be defective in DC cells. This possibility is directly in line with the notion that DDR mechanisms and telomere maintenance mechanisms are functionally related.

To this end we will

- Examine fibroblast and lymphoblastoid cell lines from DC patients for their capacity to carry out functional DDR.
- Knockdown the *DKC1* gene in normal cell lines using siRNA oligonucleotides and examine DDR relative to control cells.
- Examine whether a novel stimulator of telomerase, TA-65, derived from the plant *Astragalus membranaceus*, affects DDR in cells exposed to ionizing radiation.

Chapter 2 Materials and Methods

2.1 Cell lines

A total of 14 established cell lines were used in this project (Table 2.1). Most cell lines have been selected for their deficiencies in telomere function such as DKC1 deficient cell lines. Mouse lymphoma LY-S (radio- sensitive) and LY-R (radio-resistant) cell lines were used as a reference for cytological testing of telomere length measurements using IQ-FISH techniques.

Table 2.1 List of Cell Lines used in this project.

Cell line	**Origin and gene affected**	**Cell Type**	**Age at sampling**	**Sex**	**Clinically affected**	**Source**
GM08399	Healthy Individual	Fibroblast	19 year old	Female	No	Coriell Cell Repositories
GM01787	Dyskeratosis Congenita carrier, X-linked recessive; DKC1 +/-	Fibroblast	78 year old	Female	No	Coriell Cell Repositories
GM01774	Dyskeratosis Congenita, X-linked recessive; DKC1 -/-	Fibroblast	7 year old	Male	Yes	Coriell Cell Repositories
GM00893	Healthy Individual	Lymphobastiod	32 year old	Female	No	Coriell Cell Repositories
GM017208	Healthy Individual	Lymphobastiod	26 year old	Male	No	Coriell Cell Repositories
GM03650	Dyskeratosis Congenita carrier, X-linked recessive; DKC1 +/-	Lymphobastiod	47 year old	Female	No	Coriell Cell Repositories
GM01775	Dyskeratosis Congenita, X-linked recessive; DKC1 -/-	Lymphobastiod	7 year old	Male	Yes	Coriell Cell Repositories
GM03193	Dyskeratosis Congenita, X-linked	Lymphobastiod	15 year old	Male	Yes	Coriell Cell Repositories

	recessive; DKC1 -/-					
W12022568	Dyskeratosis Congenita, X-linked recessive; DKC1 -/-	Lymphocyte	9 year old	Male	Yes	Salisbury NHS
W1202626	Healthy individual	Lymphocyte	10 year old	Unknown	No	Salisbury NHS
W1202625	Healthy Individual	Lymphocyte	8 year old	Unknown	No	Salisbury NHS
LY -R	Mouse Lymphoma, Normal radiosensitive	Lymphoma	Unknown			Dr Andrzej Wojcik, University of Warszaw, Poland
LY-S	Mouse Lymphoma, radiosensitive	Lymphoma	Unknown			Dr Andrzej Wojcik, University of Warszaw, Poland
HeLa	Human Cervical Carcinoma	Epithelial adherent cells	31 year old	Female	Yes	ATTC (American Tissue Culture Collection)
U205	Human Osteosarcoma	Mesnchymal adherent cells	15 year old	Female	Yes	ECCC (European Collection of Cell cultures)

2.2 Cell culture and tissue culture methodology

2.2.1 Human adherent cell lines

All cell lines were kept frozen in liquid nitrogen. When we needed to culture cells, vials of frozen cells were thawed and cultured in either a 25cm^2 flask or a 75cm^2 flask with filter head (Nunc) to avoid fungus contamination. Primary human fibroblast cell lines GM08399 (normal individual), GM1787 (DC patient with a heterozygous *DKC1* mutation: *DKC1*(*+/-*), GM1774 A (DC patient with homozygous *DKC1* mutations: *DKC1*(-/-) and HeLa were cultured in Dulbecco's modified eagle medium (D-MEM) (Gibco/invitrogen) supplemented with 10% fetal bovine serum (FBS) at 37°C under

10% CO_2. The U2OS cell line was grown in McCoy's 5a medium (Fisher), supplemented with 10% foetal bovine serum (Gibco/Sigma) and 2mM glutamine (Sigma) in the atmosphere of 10% CO_2 at 37°C.

All cell lines were subcultured 1:3 by trypsinization at least every 3 to 4 days at the point when cells were ~ 80% confluent.

2.2.2 Human lymphoblastoid cell lines

All human lymphoblastoid cell lines, GM00893, GM017208, GM03650, GM01775 and GM03913 were grown in RPMI 1640 medium (Gibco/Invitrogen) containing 10% foetal calf serum and 0.1 mg/ml of streptomycin at 37°C in the atmosphere of 5% CO_2.

2.2.3 Mouse lymphoma cell lines

Mouse lymphoma cell lines were grown in standard tissue culture conditions by using the RPMI 1640 medium (Gibco/Sigma) and 10% fetal calf serum with 0.1mg/ml of streptomycin at 37°C in the atmosphere of 5% CO_2. Cells were sub-cultured at the ratio 1:5 every 3-4 days. They were used as a reference for cytological testing telomeric measurements using interphase Q-FISH (IQ-FISH) technique.

2.2.4 Tissue culture procedure

The subculturing of cells were performed as follows using the appropriate size flasks. The tissue culture hood was thoroughly cleaned with the standard laboratory disinfectant used in the Institute of Cancer Genetics & Pharmacogenomics. Tissues culture flasks (Nunc) with cells were transferred from the incubator and examined

carefully for signs of contamination or deterioration with the use of an inverted phase microscope. If cells were assessed as ready for trypsinization using trypsin-EDTA, tissue culture flasks were transferred to the hood. All solutions were brought to room temperature prior to trypsinising using a waterbath with a monitor to keep the temperature at 37ºC. The water-bath was constantly cleaned and disinfected alongside the incubator and the hood to avoid spreading any fungus or bacterial infection. Medium was aspirated from flasks by using a Pasteur pipette. Cells were washed briefly with 2-3ml of PBS (Phosphate buffered Saline, Gibco/invitrogen). Following PBS wash a total of 1ml of trypsin/EDTA (Gibco/Invitrogen) was added to the tissue culture flask which was then incubated for 5 min at 37˚C in a 10% CO_2 incubator and checked that all cells have detached from the plastic surface. Approximately 1 ml of medium was added to the flask and cell suspension was mixed several times. Cells were transferred into a 15 ml sterile tube and centrifuged at 1500 rpm for 5 min. Supernatant was removed and cell pellet flicked. The samples were then resuspended in 3ml of complete medium. 5ml of complete medium was added into three new 25cm^2 flasks (labelled with cell line, date and passage number) and 1 ml of cells resuspended in medium. Cells were incubated at 37°C under 10% CO_2. To subculture in 75cm^2 flask, the same procedure was followed but 15ml of complete medium was added into each flask.

All lymphobastiod and lymphoma cell lines were grown in suspension under tissue culture conditions as mentioned above. Cells were sub-cultured at the ratio of 1:10 every two or three days, preferably before the medium colour changed to yellow.

2.1.5 Cryopreservation of cells

After checking cells under an inverted phase microscope, cells were trypsinized as described above. Cell suspension was mixed with 1ml of freezing medium containing 90% fetal bovine serum and 10% DMSO. The cell suspension was aliquoted into

cryogenic vials for storage in liquid nitrogen. Prior to storage in liquid nitrogen the vials were kept in a Nalge nunc cooler for 24 hours at -80^{o}C. This plastic holder was filled with Isopropyl alcohol (IPA). Finally the vials were transferred into liquid nitrogen. Cells were preserved in liquid nitrogen to avoid aging and contamination.

2.1.6 Thawing of Cryopreserved cells

The medium was aliquoted in the appropriate tissue culture flask before the vial was taken out of the liquid nitrogen. The cryopreserved cells were handled with great care. The vials were thawed for two to three minutes and the content immediately put into the flask containing medium. After 24 hours the medium in flasks was changed to wash away any residual DMSO.

2.1.7 Cell counting

Cell lines were sub-cultured in tissue culture but cell suspension was mixed with 1ml of medium. Haemocytometer was used for cell counting and it was cleaned with 70% of IMS. Coverslip was placed on top of the haemocytometer and placed under the microscope. Using a Pasteur pipette, some cell suspension was drawn up carefully to fill the haemocytometer by gently resting the end of the pipette tip at the edge of the chambers. The grid lines were focussed using the 10x objective of the microscope, on one set 16 corner square as indicated on Figure 2.1.

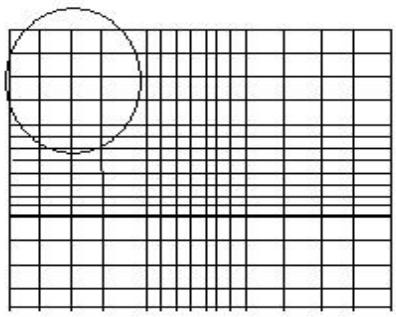

Figure 2.1. Haemocytometer. Example of 16 squares grid lines. The circled part demonstrates one part of the 16 corner square where the cells were counted. (diagram adapted from Abcam).

Using a hand tally counter, the number of cells was counted in this area of 16 squares. Cells were counted within the square and any positioned on the right hand or bottom boundary line. The same was done on all 4 sets of 16 corner squares. The haemocytometer is designed so that the number of cells in one set of 16 corner squares is equivalent to the number of cells x 10^4 /ml. Therefore to obtain the count as follows

1. Count up the total from the four corner squares and divide by 4 to find the average cell number (Cells/ml x 10^4). This is the number of cells per 1 ml, or per 1000µl.

2. To work out the amount of cells per 1ul, take the answer from above and multiple it by (1µl/1000µl).

Now, if 100,000 cells are required to be seeded, divide 100,000 by the answer from above (part 2) and multiple it by 1. This is amount of volume, in µl, required to seed 100,000 cells.

2.1.8 Irradiation

Cells were irradiated with the appropriate dose of gamma rays using a Co^{60} source. Datasheets were used to calculate dosages of radiation measured in Gray (Gy) per minute. The formula used to calculate this was:

Time (mins) = Dose Needed (Gy)/Dose rate (Gy min – 1)

Irradiated cells were incubated for different time intervals to allow recovery. Once cells were 80% confluent they were trypsinized as explained in the Cell culture section and counted using haemocytometer. The required amount of cells was seeded onto a polyprep slide (Sigma). Each polyprep slide with cells was transferred into a 10 cm sterile dish (Nunclon™) and placed into a 37˚C incubator for an overnight incubation.

Following morning cells were inspected under a contrast-phase microscope and if they looked healthy a radiation experiment was carried out. Dishes with polyprep slides were transferred into polystyrene containers and transported to radiation facility room. Cells were placed at the radiation location and exposed to the required doses. After irradiation dishes were returned to polystyrene container and transported back to a 37˚C incubator until needed for γH2AX assay (described below).

2.1.9 - Calculation of Population Doublings

When recording the phase of a cell population, age should be expressed as a population doubling, rather than passage number. The term "passage" is often used to indicate the age of cell cultures. However, it indicates only the number of trypsinisation steps performed during the culture period. It is therefore inadequate for describing the age of a culture because trypsinisation can be performed at different split ratios.

Since one population doubling (PD) means doubling the number of cells as a group, the relationship between PD and dilution factor is derived as follows:

2^{nd} = dilution factor (where n = PD)

If the logarithm of both sides is taken and rearranged

Log 2^{n} = log (dilution factor)

n(PD) = log (dilution factor)/log2 = log(dilution)/0.301

This formula was used when for each passage number the dilution factor was known.

Otherwise the cell PDs were calculated using the following formula:

PD = $(\text{Log}N_1/\text{Log}2) - (\text{Log}N_0/\text{Log}2)$

N_0 = cell number at the beginning of cell culture

N_1 = cell number at the end of the cell culture period

2.2 Cytogenetic Analysis

2.2.1 Metaphase Preparation using fibroblast cell lines

A high mitotic index is essential in scoring a large number of metaphases in a short time and it is also important to get high quality metaphase spreads. A flask with the semi-confluent cells (80-90%) was treated with colcemid (10μg/ml) (Sigma-Aldrich). Colcemid was used to arrest cells in metaphase by inhibiting the mitotic spindle formation. Cells were treated for three hours with colcemid (10μg/ml) prior to trypsinization and harvesting. Cells were washed in PBS, trypsinized, and spun down at 1000rpm for five minutes. Cells were then treated with 10ml of hypotonic buffer (75mM of KCl) for 15 minutes in a 37^{o}C water bath and this will cause cells to increase their fluid intake. Cells were then fixed in a solution consisting of methanol and glacial acidic acid (3:1) solution. The process of fixation was carried out two more times and each time 1ml of fresh fixative was added drop wise, followed by the addition of 2ml of extra fixative. The cells were left at room temperature for 10 minutes and 30 minutes respectively. Finally, the cell pellets were re-suspended in fresh fixative and 10μl of cell suspension was dropped onto pre-cleaned slides. The fresh fixative ensured that mitotic cells were spread over the surface of slide effectively. Once the slides were dried they were checked under a phase contrast microscope.

2.2.2 Metaphase preparation using lymphoblastoid cell lines

Preparations of metaphases from human lymphoblasts cell lines were performed as described above with the difference that trypsinization was not required as these cells grow in suspension.

2.2.3 Giemsa staining

Slides were stained with 7% Giemsa (Sigma-Aldrich) for five minutes in 50ml of ddH20. Giemsa stain was filtered to achieve better purity using standard filter paper (3MM Watman paper). After staining, slides were rinsed quickly with ddH20 and left to air dry while covered with paper to prevent dust settling onto the slides. Slides were mounted with DPX mountant (BDH laboratories), covered with cover slips, and left overnight to dry. DPX is a neutral solution of Polystyrene Plasticizer in Xylene. By applying this solution the coverslips were permanently attached onto the slides. A clean dust free and evenly stained slide with high mitotic index was selected for analysis using conventional microscopy (Zeiss Axioplan 2) equipped with CCD camera and MetaSystem software (Altlussheim, Germany).

2.2.4 Micro-nuclei Assay

Exponentially growing cells were treated with 6µg/ml of Cytochalasin B (Sigma-Aldrich) for 48 hours or 72 hours. The cells were then centrifuged at 800 rpm for 5 minutes and the supernatant was aspirated. A total of 3ml of KCL (75mM) was then added to the cells and left at room temperature for 5 minutes. A few drops of fixative (Methanol: Acetic Acid; 3:1) were added to the cells, and they were centrifuged at 800 rpm for 5mins. After centrifuging the supernatant was aspirated and the cells were re-suspended in 500µl of fixative. A total of 400 µl of this suspension was cytospined onto slides at 800rpm for 5 minutes. The slides were then stained with Giemsa (Sigma-Aldrich) as described in section 2.2.3.

2.2.5 Immunocytochemistry (γH2AX-assay)

This method is used for detecting DNA damage in nuclei using a monoclonal antibody against H2AX (a protein that recognizes DNA damage).

Using a haemocytometer, cell counting was preformed and approximately 100,000 cells were seeded on a poly-prep slide (poly – L- lysine coated glass slides) (Sigma-Aldrich) . Each poly-prep slide with cells was transferred into a 10 cm petri dish and they were placed in the incubator for 24 hours to allow the cells to attach and grow. Cells were then irradiated using gamma rays at doses 0.25 Gy, 0.5 Gy, and 1.0 Gy for dose response. If doing repair kinetics, cells were irradiated at 1.0 Gy and left in incubator at their appropriate time points (30 minutes, 5 hours, 24 hours and 48 hours). Petri dishes with poly-prep slides were transferred into polystyrene containers and transported to radiation facility room. The cells were placed at the radiation location and exposed to the above doses, appropriately. After irradiation dishes cells were returned to polystyrene container and transported back to a 37˚C incubator until the appropriate time points. The petri dish containing the poly-prep slides were transferred from the incubator to the molecular laboratory. Poly-prep slides were carefully transferred into 4% formaldehyde (Sigma-Aldrich) in PBS into coplin jars and were left to fix for 15 minutes. Cells were then permeabilize in 0.2% Triton-X (Sigma-Aldrich) in dH_20 at 4^0C for 10 minutes followed by blocking with 0.2 percent of milk (semi-skimmed powder, Marvel) in PBS (Phosphate buffered saline) for 1 hour covered with parafilm. A total of 100 µl of γH2AX (Anti-phospho-Histone H2A.X (Ser139)) antibody (dilution of 1:500 with 0.2 percent milk) (Millipore) was added on to each slide, covered with parafilm and left to incubate at room temperature for 1 hour. This was followed by 3 X 15 minutes washing in TBST (8.8 grams of NaCL, 0.2 grams of KCL, 3 grams of Tris base,

500ul of Tween 20 and 800ml of ddH_20), on an orbital shaker. Finally a total of 100 µl of Alexa fluor 488 (dilution of 1:1000 with 0.2 percent milk) (Biolegend) was added on to each slide and the procedure repeated as above. Alexa fluor 488 anti-mouse is used as a secondary antibody that binds to γH2AX antibody (primary antibody), to analyze the amount γH2AX foci (colour: green). After several washes in TBST and PBS in dark coplin jar and on an orbital shaker, and dehydrating them in ethanol series (70%, 90% and 100%) for five minutes each and air dried in dark, slides were analyzed for the presence of γH2AX signals by staining them with solution containing DAPI – vecta-shield (vector laboratories). The slides were analysed using the computerized Axioskop 2 Zeiss fluorescence microscope equipped with a CCD camera and Metasystems software.

2.2.6 γH2AX assay using cytospin

The protocol for DNA damage detection in lymphoblastoid cell lines required the use of cytospin. In contrast to adherent cells, which can be grown on poly-l-lysine microscope slides, lymphoblastoid cells cannot as they grow in suspension. The alternative method for spreading these cells on to microscope slides employs the cytospin procedure. Cells were irradiated in flasks or tubes as cell suspension. This cell suspension was then used to attach cells to microscope slides using cytospin at 700rpm for 5 minutes. After centrifuging cells in the Cytospin machine (Shandon), cells were fix in 1% of formaldehyde in PBS for 20 mins. They were then permeabilize in 0.25% Triton + 0.1% glycine in PBS at 4^0C for 10 minutes. They were blocked for 20 minutes using 0.5 percent BSA in PBS. The procedure from section 2.2.6 was followed with the exception that 0.5 percent BSA was used for antibody dilution.

2.2.7 Immunofluorescence TIF-assay (Telomere dysfunction Induced Foci)

The TIF assay is designed to show DNA damage at telomeres using combination of antibody detection and hybridization with cyanine-3 (Cy3) labelled telomeric PNA oligonucleotide $(CCCTAA)_3$. Firstly, the slides are fixed using 4% formaldehyde for 20 minutes, after the de-hydration as described in section 2.2.6. DAPI is not added to the slides. Instead slides were incubated overnight in a dark container at room temperature. This incubation allows better preservation of antibodies and enables them to remain intact after the subsequent hybridization procedure. This probe is hybridised on slides the following day. After adding the probe, slides were covered with coverslips, incubated for 2 min at 80^{o}C and left for 2 hours at room temperature for hybridization to take place. Slides have been washed with 70% formamide (10ml of formamide, 10ml of 20% SSC buffer and 20ml of ddH_20) for 10 minutes, twice in dark to remove excess unbound probe, washed in PBS, dehydrated with an ethanol series (70%, 90% and 100% concentration) for five minutes each and then air dried before adding 15µl Vectasheild mounting medium (Vector Laboratories) with DAPI. The slides were analysed using the computerized Axioskop 2 Zeiss fluorescence microscope equipped with a CCD camera and MetaSystems software. DNA damage on Telomeres (TIF-Foci) is displayed as yellow, with colour green (FITC) merged with red (Cy3).

2.3 Hybridisation with the telomeric probe

This procedure is used to either analyse telomeres using IQFISH protocol or for analyses of chromosome aberrations. The method is described as below.

2.3.1 Harvesting cells prior to Hybridisation

In the case of IQ-FISH addition of Colcemid was not required. The cell lines were grown until confluent, wash with PBS, trypsinized, and spun down at 1500rpm for five minutes. Cells were then treated with 3ml of hypotonic buffer (75mM of KCl) for 15 minutes in a 37ºC water bath. Fixation was followed using methanol-glacial acidic acid (3:1) as fixative by adding 3 drops to the sample and centrifuged at 1000rpm for 5 minutes. The supernatant was aspirated and 3ml of fixative was added to the cells, leaving it for 10 minutes at room temperature. Again, it was centrifuged at1000 rpm, supernatant aspirated and 3ml of fixative was added. It was left for 30 minutes at room temperature. Finally the cell pellet was re-suspended in fresh fixative and 15ul of cell suspension was dropped on pre-cleaned slides. The fresh fixative ensured that cells were spread over the surface of slide. The slides have then been aged by placing them at 55^0C on a hot plate overnight.

2.3.2 Pre Hybridisation washes

After being aged, the slides were washed in PBS for 5 minutes. After the PBS wash, the cells were fixed in a 4% formaldehyde solution for 2 minutes and then washed in PBS for 5 minutes. A total of 500µl of pepsin (10% pepsin in ddH_2O; Sigma Co.) mixed in 50ml of acidified dH_2O at pH 2 and were incubated at 37ºC for 10 minutes to remove unwanted proteins. Slides were then washed in PBS twice for 2 minutes. 4% formaldehyde was used to fix the cells for further 2 minutes in a coplain jar. The slides were then washed in PBS solution 3 times for 5 minutes, dehydrated in ethanol series (70%, 90% and 100%) and left to air dry at room temperature.

2.3.3 Hybridisation with the PNA probe

About 20ul of the FITC or Cy3 labeled peptide nucleic acid (PNA) telomeric oligonucleotide $(CCCTAA)_3$ was added to each slide. Slides were covered with coverslips, denatured for 2 min at 80°C and then incubated in a dark humidified chamber for 2 hours to allow hybridization to take place.

2.3.4 Post Hybridisation washes

Slides have been washed with 70% formamide to remove excess unbound probe, plus two times with PBS for five minutes each. Slides were then dehydrated in ethanol (starting with 70%, 90%, and 100% respectively) for five minutes each and stained with 15ul DAPI. Slides were either then analyzed using the Smart Capture software and telomere fluorescence analyzed using the software IPLAB (as described below) or analyzed for chromosome aberrations.

2.3.5 Average Telomere length analysis by IQ-FISH

A total of 50 interphase cells have been analyzed for each cell line. Each measurement was repeated 3 times. Images of interphase cells were captured using a 63X objective on an Axioplan 2 Zeiss fluorescent microscope equipped with a CCD camera and the Smart capture 2 image acquisition software. Images were used to measure telomere signal intensity which is proportional to telomere length using the IP Lab software. The software produces a combined image of the detected telomeres and the cell nucleus boundaries which are superimposed onto the telomere image. In order to maintain the accuracy of IQ-FISH methodology it was important to use appropriate controls for the experiment. This is because the fluorescence microscope lamp intensity is not constant. To ensure the accuracy of fluorescence intensity measurement we used two mouse cell lines, LY-R and LY-S, with long and short telomeres respectively, as calibration

standards (Mcllrath et al., 2001). In each experiment we captured images of LY-R and LY-S cells together with the test samples (human cells). After capturing images of interphase cells in the Smart Capture 2 software using "image segmentation" (fig 2.2), the information was imported to the program in which telomere fluorescence intensities were measured. The procedure for IQ-FISH was described in detail in a PhD thesis by another student working in Dr Slijepcevic laboratory (Ojani 2012).

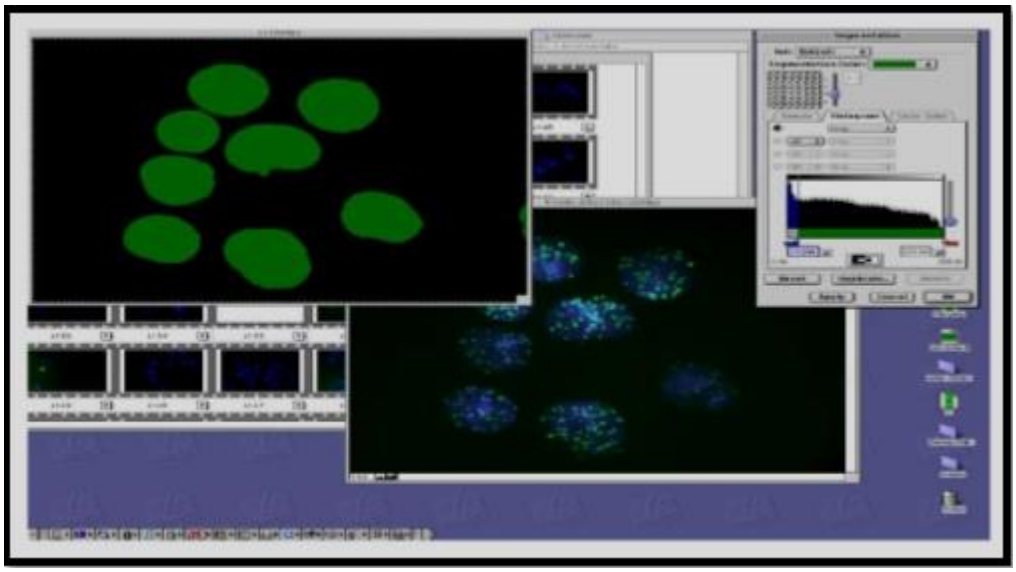

Figure 2.2) Image displays a typical segmented image with cell nuclei stained in green. This function defines the area of the image in which fluorescence intensity will be measured. In practice this means selecting exclusively cell nuclei as areas of interest and ignoring the rest of the image.

The IP-LAB software allows the "background removal" option. It is very important as the average telomere fluorescence signal was analysed from subtracting the fluorescence background noise from the total fluorescence values, so it is clear what is happening inside the nuclei. This process is performed using the "Pixel arithmetic" procedure which is shown below (Figure 2.3).

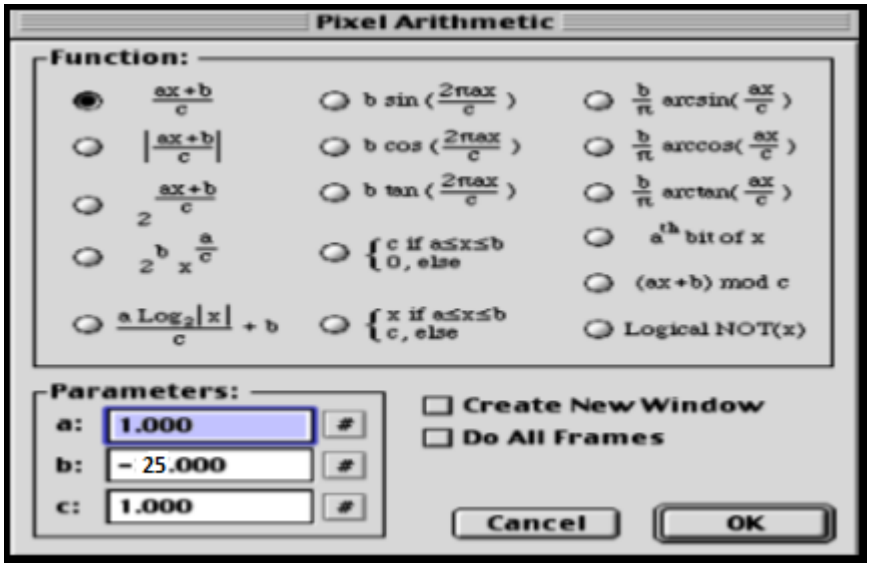

Figure 2.3) Image displays a snap-shot of the mathematical manipulations, Pixel arithmetic behind the process of telomere fluorescence intensity measurement. This is a software which subtracts the fluorescence background noise from the actual fluorescence values.

Figure 2.2 and Figure 2.3 demonstrate the procedures behind telomere fluorescence measurement. This involves steps like cell image segmentation to determine nuclear boundaries, background removal to eliminate non-specific fluorescence, and measurement of telomere fluorescence intensity. At the end of the procedure a table is generated that shows the average fluorescence intensity for each cell.

2.4 RT-Polymerase Chain Reaction (PCR)

2.4.1 RNA extraction

Total RNA is extracted using the RNeasy Plus Procedure (QIAGEN) which is designed to purify RNA from small amounts of animal cells. This kit is compatible with a range of cultured cells and it provides fast processing and effective purification of RNA from cells. Approximately 80% confluent cells were washed with PBS, trypsinized and collected as a pellet. Cells were disrupted by adding RLT buffer Plus. Beta-mercaptoethanol (β – ME) was added to the RLT buffer Plus (guanidium thiocyanate

lysis buffer) before use. The lysate was homogenised by passing the lysate at least 5 times through a 20-gauge needle fitted to an RNase-free syringe. The homogenised lysate was transferred to a gDNA elimination spin column (to remove genomic DNA for accurate gene expression analysis) and centrifuged for 30 second at 1000rpm. One volume of 70% RNA free ethanol was added to the flow-through. The sample was transferred to an RNeasy spin column placed in a 2ml collection tube and centrifuged for 15 second at 1000rpm. The flow-through was discarded and a new one was added. One volume of Buffer RW1 was added, centrifuged and flow-through was discarded with a new one used. Buffer RPE was added to the RNeasy spin column, centrifuge and flow-through discarded and it was repeated. Finally, 30µl of RNA-free water was added to the spin column membrane that was centrifuged for 1 minute at 1000rpm. The RNA quantity was measured using the spectrophotometer NanoDrop 2000C (Thermo Fisher Scientific), which enables measuring of 0.5- 2 µl samples with high accuracy and reproducibility. The spectrophotometer was blanked using the reference RNA free solution that was placed onto the measurement pedestal, and a reading was taken at 260nm wavelength. The measurement of RNA absorbance took place afterwards. The following table (2.2) demonstrates an example of the reading from the total RNA extraction of one of the experiments.

Table 2.2 Sample reading from RNA extraction of Hela, U20S and GM08399.

Sample name	A260/280 nm ratio	RNA concentration (ng/µl)	Amount of 1ug RNA (µl)
HeLa	2.05	1075.8	0.93
U2OS	2.03	1047.4	0.95
GM08399	1.99	71.4	0.99

2.4.2 Purification of RNA Sample using Deoxyribonuclease I Amplification Grade

We took 1ug of RNA sample, added 1ul of 10x DNase I Reaction Buffer, 1ul of Deoxyribonuclease I Amplification Grade (DNase I, Amp Grade) and Nuclease free water to 10ul in microcentrifuge tube. DNase I, Amp Grade digests single-and double-stranded DNA to oligo deoxy-ribonucleotides containing a 5'-phosphate, eliminating DNA to purify RNA. The tube was then incubated at room temperature for 15 minutes, followed by adding 1ul of 25mM EDTA solution in inactivate DNase I. Finally it was heated for 10 minutes at 65^{o}C. The RNA sample is now ready for reverse transcription to make cDNA.

2.4.3 The First Strand cDNA synthesis with Superscript III (Invitrogen)

The following components were added to a nuclease-free microcentrifuge tube:

- 1µl of random primers (diluted 1:11 from the original stock in nuclease free water)

- 1µl of 10mM mixed dNTP (10mM from each dATP, dGTP, dCTP and dTTP at neutral PH)
- 11µl of total RNA (purified by DNase I, Amp Grade)

Final volume 13µl reaction mix

The final mixture volume was heated to 65˚C for 5 minutes and was quickly chilled on ice for 1 minute. This step is designed for primers binding along the opened RNA configuration.

The following components were added to the collected 13 µl reaction mix.

- 4µl of 5x first strand buffer
- 1µl of 0.1 M DTT (Dithiothreitol)
- 1µl of RNAseOUT™ Recombinant Rnase Inhibitor (40 units/µl)
- 1µl of superScript™ III RT (200 units/µl)

Final volume 20µl reaction mix

The 20µl reaction mix was mixed gently and incubated at 25°C for 5 minutes, followed by 50˚C for 60 minutes. This was followed by incubation for 15 minutes at 70˚C in order to inactivate the reaction. The cDNA sample is now ready to be used as a template for amplification by PCR.

2.4.4 Primer Design

DKC1 primers were designed using the National Centre for Biotechnology Information (NCBI) (http://www.ncbi.nlm.nih.gov/), and loaded onto the primer express software. The chosen primers were then BLASTED using the NCBI website in order to confirm

their specificity. The GAPDH primers (Table 2.3) were kindly provided by Dr. Mark Pook, Brunel University.

Table 2.3 Human primer sequence for Real-time PCR

Gene Name	Orientation	GC%	Tm C°	Length bp	Sequence
GAPDH (house keeping gene)	Forward	55.5	59.2	18	5'-GAAGGTGAAGGTCGGAGT-3'
GAPDH (house keeping gene)	Reverse	45	60.8	20	5'-GAAGATGGTGATGGGATTTC-3'
DKC1-F	Forward	52.3	66.4	21	5'-GGCGAGTTGTTTACCCTTTGG-3'
DKC1-R	Reverse	52.3	66.3	21	5'-GCATAATCTTGGCCCCATAGC-3'

2.4.5 Real-Time quantitative Reverse Transcription PCR (Real-Time qRT –PCR)

Real-Time qRT –PCR technique is used to amplify cDNA and simultaneously quantify the cDNA products by utilising SYBR Green I dye. SYBR Green binds directly to double stranded DNA. Therefore, it is possible to measure the fluorescence emission of the DNA-dye complex and quantify the amount of DNA produced.

A total of 1µl cDNA was added to the following reaction mix:

5µl of SYBR Green master mix (2x concentration) (Applied Biosystem)

1µl of forward primer (10mM)

1ul of reverse primer (10mM)

Nuclease free water to 10µl

The reaction mix was then added to a MicroAmp fast optical 96-well reaction plate (Applied Biosystem). Three wells were used for each sample. The reaction plate was sealed with an ABI-prism adhesive cover (Applied Biosystem), followed by brief centrifugation for 30 second and run in 7900HT fast real time PCR machine (Applied Biosystem). Table 4 shows the real time PCR thermal cycle.

Table 2.4 Real Time PCR thermal cycle

	Temperature(°c)	**Time**	**Cycles number**
Enzyme Activation	95	5 minute	1 cycle
Denaturation	95	15 minute	30-40 cycles
Annealing (Variable)	60	1 minute	30-40 cycles
Initial Extention	72	1 minute	30-40 cycles
Extension	72	10 minutes	1 cycle

A dissociation curve analysis was performed immediately after the PCR run in order to check for non-specific products or primer dimer that may affect the data quality. The data was obtained by slowly increasing the reaction temperature to 95°C while continuously measuring fluorescence emission. The increased temperature caused product denaturation, a process accompanied by a decrease in fluorescence.

2.5 siRNA

A group of double-stranded RNA molecules that obstructs the expression of a specific gene is called Small interfering RNA (SiRNA) also known as short interfering RNA. A wide range of small RNA molecules have been recognised including microRNA (miRNA), (siRNA), and Piwi-interacting RNA (piRNA) (Ghildiyal and Zamore 2009). This happened since the identification of RNAi (RNA interference) in 1998 by Fire and Mello using C. Elegans (Fire et al. 1998). Each group of these RNAs differ in relation to their modes of target regulation, their biogeneses, and in the biological pathways in which they regulate. RNAi was described as a form of post-transcriptional gene silencing by Fire and Mello, where the ds(double stranded) RNA induces the degradation of homologous endogenous transcript, either lessening or totally inactivating the mRNA transcript of a specific gene (Fire et al. 1998). This method of post-transcriptional gene silencing is transient and the expression of the specific mRNA reverts back to normal in human cells within 7 to 10 days post transfection.

2.5.1 Effective controls for RNAi Experiment

It is important to have appropriate controls when conducting RNAi experiment (Huppi et al. 2005). This is to ensure how reliable and effective is the RNAi procedure in terms of loss of function (LOF) on the target gene. The editors of Nature cell Biology in 2003 have published a standard criteria which includes Mismatched or scrambled RNA (Also known as non-targeting siRNA). Hannon GJ 2002 provides an intensive review on the limitations of drawbacks on the pathway, so he suggests an effective use of the transient silencing, by looking at two or more siRNAs targeted at different sites on the target gene, so that the desired effect can be achieved. For this reason, we used SmartPool

SiRNA which provides four oligonucleotides to target the DKC1 gene at four different sites.

2.5.2 Re-suspension of siRNA

The siRNA oligonucleotides were purchased from Dharmacon (Thermo Scientific) and were re-suspended as recommended by the manufacturer's protocol. All siRNA oligonucleotides were delivered in a dry powder form and re-suspended in a siRNA resuspension buffer provided by the manufacturer (Table 2.5).

Table 2.5 Summary of controls in RNA Inhibition experiments

Control Type	**Function**	**Product Used**
Positive Control	Optimizes and monitors efficiency of siRNA delivery into cells	ON-TARGET GAPDH Control Pool (Silencing GAPDH)
Negative Control	Distinguish between sequence-specific silencing to non-specific effect	None-Targeting (Scrambled RNA)
Untreated Control	Determine the base level of gene expression, as well as viability and phenotype	Cells cultured without any siRNA treatment

All siRNAs were centrifuged in a tube to collect the siRNA pellet at the bottom. According to the amount of siRNA, all the siRNA stock was diluted to a final concentration of 5μM/μl in 5x siRNA re-suspension buffer (Dharmacon), containing 20mMKCl, 6mM HEPES-pH 7.5, and 0.2 mM MgCl2, diluted down to a 1x siRNA buffer with RNase free water (Dharmacon). A total of 1000 μl of 1x siRNA buffer was added to

5nmol siRNA tube to give a final concentration of 5µm/µl. The solution was resuspended with a pipette three to five times to avoid any bubbles. The solution was left on an orbital shaker set at 200rpm/minute for 30 minutes at RT. Then the solution was briefly centrifuged and the SiRNA concentration was verified using the spectrophotometer NanoDrop 2000C (Thermo Fisher Scientific). (Table 2.6) summarizes the purity, quality, and total concentration of all siRNAs used in our experiments.

Table 2.6 Summary of short interfering RNA used in RNAi experiments

siRNA	**Company**	**Stock quantity concentration**	**Working Quantity**	**A260/280 (>2.0 is pure)**
GAPDH	Dharmacon	5 µM	5 nM	2.19
Non-Target (Scrambled)	Dharmacon	5 µM	5 nM	2.29
DKC1	Dharmacon	5 µM	5 nM	2.19

2.5.3 Optimisation and RNAi procedure

We optimised the DKC1 primers (Table 2.3) at three different concentrations: 5pmol, 10pmol and 20pmol. We found 10pmol to be the optimal concentration for effective amplification as illustrated in figure 2.4. Figure 2.5 shows a dissociation curve with clear amplification products without non-specific amplification for DKC1 primers.

For the RNAi protocol we used ON-TARGETplus SMARTpool siRNA oligonucleotides from Thermo Scientific Dharmocon. SMARTpool technology that combines a cocktail of four siRNAs to mimic the natural silencing pathway, as it provides high specificity for

reduced off-targets and it is efficient for silencing. Furthermore, the SMARTpool reagents reduce false negative results by targeting four different mRNA regions at once. Details of four siRNAs oligonucleotides within the SMART Pool specific for DKC1 gene are listed in Table 2.7.

Table 2.7 - All four sequences of siRNA used in knock-down of DKC1 gene

Dharmacon Smart Pool siRNA	Target Sequence
Human DKC1 Sequence 1	CAAGGUGACUGGUUGUUUA
Human DKC1 Sequence 2	GCAGGUAGUUGCCGAAGCA
Human DKC1 Sequence 3	UCUCAUAAACGGCUGGUUA
Human DKC1 Sequence 4	GGACAGGUUUCAUUAAUCU

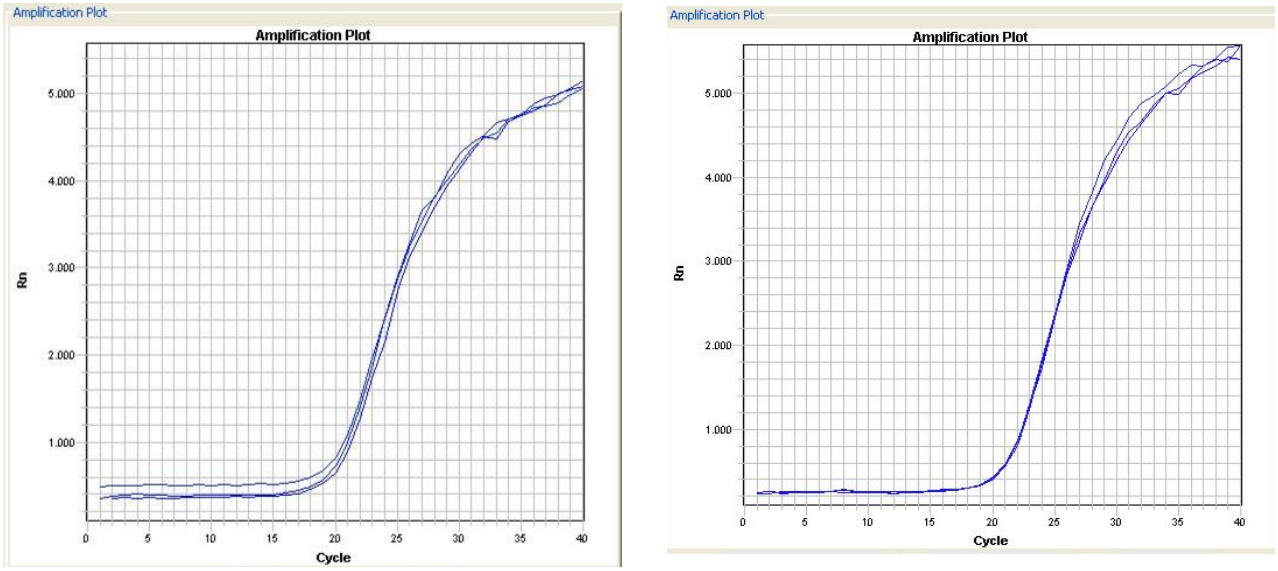

Figure 2.4) Amplification curve for DKC1 primers at concentration 10mM using a) Hela and b) U20S cell line

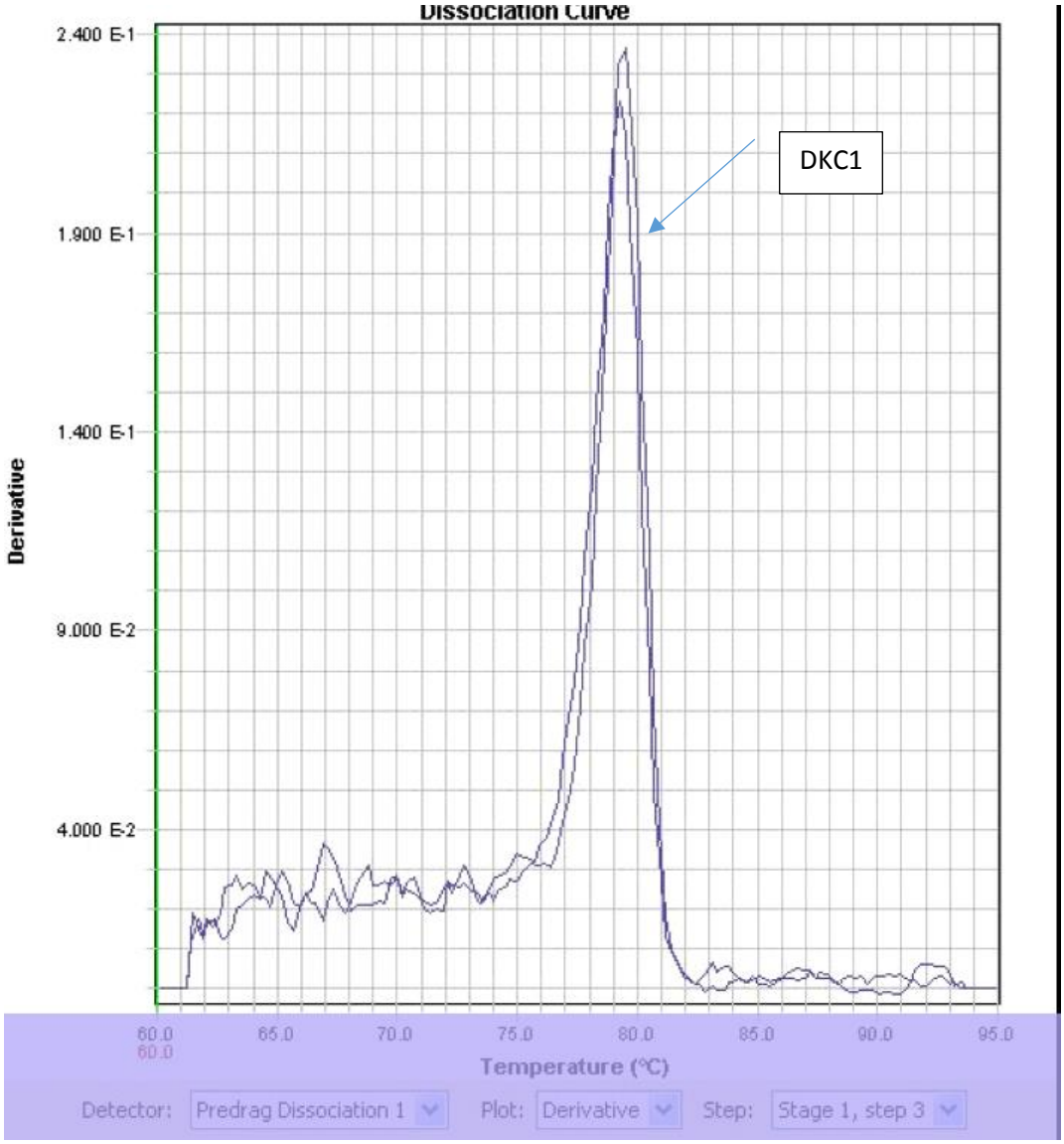

Figure 2.5) Dissociation curve analysis confirms only one amplification product without any non-specific amplification or primer dimer.

2.5.4 siRNA Transfection using DharmaFECT

It was required to have the final siRNA concentration at 25nM with the volume of 2ml of transfection medium in order to transfect the cells. So firstly, we diluted siRNA with DharmaFECT transfection reagent and with serum-free medium in separate tubes:

Tube 1: 10ul of 5um siRNA + 190ul of Serum-free Medium

Tube 2: 4ul of DharmaFECT + 196ul of Serum-free Medium

(DharmaFECT has to be optimized according to cell line + cell density easy to transfect cells + lower cell density require lower amount of DharmaFECT reagent).

Both tubes were incubated for 5 minutes at room temperature. Contents of tube 1 were added into tube 2, giving a total volume 400ul and incubated for 20 minutes at room temperature. We then added 1600ul of antibiotic-free complete medium to the transfected medium giving the final volume 2000ul and final siRNA concentration at 25nM. Finally, culture medium was removed from T25 flask and 2ml of Transfection medium was added to the flask. Cells were incubated at 37^{o}C for 24hrs and then the transfected medium removed and replaced with complete medium. mRNA (or protein) was extracted i.e. after 48 hours post transfection.

2.5.5 Procedure

U2OS, Hela and Fibroblast adherent cells were seeded in T25 flasks. A total of 400,000 cells were added to each flask containing 5ml medium. Adherent cells were seeded for 24 hours pre- siRNA addition. After 24 hours, the transfected medium was replaced with fresh medium. Cells were harvested 48 hrs, 72hrs, 96hrs and 7 days after treatment. This was followed by RNA extraction, cDNA synthesis and knockdown measurement using real-time qRT –PCR, or protein extraction for western blot analysis. When DKC1 expression was at its lowest level, extensive analysis of H2AX, TIF and MN assay was performed. The schematic below (Figure 2.6) represent the exact experimental procedure used in all siRNA experiments.

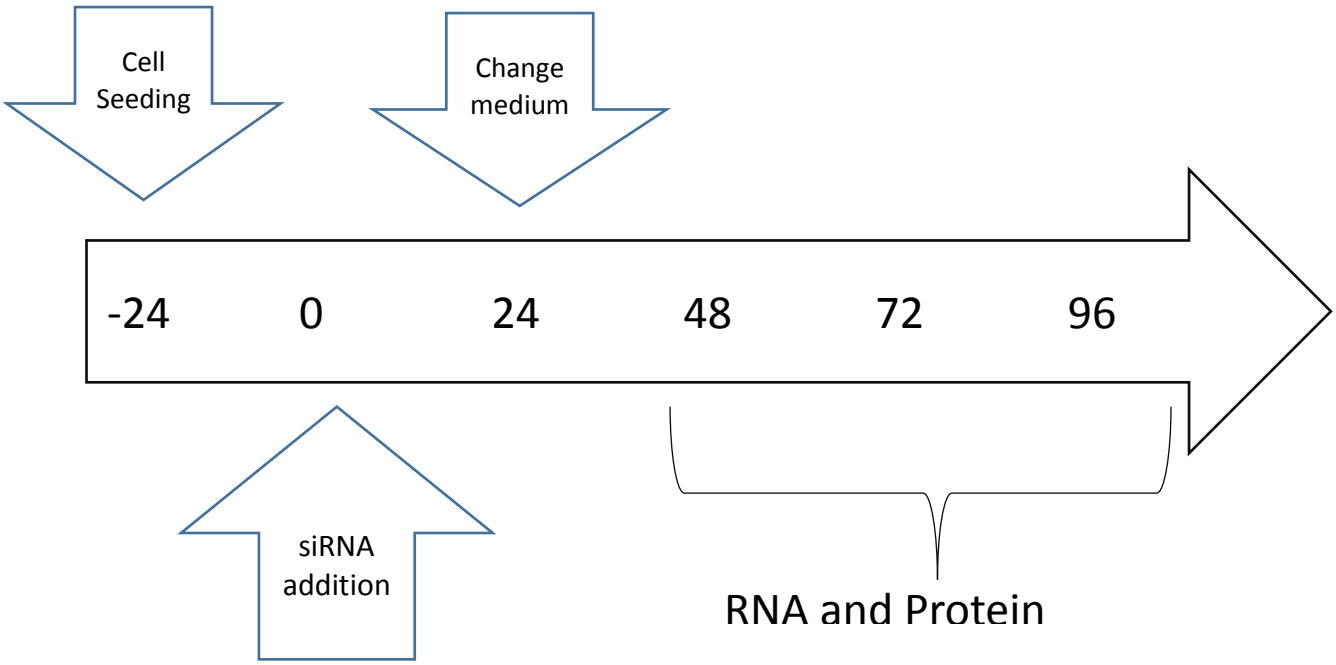

Figure 2.6 Summary of experimental plan. The long line represents time in hours.

2.6 Western blot

Western blot is a technique used to specifically detect and quantify protein from a tissue or cell samples. It uses gel electrophoresis to separate proteins according to size and mobility. Proteins are then transferred to a Polyvinylidene Fluoride (PVDF) membrane in a wet blot conditions. An appropriate primary antibody is used to detect a specific target. Enhanced Chemiluminescent dye is used to detect the Horseradish peroxidase (HRP) conjugated secondary antibody that is bound to the specific primary antibody and the protein of interest is detected on an X-ray film.

2.6.1 Protein sample preparation

Cells were grown to 80-90 percent confluence and the plate was rinsed six times with cold PBS. All the excess liquid was removed and 200µl of RIPA buffer (Radioimmunoprecipitation assay buffer) and 10µl of 25x protease inhibitor were added for at least 5 minutes onto the plate. Samples were thawed and mechanically sheared ten times using a 1ml syringe and a 23g needle. Samples were collected into Eppendorf tubes and spun at 13,000rpm for 15 minutes. The supernatant was aliquoted and transferred to clean Eppendorf tubes and stored at -20°C.

2.6.2 Protein Quantification

Each protein sample was quantified using a RC DC-protein assay (Biorad). This is a kit that comes with reagent A (contain alkaline copper tartrate solution for colorimetric assays), reagent B (contain a dilute folin reagent for colorimetric assays), reagent S (Surfactant solution for colorimetric assay), and reagent I and reagent II (reducing agents) This assay was used since it was compatible with reagents in the sample buffer and had a high concentration of SDS and a strong reducing agent such as beta-mercaptoethanol. The assay was performed according to manufacturer's instructions. In short, a serial dilution of 0.2 mg/ml – 1.6mg/ml of protein standard was made using bovine serum albumin (BSA). This was used to construct a standard curve where all unknown sample protein concentrations were measured against the standard curve. A total of 125 µl of reagent I was added to 25µl of each protein standard and protein sample vortexed and left for one minute. A total of 125 µl of reagent II was added to the sample tube vortexed briefly and centrifuged at 15,000xg (13,000rpm) for five minutes at room temperature. The supernatant was discarded by tipping it on to a dry paper

tissue. 127µl of reagent A', made earlier by 5µl of DC reagent S to 250µl of DC reagent A, was added to the tube and left for five minutes after a brief vortexing. It normally takes longer than five minutes for all the proteins to dissolve completely, as some surface membrane proteins are insoluble and difficult to dissolve. With a regular vortexing for 15 minutes all proteins were dissolved. At this point 1ml of DC reagent B was added to the tube, vortexed, and left for 15 minutes to incubate at room temperature. After 15 minutes absorbance was read at 595nm wavelength using Nano drop. The absorbance of protein standard was recorded first and a standard curve of protein concentration in mg/ml against absorbance was constructed (Figure 2.7). Absorbance of each protein sample was read using the spectrophotometer and the concentration of each protein sample was calculated from the standard curve.

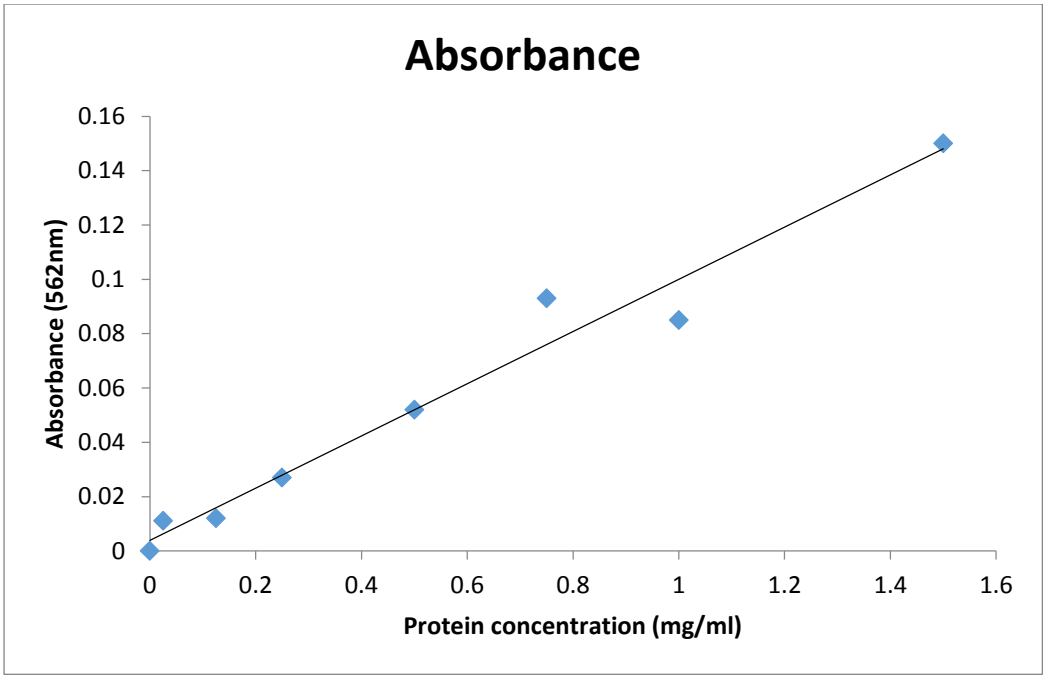

Figure 2.7 Standard curve used in protein quantification analysis. The concentration of each protein sample was calculated using the absorbance read from the spectrophotometer.

2.6.3 Making SDS-PAGE gel (Acrylamide gel)

Protein lysates were prepared from GM08399 cell line and the protein concentration determined using RC DC-protein assay as previously described. The following describes how we made the SDS –Page GEL.

2.6.3.1. Preparing Resolving Gel Tris-glycine SDS-Polyacrylamide Gel Electrophoresis

The percentage of the gel is dependent of the size of protein. The larger the protein size the lower the percentage of polyacrylamide gel. The protein size for dyskerin is 57kDa, so the percentage of the gel should be 12%.

The following ingredients were required:

dH_20	10.6ml
30% Acrylamide mix	4.0ml
1.5 m Tris (pH 8.8)	2.5ml
10% SDS	0.1ML
10% ammonium persulfate	0.1ml
Temed	0.004ml

Temed should always be added last.

2.6.3.2. Stacking Gel for Tris-glycine SDS-Polyacrylamide Gel Electrophoresis.

dH20	1.4ml
30% Acrylamide mix	0.33ml
1.5 m Tris (pH 6.8)	0.25ml
10% SDS	0.02ml
10% ammonium persulfate	0.02ml
Temed	0.002ml

For stacking gel, Temed was not added until the resolving gel was set.

The resolving gel was added to the glass stand was left to set. The stacking gel was added afterwards and combs were put in and left to set. It was then placed in the tank and fill with running buffer.

2.6.4 Preparing protein samples

We worked out the amount protein sample we needed to load by the following method. We used 10ug:

10ug/ (protein concentration* x20) = x ul
X = the sample to load
*refer to figure 2.7

We added the same amount of 4x laemmli to the protein sample (x ul).

So for example, to add 7ul of protein sample, 7ul of 4x laemmli was added.

4x Laemmli (pH 6.8) is made up from the following

- 8 % SDS
- 20 % Beta-mercaptoethanol.
- 40% glycerol
- 0.008 bromophenol blue
- 0.25 Tris HCL.

Beta-mercaptoethanol was added fresh in the laemmli.

The samples were added in eppendorf tubes, centrifuged and holes were made on top of the tubes. They were heated for 5 minutes for 95^{o}C.

Sample were then loaded onto the gel that was already inside the tank. Protein marker was added. Power pack was attached, with red to red and blue to blue, and voltage @ 100 volts. When the protein samples were evenly located on the gel, the power was switched to 150 Volts for approximately 45 minutes. The samples were checked regularly to prevent running off the samples.

2.6.5 Blotting and transfer

Once proteins were separated in the gel based on their size and mobility (heavier proteins move slower and hence were at the top of the gel, whereas smaller proteins move faster and were found near the bottom of the gel), proteins were transferred onto a blotting paper. Polyvinylidine fluoride (PVDF) is a non-reactive membrane that has a non-specific affinity to amino acids. PVDF was activated by soaking in 100 percent methanol for 10 seconds. A sandwich of filter pad, 3mm filter paper, activated PVDF membrane, gel, 3mm filter paper, and filter pad was assembled according to the manufacturer's protocol. A small magnetic stirrer was placed in the tank, topped with 1x transfer buffer made with 11.25g (w/v) of glycine, 2.42g (w/v) of tris base, 200ml (v/v) of methanol and distilled water to 1 litre. The blotter was placed inside the tank and the tank was run at 60V for 45 minutes on a magnetic stirrer to create an even distribution of the electrolysis. An ice pack was also placed inside the tank to prevent overheating of the buffer solution.

2.6.6 Blocking and antibody incubation

Once the transfer of protein from gel onto the PVDF membrane was complete the proteins were blocked with 5% blocking reagent containing 5g (w/v) of semi-skimmed milk (Marvel) in 100ml of Tris buffer saline-Tween (TBST) made with 16g (w/v) of NaCl, 0.2g (w/v) KCl, 3g (w/v) of Tris base, 0.1% (v/v) Tween-20 added to 800ml of distilled water adjusted pH to 7.6, and distilled water added to 1 litre. The membrane was left in 30ml of blocking solution for about one hour on a shaker at room temperature. The milk mixture blocks the unspecific binding of an antibody with the

membrane. After one hour of blocking, the membrane was rinsed with TSBT and the primary antibody was added. The primary antibody was diluted down according to the manufacturer's recommendation and was further optimized by the user. Below shows all antibodies used in our experiment with optimized dilution ranges.

DKC1 Primary Abcam Rabbit Polyclonal 1:1000
DKC1 Secondary DAKO Rabbit Polyclonal 1:2000
Beta-actin Primary SIGMA Rabbit Polyclonal 1:1000
Beta-actin Secondary DAKO Rabbit Polyclonal 1:2000

Primary antibodies were diluted in one in five dilutions in 5% blocking buffer in 1x TBST and added to the membrane overnight on a shaker set at medium pace (200rpm/minute) at 4°C. The following day the membrane was washed four times with 1x TBST for 15 minutes each and incubated with a secondary antibody diluted in one in five dilutions of 5 % blocking buffer on a shaker at RT for a minimum of one hour.

2.6.7 Protein detection with chemiluminescence

After 1 hour incubation with a secondary antibody the membrane was washed four times in 1x TBST for 15 minutes. Meanwhile ECL plus (Enhanced chemiluminescence) kit (GE Healthcare) was taken out of the fridge and left at RT to warm up. The amount of ECL required for detection was based on the size of the membrane and was recommended by the manufacturer to be of a final volume of 0.125m/cm2 of membrane. The manufacturer's protocol was consulted for the exact mixture of chemical A and chemical B. Chemical A is a detection reagent, a membrane probed with

antibody-enzyme conjugated (HRP, a stable peroxidase) and chemical B is a luminol solution. When chemical A and B mixed together, HRP catalyses the oxidation of luminol at alkaline conditions. As a rule of thumb, 2ml of reagent A was mixed with 50µl of reagent B. That is 1 part of reagent A mixed with 40 parts of reagent B. The ECL mixture was added onto the membrane and covered with Saran wrap for 5 minutes in a dark room. The excess of the ECL was tipped off onto a paper towel, wrapped in the membrane facing down onto a piece of clean Saran wrap and placed in an x-ray cassette. Unexposed ECL plus hyperfilm (GE healthcare) was put on top of the membrane and the cassette closed and left for exposure for 5 minutes. The x-ray films were developed using an automatic machine (Xograph). The exposure time was assessed accordingly depending on the size of the exposed bands. If the protein bands were faint and could not be visualized then a second film was exposed for a longer period. The ECL chemiluminescence was active for at least one hour.

2.7 Statistical Analysis

Basic statistical analysis such as descriptive measurements and graphical display were done using Microsoft Excel 2013 software. For chapter 3, 4 and 5, t-tests were done at 95%, 99% and 99.9% confidences where alpha was set at 0.05, 0.01 and 0.001 respectively.

For chapter 4, Anova was done because we used two control samples for our test samples, and t-test only allows comparison between two samples. In this chapter, we needed to compare three samples (two control and one test) and Anova allows comparison of two or more samples, hence we used the Anova software available on Data analysis in Microsoft Excel 2013 to compare the significance between the test sample and the two control samples. Alpha was set at 0.05, 0.01 and 0.001 for 95%, 99% and 99,9% confidences, respectively

Chapter 3 DNA Damage Response in DC Fibroblast cell lines

3.1 Introduction

Telomeres are specialized structures that cap the ends of chromosomes to help protect them from being recognised by DNA repair activities as sites of damage. Genomic stability is also ensured as telomeres prevent end-to-end chromosome fusion. The telomere ends as a single stranded, G-rich overhang able to form a t-loop, in which the overhang invades the telomeric double helix, remodelling the DNA into a circle known as the T-loop (Calado and Young 2008; Huffman et al 2000; Oeseburg et al 2010).

With each mitotic cycle, telomeres become shorter to a point that the T-loop structure is lost and the DNA damage response activated, resulting in cell cycle arrest and senescence (Diotti 2011; de lange 2005; Nigam 2011; d'Adda di Fagagna et al 2003) or cell death (Bessler et al., 2010; Calado and Young 2008). A few base pairs (50–200 bp) of telomeric DNA sequence are lost with each cell division (Callen 2004).

Shelterin, a protein complex, designed to protect the chromosomal ends from erosion and end-to-end fusion represses the DNA damage response pathway(de lange 2005). However, telomere shortening will result in destabilization of the T-loop as the platform for the shelterin complex and it will cause an inability to recruit the proteins of the shelterin complex (Oeseburg et al 2010). This view is supported by observations that the loss of function of Shelterin proteins can lead to telomere dysfunction and activating DNA damage response pathway. For example loss TRF2, a shelterin protein leads to telomeric fusion (Karlseder et al 2002; Smogorzewska et al., 2000; de Lange 2002). Furthermore, it has been found that some of the NHEJ proteins are present at telomeres and interact with the shelterin complex. It has been shown in a series of mouse knock-out experiments that deficiencies in DNA-PKcs, Ku70/80 and Artemis show a significant

increase in the amount of chromosomal aberrations which includes telomere end-to-end fusion (Rooney et al 2003; Yasaei 2010) This suggests that ku70, ku80,DNA-Pkcs and Artemis are needed for the end-capping function of telomeres (Bailey et al 1999). This also suggests that defects in the DNA damage response pathway other than telomere shortening can lead to dysfunctional telomere maintenance. Collectively, these observations revealed a potential functional link between DNA damage response and telomere maintenance. The support for this functional link comes from observations that DNA damage response factors other than NHEJ proteins have the potential to affect telomere maintenance (reviewed in Slijepcevic 2006). Another way to examine the existence of this functional link is to probe whether factors involved exclusively in telomere maintenance such as the enzyme telomerase for example, will affect DNA damage response mechanisms. The main aim of this thesis is to exploit the human genetic diseases, DC, a typical disease of dysfunctional telomeres mainly due to defects in telomerase components with a view to testing the efficiency of DNA damage response in affected cells.

DC is a bone marrow disorder caused by telomere dysfunction. Mutations directly implicated in causing DC have been identified in the following genes: *DKC1, TERC, TERT, NOP10, NHP2, TINF2* and *TCAB1* (Du et al 2008; Oeseburg et al 2010; Anderson et al 2012). All of these genes are implicated in telomere function (Kirwan 2009). As telomerase is required for functioning of stem cells highly proliferative tissues including skin and bone marrow, will be affected in DC patients generally recognized by their short telomeres (Mitchell et al 1999). DC patients have the following symptoms: short stature, hypogonadism, infertility, bone marrow failure, skin defects, hematopoietic defects and premature aging (Calado et al 2008). The most common form

of DC is the so called X linked form caused by the mutations in the *DKC1* gene encoding the dyskerin protein (Parry et al 2011). Previous studies have shown that although DC fibroblasts cell lines do show more DNA damage than normal fibroblasts cell lines, after treatment with DNA damage agents (i.e. etoposide), the difference was not statistically significant (Kirwan et al 2011). Thus the conclusion was that the response of DC cells to DNA damage is normal.

However, a careful examination of literature reveals that this conclusion may not be justified. A simple cytogenetic study published almost 25 years ago revealed sensitivity of DC cells to ionizing radiation relative to normal cells (DeBauche et al 1990). Given that the cytogenetic test used in the study was designed to reveal a faulty DNA repair kinetics that may lead to radiosensitivity, Kirwan et al (2011) should have carried out DNA repair kinetic analysis in DC cells to substantiate their conclusion.

In contrast, work done on cells derived from the mouse DC model has suggested that Dkc1 defective murine cells show an abnormal DNA damage response after exposure to etoposide (Gu et al 2008) thus contradicting the conclusion by Kirwan et al (2011).

Therefore, we decided to examine the DNA damage response in a primary fibroblast cell lines GM01774 (Homozygous, DKC1 -/-) obtained from a patient with a 3 bp deletion of nucleotides 201_203 in the *DKC1* gene (201_203delCTT) (Knight et al. 1999). In addition, we used another primary fibroblast cell line from a patient not clinically affected but shown to be a DC carrier (DKC1 +/-). A primary fibroblast cell line from a normal individual (GM08399) was used as a control.

3.2 Assessment of DNA damage using γH2AX and TIF assay

DNA damage in mammalian cells can be detected reliably using antibody against the phosphorylated form of histone H2AX (γH2AX). H2AX becomes phosphorylated whenever there is damage in DNA and it is considered one of the most reliable DNA damage markers (Rogakou et al 1997). When telomeres become dysfunctional the chromosome 'capping' function is no longer provided, with the possible collapse of the T-loop structure. Since telomere dysfunction leads to activation of DNA damage response factors as it is treated as a pathological DSB by cell DNA damage apparatus, the protocol must be designed to allow the combination of markers that detect DSB and telomeres. Thus, DNA damage markers, such as H2AX, can be used to detect DNA damage directly at telomeres by combining it with telomere-specific antibodies using the assay called Telomere dysfunction Induced Foci (TIF) assay (Takai et al 2003). Instead of antibodies specific to telomeric proteins we used Peptide Nucleic Acid (PNA) telomeric sequence (with a cy-3 fluorescence label) in combination with the DNA damage marker H2AX to detect DNA damage at telomeres.

3.2.1 Dose response curve

We reasoned that two types of experiments should be performed to clarify the uncertainty caused by Kirwan et al (2011). First, a classical dose response curve for each cell lines should be generated after exposure to different doses of ionizing radiation (IR) as the source of DNA damage. Second, given that Kirwan et al (2011) has not carried out DNA repair kinetics analysis in DC cells we thought that this kind of analysis is necessary in light of observations by Gu et al (2008).

Therefore, we started with generating dose response curves for each cell line. We decided to irradiate the cell lines with the following doses of gamma rays: 0.25 Gy, 0.5 Gy and 1.0 Gy. Each analysis was preformed three times and each time a total of 100 cells were analysed for the presence of DNA damage signal due to H2AX. Furthermore, in order to assess DNA damage at telomeres we carried out the TIF assay in parallel.

Representative examples of DC cells stained with the H2AX antibody, the telomeric PNA probe and combination of the two are shown in Fig 3.1.

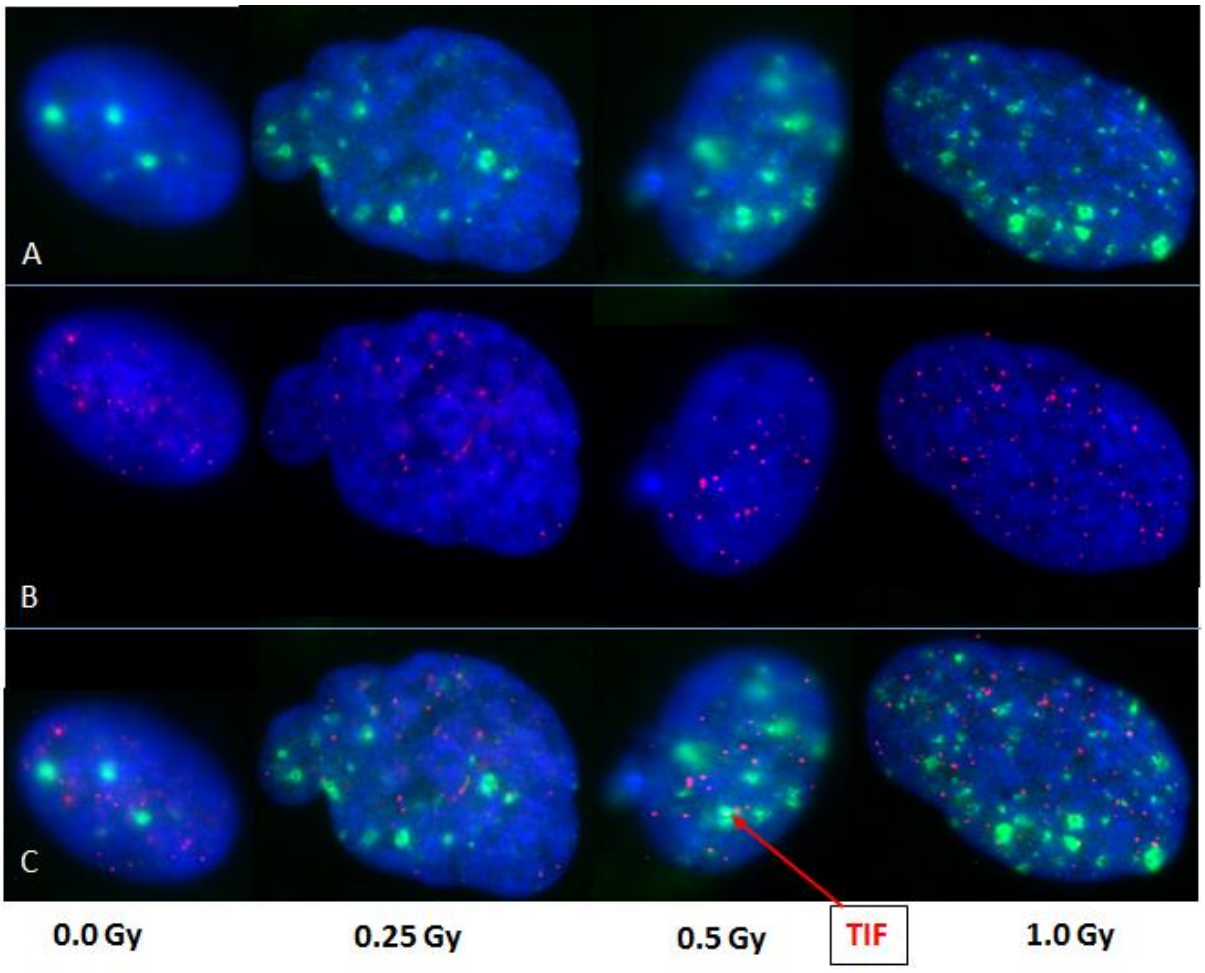

Figure 3.1) Images obtained from nuclei of the DC fibroblast cell line, after irradiation with gamma rays at 0.0Gy, 0.25Gy, 0.5Gy and 1.0Gy doses A) Detection of DNA damage γH2AX foci. B) Telomeres were detected by $(AATCCC)_3$ probe labelled with Cy-3 (red) C) Colocalization with γH2AX and telomeres represent a TIF (merged), visible as yellow spots. The nucleus was counterstained with Dapi. Examples are from the GM01774 cell line. Increase in dosage shows the increase in γH2AX foci.

Our analysis revealed that GM08399 and GM01787 cell lines had a lower spontaneous frequency of γH2AX foci than the GM01774 cell line (Fig 3.2). Furthermore, a significant difference was observed at 0.25Gy for GM1787 (heterozygous, DKC1 +/-) and GM1774 (homozygous, DKC1 -/-) cell lines relative to the control cell line (Fig 3.2). However, at 0.5 Gy and 1.0 Gy the significance was lost for the heterozygous cell line but not for homozygous cell line in comparison to the normal fibroblast cell line (Fig 3.2). Therefore, these results indicate that the homozygous DC cell line shows sensitivity to IR suggesting that the DNA damage response could be defective in DC cells.

We have also analysed DNA damage response at telomeres using the TIF assay (figure 3.3). Fig 3.3 is almost exact replica of the Fig 3.2 suggesting a similar response of used cell lines to DNA damage at telomeres. GM08399 and GM01787 cell lines showed a lower spontaneous frequency of TIF foci compared to the GM01774 cell line thus supporting the notion that DC is the disease of dysfunctional telomeres (Knight et al. 1999). Taken together these results show sensitivity of DC cells to DNA damage in contrast to Kirwan et al (2011).

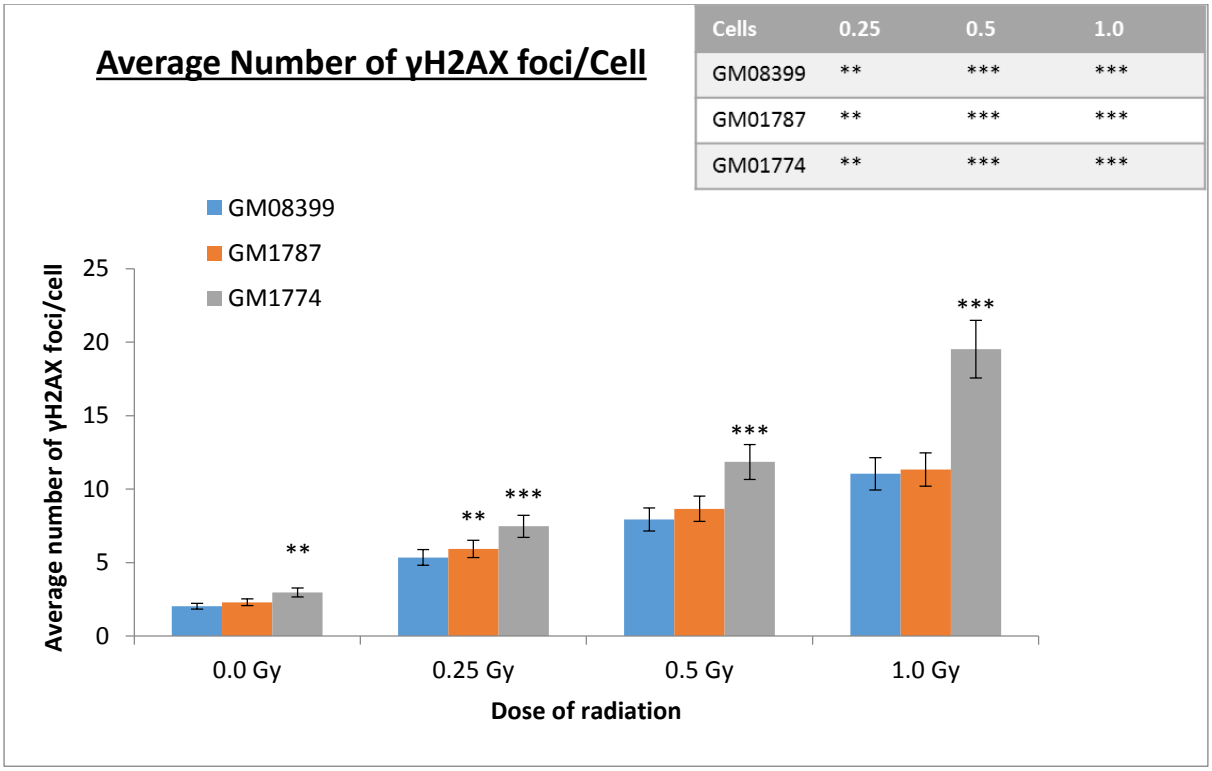

*Figure .3.2) Frequencies of γH2AX positive foci after exposure of cells to 0.0, 0.25, 0.5 and 1.0 Gy of gamma radiation. Error bars indicate SEM. Two types of statistical comparison were carried out. The inset shows comparison of DNA damage foci for each dose against unirradiated samples. Stars above bars indicate comparison between DC and control cell lines *P<0.05 **P<0.01, ***P<0.001.*

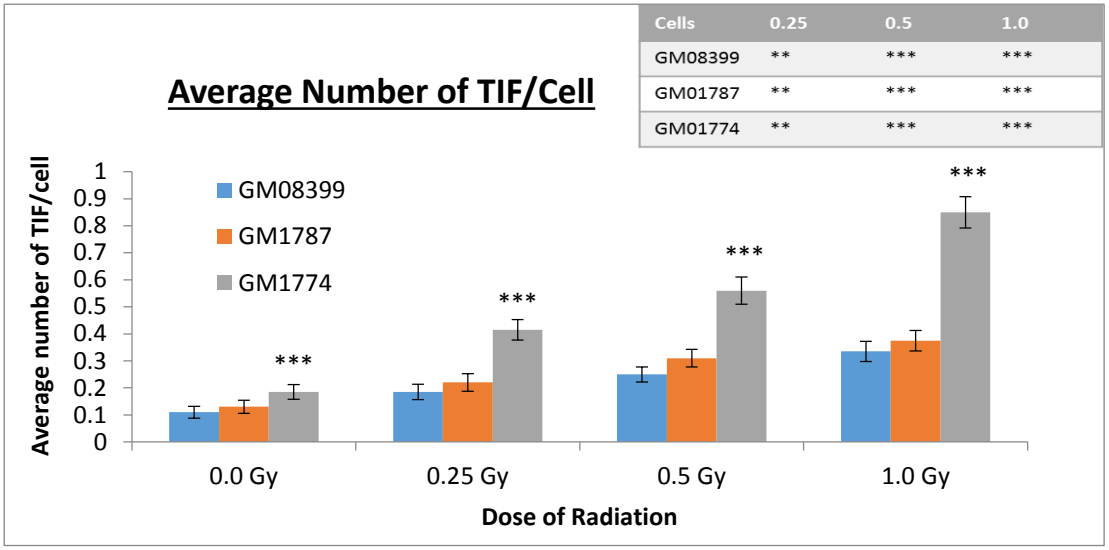

*Figure 3.3) Frequencies of TIF in 0.0, 0.25, 0.5 and 1.0 Gy doses of gamma radiation for DC cell lines with control cell line (GM08399). Error Bars indicate SEM. Two types of statistical comparison were carried out. The inset shows comparison of TIF foci for each dose against unirradiated samples. Stars above bars indicate comparison between DC and control cell lines. *P<0.05, **P<0.01, ***P<0.001 versus control.*

3.2.2 Repair kinetics curve

To substantiate further the potentially defective DNA damage response of DC cells we analysed repair kinetics of DSBs. IR induced predominantly DSBs (Rogakou et al., 1997) which are effectively detected by H2AX (Rogakou et al 1997; Bonner et al 2008). We designed experiments in the standard way for this type of study (Bonner et al 2008). The dose of IR sufficient to induce a strong degree of damage is 1.0 Gy. Following exposure of cells to the dose of 1.0 Gy gamma rays we monitored DNA damage in all cell lines 30 min, 5 h, 24 h and 48 h after irradiation (Fig 3.5). In parallel, we carried out the TIF assay in all samples (Fig 3.6). Representative images showing staining of cells with H2AX antibody or telomeric PNA probe in kinetics experiments are shown in Fig 3.4.

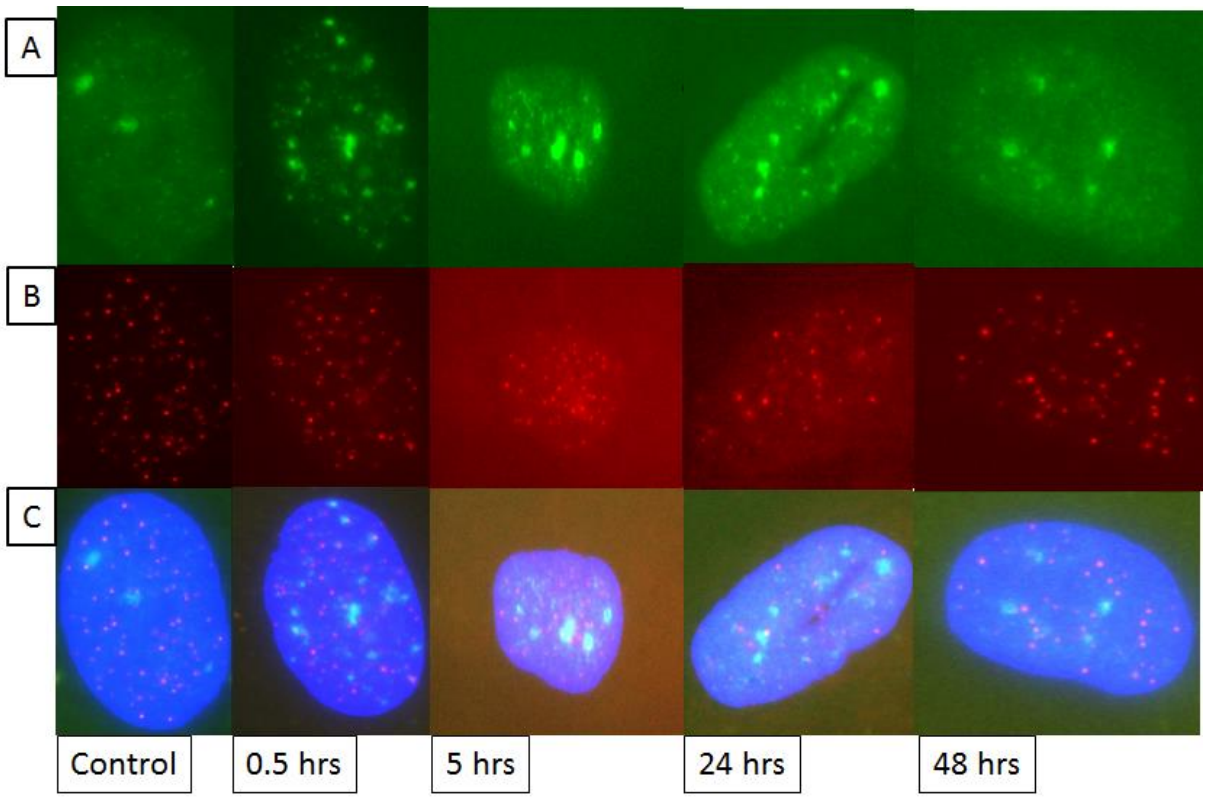

Figure 3.4) Images obtained from nuclei of the DC fibroblast cell line, after irradiation with gamma rays at 1.0Gy dose at different time points. A) Detection of DNA damage ɣH2AX foci B) Telomeres were detected by $(AATCCC)_3$ probe labelled with Cy-3 (red) C) Colocalization with γH2AX and telomeres represent a TIF (merged), visible as yellow spots. The nucleus was counterstained with Dapi. Examples are from the GM01774 cell line. The reduction of ɣH2AX foci is clearly evident.

Figure 3.5 illustrates the repair kinetics curve generated after staining of cells with the H2AX antibody. After 30 minutes, GM1774 and GM1787 cell lines exhibited significantly higher frequencies of ɣH2AX positive foci compared to the normal control cell line. However, after 5 hours the significance was lost for the GM1787 cell line although it was regained again at 24 hours. However, at 48 hours, DNA damage was repaired completely in both GM1787 and GMO8399 cell lines given the lack of statistically

significant difference relative to non-irradiated cells. However, the GM1774 cell line showed a significantly higher level of H2AX positive foci compared to control non-irradiated cells (Fig 3.5). Thus, the results indicate that the control cell line and the GM01787 cell line show normal DSB repair kinetics. By contrast the GM01774 cell line shows the residual DNA damage 48 h after irradiation suggesting that a slower repair rate relative to the other two cell lines, indicating a potential DNA damage response defect. This also supports results obtained in the case of dose response curve analysis.

Figure 3.6 shows the repair kinetics curve obtained after the TIF assay. It is interesting to note that GM1787 and GM1774 cell lines showed significantly higher frequencies of TIFs at all-time points relative to the control cell line (Fig 3.6). In all cases with the GM1774 cell line showed the highest frequencies of TIF foci (Fig 3.6). Therefore, this suggests that DNA damage at telomeres is more persistent in cells from DC patients and DC carriers relative to control cells. This observation is in line with the notion that dysfunctional *DKC1*, which eventually leads to telomere shortening and telomere loss of function, also causes dysfunctional DNA damage response.

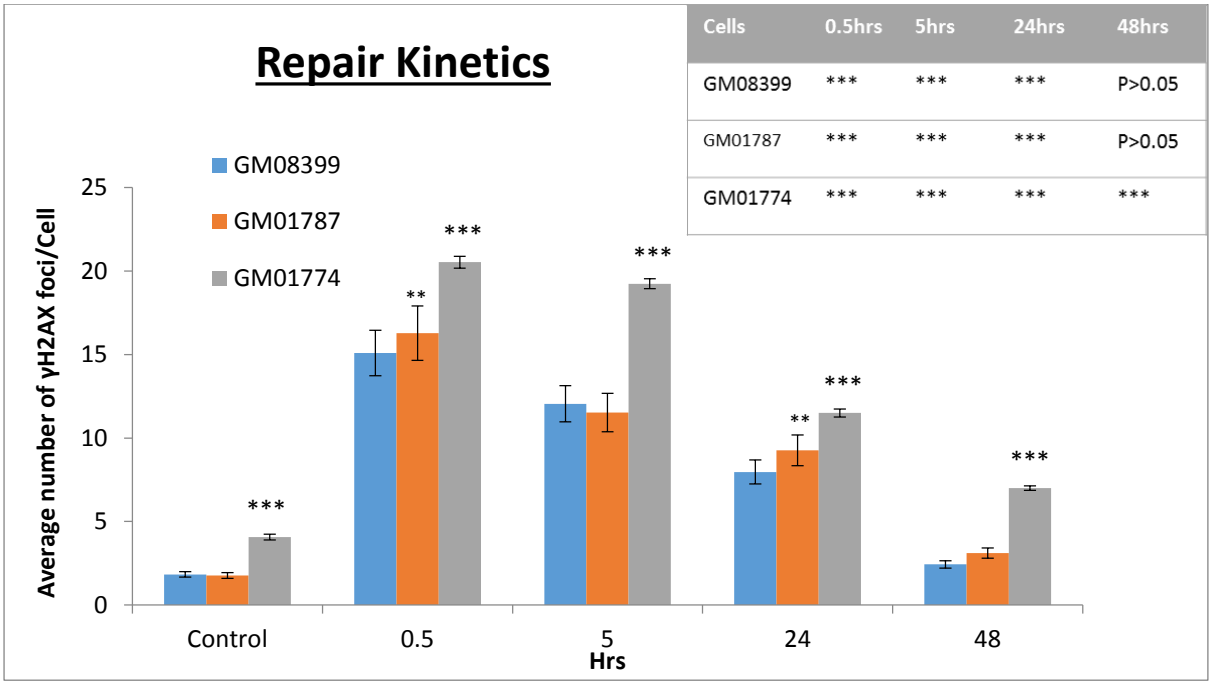

*Figure 3.5) Frequencies of γH2AX positive foci in untreated and 1.0 Gy doses of gamma radiation for DC cell lines with control cell line (GM08399). Error bars indicate SEM. Two types of statistical comparison were carried out. The inset shows comparison of DNA damage foci for each time point against unirradiated samples. Stars above bars indicate comparison between DC and control cell lines *P<0.05 **P<0.01 ***P<0.001 versus control.*

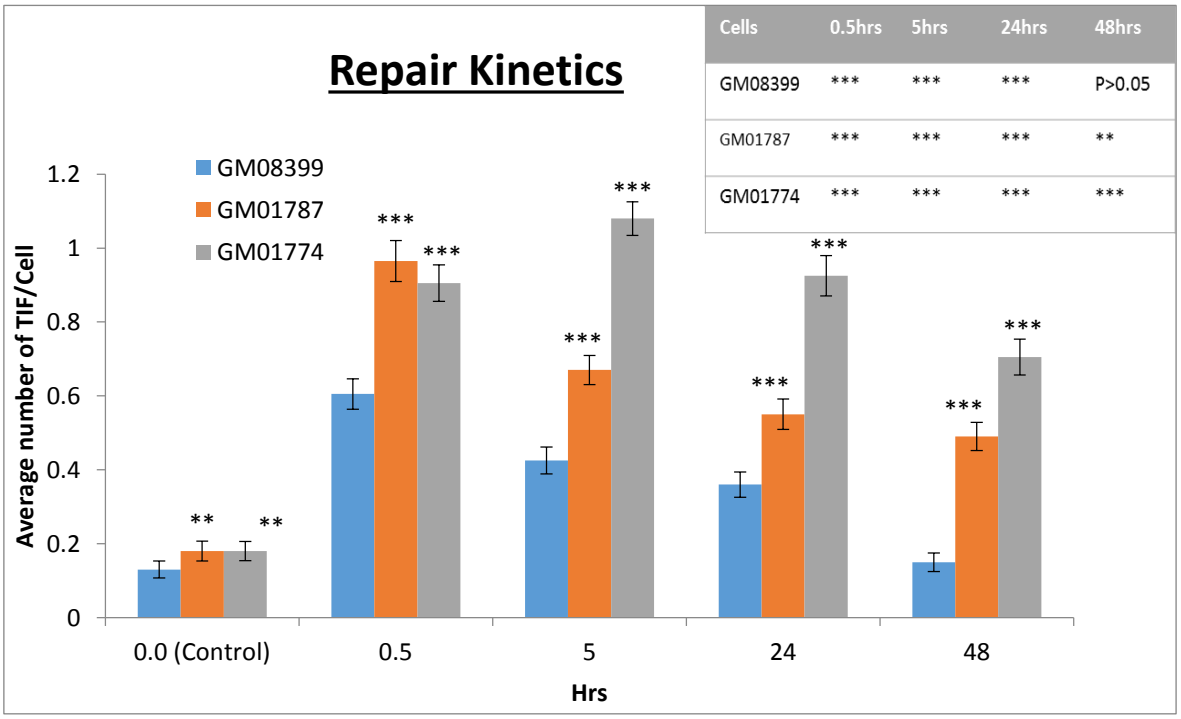

*Figure 3.6) Frequencies of TIF foci in untreated and 1.0 Gy doses of gamma radiation for DC cell lines with control cell line (GM08399). Two types of statistical comparison were carried out. The inset shows comparison of TIF foci for each time point against unirradiated samples. Stars above bars indicate comparison between DC and control cell lines *P<0.05 **P<0.01 ***P<0.001 versus control. Error bars indicate SEM.*

3.3 Chromosomal Aberrations in DC fibroblast cell line

The above observations are consistent with DNA damage response being defective in DC cells. In order to provide further evidence for this notion we thought that DNA damage response can be analysed at the cytogenetic level by investigating spontaneous and radiation induced chromosomal aberrations (CAs) in DC cells.

Double strands breaks (DSB) are the ultimate lesions for the formation of CAs which result from erroneous repair of breaks mainly by non-homologous end joining in G1 and S, or by homologous recombination in S and G2 stages of the cell cycle (Obe and Durante 2010). We started by analysing CAs in DC and control fibroblast cell line by Giemsa staining. However, DC cells are characterized by a poor growth potential. In order to obtain sufficient numbers of mitotic cells for CAs analysis a reasonable mitotic index is required. We only managed to obtain a small amount of mitotic cells in non-irradiated DC cells, a total of 15 well spread metaphases suitable for cytogenetic analysis (Table 3.1). We observed one dicentric chromosome in the DC fibroblast cell line (Figure 3.7). Exposure of cells to IR resulted in a cell cycle block and a poor mitotic index which precluded analysis of IR induced CAs. As a result of failure to analyse CAs we had to resort to alternative methods.

Table.3.1 Scoring of CA in fibroblast cell lines

Cell line	**CA**
GM08399	0
GM1787	0
GM1774	1 (Dicentric)

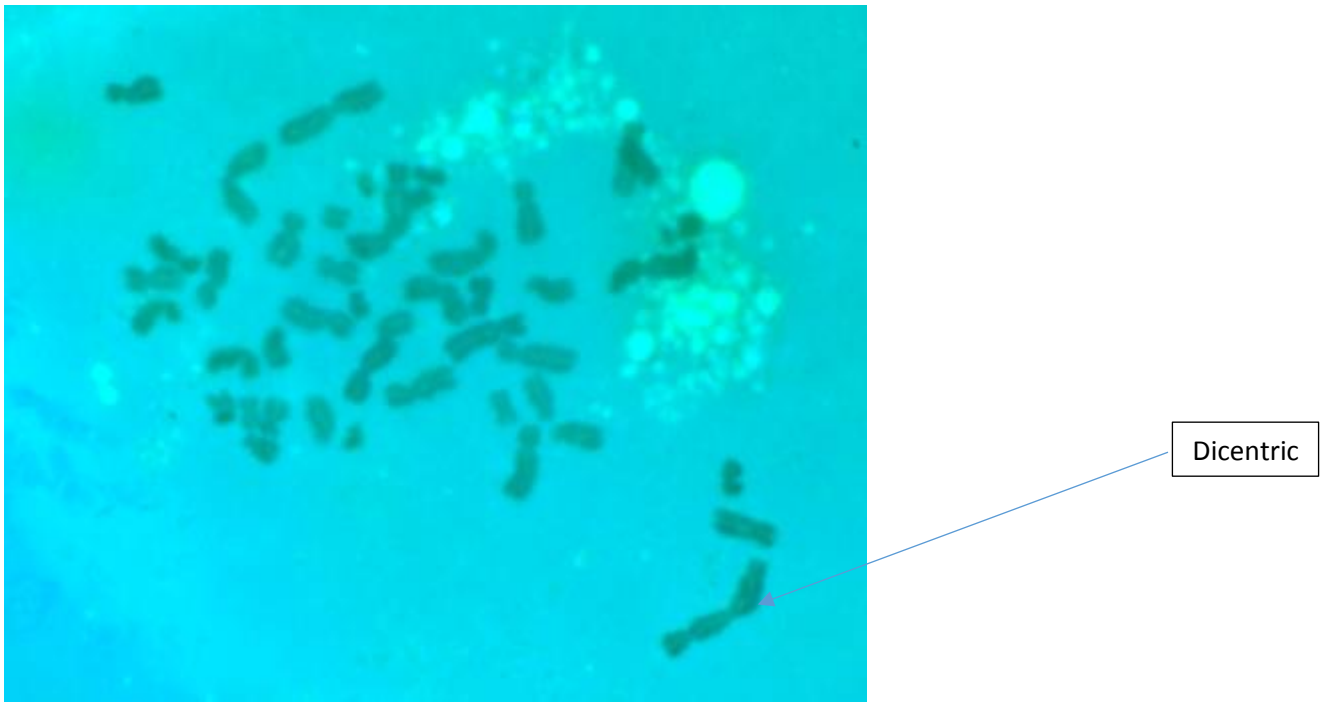

Figure 3.7. Chromosomal Abnormalities in GM01774 DC fibroblast cell line An example shows a metaphase spread with chromosomes stained with Giemsa from GM1774 with dicentric chromosome (arrowhead) as consequence of chromosome end-to-end fusions.

3.4 Micronuclei in normal and DC fibroblast cell lines

The method that is thought to be a surrogate for CAs analysis is the Cytochalasin B micronucleus tests. A micronucleus is formed during cell division when the nuclear envelope is reconstituted around chromosome fragments lacking centromere and/or lagging whole chromosome that is not incorporated into the main daughter nucleus (Gutierrez-Enriquez, 2003).

This assay involves detecting micronuclei, which can be chromosomal fragments or whole chromosomes that are not included in the daughter nuclei during division. Fenech and Morley (1985) developed the cytokinesis-block micronucleus (MN) method as a more precise measure of chromosome damage and it is used as an indication of genotoxicity and a sensitive indicator of in vivo radiation exposure (O'DriscoIll et al 1998) .

We first optimised the assay to establish the conditions for the use of micronuclei (MN) test to determine the level of chromosomal damage induced by IR exposure to fibroblast cell lines.

We used the protocol described by Gutierrez-Enriquez, 2003 which is essentially a modified version of the Fenech and Morely (1985) original protocol.

In order to compare the level of micronuclei in the three cell lines we decided to generate dose response curves for each cell line using the following doses of IR: 0.5 Gy, 1.0 Gy, 2.0 Gy and 4.0 Gy of gamma rays. Furthermore, we harvested cells 48 h after irradiation. Examples of images of the cells after the procedure designed to analyse

micronuclei are shown in figure 3.9. For each time point a total of 500 binucleated cells were analysed. The results of our analysis are presented in (Figure 3.8).

Our analysis reveals that GM08399 and GM01787 cell lines have a lower level of MN than GM01774 cell line. The basal level of MN is significantly higher in the GM1774 compared to the normal and the DC heterozygous cell line. This significance starts to increase at 2.0 Gy culminating at the dose of 4.0 Gy. Therefore, these results are consistent with the results presented in Figs 3.1 and 3.2 which suggest a defective DNA damage response in DC cells.

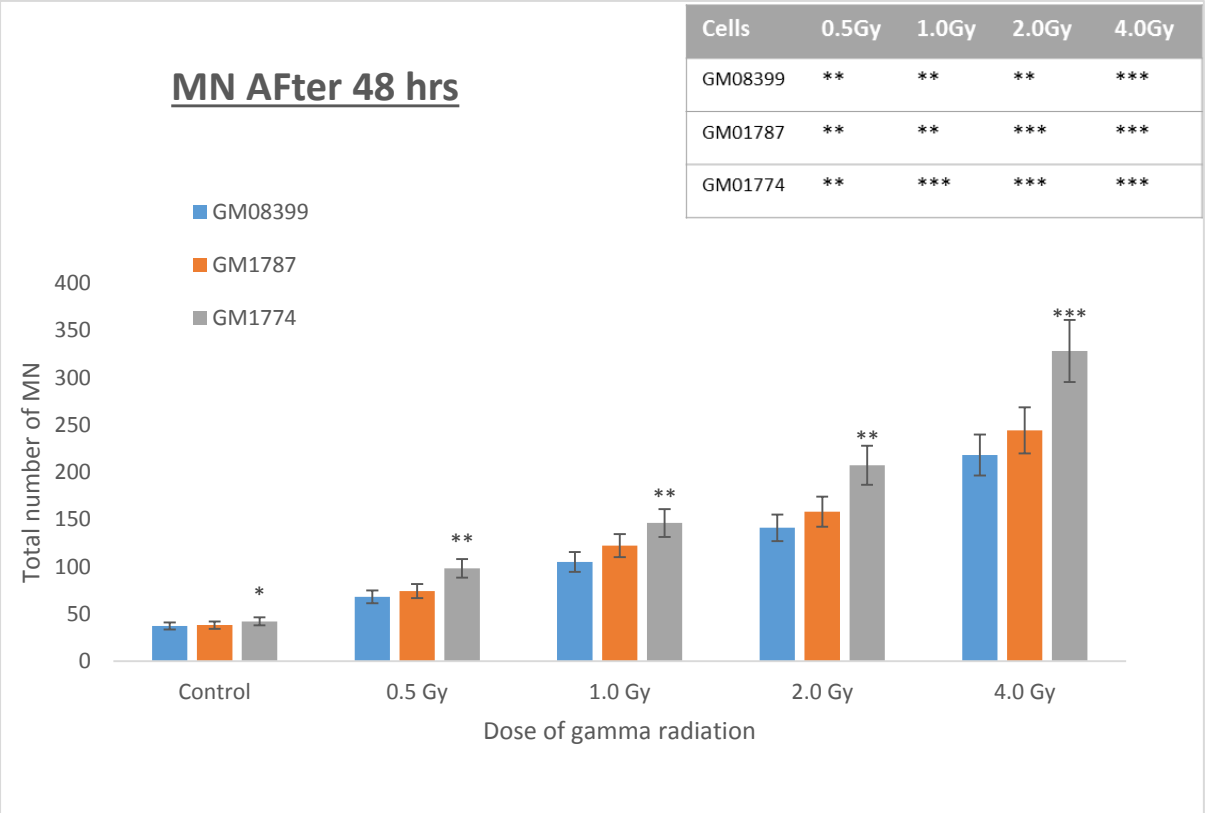

Cells	0.5Gy	1.0Gy	2.0Gy	4.0Gy
GM08399	**	**	**	***
GM01787	**	**	***	***
GM01774	**	***	***	***

*Figure.3.8) Frequencies of MN in 0.5 Gy, 1.0 Gy, 2.0 Gy and 4.0 Gy doses of gamma radiation for DC cell lines compared to control obtained after 48 hours. Two types of statistical comparison were carried out. The inset shows comparison of MN for each dose against unirradiated samples. Stars above bars indicate comparison between DC and control cell lines *P<0.05. **P<0.01 ***P<0.001 versus control. Error bars represent SEM*

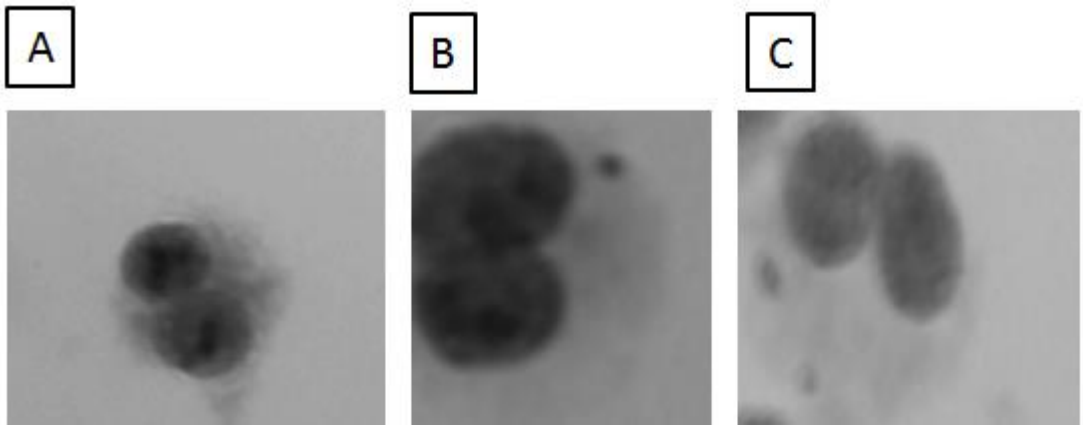

Figure.3.9) Images obtained from GM1774 (Homozygous) fibroblast cell line in the scoring of binucleated cells stained with Giesma. A) A normal binucleated cell after cytokinesis block MN assay. B&C) Examples of Mirconuclei scored in the assay.

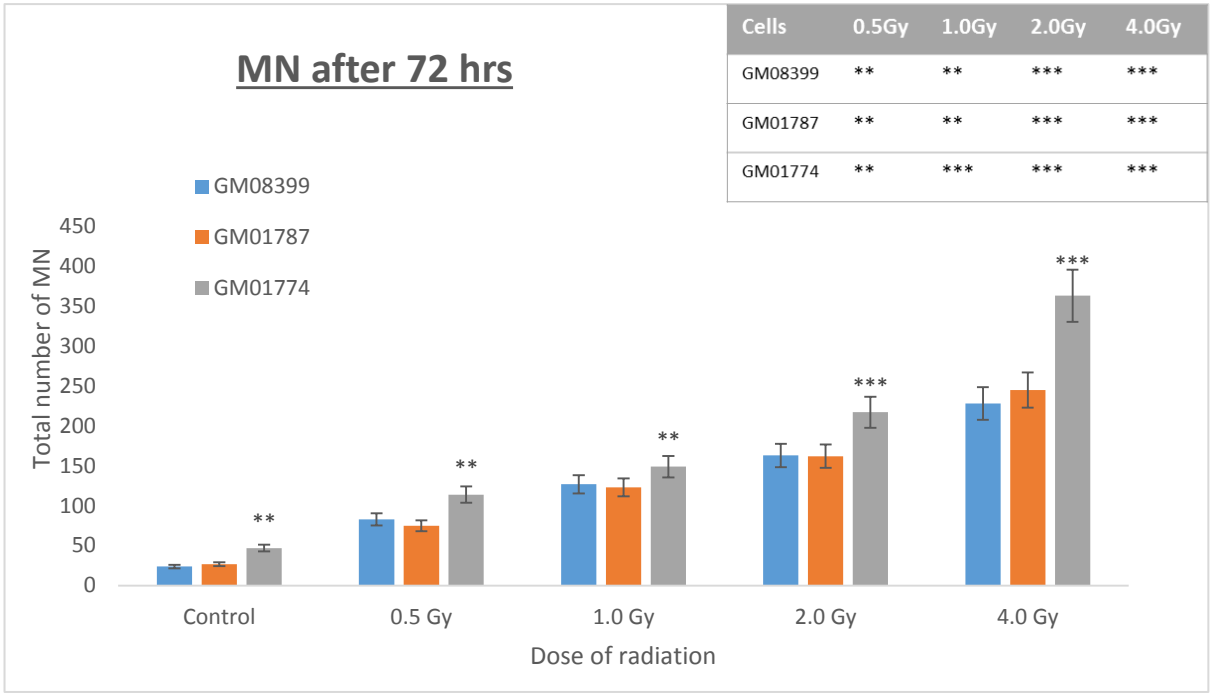

Cells	0.5Gy	1.0Gy	2.0Gy	4.0Gy
GM08399	**	**	***	***
GM01787	**	**	***	***
GM01774	**	***	***	***

*Figure.3.10) Frequencies of MN in 0.5 Gy, 1.0 Gy, 2.0 Gy and 4.0 Gy doses of gamma radiation for DC cell lines compared to control obtained after 72 hours. Two types of statistical comparison were carried out. The inset shows comparison of MN for each dose against unirradiated samples. Stars above bars indicate comparison between DC and control cell lines *P<0.05 **P<0.01 ***P<0.001 versus control. Error bars represent SEM*

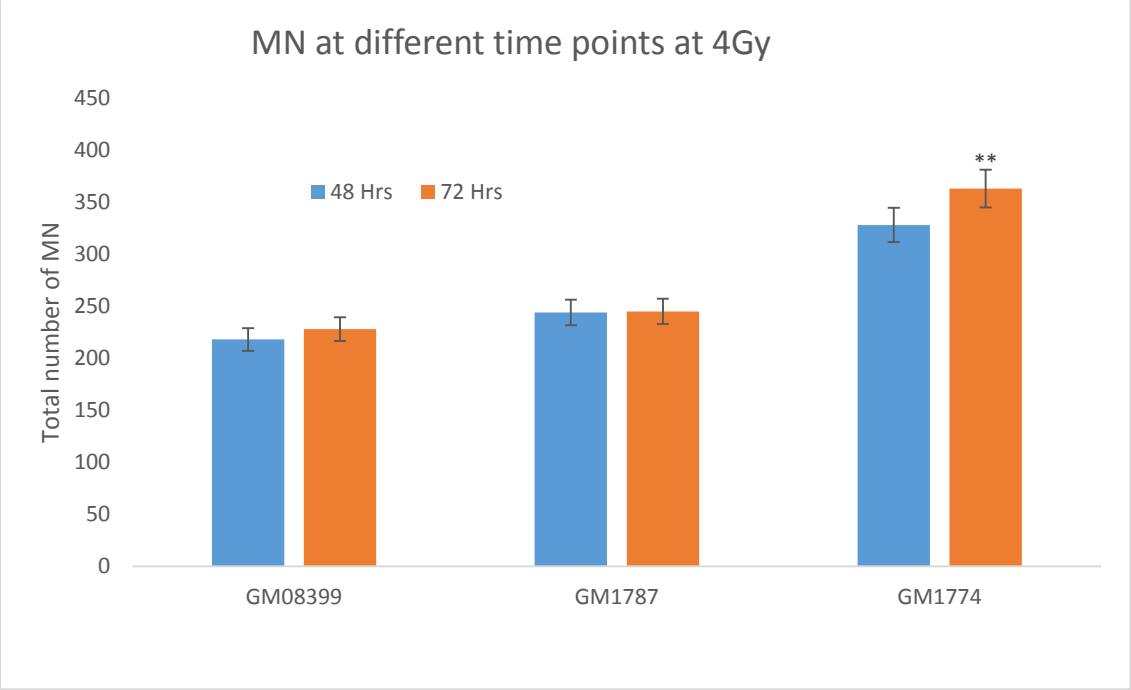

*Figure.3.11) Frequencies of MN at 4 Gy of gamma radiation at 48 and 72 hrs for DC cell lines compared to control cell line. *P<0.05. **P<0.01, ***P<0.001 versus control. Error bars represent SEM.*

We have extended MN analysis further by slightly changing the protocol. Gutierrez-Enriquez (2003) reported that in normal lymphobastiod cell line there was an elevated MN level 72 hours following exposure to IR, in particular when irradiated with higher doses such as 4.0 Gy. Figure 3.10 shows a dose response curve generated with a modified protocol in which cells were harvested 72 hrs after IR. The basal level of MN remained the same as when harvesting cells 48 hr post-treatment (figure 3.8 and 3.10). However there was an increase in the MN levels for the homozygous DC cell line. Statistical analysis showed that GM1774 cell line displayed a significantly higher level of MN at 4.0 Gy compared to the control cell line (Figure 3.10). A comparison is made in Figure 3.11 between 48 hrs and 72 hrs harvests at the dose of 4.0 Gy. Based on this analysis, treatment with 4.0 Gy increases the sensitivity of the homozygous DC cell line to IR thus further substantiating the notion of defective DNA damage response in DC cells.

3.5 Anaphase Bridge analysis in DC fibroblast cell lines

To further verify the notion that DC cells have a defective DNA damage response we investigated frequencies of anaphase bridges. Anaphase bridges are chromatin fibers connecting two separating chromosome masses and mostly result from dicentric chromosomes which may form by fusion of dysfunctional telomeres or DSBs formed at interstitial chromosome sites (Gisselsson et al 2000). In both cases DSBs are required for the formation of anaphase bridges (Acilan et al 2007).

We quantified anaphase bridges in bi-nucleated cells after treatment with Cyt-B and generated dose response curves using the same doses as for MN analysis. Examples of Anaphase Bridges observed are shown in figure 3.13.

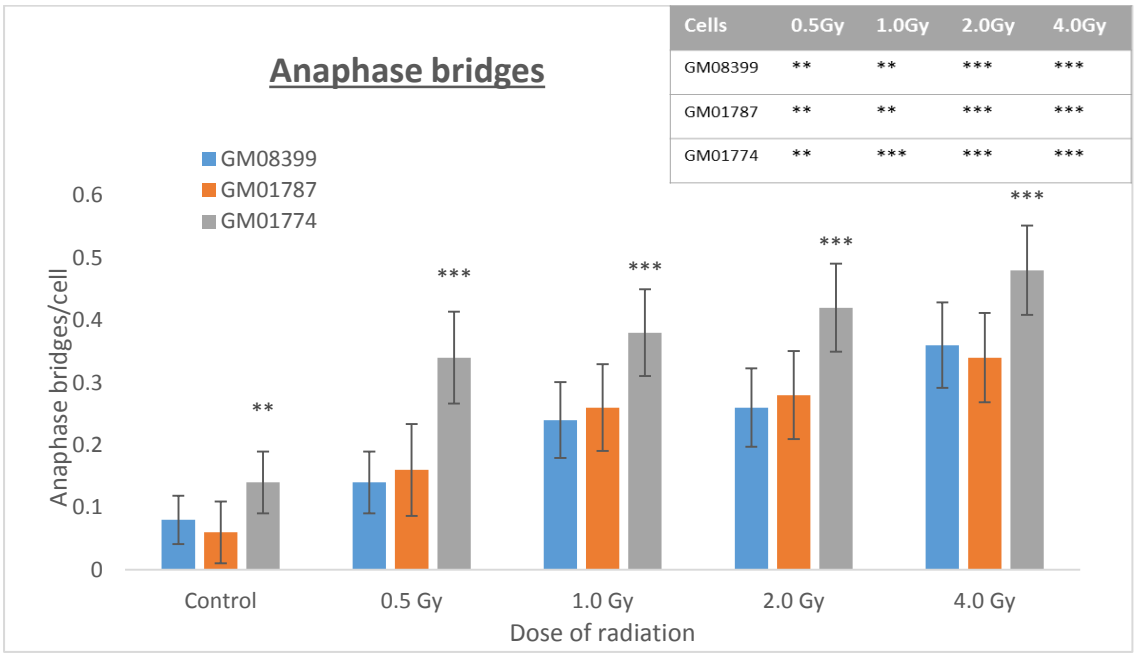

Cells	0.5Gy	1.0Gy	2.0Gy	4.0Gy
GM08399	**	**	***	***
GM01787	**	**	***	***
GM01774	**	***	***	***

Figure.3.12) *Frequencies of Anaphase Bridges in 0.5 Gy, 1.0 Gy, 2.0 Gy and 4.0 Gy doses of gamma radiation for DC cell lines compared to control Two types of statistical comparison were carried out. The inset shows comparison of Anaphase Bridges for each dose against unirradiated samples. Stars above bars indicate comparison between DC and control cell lines *P<0.05. **P<0.01, ***P<0.001 versus control.. Error bars represent SEM*

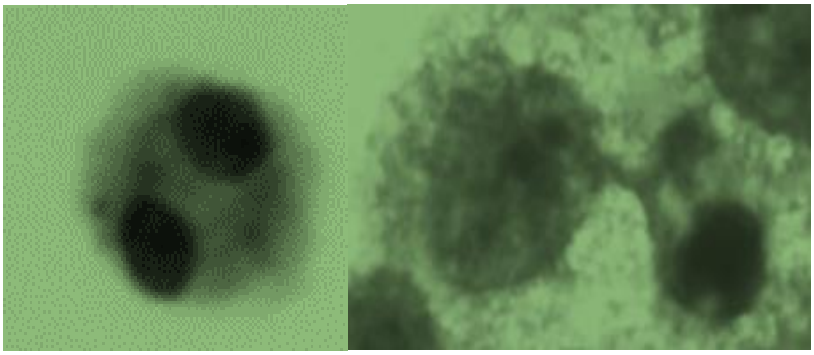

Figure.3.13) Images obtained from GM1774 (Homozygous) fibroblast cell line stained with Giemsa to score on Anaphase bridges, as a consequence of telomere end to end fusion.

We observed a pattern of anaphase bridge frequencies that was similar to the pattern of MN frequencies (Figs 3.12) thus further supporting the notion that DNA damage response ion DC cells is dysfunctional.

We also quantified Anaphase bridges in Telophase Lags (example in figure 3.14) following IR. These are telomere fusion between late anaphase- early telophase and are also referred to as Anaphase laggard (Catalan et al., 2000). The pattern of repair was similar observed with γH2AX assay (Figure 3.15).

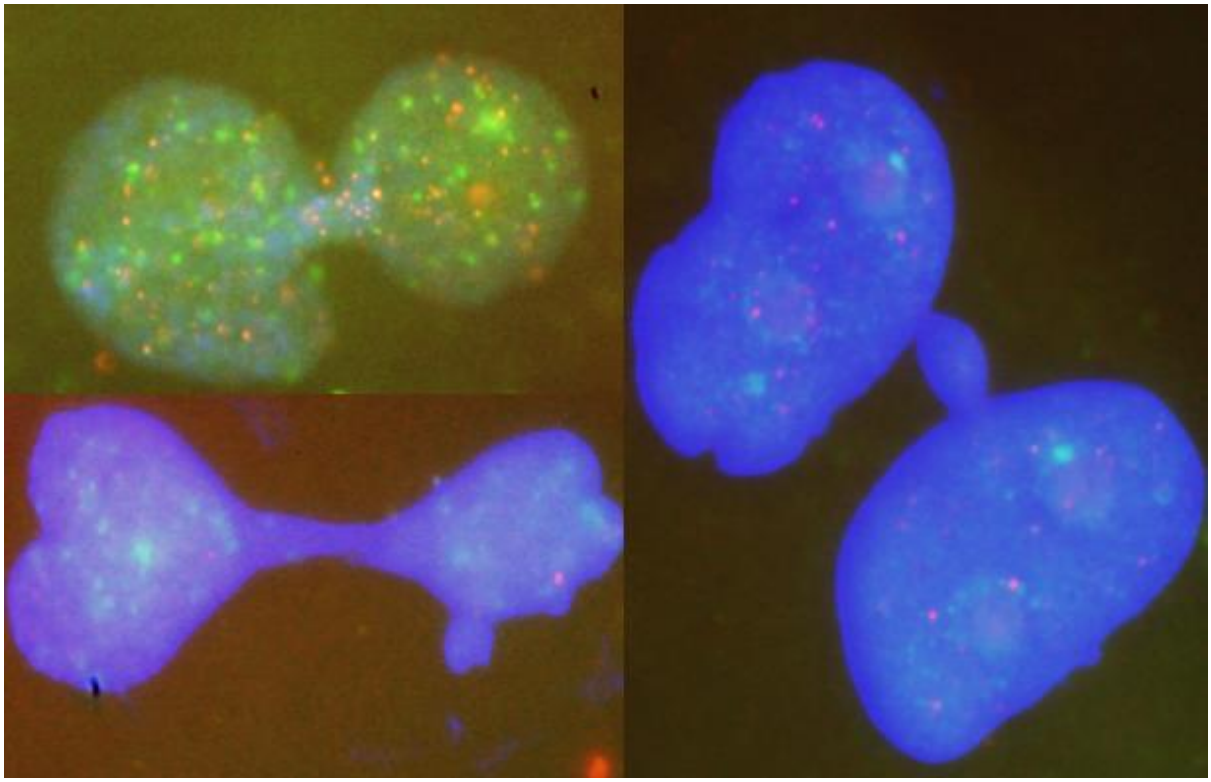

Figure.3.14) Anaphase Bridges - Telophase lags in DC fibroblast cell lines. The cells were captured in late anaphase-early telophase. Note the presence of red and green fluorescence. Red represents telomeres and green due to γH2AX

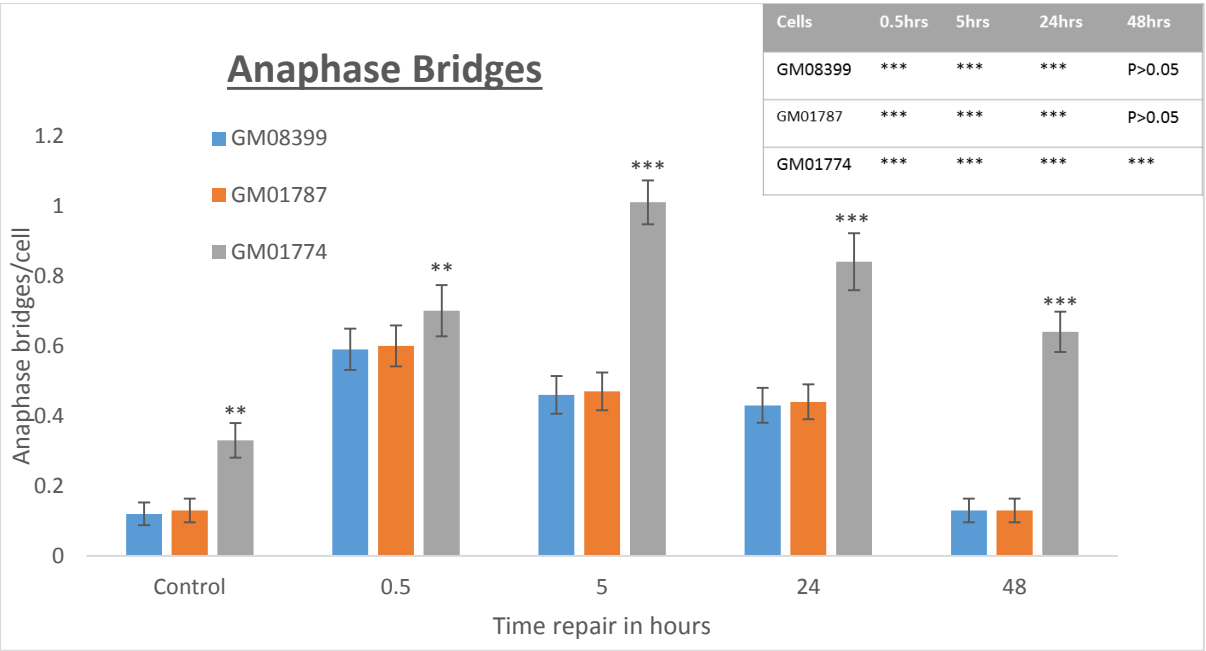

*Figure .3.15) Anaphase bridge frequencies in DC fibroblast cell lines. Graph shows frequency of anaphase bridges at different points following exposure to 1.0 Gy of gamma rays. The inset shows comparison of Anaphase Bridges for each time point against unirradiated samples. Stars above bars indicate comparison between DC and control cell lines *P<0.05 **P<0.01 ***P<0.001 versus control.. Error bars represent SEM*

3.6 Interphase Quantitative Fluorescent in situ hybridisation (IQ-FISH) analysis of normal and DC fibroblast cell lines.

In the last section of this chapter we analysed telomere length in the three cell lines using the protocol IQ-FISH as described previously in chapter 2 (see also Ojani, M 2012, PhD Thesis). We thought that it is important to identify differences in telomere length between DC and control cells as previous studies suggest telomere shortening in DC cells (Mitchell et al 1999) which may contribute to a defective DNA damage response. IQ-FISH is an accurate and reliable method for measuring telomere length in interphase cells, especially for slow growing fibroblast cells with mutations in DNA damage response genes (Ojani, M 2012). It is based on the use of peptide nucleic acid (PNA) telomere oligonucleotides and appropriate digital image analysis systems designed to quantify fluorescence signals (Slijepcevic 2001). We used a software called IPLAB, one

of the standard image analysis packages used for acquisition and analysis of fluorescence microscopy images. This interphase Q-FISH software is able to accurately recognize interphase nuclei and measure average, as well as total fluorescence intensity in individual nuclei. Uneven exposure during acquisition and variation in fluorescence bulb intensity can give rise to some inaccuracies in measuring fluorescence intensity for any cell sample. In order to tackle these problems, calibration is required that will make the acquired images comparable to each other. Researchers in the laboratory use two mouse lymphoma cell lines, LY-R (radioresistant cells) and LY-S (radiosensitive cells) for calibration purposes. These two cell lines have long telomeres (LY-R = 48 kb) and short telomeres (LY-S = 7 kb) (Mcllrath et al 2001). Hybridization efficiency after the protocol used for conventional Q-FISH immediately produced expected results. As can be seen in Figure 3.16, LY-R cells had much more intense signal than LY-S cells thus reflecting reported differences in telomere length between the two cell lines. Images of LY-R and LY-S interphase cells were acquired along with GM08399 (normal control cell line), GM1787 (DC heterozygous cell line) and GM1774 (DC homozygous cell line) and analysed telomere fluorescence (TF) using the above software. Previous experience suggested that a fixed exposure time is required for accuracy and reproducibility of Q-FISH measurements. A fixed exposure time of 0.5 seconds was therefore used. Maryam Ojani, a previous PhD student developed the method in a way that the intensity of fluorescence of LY-R and LY-S cells is measured each time a new sample is analysed by IQ-FISH, and compared against the standard based on 5 measurements presented in her thesis (Ojani 2012). This protocol generates correction factors which form the basis for calculating Corrected Calibrated Fluorescence (CCF) for each sample.

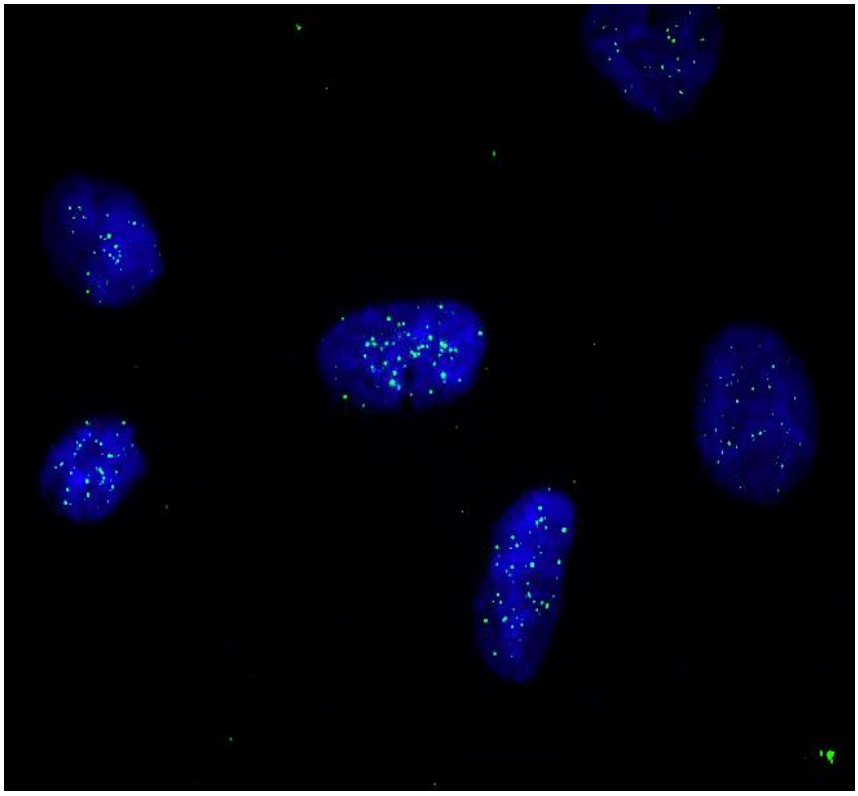

A) Example from Fibroblast cell lines

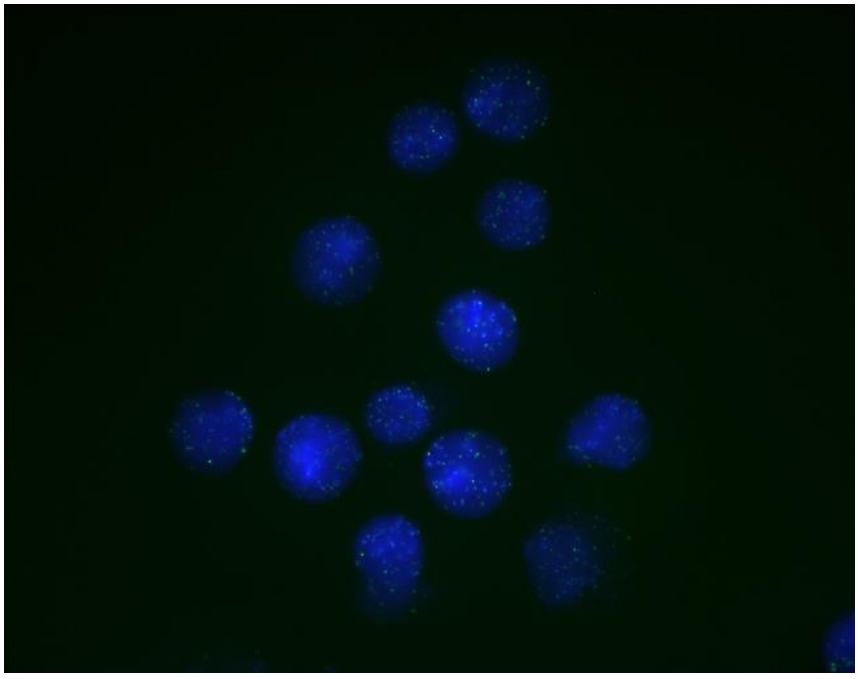

B) LY- S cell

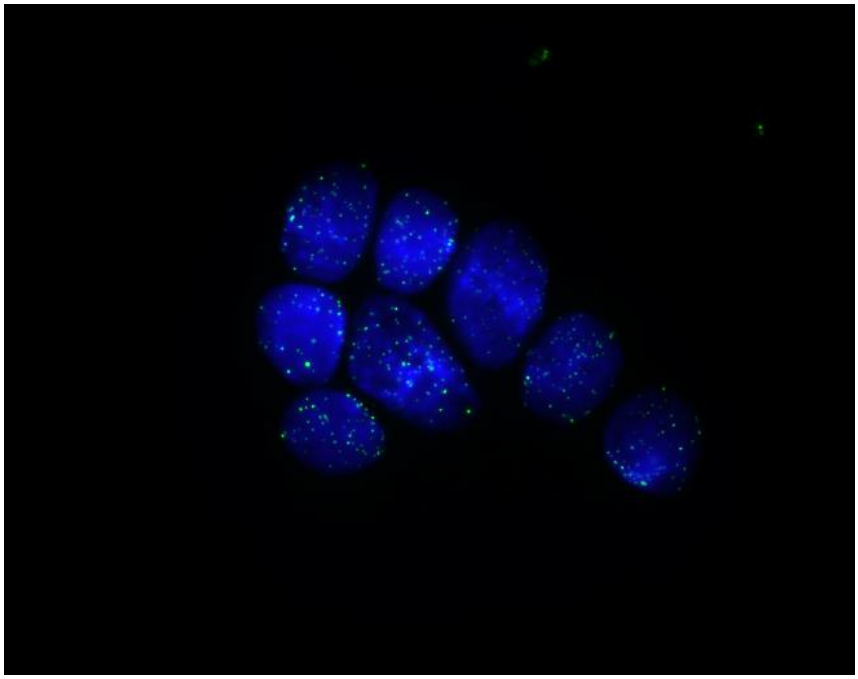

C) LY- R cell

Figure 3.16) Images to show Interphase Q-fish formation in a) GM1774 fibroblast, b)LY-S and c)LY-R cell lines. Telomeres were detected by $(AATCCC)_3$ probe labelled with FITC and were measured using IP-LAB.

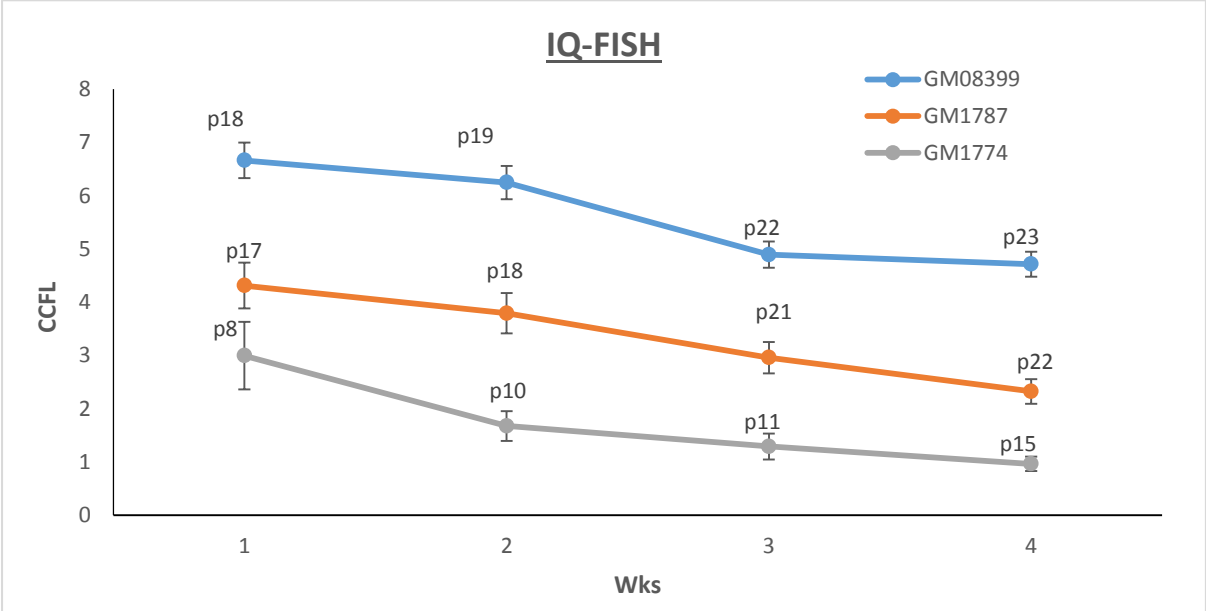

Figure.3.17) Telomere length analysis in normal and DKC1 defective cells calibrated against LY-R and LY-S mouse cells. CCFL = Corrected Calibrated Fluorescence. Error bars represent SEM.

Table 3.2 Calculation of Telomere Shortening in TFU/PD by IQ-FISH methods

Cells	Range of CCFL (TFU)	Population Doubling (PD)	Total No. of Passages	Total PD	TFU/PD
GM08399	1.9	3	6	18	0.11
GM01787	2	2.5	6	15	0.13
GM01774	0.25	1	8	8	0.25

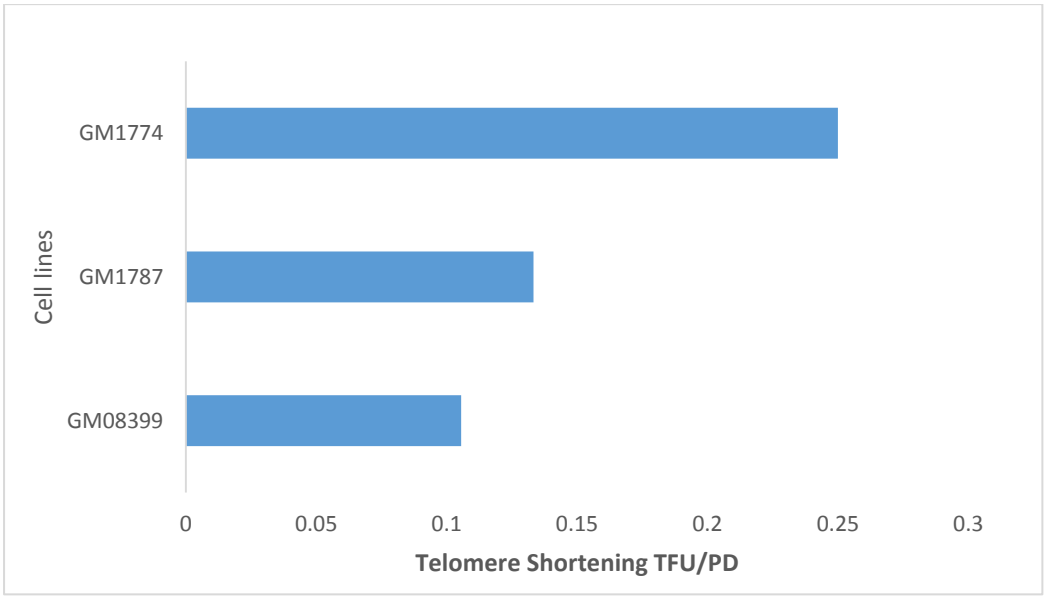

Figure 3.18) Rates of Telomere shortening in primary human cell lines in TFU/PD.

The three cell lines were analysed over a period of increasing passage numbers in GM08399, GM01787 and GM1774 cell lines to establish telomere length kinetic curves. Figure 3.17 illustrates that GM1787 have a shorter telomere length compared to GM08399. When comparing GM1787 and GM08399 at passage 18, it is clear that GM08399 have telomeres at least twice the length than GM1787. Therefore, the results suggest that GM1787 has shorter telomere length than GM08399, especially around

higher passage numbers. In addition, the results indicate that the telomere length indeed decrease over a period of 4 intervals. For GM1774 cell line, lower passage numbers were chosen as it is difficult to generate higher passages numbers. But even in this lower passages, it is interesting to note that for example at passage 15, the average telomere length is much lower than the higher passages of the normal control cell line and the heterozygous cell line. This indicates that DC homozygous cell have accelerated telomere shortening compared to the heterozygous indicating that it's difficult to form the T loop, thus activating the DNA damage response machinery, as the free ends would be recognised as broken ends. Similarly, the heterozygous has decrease levels of telomere length compare to the normal control. These ties in with the results obtained in figure 3.6, where there were higher levels of DNA damage found at telomeres.

In addition, we calculated the rate of telomere shortening in the DC fibroblast cell lines (Table 3.2) and presented the findings in Figure 3.18. We achieved this by calculating the range of the CCFL (Telomere Fluorescence) between the highest passage number to the lowest passage number in each cell line and used this value per PD to work out this rate of telomere shortening. DC homozygous fibroblast cell lines lose more Telomere Fluorescence when compared to the heterozygous and normal control cell lines. This tallies with the results presented from TIF assay (Figure 3.3 and 3.6) where there are higher levels of DDR at telomeres in DC homozygous cell lines compared to normal cells. Therefore, these results confirm the accelerated telomere shortening in DC cell lines relative to the control cells.

3.7 Discussion

Results presented in this chapter show that DC cells have a dysfunctional DNA damage response. We have selected DC fibroblast cell lines as a model with telomere dysfunction resulting from the defective *DKC1* gene. Given the extensive evidence pointing to the functional link between DNA damage response and telomere maintenance we reasoned that the *DKC1* defect will affect the DNA damage response. Our results largely support this notion. The supporting evidence can be split into two categories: evidence from telomere length analysis and evidence from DNA damage response analysis. These two sets of evidence will be discussed below.

3.7.1. Evidence from telomere length analysis

A study published by Cabuy et al. (2005) found that the rate of telomere shortening was higher in radiosensitive cells than in normal cells. Their calculation of the rate of telomere shortening was similar to what we presented in figure 3.18. in the form of telomere fluorescence loss per PD. Cabuy et al (2005) reasoned that the rate of telomere shortening may be related to the overall DNA damage response capacity. This is in line with our results which show that the rate of telomere shortening was highest in the cell line with the defective DNA damage response – the cell line from the DC patient with the homozygous mutation (Figure 3.18). Indeed, a high level of DNA damage at telomeres observed in this cell line (Figure 3.3 and 3.6) suggests that the accelerated shortening of telomeres (Figure 3.17) is a predisposing factor for a defective DNA damage response. Our results are also in line with those published by Michell et al (1997) demonstrating accelerated telomere shortening of the same DC homozygous cell line that we used. Furthermore, our results correspond well with the findings published

by M'kacher et al (2003). This study showed that cells with significantly shorter telomere length were much more sensitive to IR and other DSB inducing agents, including Bleomycin. Severely shortened telomeres become dysfunctional and this dysfunction most likely activates the DNA damage response machinery because telomeres are too short to adopt the normal t-loop structure required to form the correct platform for the shelterin complex which will eventually suppress DNA damage response activation. Therefore, our results support the notion of telomere shortening as the cause of telomere dysfunction and thus additional evidence for the view that DNA damage response mechanisms and telomere maintenance are functionally related.

3.7.2 Evidence from DNA damage response analysis

Previously, a cytogenetic study showed that DC cells may be more sensitive to X-rays (DeBauche et al., 1990). The study revealed that x-ray induced G2 chromatid gaps and breaks were significantly elevated in DC fibroblast cell lines relative to control lines (DeBauche et al., 1990). This fits well with our findings of abnormal DNA damage repair kinetics as demonstrated by quantifying γH2AX foci induced by IR at different time intervals post-exposure (Figure 3.2 and 3.5).

It is interesting to note that a recent work from the DC mouse model has revealed *Dkc1* defective mouse cells show an abnormal DNA damage response (Gu et al., 2008) thus supporting our results. Mice were exposed to etoposide, a DNA damaging agent that induces DNA lesions in the form of DNA DSBs but not as effectively as IR. However, Kirwan et al (2011) observed DNA damage response to be normal in DC human fibroblast cell lines after exposure to etoposide. We believe that their experimental design failed to appreciate the fact that DNA damage should be monitored in the form of kinetics (a time course) rather than monitoring damage at a single point immediately after the exposure. Thus, we must conclude that our results, consistent with the

observations obtained by Gu et al (2008) reflect better the DC cell capacity to carry out DNA damage response, than results obtained by Kirwan et al (2011).

This notion is supported by a more recent study by Manguan-Garcia et al. (2014), who found a defective DNA damage response in X-linked recessive DC cells in comparison with normal cells. They exposed DC cells to Bleomycin, a well-known DSB inducing agent, and used the same homozygous and heterozygous cell lines as we have used. Their results showed that the number of ɣH2AX foci was dramatically higher in DC cells than in normal cells after exposure to Bleomycin. To provide further evidence that DNA damage response is defective in DC cells we generated MN and Anaphase bridge dose response curves and shown the DNA damage defects. This also demonstrates that MN and Anaphase bridges analyses can be used as a biomarker for radiosensitivity in DC fibroblast cell lines in a similar fashion as the G2 assay (DeBauche et al 1990).

In summary our results conclusively show that the GM1774 (*DKC1* -/-) cell line exhibits a defect in cellular response to DNA damage which is in line with the hypothesis that DNA damage response and telomere maintenance are functionally related.

Chapter 4 DNA Damage Response in DC Lymphoblastoid cell lines

4.1 Introduction

In the previous chapter we looked at fibroblast cell lines from DC patients born with mutation in *DKC1*(-/-). The function of *DKC1* is to stabilise the RNA template required for synthesis of telomeric repeats. Our findings indicate that *DKC1* defective fibroblast cells have an abnormal DNA damage response suggesting, in line with numerous previous studies, the functional relationships between telomere maintenance and DNA damage response (Manguan-Garcia et al 2014; DeBauche et al 1990; Gu et al. 2008; De Lange, 2005; d'Adda di Fagagna et al, 2003). Since telomerase, the reverse transcriptase responsible for synthesis of telomeric DNA, is inactive in fibroblasts we decided to look a lymphoblastoid cell lines (B-lymphocytes transformed *with* Epstein-Barr Virus) as telomerase shows some activity in lymphocytes possibly reflecting bone marrow failure as the prinicipal cause of early mortality in the majority of DC patients (Courtlhard et al 1998).

Lymphocytes retain the abiity to express telomerase after differeniation from stem cells unlike fibroblasts. In mature and differeniated lymphoctyes telomerase synthesise telomere repeats after each mitotic cycle in a regulated fashion (Weng 2002; Ratts and Weng 2012). This prompted us to monitor whether DC lymphoblastoid cells show impaired growth due to accellerated telomere shortening. In addition, we wanted to confirm that the *DKC1* gene mutated in a different cell type contributes to the observed defective DNA damage response (Chapter 3) thus adding further evidence to the notion of the functional interplay between telomere maintenance mechanisms and DNA damage response.

In this chapter, we used cell lines from two different DC patients, both homozygous recessive mutant with respect to the *DKC1* gene: GM01775, a cell line from a patient

with a 3 bp deletion of nucleotides 201_203 of the DKC1 gene (201_203delCTT) (Knight et al. 1999) and GM03193, a cell line from a patient with A>G transition at nucleotide 193 in exon 4 of the DKC1 gene resulting in the substitution of alanine for threonine at codon 66 [Thr66Ala (T66A)] (Knight et al 1999; Hassock et al 1999). We examined DNA damage response in the two cell lines and the acompanying control lines, GM008933 and GM017205, a 26 year male (Hu et al 2004). Furthermore, we included a cell line from a patient with the heterozygous mutation: GM03650, belongs to the same family as GM03193 (Knight et al 1999; Hassock et al 1999). We were also interested to see whether different *DKC1* mutations produce different or similar effects in a different cell environments. For example, the GM01775 (lymphoblastoid) and GM1774 (fibroblast) are from the same patient whereas the GM03193 cell line is derived from a patient with a different mutation.

4.1.1 Assessment of DNA damage response

The assessment of DNA damage response was carried out using the same techniques and principles as in the previous chapter. We started to analyse DNA damage response following exposure of cells to IR by using the γH2AX assay and first generated a dose response curve as in the previous chapter. In constrast to adherent fibroblast cell lines that are seeded on poly-l-lysine coated slides and then irradiated (Chapter 3) lymphoblastoid cell lines required different treatment for staining with the **γ**-H2AX antibody. Cells were irradiated in suspension and processessed using the standard cytospin procedure. A cytospin machine (Shandon) was used to spread a single layer of cells on to microscope slides. We noticed that DC lymphoblastoid cell lines were sensitive to the cytospin treatment relative to normal cells, resulting in the greater mechanical fragmentation of DC cells which almost certainly would interfere with the subsequent analysis. Therefore, we resorted to developing a suitable cytospin protocol

for DC cells. After a series of experiments with different conditions (speed and time of centrifugation, different fixative solution etc) we optimized the protocol for DC cells that resulted in depositing intact cells on microscope slides for **γ**H2AX staining.

The summary of the protocol optimization is provided below. The standard centrifugation speed of 1500 rpm and a fixative solution consisting of formaldehyde, Pbs and distilled water were used for normal cell lines with good results. This was not suitable for DC lymphobastiod cell lines as the cell nuclei were irregularly shaped or disrupted. So, different speed seetings, 1000rpm, 800 rpm, 700 rpm and 600rpm, for 5 minutes were used. The speed of 700rpm provided analysable microscope slides containing intact cells. Regarding the fixative procedure, we found that a mixture of PBS and water was not required for fixing the cells. For the permablising step, we added glycine as it captures unbound fixative (Formaldehyde) thus eliminating the need for additional washing. This protocol for lymphobastiod cell lines treatment for cytospin was adapted from Horn et al (2013). Furthermore, Dr Kai Rothkamm (Public Health England) gave advice via email based on the protocol for peripheral blood lymphocytes used in his laboratory. The protocol we established is fully described in the Materials and Method section (Chapter 2).

The dose response curves were generated as in previous chapter with the difference that the dose of 0.25 Gy was ommited. The experiment was performed three times and each time, a total of 100 cells were analysed. Representative images of lymphoblastoid cell nuclei stained with the **γ**-H2AX antibody are shown in Fig 4.1.

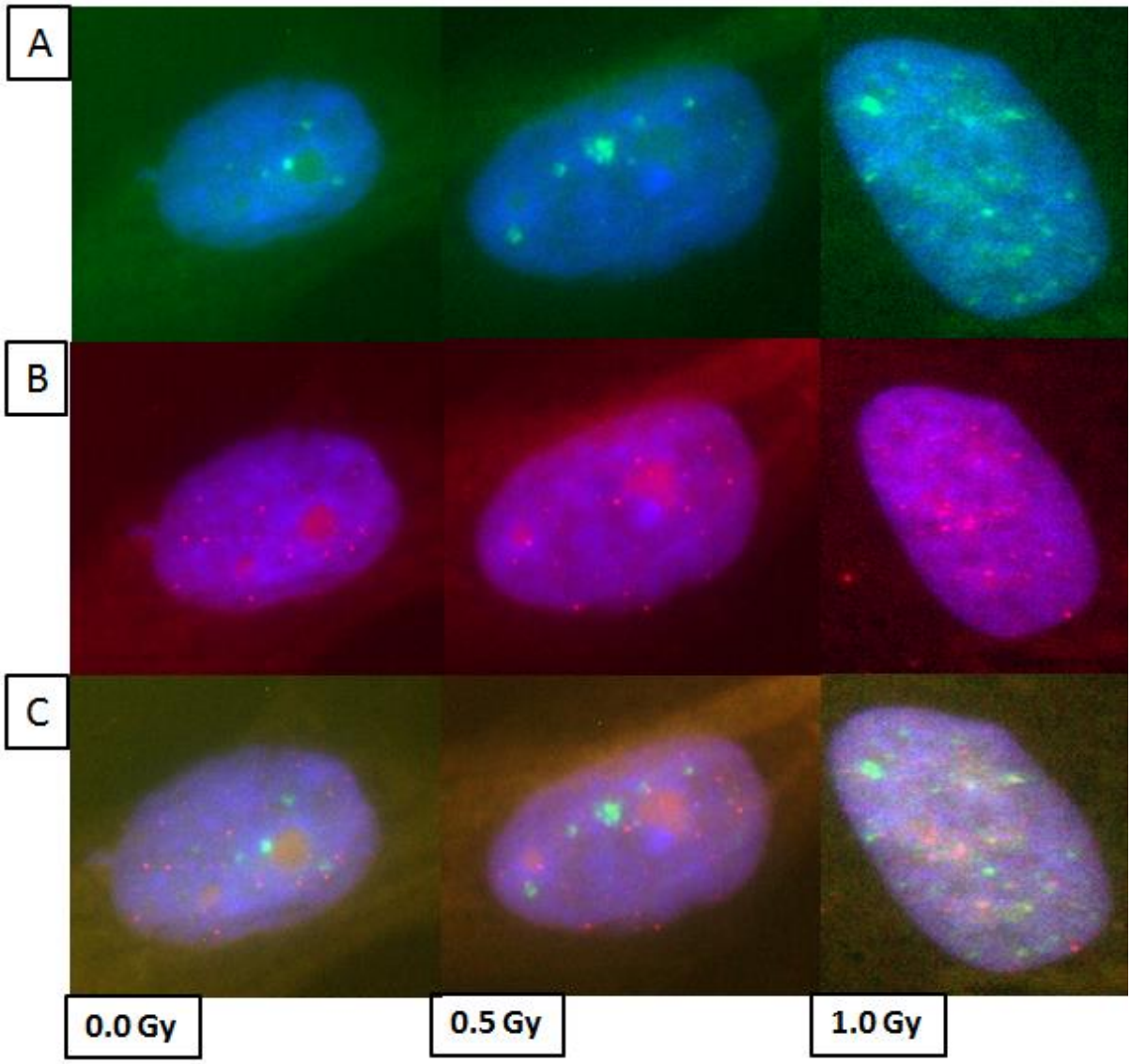

Figure 4.1) Images obtained from nuclei of the DC lymphoblastoid cell line, after irradiation with gamma rays at 0.0Gy, 0.5Gy and 1.0Gy doses A) detection of DNA damage γH2AX foci. B) Telomeres were detected by $(AATCCC)_3$ probe labelled with Cy-3 (Red) C) Colocalization with γH2AX and telomeres, represent TIF (merged) shown as yellow spots. The nucleus was counterstained with Dapi. Examples are from the GM01775 cell line.

The results of our analysis are shown in Fig 4.2. The Anova reveals that the control cell lines (GM00893 and GM17208) and the heterozygous cell line (GM03650) had lower spontaneous frequencies of ɣH2AX foci relative to the homozygous cell lines (GM01775 and GM03193) (Fig 4.2). Exposure of cells to IR results in a significant difference in frequencies of DNA damage foci between homozygous cell line on one side and control and heterozygous cell lines on the other (Fig 4.2). For example, the frequency of ɣH2AX

positive foci is much higher at 1.0 Gy for GM03193 (P = 8.66112E-20) and GM1775 (P=4.97503E-14) homozygous cell lines relative to the remaining three lines (Fig 4.2). Anova indicates there is no significant difference between GM0350 (Heterozygous cell line, DKC1+/-) and control cell lines (Fig 4.2). Therefore, in line with the results obtained for fibroblast cell lines, these results indicate that both homozygous cell lines are more sensitive to radiation than control lines, suggesting DNA damage response to be defective in *DKC1* defective cells.

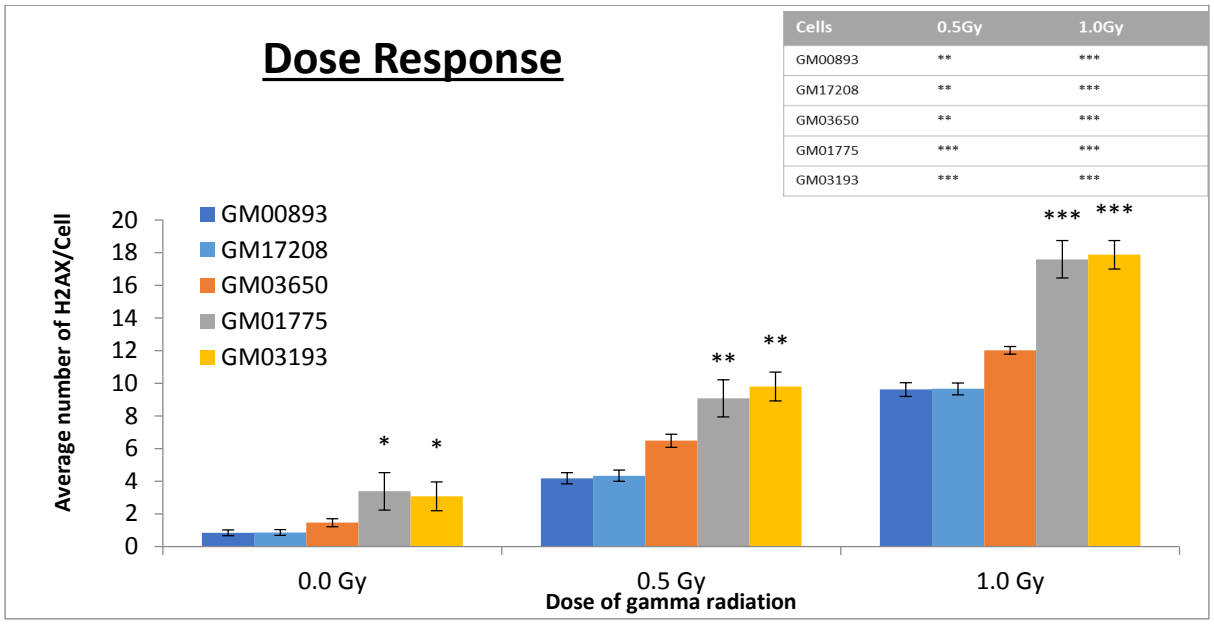

*Figure 4.2) Frequencies of γH2AX positive foci in 0.0, 0.5 and 1.0 Gy doses of gamma radiation for DC cell lines with control cell lines (GM00893 and GM017208). The inset shows comparison of DNA damage foci for each dose against unirradiated samples. Stars above bars indicate comparison between DC and control cell lines.*P<0.05 **P<0.01 ***P<0.001 versus control. Error bars represent SEM.*

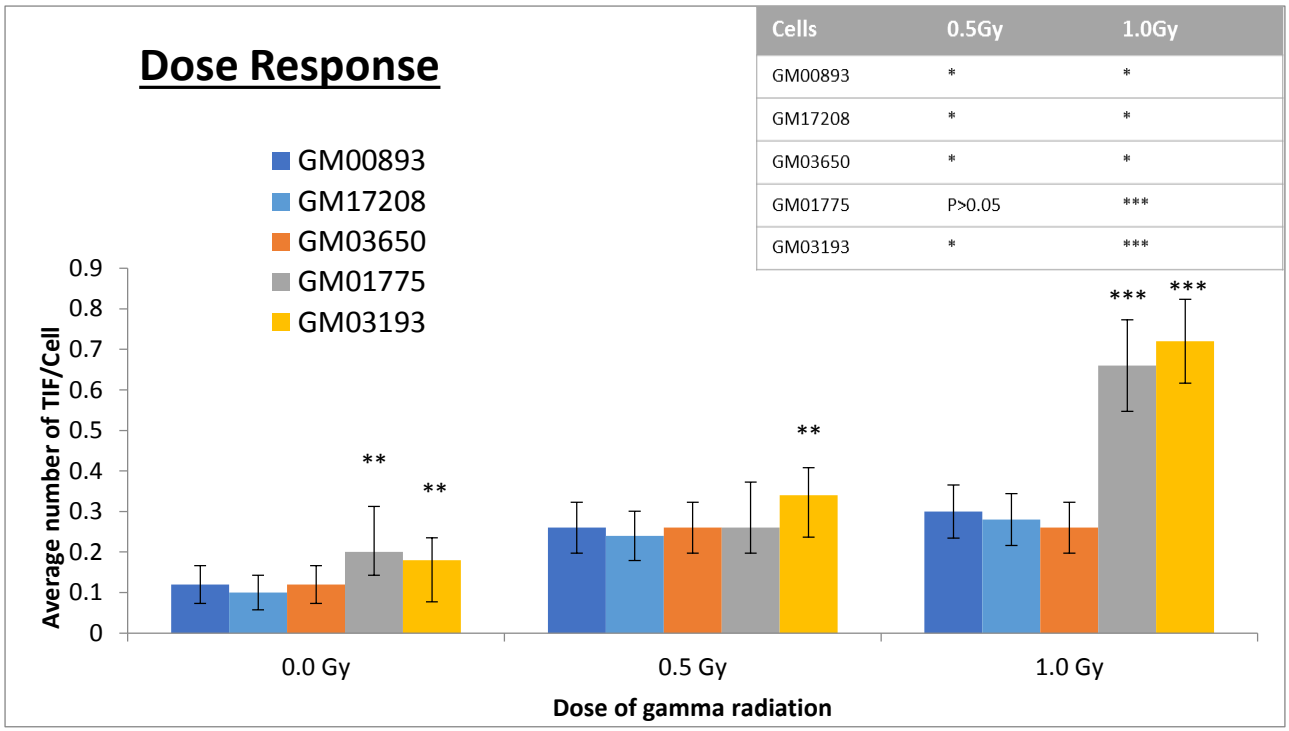

Cells	0.5Gy	1.0Gy
GM00893	*	*
GM17208	*	*
GM03650	*	*
GM01775	P>0.05	***
GM03193	*	***

Figure 4.3) *Frequencies of TIF positive foci in 0.0, 0.5 and 1.0 Gy doses of gamma radiation for DC cell lines with control cell lines (GM00893 and GM017208). The inset shows comparison of TIF foci for each dose against unirradiated samples. Stars above bars indicate comparison between DC and control cell lines. *P<0.05 **P<0.01 ***P<0.001 versus control. Error bars represent SEM.*

We have also analysed DNA damage response at telomeres using TIF (Telomere dysfunction induced foci) assay method to generate a dose response curve (figure 4.3) as in previous chapter. This is a relatively quick way of analysing telomere function in human cells (Takai et al 2003). When telomeres become dysfunctional this leads to activation of DNA damage response factors which accumulate at the damage site which is considered to be a DNA double strand break (DSB). Therefore, the protocol must be designed to allow the combination of markers that detect DSB and telomeres. We have used the antibody against ɣH2AX in combination with Peptide Nucleic Acid (PNA) telomeric sequence (with a cy-3 fluorescence label).

The analysis of TIF foci revealed that control cell lines showed a lower spontaneous frequency of TIF foci than homozygous DC cell lines (Figure 4.3), an observation in line

with Fig 4.2. However, the dose of 0.5 Gy produced a significantly higher frequency of TIFs relative to control lines only in the case of the GM03193 cell line (Fig 4.3). Only at the dose of 1.0 Gy both homozygous DC lines showed significantly higher frequencies of TIFs relative to control and heterozygous cell lines (Fig 4.3).

4.1.2 Repair kinetics analysis

To examine further the DNA damage response in lymphoblastoid cell lines, we analysed repair kinetics for each of the DC cell lines with respect to control lines. Examples of digital images showing staining of cell nuclei with the DNA damage marker, γH2AX, and telomeres for each time point are shown in figure 4.4.

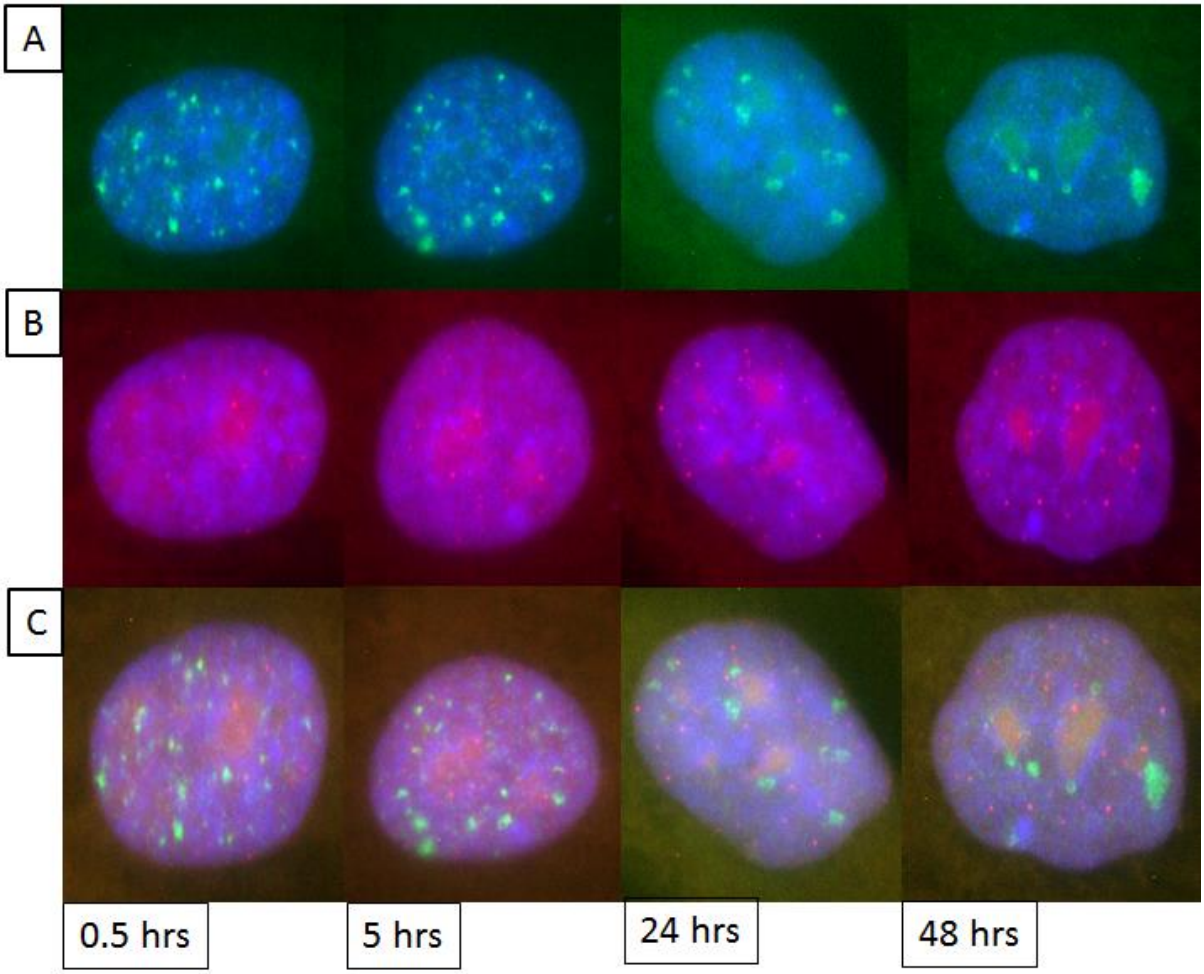

Figure 4.4) Images obtained from nuclei of the DC lymphoblastoid cell line, after irradiation with gamma rays at 1.0Gy dose at different time points. A) detection of DNA damage γH2AX foci. B) Telomeres were detected by $(AATCCC)_3$ probe labelled Cy-3 (red) C) Colocalization with γH2AX and telomeres represent TIF (merged) visible as yellow spots. The nucleus was counterstained with Dapi. Examples are from the GM01775 cell line.

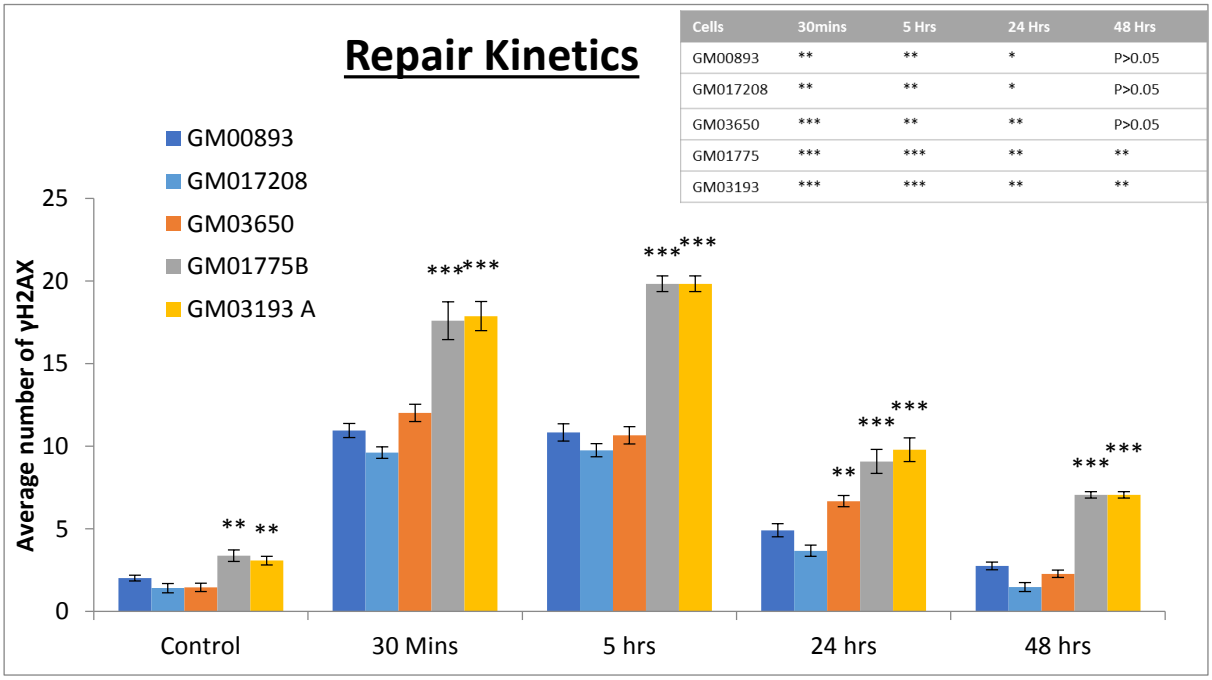

Cells	30mins	5 Hrs	24 Hrs	48 Hrs
GM00893	**	**	*	P>0.05
GM017208	**	**	*	P>0.05
GM03650	***	**	**	P>0.05
GM01775	***	***	**	**
GM03193	***	***	**	**

*Figure 4.5) Frequencies of γH2AX positive foci in untreated and 1.0 Gy doses of gamma radiation for DC cell lines with control cell lines (GM00893 and GM017208). The inset shows comparison of DNA damage foci for each time point against unirradiated samples. Stars above bars indicate comparison between DC and control cell lines. *P<0.05 **P<0.01 ***P<0.001 versus control. Error bars represent SEM.*

We irradiated all cell lines with 1.0 Gy of gamma rays and harvested them for analysis 0.5 h, 5 h, 24 h and 48 h after irradiation. Figure 4.5 shows the repair kinetics curve generated using the γH2AX assay. After 30 minutes, GM1775 and GM3193 cell lines showed significantly higher frequencies of γH2AX positive foci compared to normal control cell lines. DC homozygous cell lines (GM1775 and GM3193) have higher level of γH2AX foci at the basal level. This increased at least 2-fold after 30 minutes and especially after 5 hours (Figure 4.5). After 48 hours, control cell lines and the heterozygous cell line showed the same level of γ-H2AX foci compared to untreated cell lines indicating their capacity for a proficient repair (Figure 4.5). By contrast, the homozygous cell lines still showed residual level of DNA damage foci at 48 hours

indicating an impaired repair capacity. This further suggests an abnormal DNA damage response mechanisms in homozygous DC cell lines. This observation is in line with figure 4.2 which revealed a defective DNA damage response through generating dose response curves but also with the results presented in the previous chapter (figures 3.2 and 3.5).

We next monitored the rate of the TIF repair in the same set of cell lines (Fig 4.6). Examples of TIF images at various time points following irradiation are shown in Fig 4.5.

It is interesting to note that our results are generally in line with the recent study by Fumagalli et al 2012, which suggested that DNA damage at telomeres is potentially irreparable. All cell lines, including normal control cell lines showed residual DNA damage at telomeres 48h after irradiation (Fig 4.6). This is in line with the DNA repair kinetics monitored using the γH2AX assay which revealed proficiency of normal cells to fully complete the repair process (Fig 4.5). With regard to differences between DC and normal cell lines the statistical analysis revealed significantly higher levels of TIF foci in DC cells compared to control.

Taken together, our results suggest that, similarly to DC fibroblast cell lines, DC lymphoblastoid cell lines show a defective DNA damage response when analysed for the presence of a DNA damage marker after irradiation.

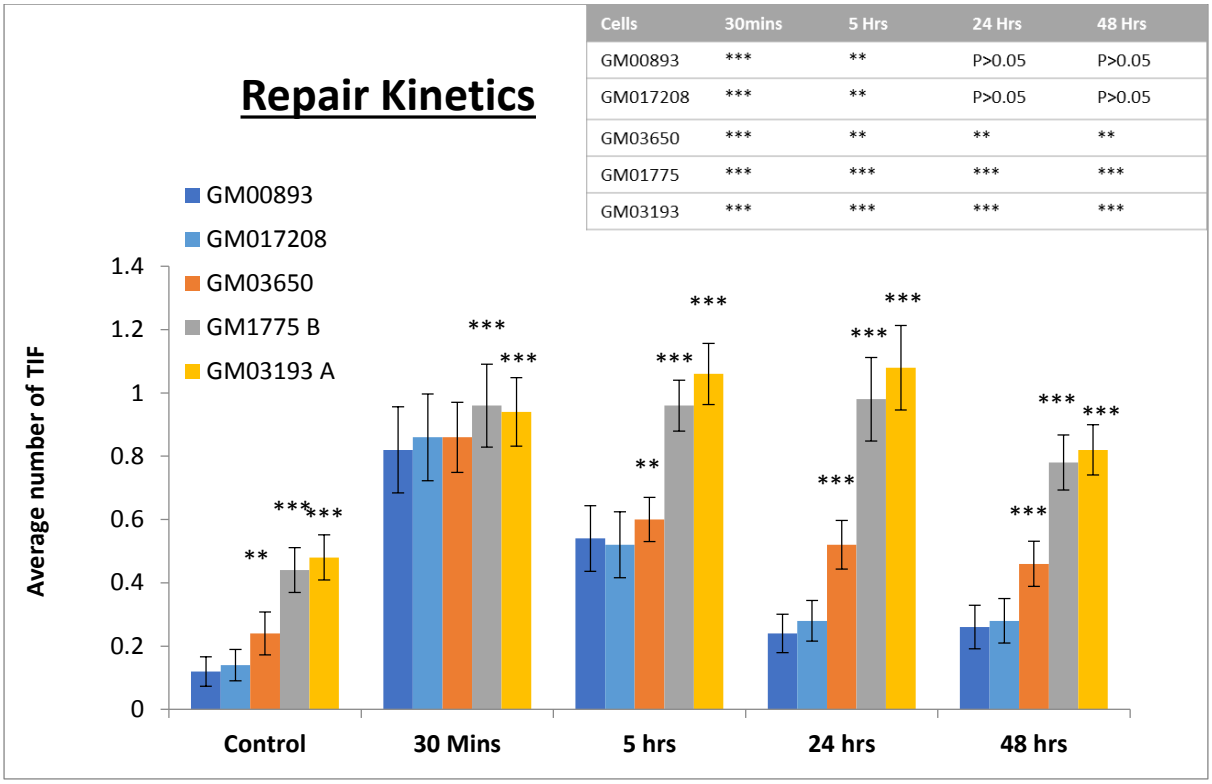

Cells	30mins	5 Hrs	24 Hrs	48 Hrs
GM00893	***	**	P>0.05	P>0.05
GM017208	***	**	P>0.05	P>0.05
GM03650	***	**	**	**
GM01775	***	***	***	***
GM03193	***	***	***	***

*Figure 4.6) Frequencies of TIF positive foci in untreated and 1.0 Gy doses of gamma radiation for DC cell lines with control cell lines (GM00893 and GM017208). The inset shows comparison of TIF foci for each time point against unirradiated samples. Stars above bars indicate comparison between DC and control cell lines. *P<0.05 **P<0.01 ***P<0.001 versus control Error bars represent SEM.*

4.2 Interphase Quantitative Fluorescent in situ hybridisation (IQ-FISH) analysis of normal and DC lymphoblastoid cell lines.

Given the functional relationship between DNA damage response and telomere maintenance we next monitored telomere length in DC lymphoblastoid cell lines using IQ-FISH as in Chapter 3. Telomere length was analysed over a period of increasing passage numbers. Representative images of cell nuclei used for IQ-FISH are shown in Fig 4.7. Telomere length analysis was carried out using the calibration method developed earlier and fully described in the Material and methods section.

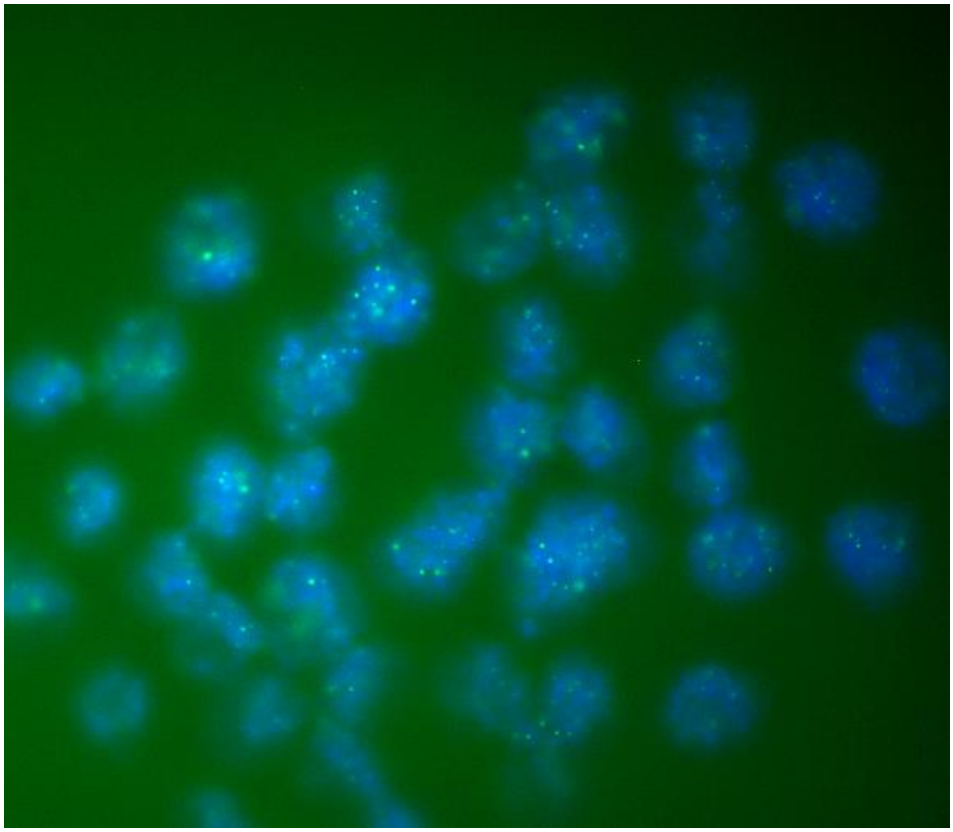

Figure 4.7) Images to show Interphase Q-fish formation in lymphoblastoid cell line. Example taken from GM01775 DC Cell line. Telomeres were detected by $(AATCCC)_3$ probe labelled with FITC and were used to measure the average telomere length.

Figure 4.8 showed that the GM3650 cell line had a shorter telomere length compared to the control cell lines. Even at lower passage numbers, GM3560 had at least twice as short telomeres compared to the controls at higher passages (P5, GM3650 and P12 GM00893). This is consistent with the existing literature and the notion that telomere length measurement is used as a diagnostic marker for DC (Wong and Collins, 2006; Mitchell et al 1999; Gu et al 2008). It was difficult to generate higher passage numbers for the DC cell lines due to their slow and poor growth. Therefore, only lower passage numbers were used for the comparison with control cell lines. Interestingly, telomere length had a tendency to go down in all DC cell lines (Fig 4.8). In contrast, in normal lines fluctuations in telomere length over the period of measurement generated a trend

indicating relatively stable length (Fig 4.8). This is consistent with the fact that lymphoblastoid cell lines express robust telomerase activity and maintain telomere length in a stable fashion (Cabuy et al 2004). Telomere Loss in DC cells over time (Fig 4.7) is consistent with the lack of functional telomerase (Zeng et al 2012; Mitchell et al 1999). Therefore, the analysis of telomere length in DC cells confirms the functional relationship between DNA damage response and telomere maintenance.

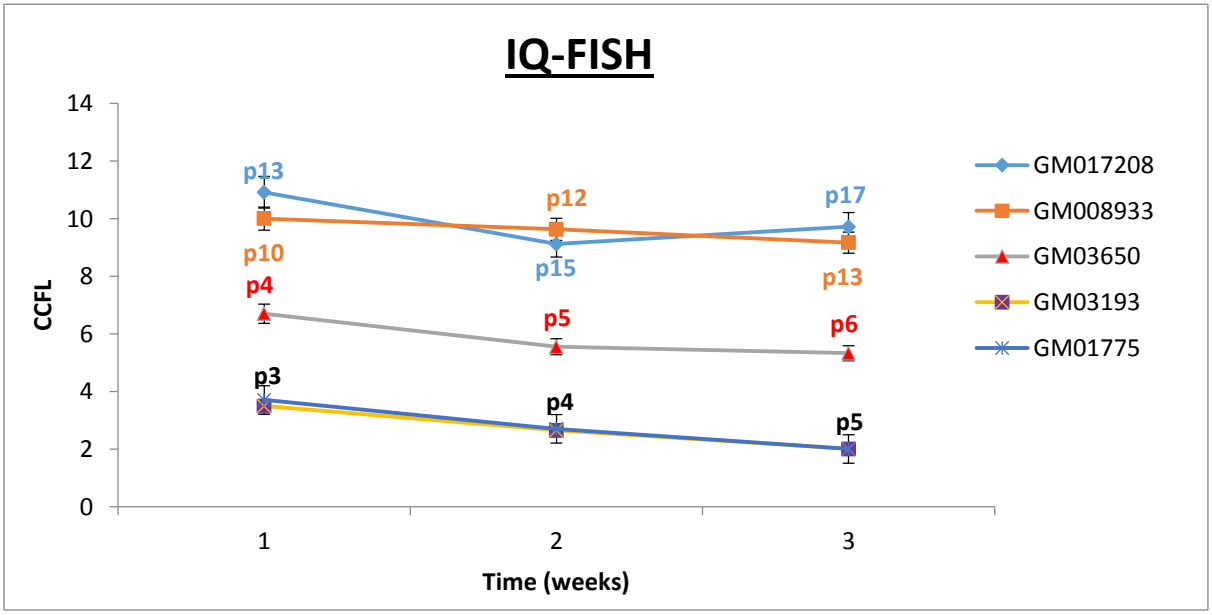

Figure 4.8) Telomere length analysis in normal and DKC1 *defective cells calibrated against LY-R and LY-S mouse cells. Each cell line was measured over a period of three passages to determine the telomere length of DC cell lines compared to control cell line. CCFl = Corrected Calibrated Fluorescence, protocol developed in Dr Slijepcevic lab. Errors bars represent SEM.*

4.3 Micronuclei in normal and DC lymphoblastoid cell lines.

Next, we wanted to assess DNA damage response in lymphoblastoid DC cell lines using two extra assays as in Chapter 3: the MN assay and anaphase bridge analysis. The MN assay required some modification in order to make it working properly in the case of

lymphoblastoid lines. The protocol from Gutierrez-Enriquez, 2003, used earlier resulted in poor quality images in which it was difficult to distinguish between two nuclei and the cytoplasm (Fig 4.9).

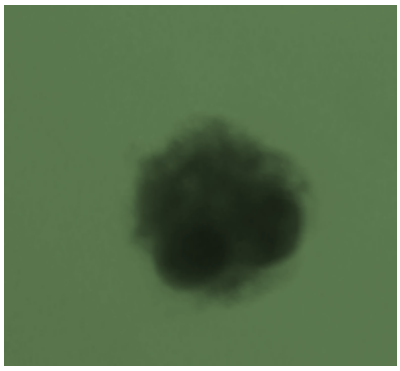

Figure 4.9) Image obtained from optimisation of the MN protocol for lymphoblastoid cell lines stained with Giemsa. The binucleated cell is not visible so the formaldehyde fixation step was removed.

The formaldehyde fixation step is removed. Furthermore, we used the standard fixative only harvested cells 48 hours after treatment with Cyt-B. We found that the modified protocol suits the lymphobastiod cell lines especially DC homozygous cell lines resulting in better quality slides (Figure 4.10).

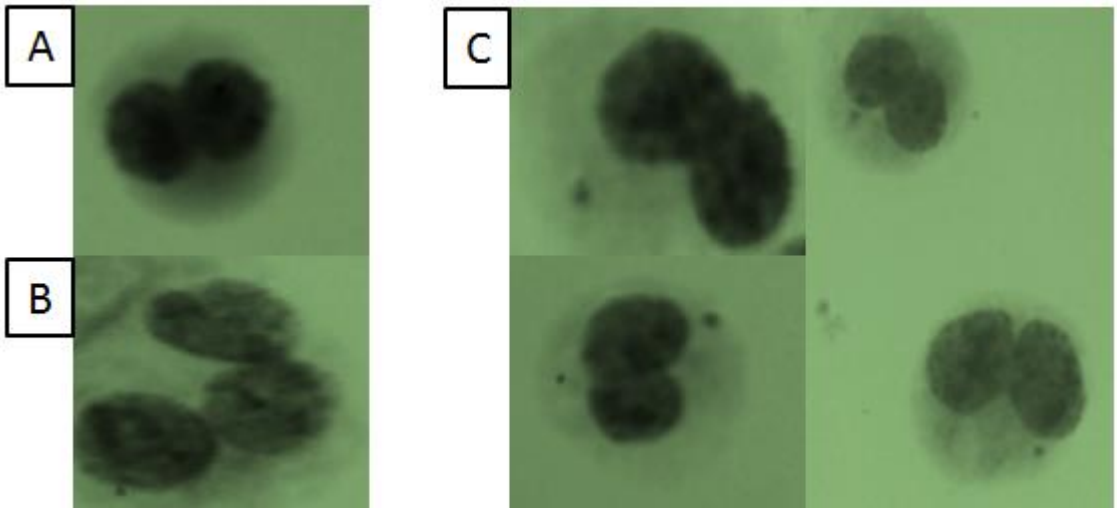

Figure 4.10) *Images obtained from GM1775 (Homozygous) lymphoblastoid cell line stained with Giemsa in the scoring of binucleated cells A) A binucleated cell b) Trimucleated cell excluded from analysis C) Examples of Micronuclei.*

Our analysis revealed that control and heterozygous cell lines have a lower level of MN than GM01775 and GM03193 cell lines (Figure 4.11). The basal level of MN was significantly higher in homozygous cell lines compared to the normal and heterozygous cell lines. Interestingly, this significance is lost at 0.5 Gy (Fig 4.11). However, at higher doses of 1.0 Gy and 2.0 Gy the significant difference between normal and DC cells is regained (Fig 4.11). It is important to stress that when the basal levels of MN are removed from the dose of 2.0 Gy which resulted in the highest level of DNA damage the difference between the normal and DC lines is lost (figure 4.11). For example, the significant different between DC lines and normal at 2Gy is the same significant at the basal level Therefore, using the MN assay we were not able to confirm the difference in DNA damage response between normal and DC cell lines.

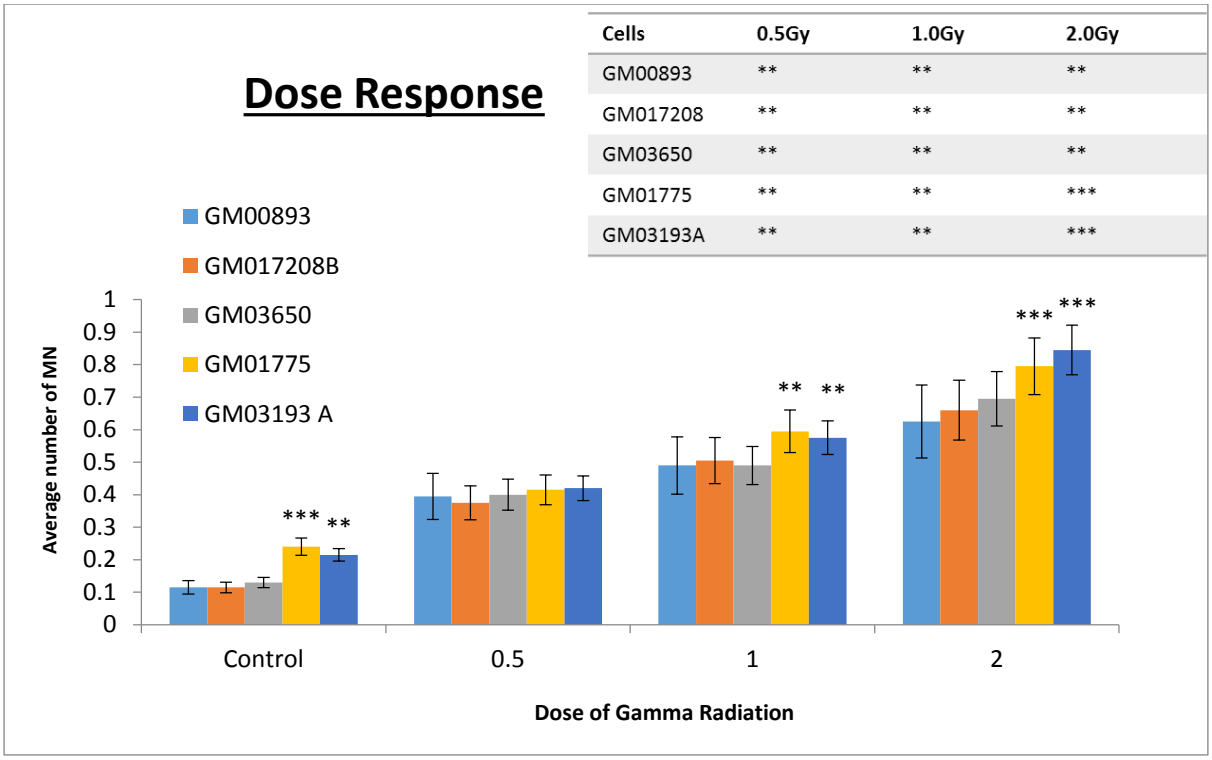

*Figure 4.11) Frequencies of MN in 0.5 Gy, 1.0 Gy and 2.0 Gy doses of gamma radiation for DC cell lines compared to control obtained after 48 hours. The inset shows comparison of MN for each dose against unirradiated samples. Stars above bars indicate comparison between DC and control cell lines. *P<0.05 **P<0.01 ***P<0.001 versus control. Error bars represent SEM.*

4.4 Anaphase bridges in normal and DC Lymphoblastoid cell lines.

We quantified anaphase bridges in all lymphobastiod cell lines following irradiation with the dose of 1.0 gamma rays 48 h after irradiation (Figure 4.12). Examples of Anaphase Bridges are shown in figure 4.13.

The basal level of anaphase bridges was higher in DC homozygous cell lines relative to the rest of cell lines (Fig 4.12). In contrast to the MN analysis the frequency of anaphase bridges was significantly higher in the homozygous DC cell lines after irradiation relative to control lines (Fig 4.12). Therefore, unlike the MN assay the anaphase bridge analysis confirmed defective DNA damage response in DC cells. We cannot rule out the possibility that the MN assay we used is sub-optimal for detecting DNA damage given

that all other assays used clearly indicate differences between homozygous DC cell lines and control or heterozygous cell lines.

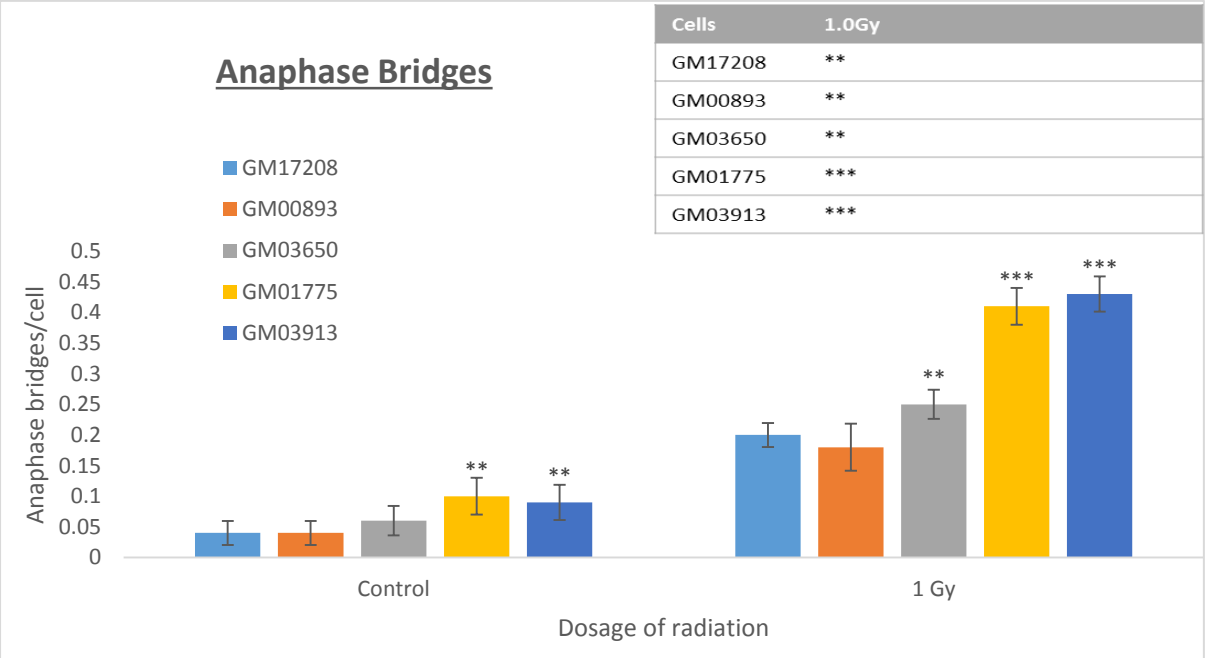

*Figure 4.12) Frequencies of Anaphase Bridges in untreated and treated doses of gamma radiation (1 Gy) for DC cell lines compared to control. The inset shows comparison of Anaphase Bridges for each dose against unirradiated samples. Stars above bars indicate comparison between DC and control cell lines. *P<0.05 **P<0.01 ***P<0.001 versus control. Error bars represent SEM.*

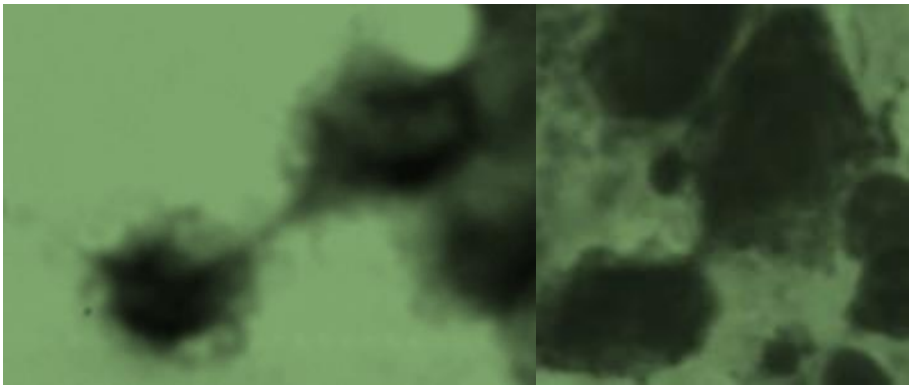

Figure 4.13) Images obtained from GM1775 (Homozygous) lymphoblastoid cell line stained with Giemsa to score on Anaphase bridges, as a consequence of telomere end to end fusion.

4.5 Analysis of Anaphase bridges in DC lymphocytes

While doing the above analysis we received a request from a clinic investigating a new DC patient to perform cytogenetic analysis on the lymphocytes from this patient. We also received the material from two control patients of similar ages. Thus our three samples are identified as follows: W1202626 and W1202625 (control lymphocytes) and W12022568 (Lymphocytes from a DC patient). The samples were not processed in our laboratory but sent to us as cells in the standard cytological fixative after chromosome preparation procedure. The number of metaphase spreads in the sample from a DC patient was low and we could only analyse 25 metaphases for chromosomal aberrations. However, it was difficult to observe them as the metaphase were not spread effectively and we were unable to quantify them. The reason could be the suboptimal concentration of KCL for this cell type or suboptimal incubation period with the same. We had a similar problem with our DC lymphoblastoid cell lines. Numerous attempts to achieve a suitable level of well-spread mitotic cells failed. Otherwise, it would have been interesting to observe whether DC lymphocytes have elevated frequencies of spontaneous chromosomal aberrations, as previous studies demonstrated (Pai et al 1989; Coulthard et al 1998).

Having said that, we analysed anaphase bridges from the same set of cells using FISH with the PNA telomeric probe labelled with Cy3. Examples of late anaphase – early telophase cells observed are shown in Fig 4.14. The analysis revealed a statistically significant difference between the DC patient lymphocytes and control lymphocytes thus further substantiating the notion that DNA damage response in DC cells is defective judging by the high frequencies of spontaneous anaphase bridges (Fig 4.15).

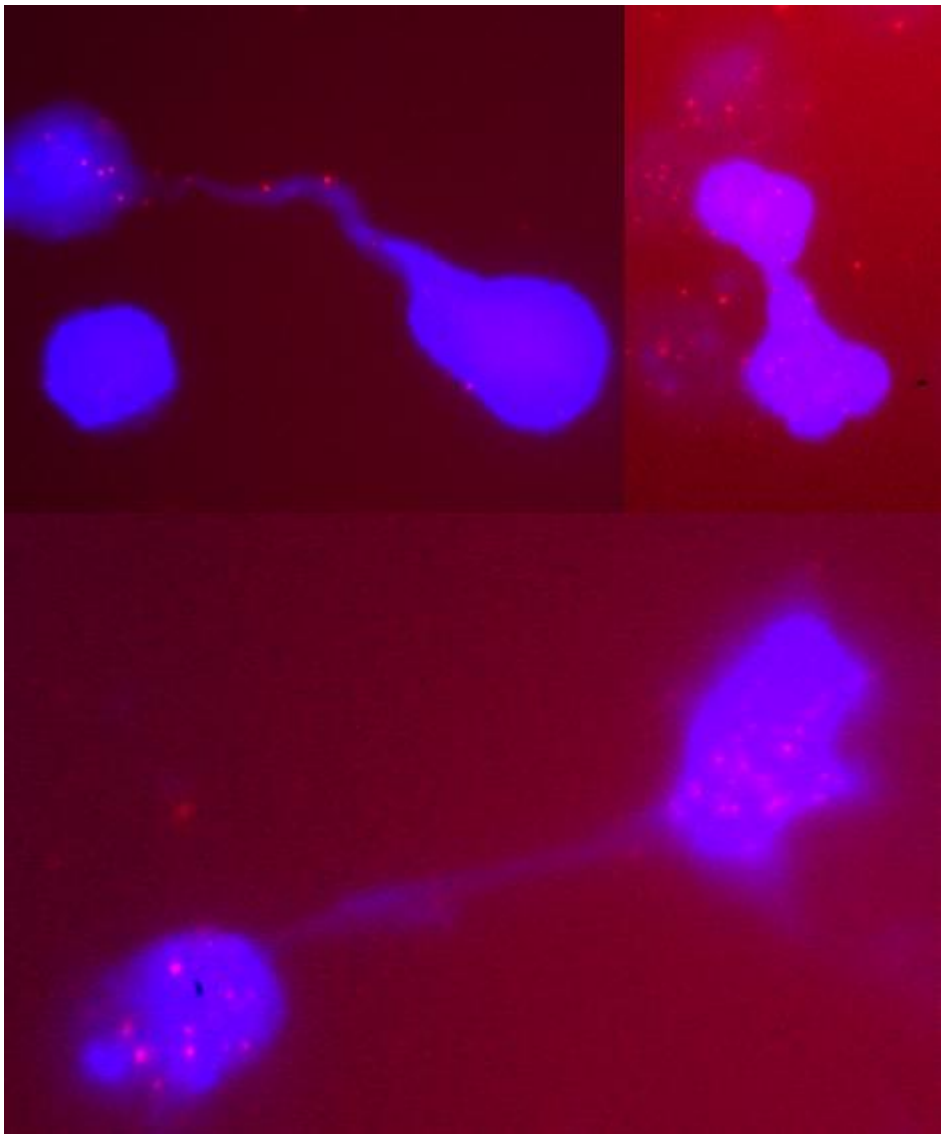

Figure 4.14) Examples of Anaphase bridges in Lymphocytes cells. The cells were captured in late anaphase-early telophase. Note the presence of red fluorescence. Telomeres were detected by $(AATCCC)_3$ probe labelled with Cy-3.

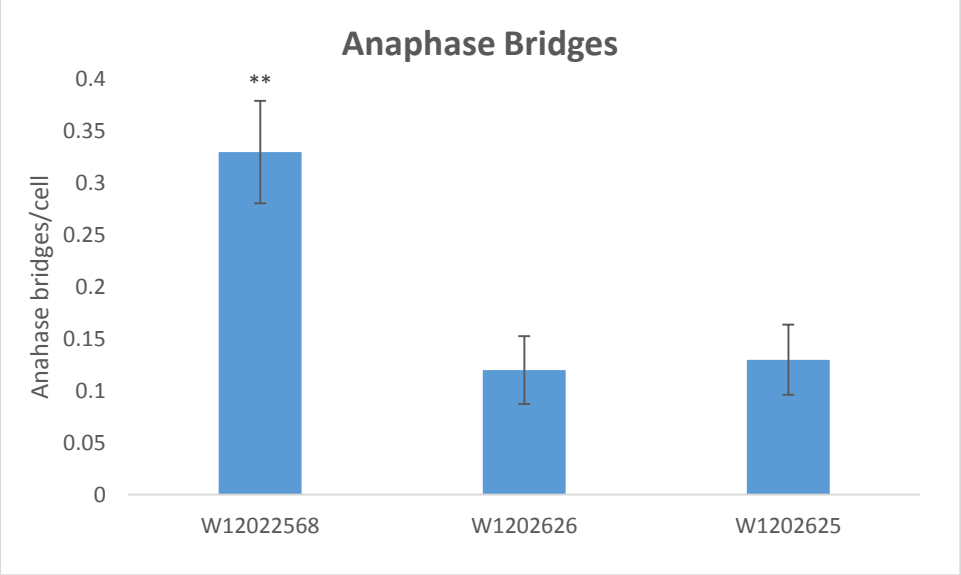

*Figure 4.15) Anaphase bridge frequencies in DC lymphocytes.. Statistical significance for Anaphase bridges of DC cell lines with respect to control cell line at each dose rate was evaluated. *P<0.05 **P<0.01 ***P<0.001 versus control. Error bars represent SEM.*

4.6 Discussion

Results presented in this chapter generally support the main findings from the previous chapter, in that lymphoblastoid cell lines from two DC patients with homozygous *DKC1* mutations show a defective DNA damage response relative to control cell lines and a single cell line from a DC patient with a heterozygous mutation. The only test which did not reproduce the difference between two sets of cell lines was the MN assay (Fig 4.11). It is possible that the MN assay in our hands is sub-optimal and that further modification of the protocol is required in order to capture differences existing between cell lines when analysed using other tests. It is important to note that in the case of fibroblast cells the difference in the frequency of MN between control and DC cells was significant, further supporting the notion that the MN test for lymphoblastoid cells in our hands may be sub-optimal.

Kirwan et al (2011) suggested that DNA damage response is normal in T lymphoctyes from their DC patients, after treatment of cells with the DNA damaging agent, etoposide. A total of 6 patient samples were used, with two of the samples being from patients with *DKC1* mutations and the rest being controls. Their analysis failed to identify differences between DC and control samples. The most important missing part in their study the analysis of DNA damage kinetics. They only analysed DNA damage immediately after exposure of cells to the genotoxic treatment.

By contrast, our results contradict those generated by Kirwan et al (2011). First, we found a clear difference in dose response between DC and control cells (Fig 4.2). Second, we found a clear difference in the repair kinetics of DNA damage between DC and control cells (Figure 4.5). Furthermore, anaphase bridge analysis revealed a similar situation (Fig. 4.12-4.15). Therefore, as in the previous chapter in which we analysed DC fibroblasts, our results suggest that DC lymphoblastoid cells show a defective DNA response. Pai et al (1989) studied DC lymphocytes and lymphoblasts cells, and they found that DC lymphocytes exposed to bleomycin showed higher levels of chromosomal abnormalities (CA) compared to normal cells, a finding in line with our results.

Interestingly, Coulthard et al (1998) found that treatment with various of clastogens including IR failed to generate significant differences in chromosomal breakage between DC and normal controls. It is therefore possible that responses from cells originating from different patients may differ in terms of DNA damage response at chromosomal level. Unfortunately we were not able to detect and observe CAs in our cell lines (Lymphobastiod and lymphocytes) as firstly, we were unable to get a good mitotic index and secondly, the metaphase spreads were not suitable for a reliable analysis. Having said that, we were able to observe a defective DNA damage response in

DC cells using more sophisticated assays such as the analysis of ɣH2AX foci. Similarly, the findings presented by Gu et al (2008), indicate that MEFs with the mutant *Dkc1* show much higher levels of ɣH2AX foci after genotoxic stress compared to cells expressing wild type Dyskerin, which is in line with our findings (Figure 4.1-4.6). Furthermore, a more recent study using exactly the same set of DC fibroblast cell lines used by us and a sophisticated methodology agreed with our findings (Manguan-Garcia, et al 2014).

As expected, we found that telomere length varies between cell lines (Fig 4.8) with DC cells having shorter telomeres and greater rate of telomere loss (Fig 4.8). Unfortunately, we have been unable to use the telomerase assay to show that shortening of telomeres in DC lymphoblastoid cell lines is caused by lower or absent telomerase activity. *DKC1* is an important component of the telomerase enzyme (Armanios and Blackburn 2013, and it is active in lymphocytes (Oeseburg et al 2010) indicating that *DKC1* mutation in DC lymphobastiod cell lines would lead to the decreased levels of telomerase activity as we observed shorter telomere lengths in these cells.

In summary our results conclusively show that GM1775 (*DKC1* -/-) and GM3193 (DKC -/-) cell lines exhibit a defect in cellular response to DNA damage which is in line with what we have observed with DC fibroblast cell line in Chapter 3. Therefore, this establishes that, the *DKC1* gene contributes to the DNA damage response, strengthening the hypothesis of the functional interplay between DNA damage response and telomere maintenance.

Chapter 5 Effects of *DKC1* knockdown on DNA Damage Response

5.1 Introduction

In the previous two chapters we demonstrated that cells derived from DC patients, defective in DKC1, showed a defective DNA damage response relative to control cells. This was apparent across two different cell types, primary fibroblasts and immortalized lymphoblastoid cells, when these were assessed for their capacity to respond to DNA damage using several different assays. Our results are consistent with some published studies. For example, DC fibroblasts showed sensitivity to IR when assessed with the G2 assay (DeBauche et al 1990), a cytogenetic test that detects chromatid type damage in metaphase cells (Parshad et al 1983). Similarly, when lymphocytes from a patient suffering from the most severe form of DC, also known as the Hoyeraal-Hreidarsson syndrome, were exposed to genotoxic stress they showed hypersensitivity indicating a defective DNA damage response (M'kacher et al 2003). Another study reported sensitivity of a DC patient to radiation therapy (Cengiz et al 2004) thus adding further evidence to the notion that DNA damage response in DC cells is defective. This notion was confirmed in the case of a mouse DC model which was characterized by a defective DNA damage response (Gu et al 2008).

However, the above studies were contradicted by Kirwan et al (2011) reporting a normal DNA damage response in cells from DC patients. For the reasons outlined earlier (see page 92) we think that the study by Kirwan et al (2011) is misleading because it was based on the version of the H2AX assay that is oversimplified and it failed to analyse DNA repair kinetics in DC cells.

Therefore, the next logical step in our study was to see whether the defective DNA damage response that typifies DC cells can be reproduced in normal cells when the *DKC1* gene is knocked-down by RNAi.

The knock-down experiments in our laboratory were initially carried out by the previous PhD student, Maryam Ojani. However, she carried experiments only once without reproducing them. Therefore, her results were considered preliminary. My task was to continue the initial experiments with the aim of completing this part to the conclusion with sufficient experimental repeats to ensure reproducibility and completeness of results. The key cell line for the experiments was the normal primary fibroblast cell line, GM08399. However, we used the HeLa cell line and the U2OS cell line for primer optimization in order to carry out knockdown experiments. We used Dharmacon Smart Pool siRNA approach as this approach worked well before in our laboratory.

Before proceeding to the actual knock-down experiments it was important to optimise the primers concentration in HeLa and U20S cell lines using Real-Time PCR. The optimization step excluded primary fibroblasts because they grew much slower than established cell line thus significantly delaying the preparatory efforts. Nevertheless, there is no reason to doubt that the same primers will work in fibroblasts. The optimisation of primers concentration and the complete protocol for the knockdown is described fully in chapter 2.

The quality control to ensure efficient delivery of the siRNA oligonucleotides into the cells by knock-down of the housekeeping gene GAPDH was done in our lab by M. Ojani. This was done in order to ensure the delivery of siRNA oligonucleotides was effective. She found the expression of GAPDH was reduced to between 20% and 40% and the effect lasted up to 72 hrs (see PhD thesis by M. Ojani).

5.1 Knock-down of DKC1 through siRNA

Having optimised the primer concentration and verified the initial steps required for Q-PCR the next step was to start the RNAi procedure and introduce Si(small interfering) RNA oligonucleotides into cells, verify the gene expression using quantitative Real Time PCR and western blot, and probe the phenotype using ɣH2AX, TIF, IQ-FISH and MN assays.

We started with the knock-down experiments using HeLa, U20S and GM08399 cell lines. Cocktails of siRNA oligonucleotides were transfected into cells as described (Chapter 2). DKC1 expression was measured by real time PCR at 4 different time points after transfection. The experiment was preformed twice in order to ensure reproducibility of results. Figures 5.1 and 5.2 show pooled results from two experiments.

The lowest expression of DKC1 was obtained 48 hours after transfection in the U20S cell line with the 85% knockdown. The lowest obtained expression of DKC1 in Hela and GM08399 cell lines were at the 72 hours' time-point with the expression of DKC1 reduced by 77% and 62 % respectively. As time progressed the expression of *DKC1* started to recover and a strong recovery was reached 7 days after transfection as expected (Figure 5.2). A scrambled siRNA was used as a negative control to show that the knock-down was not random and was due to degradation of target mRNA (Figure 5.2).

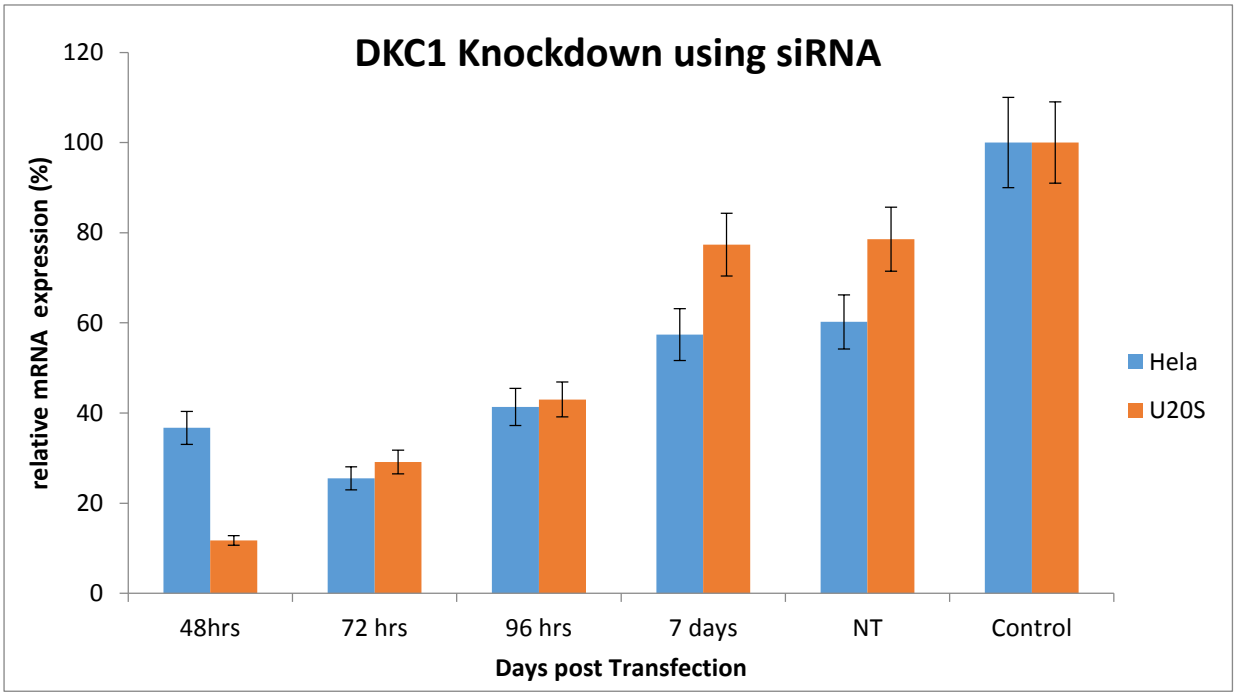

Figure 5.1) DKC1 expression at different time points after transfection with HeLa and U20S cell lines. Relative quantities (RQ) of DKC1 mRNA assessed by quantitative real time PCR after various times following transfection with siRNA oligonucleotides specific for DKC1. Additional controls, ensuring reliable results, were cells treated with only transfection reagent and cells treated with non-targeting siRNA. NT-non targeting control; Control -Transfection only (transfection reagent with no siRNA oligonucleotides). A 85 % knock-down was achieved 48 hrs after transfection in the U20S cell line and 77% knock-down was achieved 72 hours after transfection in the HeLa cell line.

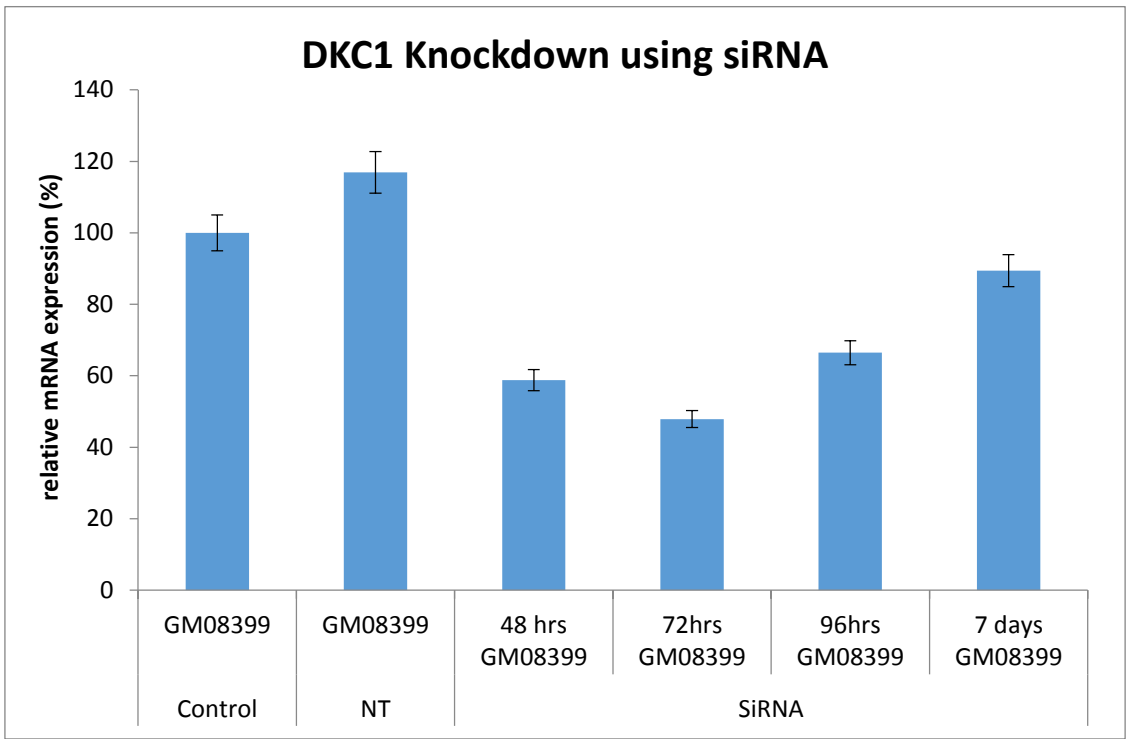

Figure 5.2) *DKC1 expression at different time points after transfection in GM08399 fibroblasts. Relative quantities (RQ) of DKC1 mRNA assessed by quantitative real time PCR after various times following transfection with siRNA oligonucleotides specific for DKC1. Additional controls, ensuring reliable results, were cells treated with only transfection reagent and cells treated with non-targeting siRNA. NT-non targeting control; Transfection only – transfection reagent with no siRNA oligonucleotides. A 62 % knock-down was achieved 72 hrs after transfection*

To confirm the knock-down at the protein level we use Western blot (Figure 5.3) for GM08399 human fibroblast. Densitometry analysis using ImageJ software showed that there was a 62% reduction at 72 hrs and 76% reduction at 96 hrs in DKC1 (Figure 5.4). It has been shown that mRNA are produced at a lower rate compared to proteins in mammalian cells, and mRNA are less stable than proteins (approximately half-life of 7 hours for mRNA versus 48 hours for proteins) (Vogel and Marcotte 2012). This is confirmed in our results when quantifying mRNA and protein after transfection, where mRNA levels start to come back to normal at 96 hours and protein levels were reduced at 96 hours. Taken together, our results show that the DKC1 expression was reduced at 72 and 96 hours post-transfection. The expression was recovered after 7 days.

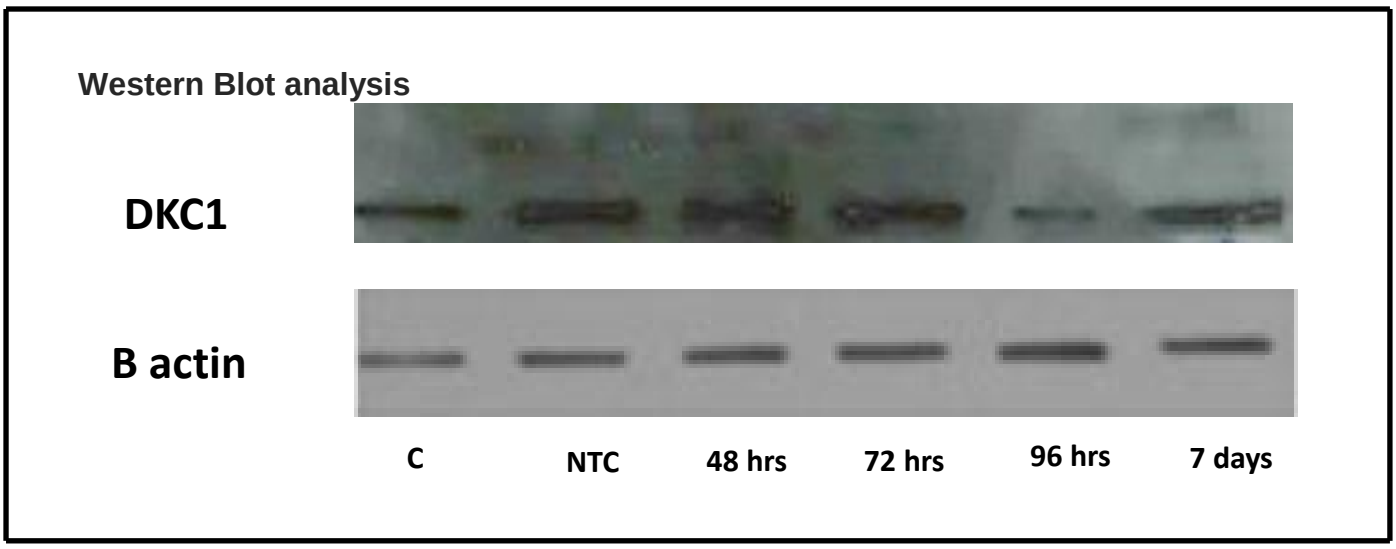

Figure 5.3) Western blot analysis of DKC1 *expression following transfection with siRNA oligonucleotides.*

The level of β-actin protein expression confirms equal protein loading in GM08399. Additional controls, ensuring reliable results, were cells treated with only transfection reagent (WT) and cells treated with non-targeting siRNA (NTC). Densitometry analysis shows a 62% reduction at 72 hrs and 76% reduction at 96 hrs in Dyskerin levels in the normal fibroblast cell line.

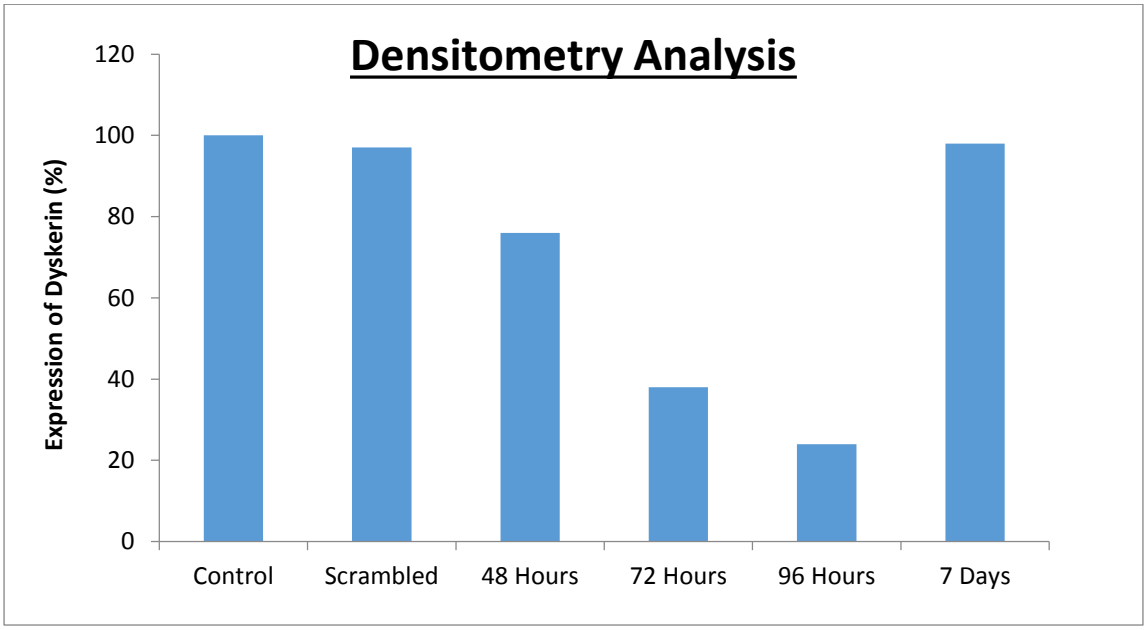

Figure 5.4) Densitometry Analysis showing the expression of Dyskerin post transfection. The lowest level is achieved is at 96 hours expressing only 24% of the control value.

.

5.2 Elevated DNA damage after DKC1 knockdown in the normal fibroblast cell line

Having verified the *DKC1* knockdown in the normal fibroblast cell line, we next investigated the efficiency of DNA damage response at post-transfection points showing the lowest expression of *DKC1* e.g. 72 and 96 h post-transfection (Fig 5.5-5.12). In brief, we transfected cells with siRNA oligonucleotides and waited for 72 and 96 hrs at which points we irradiated cells with 1.0 Gy of gamma rays and assessed the relevant phenotype: the DNA damage response efficiency using the same methods as in the previous two chapters.

In order to check the DNA damage response upon depletion of DKC1, we first probed the phenotype using GM08399 cells that had the lowest expression observed at 72 hours after transfection (Figure 5.2) with the expression reduced by 62%. In addition, we examined the phenotype 96 hours post-transfection as the lowest protein level was observed with a reduction at 76 % (Figure 5.3 and 5.4). Immunocytochemical analysis based on detecting the phosphorylated form of histone H2AX (ɣH2AX) was used to compare the DNA damage response at both time points as well as TIF assays (combination of ɣH2AX detection with detection of telomeric repeat sequences) used to compare DNA damage at telomeres. We also analysed the average telomere length at both time points using IQ-FISH protocol in order to determine if the telomere length was affected post-transfection.

All experiments were carried out using the same protocols as in the previous chapters In brief, GM08399 cells were transfected with siRNA oligonucleotides and left for 72 hours or 96 hours depending on which time point post-transfection is to be examined. At the required time point, cells were irradiated for either dose response (0.25 Gy, 0.5 Gy and 1.0 Gy) or with the dose of 1.0 Gy of gamma rays for the repair kinetics curve. When generating a dose response curve ɣH2AX and TIF assays, we processed the

samples 30 minutes after irradiation. However, when generating a repair kinetics curve, cells were left to incubate for 30 minutes, 5 hours, 24 hours and 48 hours intervals after irradiation. A non-template siRNA control oligonucleotides were also used to represent scrambled siRNA (labelled as Scrambled). Images with DNA damage foci observed are shown in Figure 5.15, using cells transfected with DKC1 siRNA oligonucleotides. Thus, the following samples were included (i) unexposed GM08399 cells to serve as a negative control for irradiation, (ii) GM08399 cells transfected with scrambled oligonucleotides to serve as a control for knock-down and (iii) irradiated GM08399 cells with no transfection to serve as a positive control for radiation and (iv) irradiated and transfected GM08399 cells to serve as the key test in the experiment. Dose response curves are shown in Figure 5.5 – 5.8. Repair kinetics curves are shown in figure 5.9–5.12.

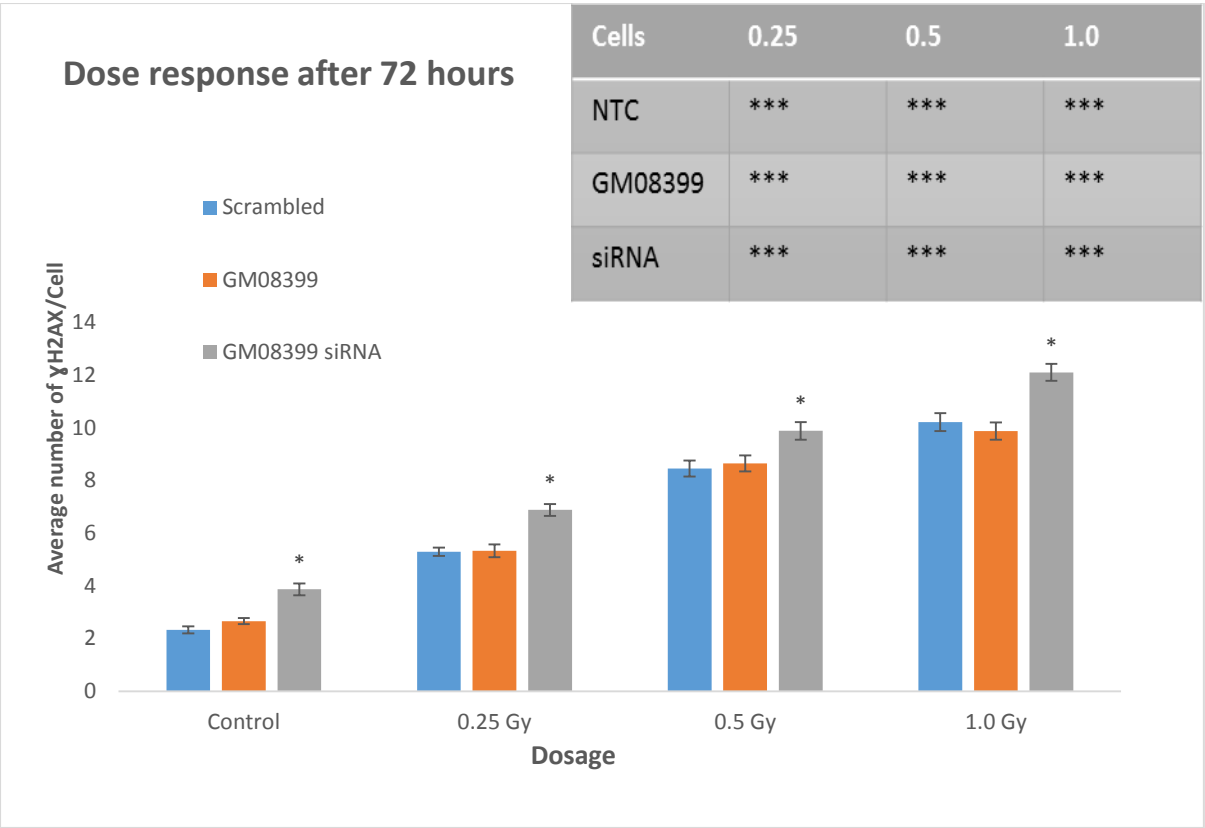

*Figure 5.5) Frequencies of γH2AX positive foci in 0.0, 0.25, 0.5 and 1.0 Gy doses of gamma radiation for transfected cell line with control cell line (GM08399) at 72 hours post transfection. The inset shows comparison of DNA damage foci for each dose against unirradiated samples. Stars above bars indicate comparison between transfected cell lines and control cell lines. *P<0.05 **P<0.01 ***P<0.001 versus control Error bars indicate SEM.*

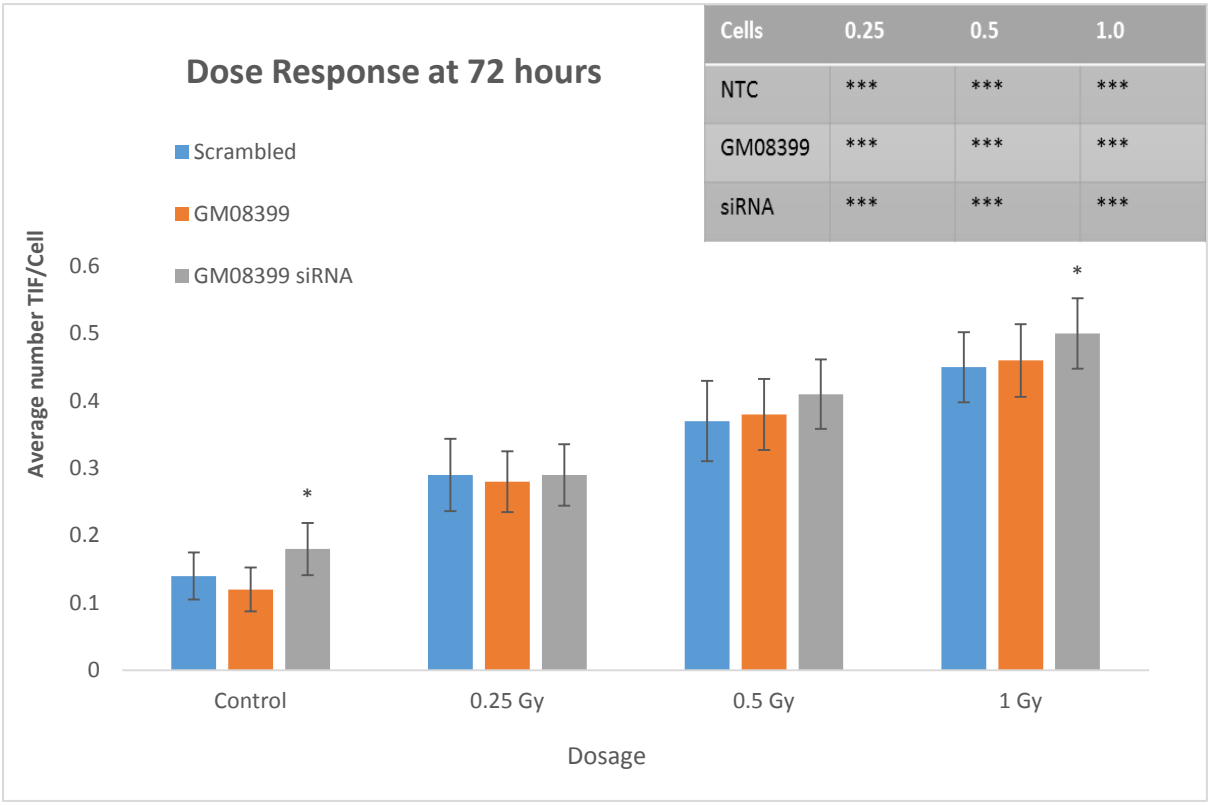

*Figure 5.6) Frequencies of TIF foci in 0.0, 0.25, 0.5 and 1.0 Gy doses of gamma radiation for transfected cell line with control cell line (GM08399) at 72 hours post transfection. The inset shows comparison of TIF foci for each dose against unirradiated samples. Stars above bars indicate comparison between transfected cell lines and control cell lines. *P<0.05 **P<0.01 ***P<0.001 versus control Error bars indicate SEM.*

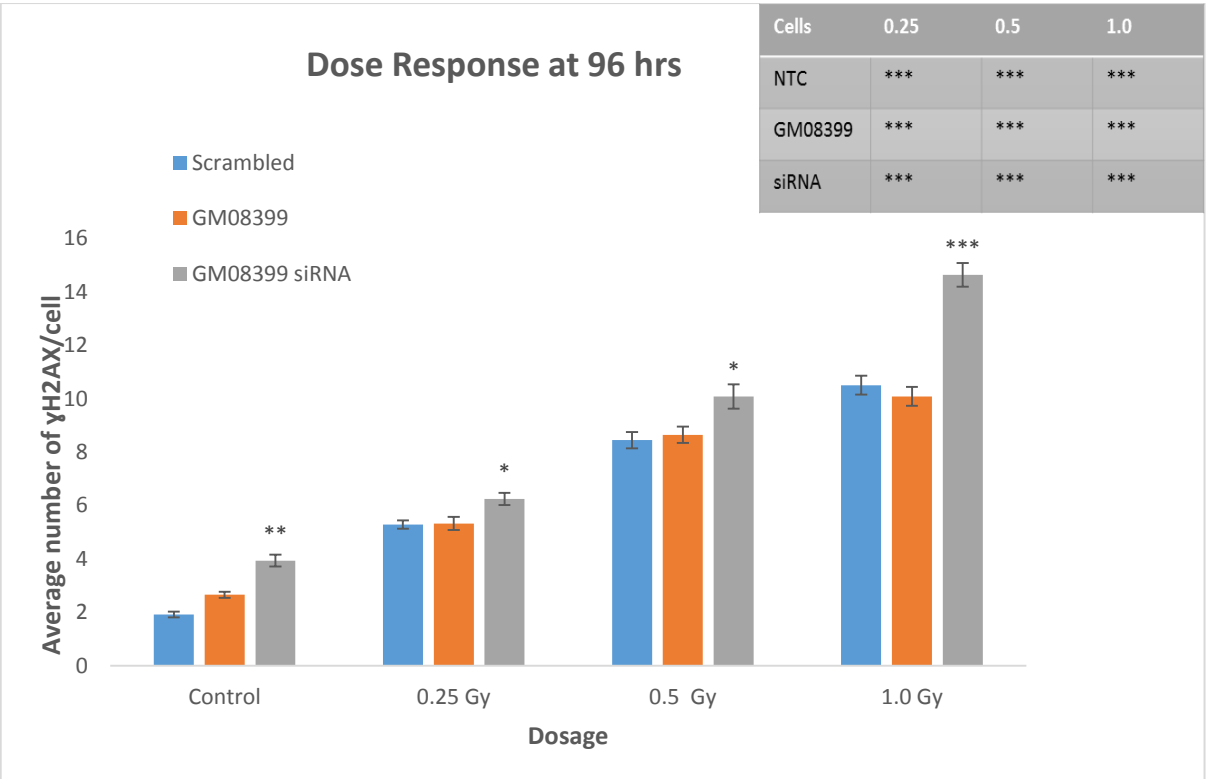

*Figure 5.7) Frequencies of γH2AX positive foci in 0.0, 0.25, 0.5 and 1.0 Gy doses of gamma radiation for transfected cell line with control cell line (GM08399) at 96 hours post transfection. The inset shows comparison of DNA damage foci for each dose against unirradiated samples. Stars above bars indicate comparison between transfected cell lines and control cell lines. *P<0.05 **P<0.01 ***P<0.001 versus control Error bars indicate SEM*

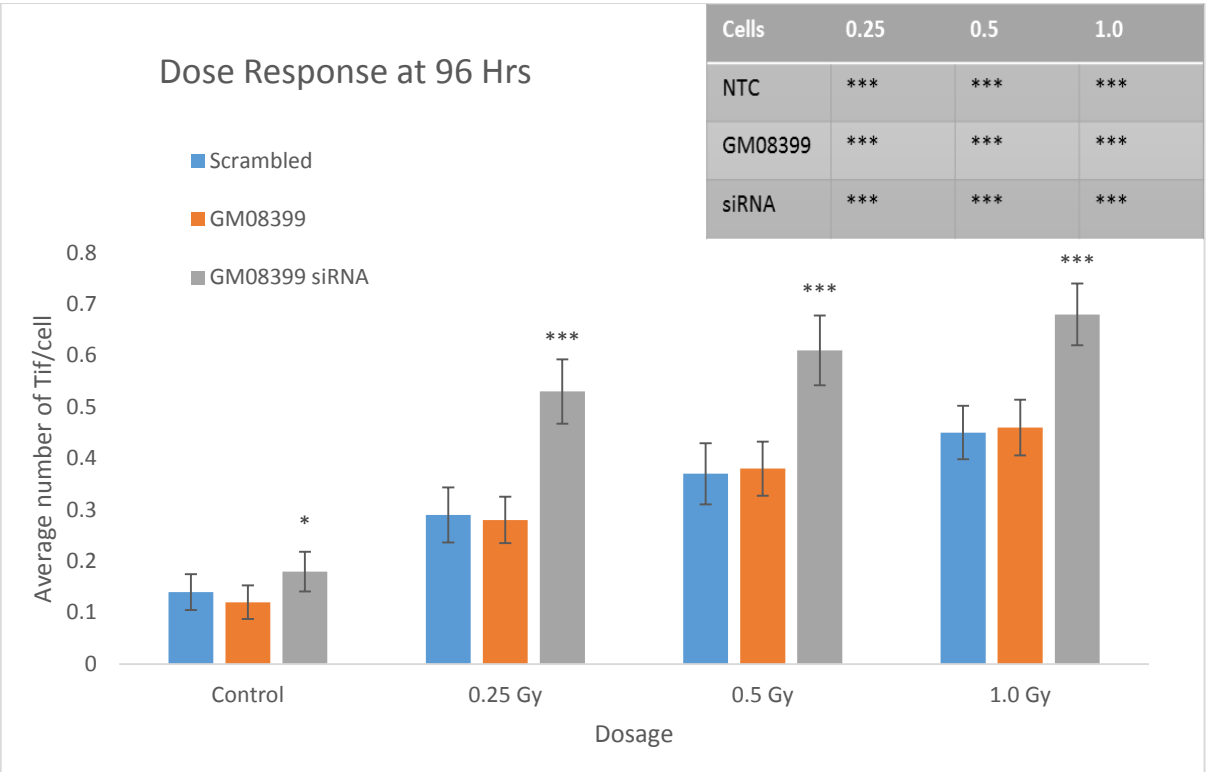

*Figure 5.8) Frequencies of TIF foci in 0.0, 0.25, 0.5 and 1.0 Gy doses of gamma radiation for transfected cell line with control cell line (GM08399) at 96 hours post transfection. The inset shows comparison of TIF for each dose against unirradiated samples. Stars above bars indicate comparison between transfected cell lines and control cell lines. *P<0.05 **P<0.01 ***P<0.001 versus control Error bars indicate SEM.*

At the time-point of 72 hrs we observed a typical dose-response pattern i.e. increase of DNA damage foci and TIFs with the dose of irradiation (Figures 5.5 and 5.6). However, statistical analysis failed to detect differences between samples transfected with scrambled oligonucleotides and DKC1 oligonucleotides at some doses in the case of TIF analysis (Figures 5.6). However, at the 96 hrs time-point differences between relevant samples were more pronounced and in the case of all TIF samples differences were statistically significant at all doses of irradiation (Figures 5.7-5.8). These results are in line with the western blot results showing the lowest expression of DKC1 at the 96 hours post-transfection time point post (Figure 5.3-5.4).

5.3 Repair of DNA damage following the knock-down

The analysis of repair kinetics has revealed similar differences between the 72 and 96 hrs post-transfection time points. The 72 hrs post-transfection time point showed efficient repair even in the case of cells transfected with siRNA DKC1 oligonucleotides as there was no statistically significant differences between non radiated cells and those irradiated and monitored 48 h post-irradiation (Fig 5.9-5.12). This suggests that the reduction in DKC1 expression is insufficient to alter the repair kinetics, the result in line with the Western blot analysis which showed smaller reduction in DKC1 expression at 72 hrs relative to 96 hrs time point (Fig 5.3 -5.4). In line with this speculation the analysis carried out at the 96 hrs time point showed statistically significant differences between relevant samples at the end of monitoring period of 48 hrs suggesting the presence of unrepaired DNA damage either in the whole genome or only at telomeres (Figures 5.10 & 5.12). The presence of residual DNA damage 48 hrs after irradiation is normally taken as the sign of a defective DNA damage response.

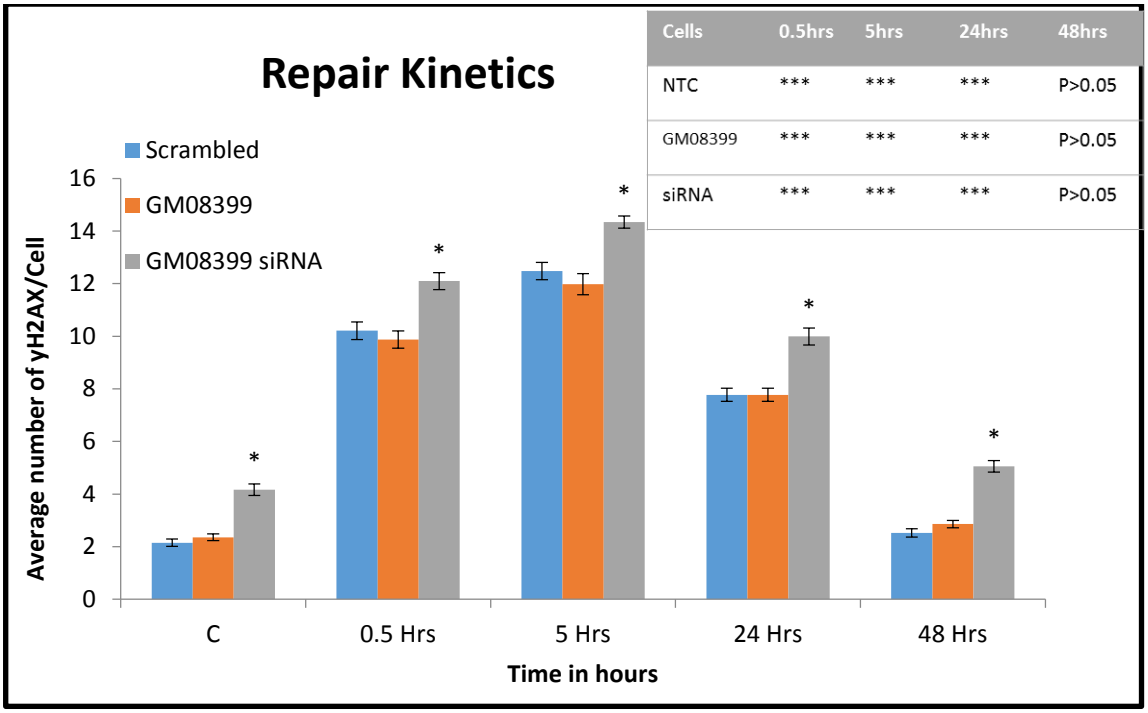

*Figure 5.9) Frequencies of γH2AX positive foci in untreated and 1.0 Gy doses of gamma radiation for transfected cell line with control cell line (GM08399) 72 hours post transfection. The inset shows comparison of DNA damage foci for each time point against unirradiated samples. Stars above bars indicate comparison between transfected cell lines and control cell lines. *P<0.05 **P<0.01 ***P<0.001 versus control Error bars indicate SEM.*

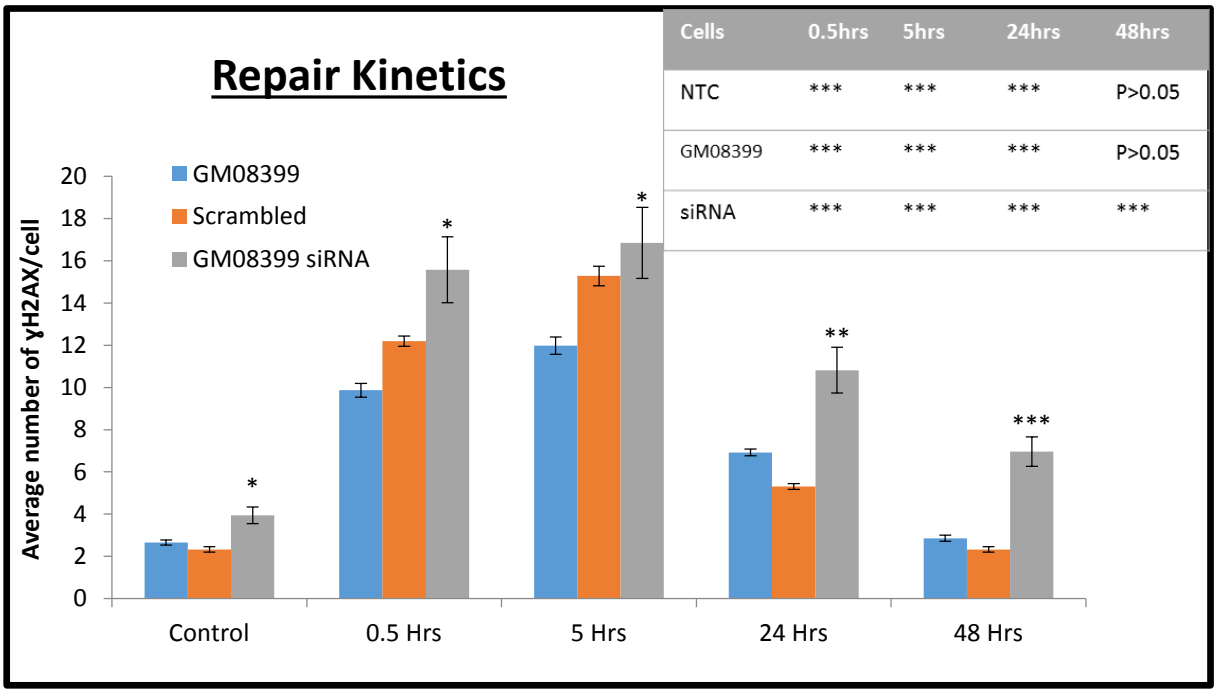

*Figure 5.10) Frequencies of γH2AX positive foci in untreated and 1.0 Gy doses of gamma radiation for transfected cell line with control cell line (GM08399) 96 hours post transfection. The inset shows comparison of DNA damage foci for each time point against unirradiated samples. Stars above bars indicate comparison between transfected cell lines and control cell lines. *P<0.05 **P<0.01 ***P<0.001 versus control. Error bars indicate SEM.*

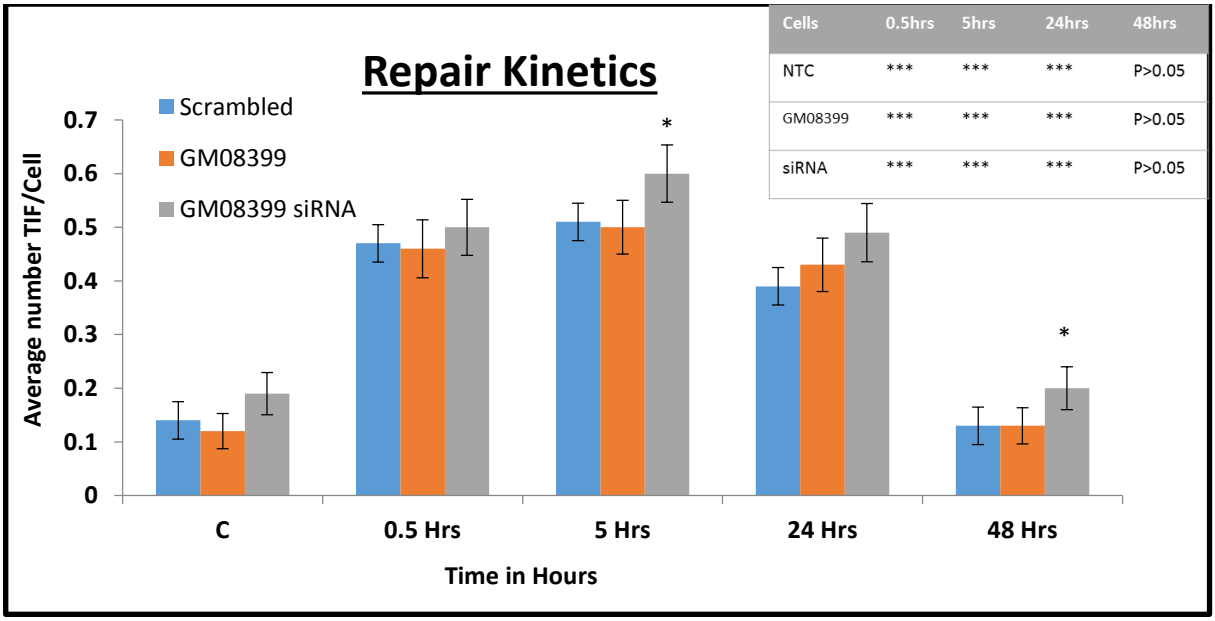

*Figure 5.11) Frequencies of TIF positive foci in untreated and 1.0 Gy doses of gamma radiation for transfected cell line with control cell line (GM08399) 72 hours post transfection. The inset shows comparison of TIF foci for each time point against unirradiated samples. Stars above bars indicate comparison between transfected cell lines and control cell lines. *P<0.05 **P<0.01 ***P<0.001 versus control. Error bars indicate SEM.*

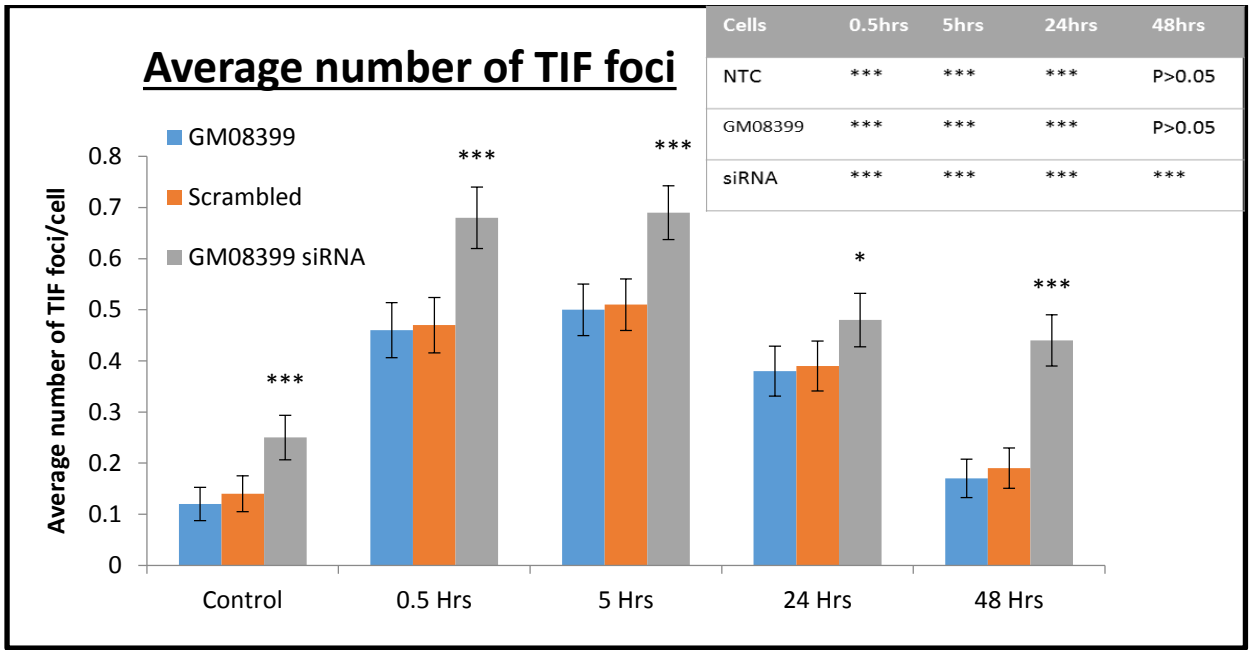

*Figure 5.12) Frequencies of TIF foci in untreated and 1.0 Gy doses of gamma radiation for transfected cell line with control cell line (GM08399) 96 hours post transfection. The inset shows comparison of TIF foci for each time point against unirradiated samples. Stars above bars indicate comparison between transfected cell lines and control cell lines. *P<0.05 **P<0.01 ***P<0.001 versus control. Error bars indicate SEM.*

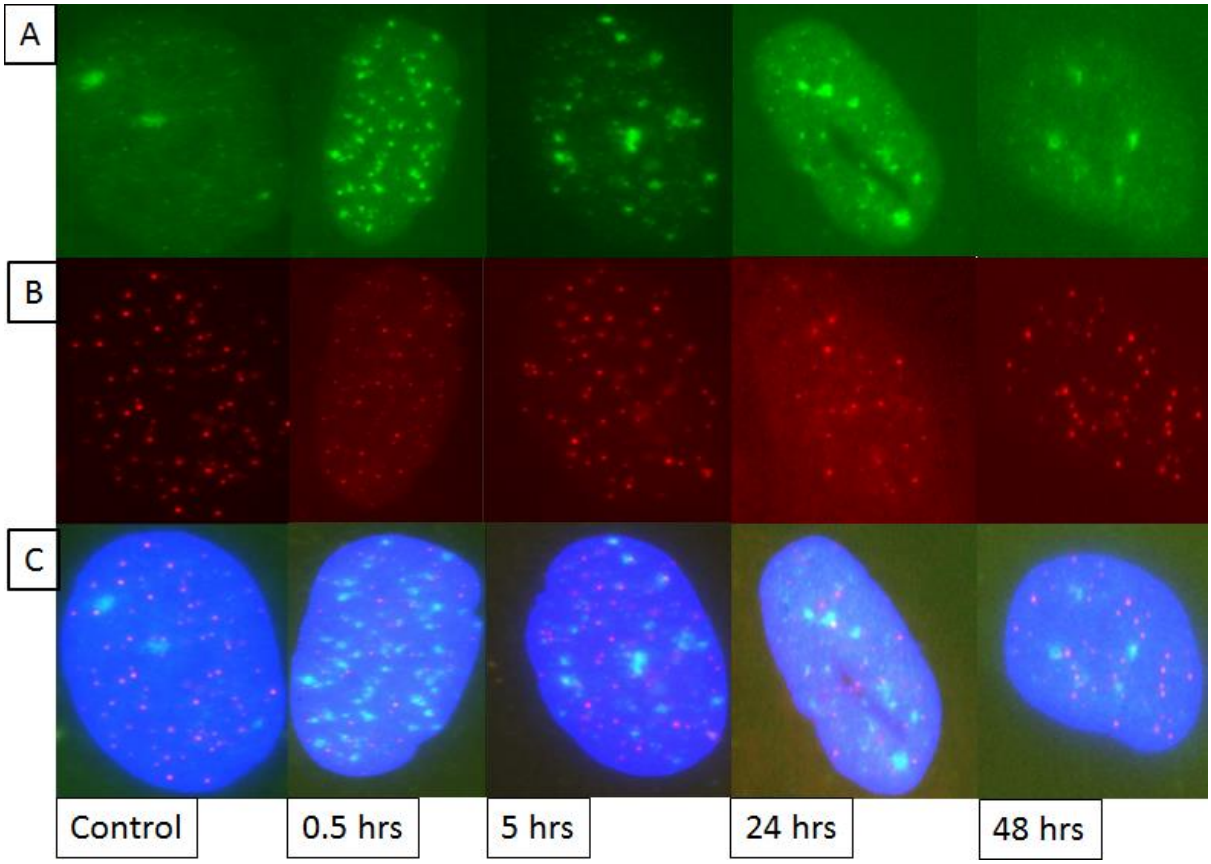

Figure 5.13) Images obtained from nuclei of the transfected cell line with siRNA oligonucleotides, after irradiation with gamma rays at 1.0Gy dose at different time points. A) detection of DNA damage γH2AX foci. B) Telomeres were detected by $(AATCCC)_3$ probe labelled with Cy-3 (red) C) Colocalization with γH2AX and telomeres represent a TIF (merged), visible as yellow spots. The nucleus was counterstained with Dapi.

5.4 DNA Damage response in HeLa and U20S upon DKC1 knockdown

As part of quality control, we also measured ɣH2AX in HeLa and U20S cells post transfection as we wanted to probe the efficiency of the siRNA transfection. Since we observed unrepaired DNA damage in DC cells 48 hrs after irradiation (Chapter 3 and 4) and elevated DNA damage response at 1 GY (Chapter 3 and 4) which is potentially indicative of a defective DNA damage response we decided to plan the experiment to take into account this point. We generated dose response and repair curves upon IR with gamma rays (Figure 5.14-5.15). In the case of HeLa cells the lowest expression was 23% and this expression was observed 48 hrs after transfection with siRNA oligonucleotides (Figure 5.1). In the case of U2OS cells the lowest expression was 15% and it was observed 72 h after transfection (Figure 5.1). We have selected exclusively

the above time points in each cell line respectively and examined DNA damage response.

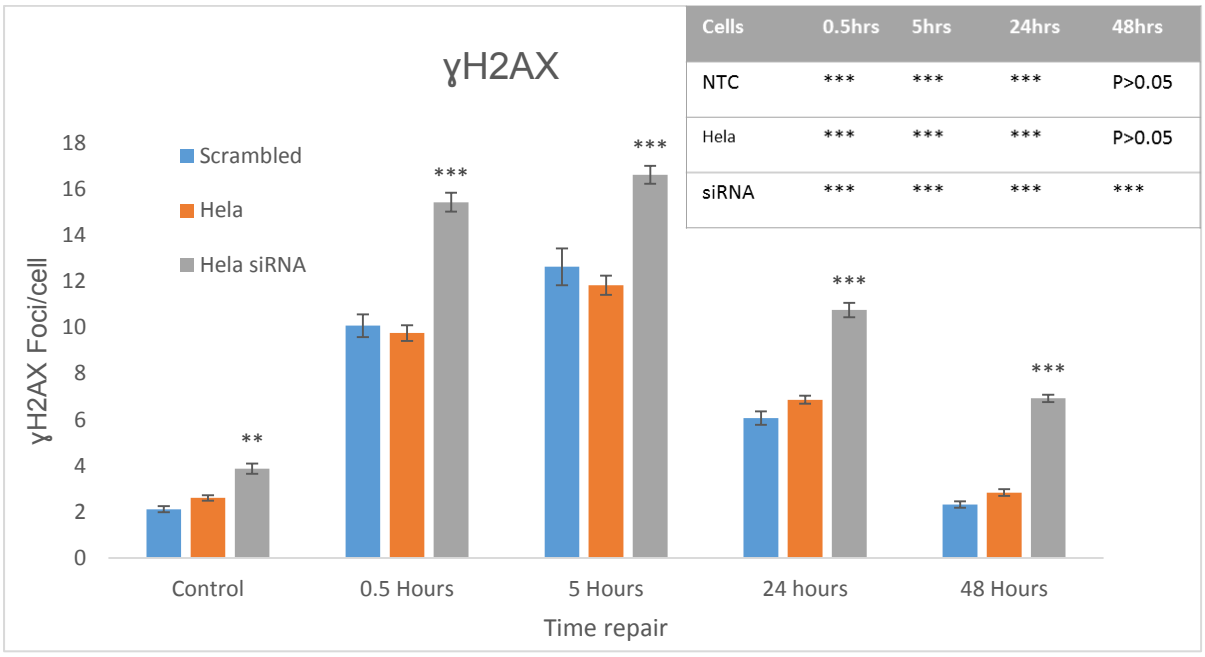

*Figure 5.14) Frequencies of γH2AX positive foci in untreated and 1.0 Gy doses of gamma radiation for transfected HeLa cell line with the untreated 72 hrs post transfection. The inset shows comparison of DNA damage foci for each time point against unirradiated samples. Stars above bars indicate comparison between transfected cell lines and control cell lines. *P<0.05 **P<0.01 ***P<0.001 versus control. Error bars indicate SEM.*

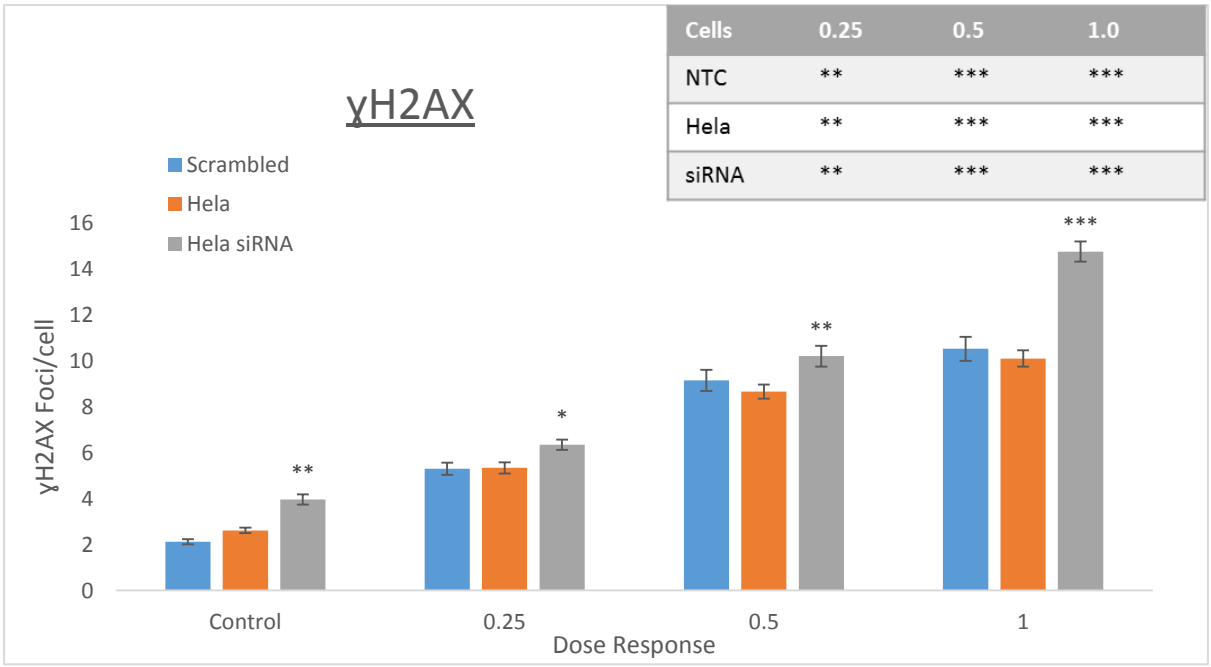

*Figure 5.15) Frequencies of γH2AX positive foci in 0.0, 0.25, 0.5 and 1.0 Gy doses of gamma radiation for HeLa transfected cell line with untreated cell line 72hrs post transfection. The inset shows comparison of DNA damage foci for each dose against unirradiated samples. Stars above bars indicate comparison between transfected cell lines and control cell lines. *P<0.05 **P<0.01 ***P<0.001 versus control. Error bars indicate SEM.*

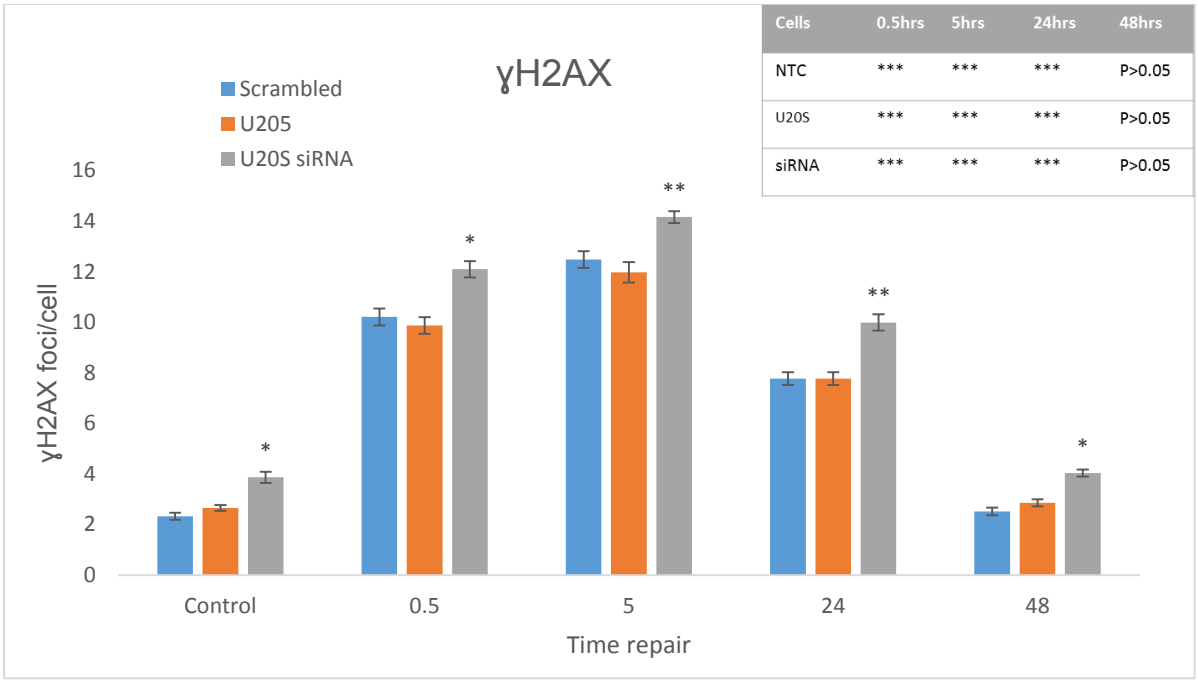

*Figure 5.16) Frequencies of γH2AX positive foci in untreated and 1.0 Gy doses of gamma radiation for transfected U205 cell line with the untreated 48 hrs post transfection. The inset shows comparison of DNA damage foci for each time point against unirradiated samples. Stars above bars indicate comparison between transfected cell lines and control cell lines. *P<0.05 **P<0.01 ***P<0.001 versus control. Error bars indicate SEM.*

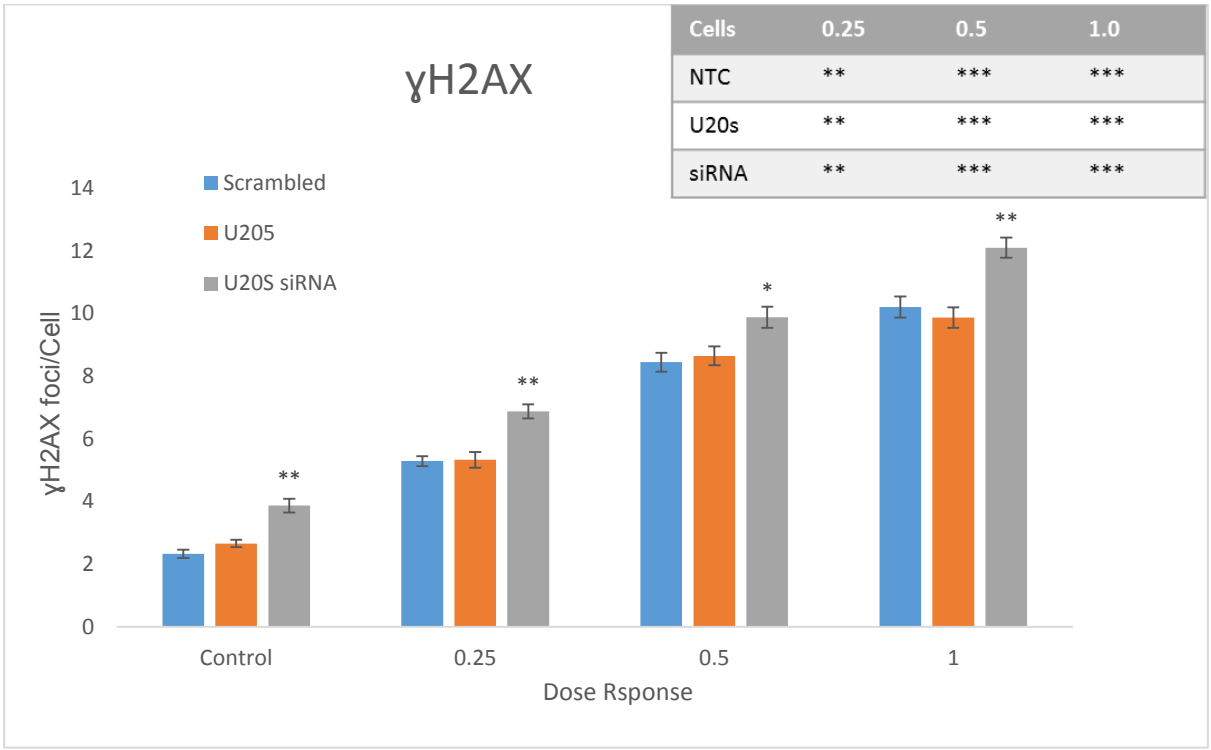

*Figure 5.17) Frequencies of γH2AX positive foci in 0.0, 0.25, 0.5 and 1.0 Gy doses of gamma radiation for U20S transfected cell line with untreated cell line 48 hrs post transfection. The inset shows comparison of DNA damage foci for each dose against unirradiated samples. Stars above bars indicate comparison between transfected cell lines and control cell lines. *P<0.05 **P<0.01 ***P<0.001 versus control. Error bars indicate SEM.*

Overall, we found that transfected Hela cell line significantly higher levels of ɣH2AX foci than the transfected U2OS cell line (Figure 5.14-5.17). The reasoning for higher levels of ɣH2AX foci in HeLa cells is that they are telomerase positive, whereas U20S are ALT positive cell lines and do not have telomerase activity. Therefore, our reasoning is that whether *DKC1* becomes dysfunctional will not have a direct effect on the function of this particular cell line and then no effect on the DNA damage response. As for transfected GM08399, post 96 hours, we observed a similar pattern for transfect Hela cell lines, thus supporting the notion that dysfunctional *DKC1* contributes towards abnormal DNA damage response.

5.5 Shorter telomere length observed in DKC1 knockdown in normal fibroblast cell lines

Apart from the effects of DKC1 depletion on DNA damage response efficiency we also assessed telomere lengths in all samples using the same methodology as in Chapter 3 and 4. Shorter telomeres lead to loss of telomere function triggering abnormal DNA damage response. Furthermore, given that DKC1 is an integral component of telomerase this indirectly implicates telomerase in DNA damage response. Therefore, we analysed the average telomere length using the IQ-FISH protocol. Results of our analysis are shown in Fig 5.18.

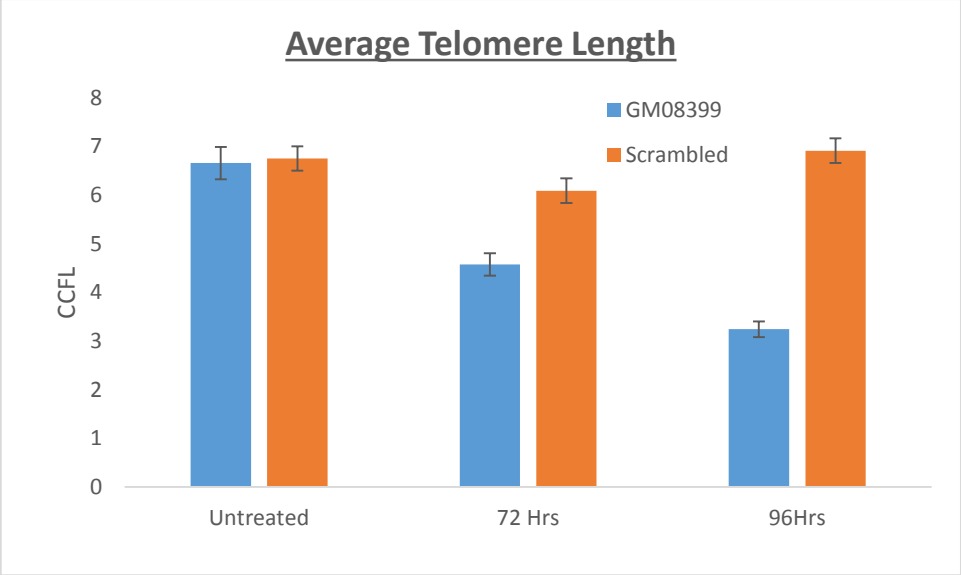

Figure 5.18) Telomere length analysis in normal and transfected cell lines calibrated against LY-R and LY-S mouse cells. Same passage number was chosen. CCFl = Corrected Calibrated Fluorescence, protocol developed in Dr Slijepcevic lab. Errors bars represent SEM.

Interestingly, normal fibroblasts do not show telomerase activity as detected by the TRAP assay (Armanios and Blackburn 2013; Scheel et al 2001). Yet, telomere length was significantly reduced at both post-transfection time points (Figure 5.18). This suggest that although telomerase is inactive in fibroblast cells, DKC1 becoming dysfunctional perhaps causes alteration in the telomerase activity that causes accelerated telomere shortening when compared to cells that are not transfected.

5.6 Micronuclei analysis in DKC1 knockdown in normal fibroblast cell lines

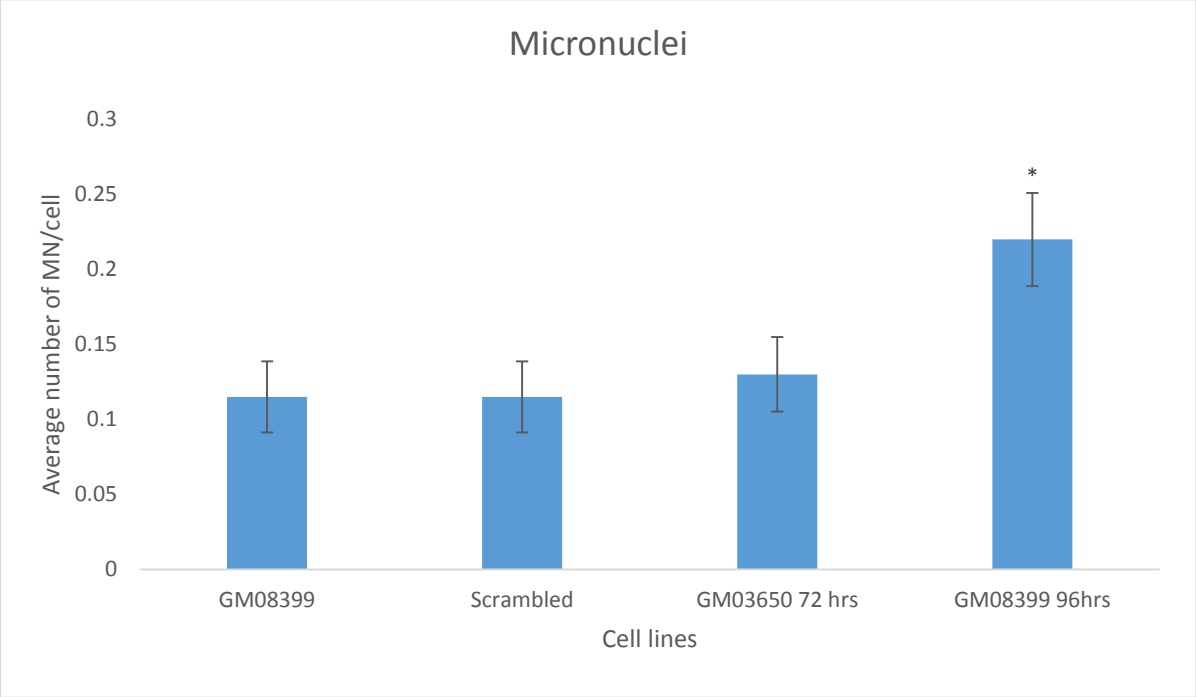

*Figure 5.19) Frequencies of micronuclei after DKC1 knockdown compared to control obtained. 500 binucleated cells/samples were analysed. Statistical significance of micronuclei with respect to control cell line *P<0.05 versus control. Error bars represent SEM.*

Finally, we wanted to examine the level of micronuclei in transfected cell lines higher levels of micronuclei was observed in DC fibroblast and DC lymphobastiod cell lines. As expected, post transfection at 96 hours, significantly higher levels of Micronuclei was observed upon depletion of *DKC1*, as shown in figure 5.14 for TIF analysis. Higher levels were observed 72 hours post transfection however there is no significant compared to the controls when statistical analysis was applied (Figure 5.19). Thus, this supports the notion that loss of telomere function leads to defective DNA damage response as observed from DC cell lines in previous chapters.

5.8 Discussion

The aim of this chapter was to knockdown *DKC1* in normal fibroblast cell line (GM08399) and to see whether it has an impact on DDR. As we observed in Chapter 3, DC fibroblast cell line exhibit an abnormal DDR so we wanted to reproduce this finding in the normal fibroblast cell line by reducing expression of *DKC1* through transfection with siRNA oligonucleotides.

Our western blot results suggested that the lowest expression of *DKC1* was found at the 96 hours' time point post transfection (Figure 5.3). The rt-PCR results indicated that the lowest expression was at the 72 time point post transfection (Figure 5.2). However, this is most likely due to mRNA being less stable than protein (Vogel and Marcotte, 2012). Therefore, for checking the phenotype of our cells we selected the time points at which the protein expression (Figure 5.3-5.4) was lowest. All the relevant tests for the assessment of DDR in cells with reduced *DKC1* expression indicated a defective DDR (Figures 5.5-5.12).

Therefore, our RNAi experiments in the normal fibroblast cell line confirm that *DKC1* is involved in DDR. The expression of *DKC1* is reduced for a short period leading to low protein levels. Dyskerin is used to stabilise the hTERT component of telomerase to synthesis telomere repeats (Shcherbakova et al 2006; Venteicher et al 2009). Shorter telomere length observed in fig 5.18 suggests that the telomeres cannot form the T loop to protect the ends from being recognised as DSBs and thus stop the DDR machinery from activation (Griffith et al. 1999). However, it is important to stress that fibroblasts do not normally have active telomerase (Wyatt et al 2010). It seems likely that *DKC1* must have roles in DDR that are different from simple telomerase regulation.

This finding further supports the notion that the loss of telomere function leads to defective DDR. This is supported by the findings in this chapter that 96 hrs post transfection, elevated ɣH2AX, TIF and MN levels were observed in fibroblast cells with the lowest *DKC1* expression level relative to their counterparts with the normal *DKC1* levels (Figures 5.7, 5.8, 5.10 & 5.12). Kirwan et al (2011) argued that DC cells have a normal DDR as explained earlier (see page 92). However, our results refute this finding and are in line with several studies which found evidence of a defective DDR in DC cells. In particular, a recent study by Manguan-Garcia, *et al*., et al. (2014) using the same DC fibroblast cell lines as our study identified a defective response of DC cells to Bleomycin treatment. Bleomycin is an agent that mimics effects of IR through inducing DSBs in DNA (Liu et al 2014).

Experiments carried out in prostate cancer cells using siRNA knockdown of *DKC1* showed a strong inhibitory effects on cell proliferation (Sieron et al 2009). We observed the same effect as the mitotic index was generally low in all post-transfected cells (not shown). The same effect was observed by Gu et al (2008).

In conclusion, this chapter shows a defective DDR in normal fibroblasts transfected with siRNA oligonucleotides specific for DKC1.

We have shown that *DKC1* knock-down causes: a) an increase in spontaneous and induced levels of DNA damage foci b) higher level of TIFs and c) reduces average telomere length.

Chapter 6 DNA damage response in TA 65 treated cell lines

6.1 Introduction

In the previous chapters we looked at the effects of DKC1 dysfunction in fibroblast and lymphobastiod cell lines from DC patients with the X-linked form of disease and identified the defective DNA damage response using several approaches (Chapters 3 & 4). In Chapter 5 we have shown that the knockdown of DKC1 in the normal cell line with the proficient repair capacity results in the reduced repair capacity suggesting the phenotype change and further confirming the notion that DKC1 is involved in DDR. This finding is in line with several publications suggesting failure of DNA damage response as the general phenotypic feature of DC cells (Mitchell et al 1999; DeBauche et al 1990; Manguan-Garcia et al 2014). Our findings are in line with the hypothesis that DNA damage response and telomere maintenance are functionally linked (de Lange 2005; Huda et al 2009; Tanaka et al 2005). In order to test this hypothesis so far we have relied on cell lines that have dysfunctional telomeres by assessing the efficiency of the DNA damage response. For example, in the case of a fibroblast cell line that is homozygous for the *DKC1* mutation, we found higher level of gamma-H2AX foci compared to the control cell line indicating a defective DNA damage response (Chapter 3). This result was confirmed when the normal fibroblast cell line was used to knock down the DKC1 expression using siRNA oligonucleotides (Chapter 5).

Another way for testing the functional link between telomeres and DNA damage response would be to probe the efficiency of the DDR by manipulating telomerase as the key enzyme involved in telomere maintenance. It seemed interesting for us to use a telomerase activator, TA-65, that is extracted from the root of *Astragalus membranaceus*, a well-known Chinese medicinal herb, and is one of many extracts that are used to study for their capacity to enhance telomerase activity (Molgora et al

2013). In January, 2007, a commercial health maintenance program, PattonProtocol-1, was launched that included a natural product-derived telomerase activator (TA-65) (Harley et al 2011). It was found that TA-65 increased Telomerase activity significantly in T human cells when compared with the effects of HTA, another compound with telomerase effects from *Astragalus* (Molgora et al 2013).

Based on these findings, we thought that it may be appropriate to use the telomerase activator TA-65 in a lymphoblastoid cell line to analyse the effect on DDR after exposure to gamma-radiation. Even though lymphoblastoid cell lines express telomerase activity we reasoned that TA-65 may enhance this activity. The enhanced telomerase activity usually manifests in elongation of telomeres. Our aim in this chapter was to assess whether elongation of telomere length by treating cells with TA-65 affects cellular capacity to respond to IR induced DNA damage.

Samples consisting of TA-65 treated cells were compared to samples of untreated cells using different doses of gamma-irradiation (dose response) and DNA damage at different time points after exposure to gamma irradiation (repair kinetics) were measured and analysed. The detection of chromosome damage was performed using the MN assay. Furthermore, anaphase bridges were quantified at two different points and at different doses of gamma irradiation.

The TA-65 powder was kindly provided by TA sciences (New York). To gain a 10mM stock of TA-65 0.049mg were dissolved in 10ml DMSO (dimethylsulfoxide) and frozen in aliquots of 0.5 ml or 1ml. To stimulate the cells 10uM of telomerase activator TA-65 (stock: 10mM) were added to one flask of cells 48 or 72 hours prior to experiments. For repair kinetics analysis cells were harvested 0.5, 5, 24 and 48 hours after exposure to 1.0 Gy or 2 Gy gamma irradiation. We used the GM008933 the lymphoblastoid cell line

established from a normal donor to determine the effects of this telomerase activator. Here we report the initial findings on the effect of TA65 upon DNA damage response mechanism.

6.2 Average telomere length in TA-65 treated lymphoblastoid cells

We started by measuring telomere length in the TA-65 treated lymphoblastoid cell line to determine the effects of the telomerase activator on telomere length. The same untreated lymphoblastoid cell line was used for control purposes. A total of 50 interphase cells per cell line were analysed by IQ-FISH to determine the mean telomere length for each sample as described in Chapter 3. Telomere length measurements were carried out over a period of four passages (Figure 6.1). Our results show that cells treated with TA-65 show significantly longer telomeres relative to control untreated cells. The effect is observed throughout the period of measurement. Our results are in line with the published study De Jesus et al 2011, demonstrating similar effects in mouse embryonic fibroblasts (MEFs).

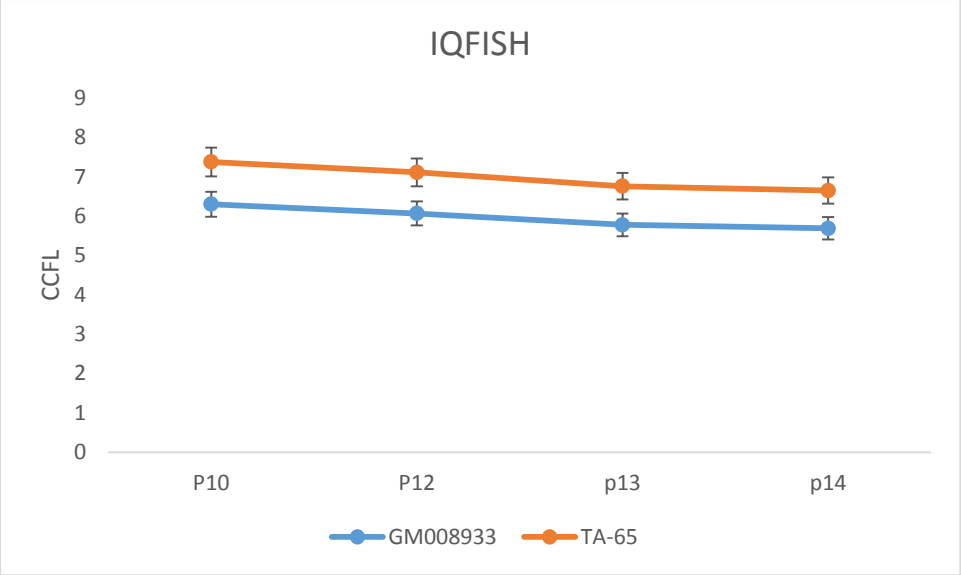

Figure 6.1) Telomere length analysis in treated and untreated TA-65 lymphoblastoid cell lines calibrated against LY-R and LY-S mouse cells. Each cell line was measured over a period of four passages to determine the telomere length of TA-65 treated cell lines compared to control cell line. CCFl = Corrected Calibrated Fluorescence, protocol developed in Dr Slijepcevic lab. Errors bars represent SEM.

6.3 Measuring Anaphase bridges 48 and 72 hours after irradiation

Given the longer telomeres in the TA-65 treated samples and the functional link between telomeres and DNA damage response (de lange 2005; Slijepcevic 2008; Blasco et al 1997; Gu et al 2008; DeBauche et al 1990; M'kacher et al 2003) we reasoned that we could test this link further by comparing DNA damage responses in the samples with normal telomeres and those in which telomeres are elongated after treatment with TA-65. Therefore the next step was to analyse the Anaphase bridges and Micronuclei. We quantified anaphase bridges observed in TA-65 treated cells following irradiation. We generated dose response curves by irradiating the cells using the set of following doses: 0.5 Gy, 1.0 Gy and 2.0 Gy and harvesting them after 48 hours (Figure 6.2) or 72 hours (Figure 6.4) . Examples of Anaphase Bridges are shown in figure 6.6. TA-65 treatment on its own did not induce increases in anaphase bridge frequencies after 48hours (Fig

6.2) but there was a slight drop in this frequency after 72 hours (figure 6.4). At the doses of 1.0 Gy and 2.0 Gy we observed statistically significant differences at both 48 h and 72 h post-irradiation suggesting that TA-65 treatment has the effect on DNA damage response presumably via telomere length elongation.

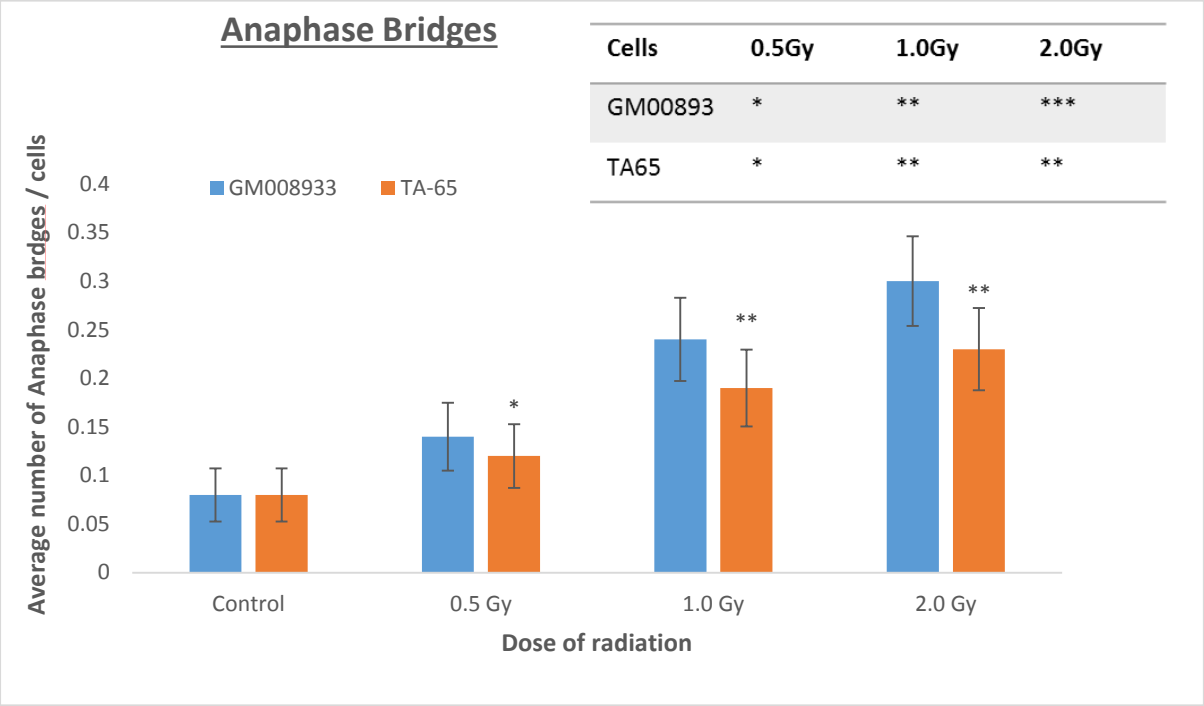

*Figure 6.2) Frequencies of Anaphase Bridges in 0.5 Gy, 1.0 Gy and 2.0 Gy doses of gamma radiation for TA-65 treated and untreated lymphoblastoid cell lines after 48 hours. Two types of statistical comparison were carried out. The inset shows comparison of Anaphase Bridges for each dose against unirradiated samples. Stars above bars indicate comparison between TA65 treated and control cell lines *P<0.05 **P<0.01 ***P<0.001 versus control. Error bars represent SEM.*

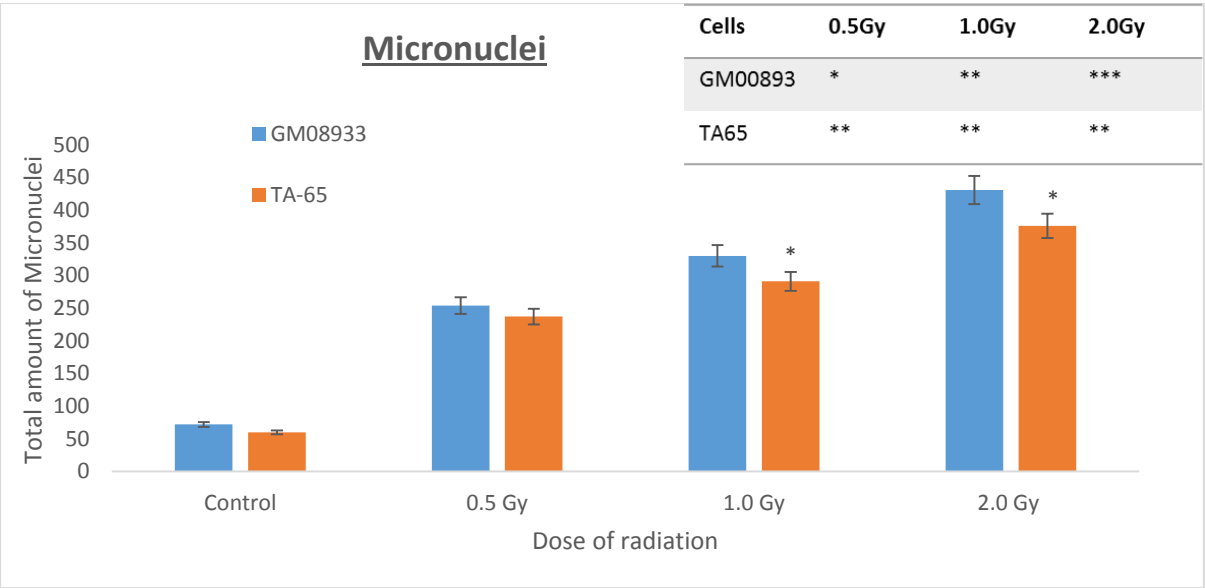

*Figure 6.3) Frequencies of MN in 0.5 Gy, 1.0 Gy and 2.0 Gy doses of gamma radiation for TA-65 treated and untreated lymphoblastoid cell lines after 48 hours. Two types of statistical comparison were carried out. The inset shows comparison of MN for each dose against unirradiated samples. Stars above bars indicate comparison between TA65 treated and control cell lines *P<0.05 **P<0.01 ***P<0.001 versus control. Error bars represent SEM.*

6.4 Measuring Micronuclei after 48 and 72 hours after irradiation

Next, we assessed the amount of micronuclei in the TA-65 treated cells relative to untreated samples. The same doses and timing after irradiation were used as in the case of anaphase bridge analysis. Examples of Micronuclei are shown in figure 6.7.

We observed almost entirely the same situation as with the anaphase bridge analysis (Fig 6.2 and 6.4) suggesting further the effect of TA-65 treatment on DNA damage response.

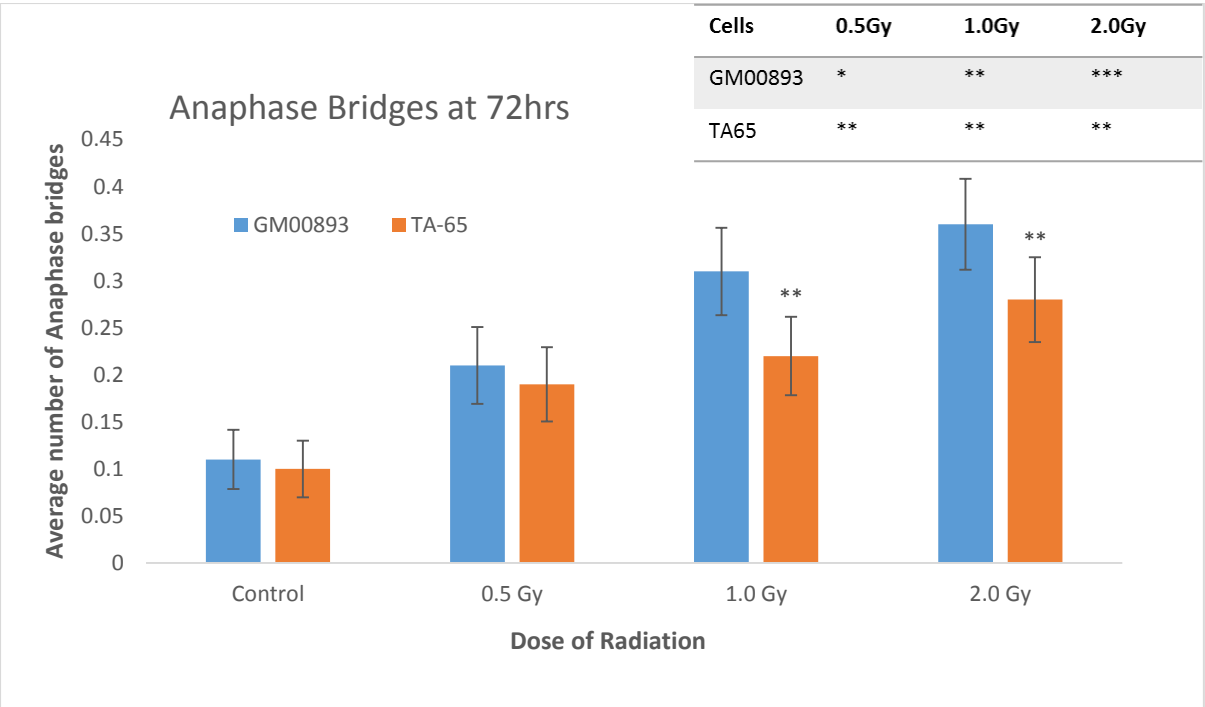

Cells	0.5Gy	1.0Gy	2.0Gy
GM00893	*	**	***
TA65	**	**	**

*Figure 6.4) Frequencies of Anaphase Bridges in 0.5 Gy, 1.0 Gy and 2.0 Gy doses of gamma radiation for TA-65 treated and untreated lymphoblastoid cell lines after 72 hours. Two types of statistical comparison were carried out. The inset shows comparison of Anaphase bridges for each dose against unirradiated samples. Stars above bars indicate comparison between TA65 treated and control cell lines *P<0.05 **P<0.01 ***P<0.001 versus control. Error bars represent SEM.*

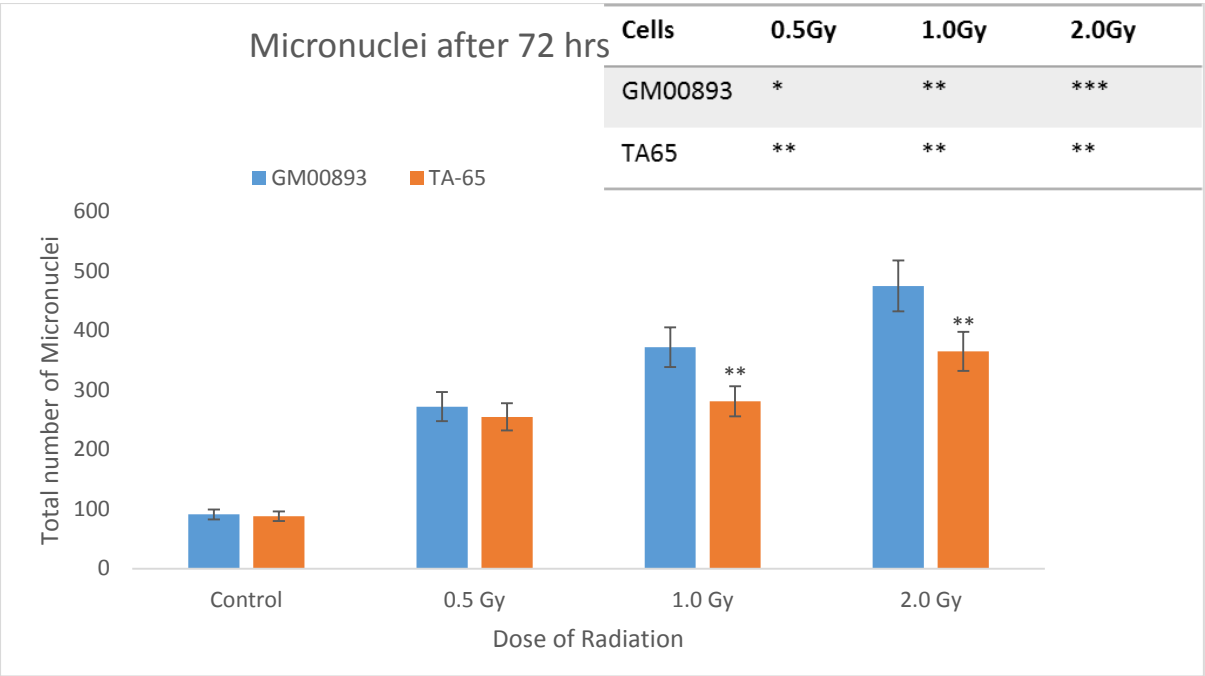

Cells	0.5Gy	1.0Gy	2.0Gy
GM00893	*	**	***
TA65	**	**	**

*Figure 6.5)Frequencies of MN in 0.5 Gy, 1.0 Gy and 2.0 Gy doses of gamma radiation for TA-65 treated and untreated lymphoblastoid cell lines after 72 hours. Two types of statistical comparison were carried out. The inset shows comparison of MN for each dose against unirradiated samples. Stars above bars indicate comparison between TA65 treated and control cell lines *P<0.05 **P<0.01 ***P<0.001 versus control. Error bars represent SEM.*

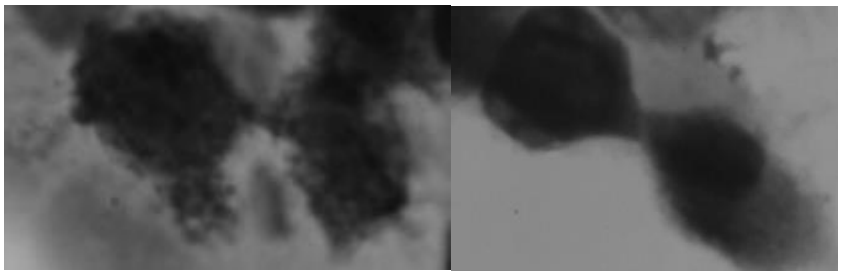

Figure 6.6) Images obtained from TA 65 treated lymphobastiod cell line stained with Giemsa in scoring Anaphase bridges, as a consequence of telomere end to end fusion.

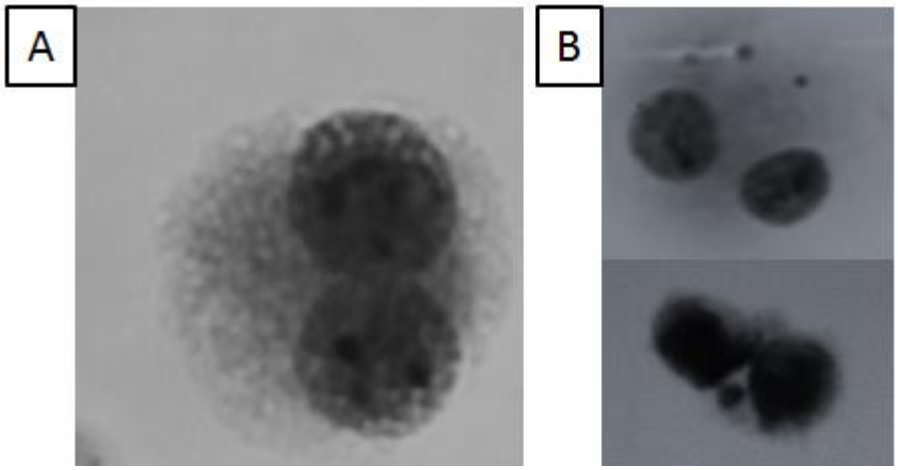

Figure 6.7) Images obtained from TA 65 treated lymphoblastoid cell line stained with Giemsa in scoring Micronuclei. A) Binucleated cell B) An example of Micronuclei scored in the assay.

6.5 Assessment of DNA damage response using gamma-H2AX and TIF assay

6.5.1 Dose response in TA-65 treated lymphoblastoid cells

Next, as in the previous chapters we carried out the assessment of DNA damage using the gamma-H2AX and TIF tests (dose response and repair kinetics) in samples treated or not with TA-65. Our results are shown in Figures 6.8 – 6.11. Our dose-response results are very similar to results obtained after anaphase bridge and MN analysis: treatment of cells with TA-65 reduces the level of damage at doses of 1.0 Gy and 2.0 Gy (Figure 6.8).

However, repair kinetics analysis after exposure of cells to 1.0 Gy of gamma rays showed no differences in the amount of damage 24 h and 48 h after irradiation

suggesting that treatment with TA-65 is insufficient to reverse effects of radiation on a long term basis given that the amount of damage was reduced 30 min and 5 h after irradiation (Fig 6.9). However, the TIF analysis yielded different results indicating the ability of Ta-65 to reduce damage at telomeres relative to untreated cells (Fig 6.10). Thus, these results suggest that TA-65 treatment is more effective at reducing damage at telomeres rather than damage in the rest of the genome as far as the repair kinetics is concerned.

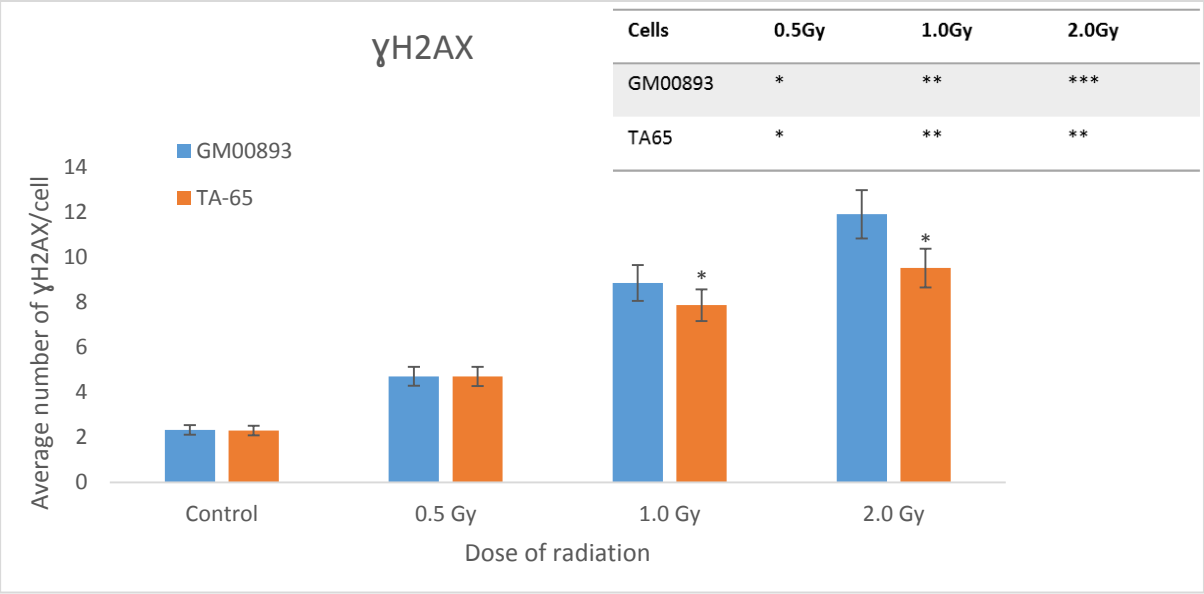

Cells	0.5Gy	1.0Gy	2.0Gy
GM00893	*	**	***
TA65	*	**	**

*Figure 6.8) Frequencies of γH2AX positive foci in 0.0, 0.25, 0.5 and 1.0 Gy doses of gamma radiation for TA-65 treated lymphoblastoid cell lines compared to the untreated cell line. Two types of statistical comparison were carried out. The inset shows comparison of DNA damage foci for each dose against unirradiated samples. Stars above bars indicate comparison between TA65 treated and control cell lines *P<0.05 **P<0.01 ***P<0.001 versus control. Error bars indicate SEM.*

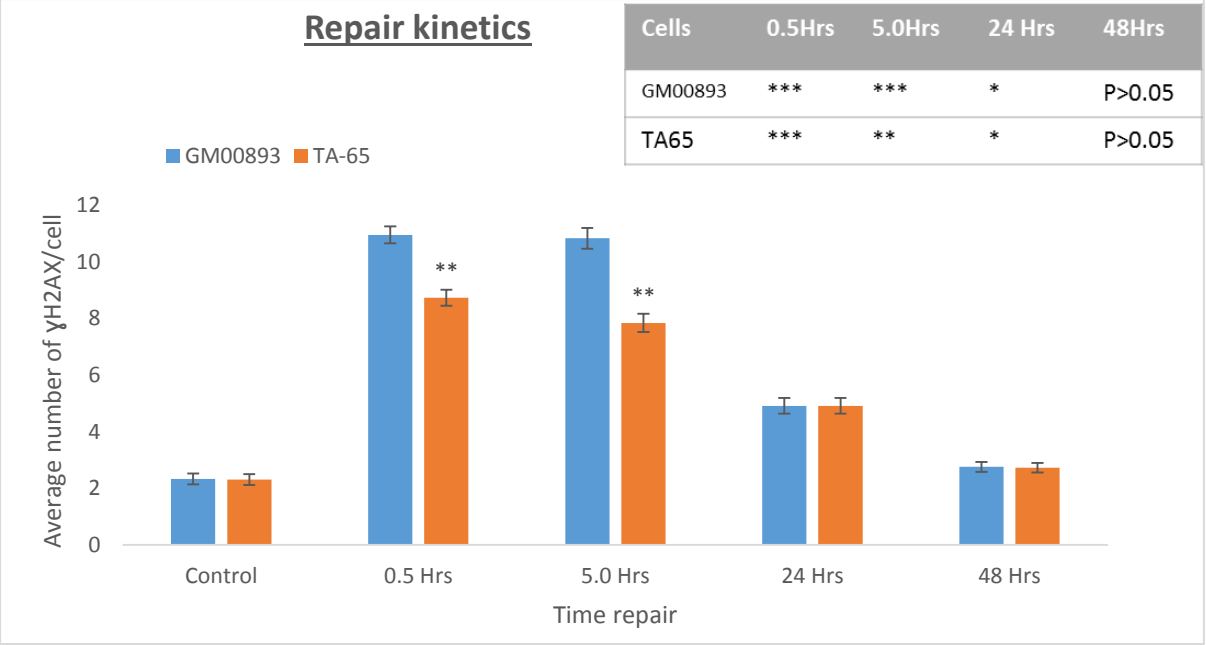

*Figure 6.9) Frequencies of γH2AX positive foci in untreated and 1.0 Gy doses of gamma radiation for TA-65 treated lymphoblastoid cell lines compared to the untreated cell line Two types of statistical comparison were carried out. The inset shows comparison of DNA damage foci for each time point against unirradiated samples. Stars above bars indicate comparison between TA65 treated and control cell lines *P<0.05 **P<0.01 ***P<0.001 versus control. Error bars indicate SEM.*

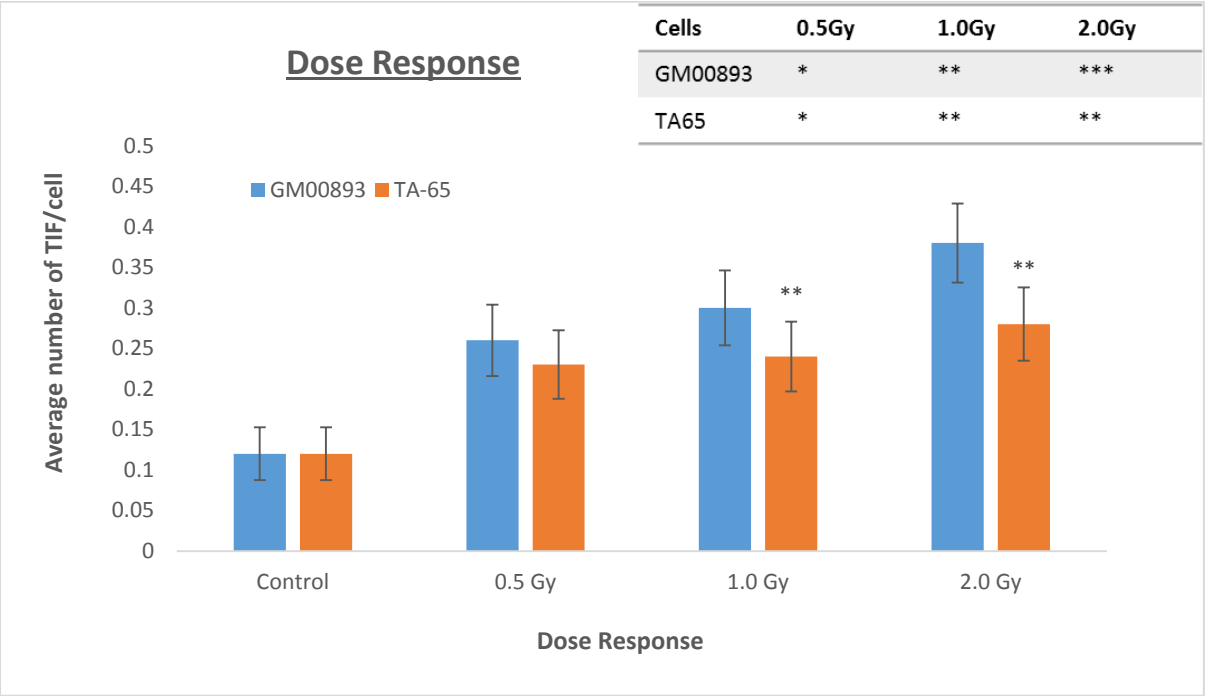

*Figure 6.10) Frequencies of TIF foci in 0.0, 0.25, 0.5 and 1.0 Gy doses of gamma radiation for TA-65 treated lymphoblastoid cell lines compared to the untreated cell line. Two types of statistical comparison were carried out. The inset shows comparison of TIF foci for each dose against unirradiated samples. Stars above bars indicate comparison between TA65 treated and control cell lines *P<0.05 **P<0.01 ***P<0.001 versus control. Error bars indicate SEM.*

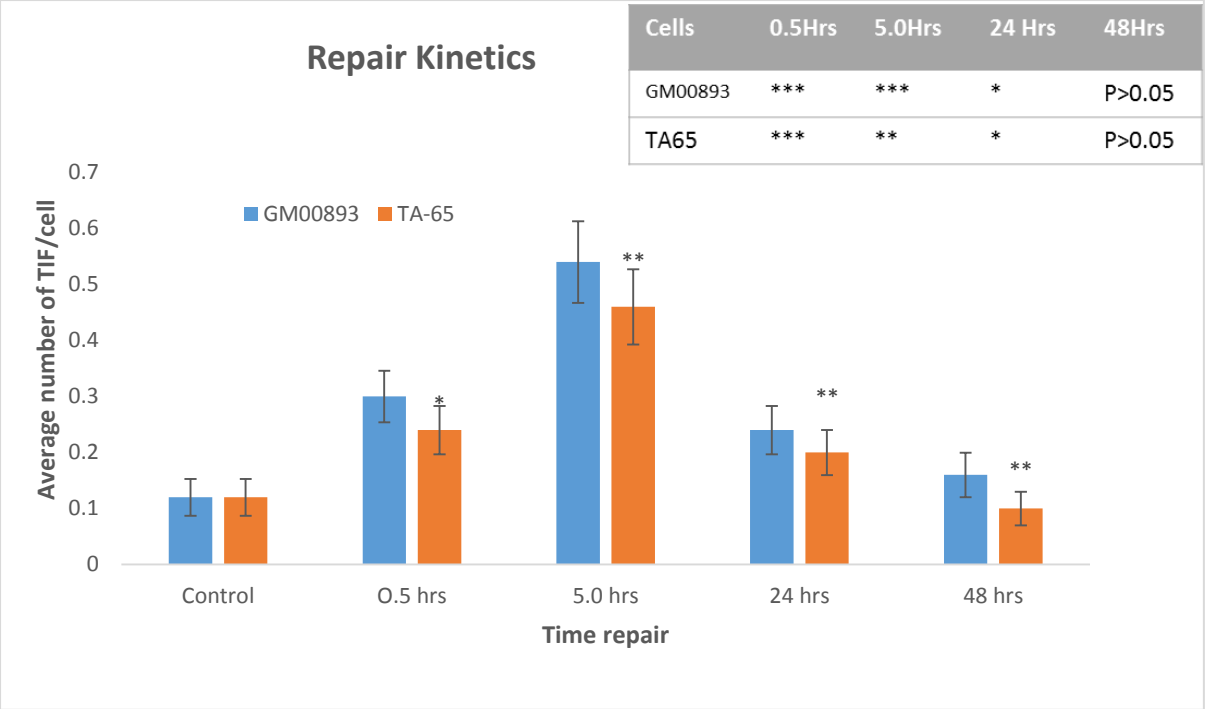

*Figure 6.11) Frequencies of TIF foci in untreated and 1.0 Gy doses of gamma radiation for TA-65 treated lymphoblastoid cell lines compared to the untreated cell line. Two types of statistical comparison were carried out. The inset shows comparison of TIF foci for each time point against unirradiated samples. Stars above bars indicate comparison between TA65 treated and control cell lines *P<0.05 **P<0.01 ***P<0.001 versus control. Error bars indicate SEM.*

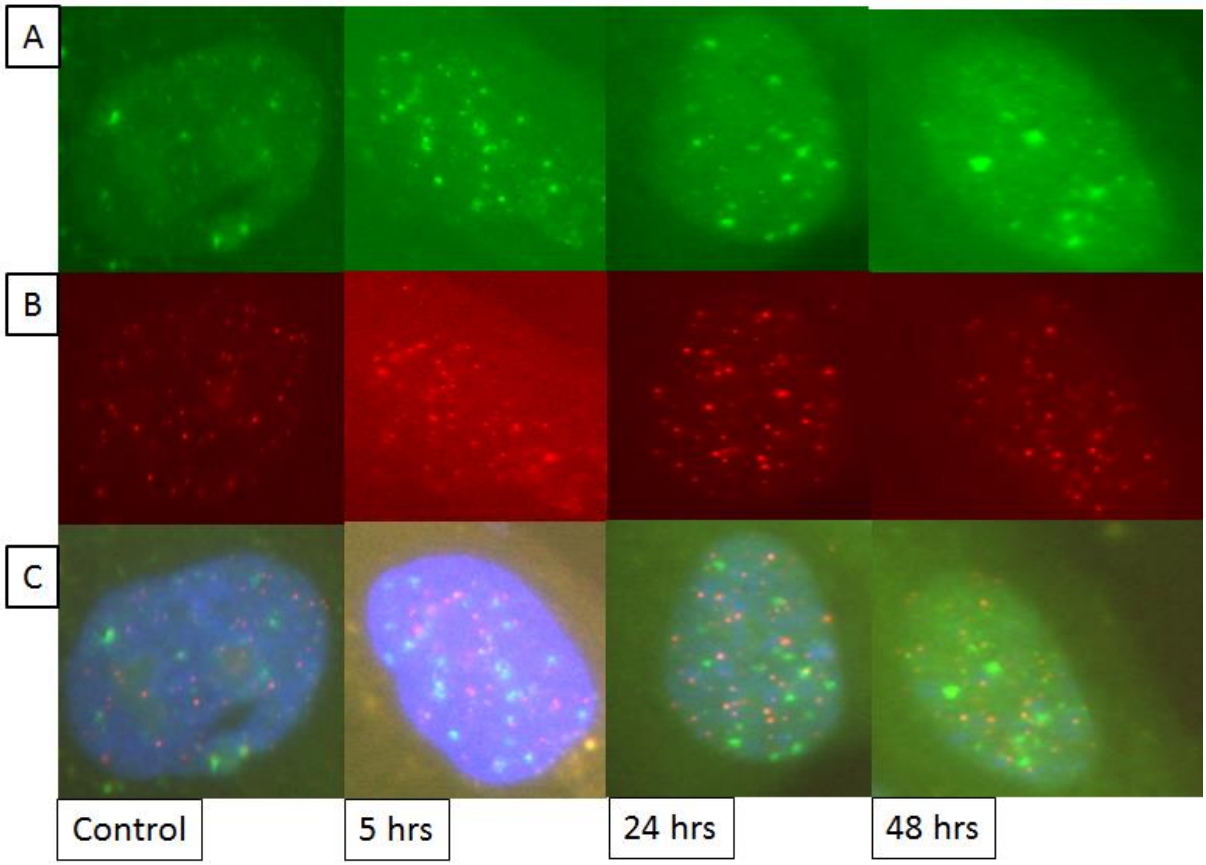

Figure 6.12) Images obtained from nuclei of the TA-65 treated lymphoblastoid cell line, after irradiation with gamma rays at 1.0Gy dose at different time points. A) detection of DNA damage γH2AX foci. B) Telomeres were detected by $(AATCCC)_3$ probe labelled with Cy-3 (red) C) Colocalization with γH2AX and telomeres represent a TIF (merged) visible by yellow spots. The nucleus was counterstained with Dapi.

6.5.2 Repair Kinetics in TA 65 treated lymphoblastoid cells at 2.0 Gy

However, it is possible that the effect of TA-65 on the repair capacity of cells may be more pronounced at higher doses of radiation. Therefore, we repeated the repair kinetics experiment using the dose of 2.0 Gy instead of 1.0 Gy used earlier (Fig 6.8). Interestingly, we observed a significant differences in the repair capacity between TA-65 treated and untreated cells 24 h after irradiation but not 48 h after irradiation (6.13) suggesting that TA-65 effects may be dose-dependent when assessing its effects on repair kinetics. We did not have time to carry out the same analysis on even higher

doses i.e. 4.0 Gy. The analysis of TIF repair kinetics at the dose of 2.0 Gy (6.14) revealed a similar situation as in the case of Fig 6.11.

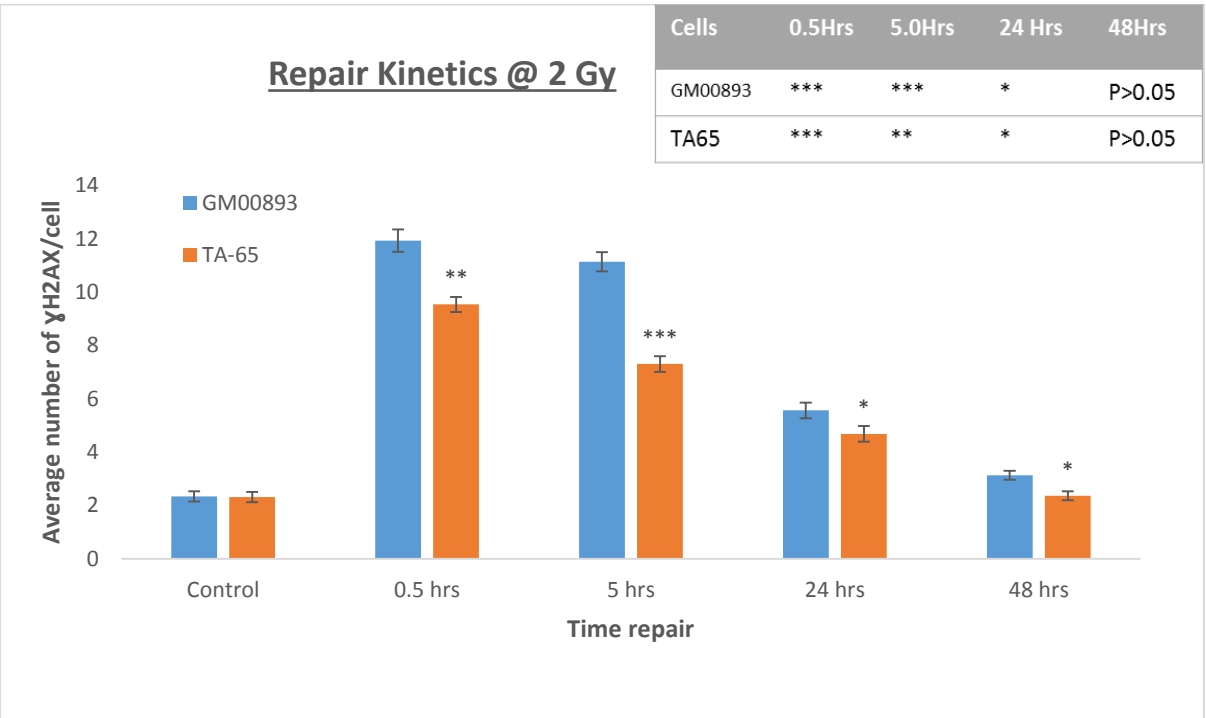

*Figure 6.13) Frequencies of γH2AX positive foci in untreated and 2.0 Gy doses of gamma radiation for TA-65 treated lymphoblastoid cell lines compared to the untreated cell line. Two types of statistical comparison were carried out. The inset shows comparison of DNA damage foci for each time point against unirradiated samples. Stars above bars indicate comparison between TA65 treated and control cell lines *P<0.05 **P<0.01 ***P<0.001 versus control. Error bars indicate SEM.*

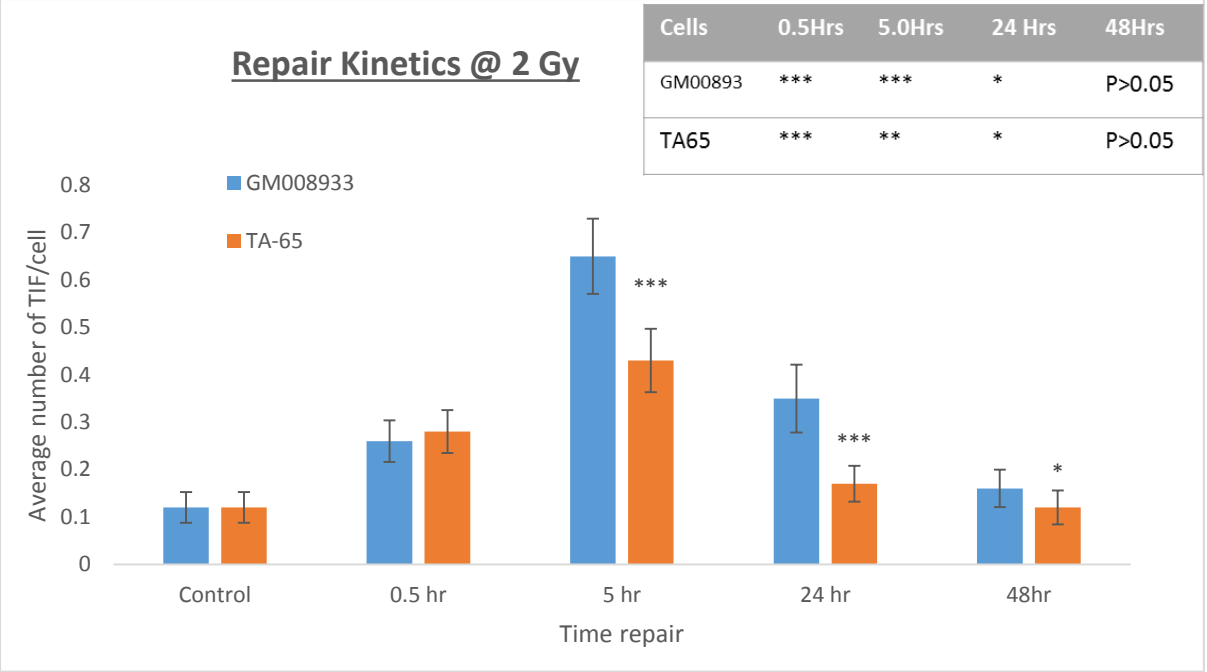

*Figure 6.14) Frequencies of TIF foci in untreated and 2.0 Gy doses of gamma radiation for TA-65 treated lymphoblastoid cell lines compared to the untreated cell line. Two types of statistical comparison were carried out. The inset shows comparison of TIF foci for each time point against unirradiated samples. Stars above bars indicate comparison between TA65 treated and control cell lines *P<0.05 **P<0.01 ***P<0.001 versus control. Error bars indicate SEM.*

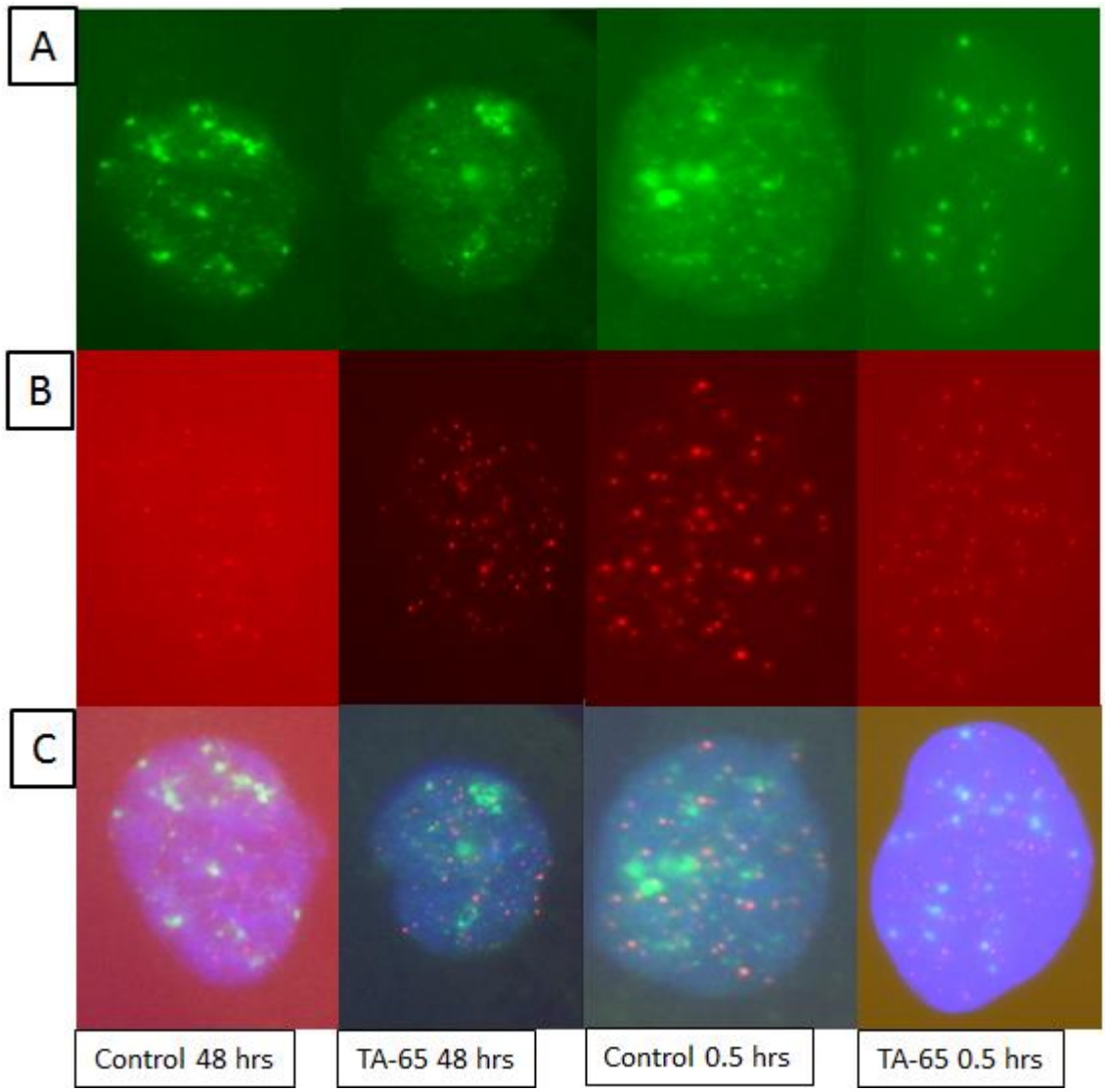

Figure 6.15) Images obtained from nuclei of the TA 65 treated lymphoblastoid cell line, after irradiation with gamma rays at 2.0Gy dose at 0.5 and 48 hrs time point. A) detection of DNA damage γH2AX foci. B) Telomeres were detected by $(AATCCC)_3$ probe labelled with Cy-3 (red) C) Colocalization with γH2AX and telomeres represent a TIF (merged) visible by yellow spots. The nucleus was counterstained with Dapi.

6.6 Testing the ability of TA 65 treated cell lines at different concentrations

Previously, different concentrations of TA 65 were tested in Mouse embryonic fibroblasts (MEFs) with respect to DNA damage response (de Jesus et al 2011). Increasing concentrations of TA 65 resulted in reducing the percentage of short telomeres. Thus, one explanation for lack of radioprotective effects of TA-65 in our

repair kinetics analysis 48 h after irradiation (Figures 6.9 and 6.13) could be explained by an insufficient dose of TA-65 used. In order to test for this possibility determined frequencies of MN at different concentrations of TAS-65 : 1uM, 10uM and 20 uM. (Our standard dose in all experiments in this chapter was 10uM). Interestingly, we observed that increasing doses of TA-65 resulted in reducing MN levels. However, we did not have enough time to carry out radiation experiments to test the above possibility more stringently.

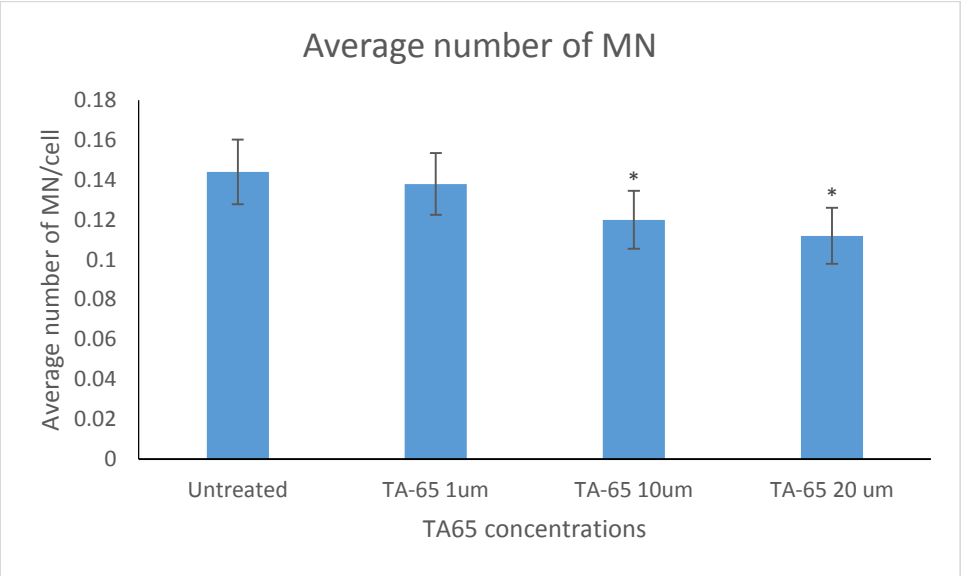

*Figure 6.16) Frequencies of MN obtained in TA-65 treated and untreated lymphoblastoid cell line. *P<0.05. **P<0.01, ***P<0.001 versus control. Error bars represent SEM.*

6.7 Discussion

The effect of the telomerase activator TA 65 on DNA damage response in lymphoblastoid cells was tested. By using the ɣH2AX assay, DSBs in the nucleus can be detected after IR treatment (Rogakou et al 1997). The dose-response experiments with the lymphobastiod cell line have shown that the treatment with the natural telomerase activator, TA 65, generally reduces frequencies of IR-induced ɣH2AX foci (Figures 6.8 & 6.9). This supports the assumption that telomere maintenance and DDR are functionally linked. Additionally, TA 65 appears to have impact on repair kinetics in irradiated cells. Almost half of the DSBs induced by IR seemed to be repaired within the first 5 hours when the cells were previously treated with TA-65 (Figure 6.9). At higher dosages TA 65 seem to have the ability to repair the DNA damage at a faster rate compared to lower doses (Figure 6.8 & 6.13). Thus, TA 65 may have a radioprotective effects.

Our experiments also revealed that TA 65 appears to reduce the DNA damage at telomeric DNA as lower levels of TIFs were present and the repair rate was faster (Figure 6.10 & 6.11).

Our findings are generally in line with those of De Jesus et al (2011) showing DDR protective effects of TA65 on mouse cells with defective telomerase.

The capacity of TA 65 to increase the average telomere length (Figure 6.1) is also in line with the observation of de Jesus et al (2011) who showed the same capacity of TA65 in MEFs (Mouse embryonic Fibroblast). TA65 elongated critically short telomeres in the group of human subjects who agreed to take TA65 pills (Harley et al, 2011). Telomerase activity generally increases upon treatment with TA65 (Molgora et al 2013; de Jesus et

al., 2011; Harley et al 2011) suggesting that this may have a favourable outcome in the case of exposure to IR. Furthermore, TA65 appears to reduces ageing in human subjects (Harley et al. 2011).

Unfortunately, we have not been able to measure telomerase activity in TA 65 treated lymphoblastoid cells by using TRAP assay due to time constraints. It would be useful to support our findings of telomere elongation by the assay for telomerase activity known as telomeric repeat amplification protocol or TRAP (Kim et al 1994). This would verify the telomerase activity in the TA 65 treated cells and we would expect the activity to increase since the average telomere length is elongated as per our result.

The protective effect of TA 65 against IR is further substantiated by scoring IR induced MN and anaphase bridges (Figures 6.2-6.5). We have also compared different concentrations of TA 65 when scoring MN and found that increasing the concentration of TA65 resulted in significantly lower levels of MN (Figure 6.16). This was in contrast to what de Jesus et al (2011) observed as they found that increased TA65 concentrations did not affect in the critically short telomeres with cells that were Terc+/-. Having said that, these cells were haploinsufficient for telomerase RNA component and we tested TA65 in normal cells.

It would be useful to score MN upon irradiation to determine the protective effect of increasing concentration of TA65. Furthermore, investigations of IR induced ɣH2AX foci in the presence of higher concentrations of TA 65 would be useful assess protective effects of TA 65 further.

This chapter showed a possible radioprotective effects of the telomerase activator TA 65. We demonstrated here that TA 65 leads to a significant increase in telomere length, rescuing telomere length to provide the protective cap on telomeres. It is possible that

this effect may be radioprotective through mechanisms that are still unknown. However, these are the initial findings and more work is required to verify radioprotective effects of TA65.

Chapter 7 General Discussion

7.1 General Discussion

It has become substantially clear that there is a link between DNA damage response and telomere maintenance and that they are functionally linked. For example, a study conducted by d'Adda di Fagagna et al (2003) established that critically short telomeres lead to cell cycle arrest and cell senescence through activating DNA damage response, as the uncapped telomeres associate directly with DDR proteins. A genetic manipulation of the shelterin component, TRF2, caused activation of DDR by turning telomeres dysfunctional (de lange 2005) and these studies clearly revealed that telomeres function to hide the free DNA ends from being recognised as DSBs by DDR mechanisms through forming the T-loop structure.

The work presented in this thesis was aimed at probing the possibility whether DDR would be affected when telomere dysfunction is present as a result of defects in factors that participate exclusively in telomere maintenance such as components of telomerase and shelterin. From here, we wanted to examine DDR in cells from DC patients as DC cells show clear telomere dysfunction as discussed in chapter one and we had three clear aims when investigating the efficiency in the DDR in these cells:

- Examine fibroblast and lymphoblastoid cell lines from DC patients for their capacity to carry out functional DDR.
- Knockdown the *DKC1* gene in normal cell lines using siRNA oligonucleotides and examine DDR relative to control cells.
- Examine whether a novel stimulator of telomerase, TA-65, derived from the plant *Astragalus membranaceus*, affects DDR in cells exposed to ionizing radiation.

As discussed previously, most of the research for DC cells focused on analysing telomere length and only marginally assessed DDR. The first study focusing on DDR in DC cells was done 25 years ago by examining chromatid breaks induced by x-radiation (DeBauche et al 1990). The study suggested elevated radiosensitivity associated with the DC defect. However, in our hands chromosomal analysis did not provide concrete results. In order to obtain sufficient numbers of mitotic cells for CAs analysis a reasonable mitotic index is required. All our DC cell lines had a low growth potential leading to poor mitotic indices and lack of sufficient numbers of mitotic cells. Therefore, it was not possible to assess frequencies of IR induced CAs. Instead, we focused on the surrogate method for CA analysis: the Cytochalasin-B method for MN assay (Gutierrez-Enriquez, 2003). Our MN analysis in generally corroborated with the results of DeBauche et al. (1990) (Chapters 3 and 4).

However, a more sophisticated analysis of DDR in DC cells was carried out using immunofluorescence with DNA damage marker H2AX. Results presented in Chapters 3 and 4 clearly indicate radiosensitivity of DC cells relative to control cells. The presence of radiosensitivity is the hallmark of a defective DDR (Brugat et al 2010; M'kacher et al 2003; Cabuy et al 2005; Yasaei 2010). Therefore, our results refute those of Kirwan et al (2011) who argued that DC cells have normal DDR mechanisms but are in line with several studies which showed defective DDR associated with the DC defect (DeBauche et al 1990; Pereboeva et al 2013; Gu et al 2008). In particular, the most recent study (Manguan-Garcia et al 2014) used exactly the same DC cell lines as we used in Chapter 3 and essentially demonstrated a defective response of these cells to Bleomycin thus supporting our conclusion that DC cells have a defective DDR.

In order to substantiate further our main finding of a defective DDR in DC cells we have shown in Chapter 5 that the reduction of DKC1 expression by RNAi leads to a defective DDR relative to control cells. Therefore, the main conclusion of this dissertation is that DC cells show a defective DDR and that DKC1 is involved in DDR mechanisms. Given that DKC1 is the protein that plays an important role in telomere maintenance through its association with telomerase it is reasonable to argue that the involvement of DKC1 in DDR is the result of its involvement in telomere maintenance. A substantial body of literature supports this notion by providing evidence that DDR and telomere maintenance mechanisms are functionally related (d'Adda di Fagagna et al 2003; Gu et al 2008; DeBauche et al 1990; Pereboeva et al 2013; M'kacher et al 2003; Manguan-Garcia et al 2014).

Another line of investigation covered in this dissertation supports the notion of a functional interplay between DDR and telomere maintenance. In the final Chapter (Chapter 6) we used a natural stimulator of telomerase called TA65, and showed that treatment of lymphoblastoid cells with this compound prior to IR has a radioprotective effects. TA65 has been previously shown to reduce signs of ageing in human subjects (Harley et al 2011) and improves the DDR capacity of mouse cells (de Jesus et al 2011). Our results show for the first time that TA65 may have radioprotective effects.

7.2 Future work

The work presented in this thesis focused heavily upon cells from patients with the X linked recessive form of DC caused by dysfunctional DKC1. It would be useful to examine another mutation causing DC to see whether it will lead to radiosensitivity. For example, the TINF2, a shelterin protein that is used to complete the capping for the telomere (Calado and Young 2008) has been recently implicated in DC (Nishio and Kojima 2010). It is important to stress that mouse cells lacking functional mTERC show

radiosensitivity (Finnon et al 2000; Strong et al 2011; Newman JP, 2008). The TERC mouse model is essentially equivalent of the DC form of disease caused by mutations in hTERC (autosomal dominant) (Marrone 2004).

Another point for future research would be the exploration of the telomerase activator TA 65 and its potential radioprotective capacity. Our results (Chapter 6) are still preliminary. In addition, it would be useful to test out the other natural telomerase activator, HTA as this activator is also derived from the same plant (Molgora et al 2013) and compare it to TA 65.

References

Acilan, C., Potter, DM., and Saunders WS. (2007). DNA repair pathways involved in anaphase bridge formation. *Genes Chromosomes Cancer. 46*(6), 522-531.

Alberts, B., Johnson, A., Lewis, J., Raff, M., Roberts, K., and Walter, P. (2008). *Molecular biology of the cell* (5th edition ed.). New York: Garland Science.

Alexander, P., and Mikulski, Z, B., (1961). Mouse lymphoma cells with different radiosensitivities. *Nature (Lond), 192*, 572-573.

Anderson, B, H., Kasher, P, R., Mayer, J., Szynkiewicz, M., Jenkinson, E, M. and Bhaskar S S (2012). Mutations in CTC1, encoding conserved telomere maintenance component 1, cause coats plus. *Nature Genetics, 44*(3), 338-U1604.

Armanios, M. (2013). Telomeres and age-related disease: How telomere biology informs clinical paradigms. *The Journal of Clinical Investigation, 123*(3), 996-1002.

Armanios, M., & Blackburn, E. H. (2012). The telomere syndromes. *Nature Reviews. Genetics, 13*(10), 693-704.

Bailey, S. M., J. Meyne, D. J. Chen, A. Kurimasa, G. C. Li, B. E. Lehnert and E. H. Goodwin (1999). "DNA double-strand break repair proteins are required to cap the ends of mammalian chromosomes." Proc Natl Acad Sci U S A 96(26): 14899-14904.

Bakkenist, C., & Kastan, M. (2003). DNA damage activates ATM through intermolecular autophosphorylation and dimer dissociation. *Nature, 421*(6922), 499-506.

Baran, I., Nalcaci, R., & Kocak, M. (2010). Dyskeratosis Congenita: Clinical report and review of the literature. *International Journal of Dental Hygiene, 8*(1), 68-74.

Barretaa, M. H., Gasperin, B. G., Rissi, V. B., Cesaro, M. P., Ferreira, R., de Oliveira, J. F., et al. (2012). Homologous recombination and non-homologous end-joining repair pathways in bovine embryos with different developmental competence. *Experimental Research, 318*, 2049-2058.

Beels L, Werbrouck J, Thierens H. (2010). Dose response and repair kinetics of gamma-H2AX foci induced by in vitro irradiation of whole blood and T-lymphocytes with X- and gamma-radiation.. *J.Radiat. Biol, 86*, 760-768.

Beer J. Z., Budzicka E., Niepokojczycka E., Rosiek O., Szumiel I., Walicka M. (1983). Loss of tumorigenicity with simultaneous changes in radiosensitivity and photosensitivity during *in vitro* growth of L5178Y murine lymphoma cells. *Cancer Res, 43*, 4736-4742.

Bekaert, S., Derradji, H., & Baatout, S. (2004). Telomere biology in mammalian germ cells and during development. *Developmental Biology, 274*(1), 15-30.

Bessler, M., Wilson, D., & Mason, P. J. (2010). Dyskeratosis congenita. *FEBS Lett, 584*(17), 3831-3838.

Blackburn, E. H. (1991). Structure and function of telomeres. *Nature, 350*, 569-573.

Blasco MA, Lee HW, Hande MP, Samper E, Lansdorp PM, DePinho RA, Greider CW (1997) Telomere shortening and tumor formation by mouse cells lacking telomerase RNA. *Cell* 91(1):25-34

Bonner, W. M., E. Redon, C., Dickey, J. S., Nakamura, A. J., Sedelnikova, O. A., & Solier, S. a. P., Yves. (2008). γH2AX and cancer. *Nat Rev Cancer, 8*(12), 957-967.

Boukamp, P., & Mirancea, N. (2007). Telomeres rather than telomerase a key target for anti-cancer therapy? *Experimental Dermatology, 16*(1), 71-79.

Bradshaw P S , Dimitrios J Stavropoulos, & M Stephen Meyn. (2005). Human telomeric protein TRF2 associates with genomic double-strand breaks as an early response to DNA damage. *Nature Genetics, 37*, 193-197.

Brown, C. (2000). Dyskeratosis congenita: Report of a case. *International Journal of Pediatric Dentistry, 10*, 328-344.

Brugat, T., Nguyen-Khac, F., Grelier, A., Merle-Béral, H., & Delic, J. (2010). Telomere dysfunction-induced foci arise with the onset of telomeric deletions and complex chromosomal aberrations in resistant chronic lymphocytic leukemia cells. *Blood, 16*(2), 239-249.

Bryan T M , A Englezou, J Gupta, S Bacchetti, and R R Reddel. (1995). Telomere elongation in immortal human cells without detectable telomerase activity. *Embo, 14*(17), 4240-4248.

Bryan, T. M., Englezou, A., Dalla-Pozza, L., Dunham, M. A., & Reddel, R. R. (1997). Evidence for an alternative mechanism for maintaining telomere length in human tumors and tumor-derived cell lines. *Nature Medicine, 3*(11), 1271-1274.

Buseman, C. M., Wright, W. E., & Shay, J. W. (2012). Is telomerase a viable target in cancer?. . *Mutation Research, 730*(1-2), 90-97.

Cabuy, E., Newton, C., Joksic, G., Woodbine, L., Koller, B., Jeggo, P.A., and Slijepcevic, P (2005). Accelerated telomere shortening and telomere abnormalities in radiosensitive cell lines *Radiation Research, 164*(1), 53-62.

Calado, R. T., & Young, N. S. (2008). Telomere maintenance and human bone marrow failure. *Blood, 111*(9), 4446-4455.

Callen, E., & Surralles, J. (2004). Telomere dysfunction in genome instability syndromes . *Mutation Research-Reviews in Mutation Research, 567*(1), 85-104.

Catalán J, Falck GC-M, Norppa H. (2000). The X chromosome frequently lags behind in female lymphocyte anaphase. *American Journal of Human Genetics, 66*(2), 687-691.

Cawthon, R., Smith, K., O'Brien, E., Sivatchenko, A., & Kerber, R. (2003). Association between telomere length in blood and mortality in people aged 60 years or older. *Lancet, 361*(9355), 393-395.

Cengiz, M., Celebioglu, B., Ozyar, E., & Lale Atahan, I. (2004). Unusual hypersensitivity to radiation therapy in a patient with dyskeratosis congenita syndrome. *Oral Oncology, 40*(7), 758-759.

Cesare, AJ., Reddel, R.R. (2010). Alternative lengthening of telomeres: Models, mechanisms and implications. *Nat.Rev.Genet., 11*, 319-330.

Coulthard, S., Chase, A., Pickard, J., Goldman, J., & Dokal, I. (1998). Chromosomal breakage analysis in dyskeratosis congenita peripheral blood lymphocytes. *British Journal of Haematology, 102*(5), 1162-1164.

d'Adda di Fagagna, F., Reaper, P., Clay-Farrace, L., Fiegler, H., Carr, P., von Zglinicki, T., et al. (2003). A DNA damage checkpoint response in telomere-initiated senescence. *Nature, 426*(6963), 194-198.

Davis, A. J., & Chen, D. J. (2013). DNA double strand break repair via non-homologous end-joining. *Translational Cancer Research, 2*(3), 130-143.

De Jesus, B. B., Schneeberger, K., Vera, E., Tejera, A., Harley, C. B., & Blasco, M. A. (2011). The telomerase activator TA-65 elongates short telomeres and increases health span of adult/old mice without increasing cancer incidence. *Aging Cell, 10*(4), 604-621.

de Lange, T. (2002). Protection of mammalian telomeres. *Oncogene, 21*, 532-540.

De Lange, T. (2009). How telomeres solve the end-protection problem. *Science(New York, N.Y.), 326*(5955), 948.

de Lange, T. (2005). Shelterin: The protein complex that shapes and safeguards human telomeres. *Genes & Development, 19*(18), 2100-2110.

DeBauche, D. M., Pai, G. S., & Stanley, W. S. (1990). Enhanced G2 chromatid radiosensitivity in dyskeratosis congenita fibroblasts.
. *American Journal of Human Genetics, 46*(2), 350-357.

Diotti, R., & Loayza, D. (2011). Shelterin complex and associated factors at human telomeres. *Nucleus, 2*(2), 119-135.

Doherty, A. J., & Jackson, S. P. (2001). DNA repair: How ku makes ends meet. *Current Biology,* (11), 920-924.

Dokal, I. (2000). Dyskeratosis congenita in all its forms. *Br J Haematol* 110(4): 768-779

Du, H., Pumbo, E., Ivanovich, J., An, P., Maziarz, R. T., Reiss, U. M., et al. (2009). TERC and TERT gene mutations in patients with bone marrow failure and the significance of telomere length measurements. *Blood, 113*(2), 309-316.

Evans, H., Mencl, J., Horng, M., Ricanati, M., Sanchez, C., & Hozier, J. (1986). Locus specificity in the mutability of L5178y mouse lymphoma-cells - the role of multilocus lesions. *Proceedings of the National Academy of Sciences of the United States of America, 83*(12), 4379-4383.

Fattah, F., Lee, E. H., Weisensel, N., Wang, Y., Lichter, N., & Hendrickson, E. A. (2010). Ku regulates the non-homologous end joining pathway choice of DNA double-strand break repair in human somatic cells. *Plos Genetics, 6*(2), e1000855.

Fenech M, Morley AA. (1985) Measurement of micronuclei in lymphocytes. *Mutat Res*. 147(1-2):29-36

Filippo, J. S., & Sung, Patrick and Klein, Hannah. (2008). Mechanism of eukaryotic homologous recombination. *Annual Review of Biochemistry, 77*, 229-257.

Finnon, P., Silver, A. R. J., & Bouffler, S. D. (2000). Upregulation of telomerase activity by X-irradiation in mouse leukaemia cells is independent of tert, terc, tnks and myc transcription. *Carcinogenesis, 21*(4), 573-578

Fire, A., S. Xu, M. K. Montgomery, S. A. Kostas, S. E. Driver and C. C. Mello (1998). "Potent and specific genetic interference by double-stranded RNA in Caenorhabditis elegans." Nature 391(6669): 806-811

Frescas, D., & De Lange, T. (2014). A TIN2 dyskeratosis congenita mutation causes telomerase-independent telomere shortening in mice.. *Genes & Development, 28*, 153-166.

Fumagalli M, Rossiello F and Clerici M (2012). Telomeric DNA damage is irreparable and causes persistent DNA damage response activation. *Nature Cell Biology, 14*(4), 355-365.

Gisselsson D, Pettersson L, Höglund M, Heidenblad M, Gorunova L, Wiegant J, Mertens F, Dal Cin P, Mitelman F, Mandahl N. (2000). Chromosomal breakage-fusion-bridge events cause genetic intratumor heterogeneity**.**. *Proc Natl Acad Sci U S A., 97*(10), 5357-5362.

Ghildiyal, M. and P. D. Zamore (2009). "Small silencing RNAs: an expanding universe." Nat Rev Genet 10(2): 94-108.

Gorgoulis, V. G., Vassiliou, L. V. F., Karakaidos, P., Zacharatos, P., Kotsinas, A., Liloglou, T., et al. (2005). Activation of the DNA damage checkpoint and genomic instability in human precancerous lesions. *Nature, 434*(7035), 907-913.

Grandin N and Michel Charbonneau. (2009). Telomerase- and Rad52-independent immortalization of budding yeast by an inherited-long-telomere pathway of telomeric repeat amplification *Mol Biol Cell., 29*(4), 965-985.

Greider, C W and Blackburn, E H. (1985). Identification of a specific telomere terminal transferase activity in tetrahymena extracts. *Cell, 43*(2.1), 405-413.

Griffith, J. D., Comeau, L., Rosenfield, S., Stansel, R. M., Bianchi, A., Moss, H., et al. (1999). Mammalian telomeres end in a large duplex loop. *Cell, 97*(4), 503-514.

Gu, B., Bessler, M., & Mason, P. J. (2008). A pathogenic dyskerin mutation impairs proliferation and activates a DNA damage response independent of telomere length in mice. *Proceedings of the National Academy of Sciences of the United States of America, 105*(29), 10173-10178.

Gutiérrez-Enríquez S1, H. J. (2003). Use of the cytokinesis-block micronucleus assay to measure radiation-induced chromosome damage in lymphoblastoid cell lines**.***535*(1), 1-13.

Haber, J. E. (2000). Partners and pathways repairing a double-strand break. *Bacterial Artificial Chromosomes and Herpesvirus Genomics, 16*(6), 259-264.

Hande P, P. Slijepcevic, A. Silver, S. Bouffler, P.P. van Buul, P. Bryant, P. Lansdorp. (1999). Elongated telomeres in scid mice *Genomics, 56*, 221-223.

Hannon GJ. (2002). RNA interference. *Nature PublishingGroup, 418*, 244.

Harley CB, Weimin Liu, Maria Blasco, Elsa Vera, William H. Andrews, Laura A. Briggs, and Joseph M. Raffaele. (2011). A natural product telomerase activator as part of a health maintenance program. *Rejuvenation Research, 14*(1), 45-56.

Harley, CB. A. Futcher, B. & Greider, CW. (1990). Telomeres shorten during ageing of human fibroblasts. *Nature, 345*, 458-460.

Hassock S, Vetrie D, Giannelli F. (1999). Mapping and characterization of the X-linked dyskeratosis congenita (DKC) gene**..** *Genomics, 55*(1), 21-27.

Heiss NS, Knight SW, Vulliamy TJ, Klauck SM, Wiemann S, Mason PJ, Poustka A, Dokal I. (1998). X-linked dyskeratosis congenita is caused by mutations in a highly conserved gene with putative nucleolar functions**..** *Nat Genet., 19*(1), 32-38.

Helt CE, Cliby WA, Keng PC, Bambara RA, O'Reilly MA. (2005). Ataxia telangiectasia mutated (ATM) and ATM and Rad3-related protein exhibit selective target specificities in response to different forms of DNA damage**..** *J Biol Chem, 280*(2), 1186-1192.

Henrique Barreta, M., Garziera Gasperin, B., Braga Rissi, V., Cesaro, M. P. d., Ferreira, R., Oliveira, J. F. d., et al. (2012). Homologous recombination and non-homologous end-joining repair pathways in bovine embryos with different developmental competence. *Experimental Cell Research, 318*(16), 2049-2058.

Holmes, K., Williams, C. M., Chapman, E. A., & Cross, M. J. (2010). Detection of siRNA induced mRNA silencing by RT-qPCR: Considerations for experimental design. *3*, 53. *BMC Research Notes, 3*(53)

Horn S, Barnard S, Brady D, Prise KM, Rothkamm K. (2013). Combined analysis of gamma-H2AX/53BP1 foci and caspase activation in lymphocyte subsets detects recent and more remote radiation exposures *Radiat Res.* 180(6):603-9

Hu X, Schrodi SJ, Ross DA, Cargill M. (2004). Selecting tagging SNPs for association studies using power calculations from genotype data**..** *Hum Hered, 57*(3), 156-170.

Huda N, Hiromi Tanaka,Marc S. Mendonca,and David Gilley. (2009). DNA damage-induced phosphorylation of TRF2 is required for the fast pathway of DNA double-strand break repair▿ *Mol Cell Biol., 29*(13), 3597-3604.

Huen, M. S., & Chen, J. (2008). The DNA damage response pathways: at the crossroad of protein modifications . *Cell Research, 18*(1), 8-16.

Huffman, K. E., Levene, S. D., Tesmer, V. M., Shay, J. W., & Wright, W. E. (2000). Telomere shortening is proportional to the size of the G-rich telomeric 3'-overhang. *Journal of Biological Chemistry, 275*(26), 19719-19722.

Huppi, K., S. E. Martin and N. J. Caplen (2005). Defining and assaying RNAi in mammalian cells. *Mol Cell* 17(1): 1-10.

I Baran, R Nalcaci, M Kocak. (2010). Dyskeratosis congenita: Clinical report and review of the literature. *International Journal of Dental Hygiene, 8*, 68-74.

IJpma AS and Carol W. Greider. (2003). Short telomeres induce a DNA damage response in *saccharomyces cerevisiae Mol Biol Cell., 14*(3), 987-1001.

Jaco I, P. Munoz, F. Goytisolo, J. Wesoly, S. Bailey, G. Taccioli, M.A. Blasco. (2003). Role of mammalian Rad54 in telomere length maintenance *Molecular and Cellular Biology, 23*, 5572-5580.

Karlseder, J., A. Smogorzewska, and T. de Lange. (2002). Senescence induced by altered telomere state, not telomere loss. *Science, 295*, 2446-2449.

Kastan, Michael B. and Bartek, Jiri. (2004). Cell-cycle checkpoints and cancer. *Nature Publishing Group, 432*, 316-323.

Khare V, E. K. (2002). The proofreading 3'-->5' exonuclease activity of DNA polymerases: A kinetic barrier to translesion DNA synthesis. *Mutat Res., 510*(1-2), 45-54.

Kim, N. W., Piatyszek, M. A., Prowse, K. R., Harley, C. B., West, M. D., HO, P. L. C., Coviello, G. M., Wright, W. E., Weinrich, S. L. & Shay, J. W. 1994. Specific Association of Human Telomerase Activity with Immortal Cells and Cancer. Science, 266, 2011-2015

Kirwan, M., & Dokal, I. (2008). Dyskeratosis congenita: A genetic disorder of many faces. *Clinical Genetics, 73*(2), 103-112.

Kirwan, Michael and Dokal, Inderjeet. (2009). Dyskeratosis congenita, stem cells and telomeres. *Biochimica Et Biophysica Acta (BBA) - Molecular Basis of Disease, 1792*(4), 371-379.

Kirwan, M., Beswick, R., Walne, A. J., Hossain, U., Casimir, C., Vulliamy, T., et al. (2011). Dyskeratosis congenita and the DNA damage response. *British Journal of Haematology, 153*(5), 634-643.

Knight S.W., Heiss, N.S., Vulliamy, T.J., Greschner, S., Stavrides, G., Pai, G.S.,Lestringant, G., Varma, N., Mason, P.J.,Dokal, I., Poustka, A. (1999). X-linked dyskeratosis congenita is predominantly caused by missense mutations in the DKC1 gene *The American Journal of Human Genetics, 65*(1), 50-58.

Koering, C. E., G. Fourel, E. Binet-Brasselet, T. Laroche, F. Klein, and E. Gilson. (2000). Identification of high affinity Tbf1p-binding sites within the budding yeast genome. *Nucleic Acids Res., 28*, 2519-2526.

Lafferty-Whyte K, C J Cairney, M B Will, N Serakinci, M -G Daidone, N Zaffaroni, A Bilsland and W N Keith. (2009). A gene expression signature classifying telomerase and ALT immortalization reveals an hTERT regulatory network and suggests a mesenchymal stem cell origin for ALT *Oncogene, 28*, 3765-3774.

Li Bibo, Amin Espinal and George A. M. Cross. (2005). Trypanosome telomeres are protected by a homologue of mammalian TRF2. *Molecular and Cellular Biology, 25*(12), 5011-5021.

Li, Xuan and Heyer, Wolf-Dietrich. (2008). Homologous recombination in DNA repair and DNA damage tolerance. *Cell Research, 18*(1), 99-113.

Liu, M., Hales, B. F., & Robaire, B. (2014). Effects of four chemotherapeutic agents, bleomycin, etoposide, cisplatin, and cyclophosphamide, on DNA damage and telomeres in a mouse spermatogonial cell line. *Biology of Reproduction, 90*(4), 72.

Löbrich M and Jeggo PA (2007) The impact of a negligent G2/M checkpoint on genomic instability and cancer induction. *Nat Rev Cancer* 7(11):861-9

Lopes, M., Cotta-Ramusino, C., Pellicioli, A., Liberi, G., Plevani, P., Muzi-Falconi, M., et al. (2001). The DNA replication checkpoint response stabilizes stalled replication forks. *Nature, 412*, 557-561.

Lovejoy CA, Li W, Reisenweber S, et al. (2012). . Loss of ATRX, genome instability, and an altered DNA damage response are hallmarks of the alternative lengthening of telomeres pathway. . *PLoS Genet, 8*(7)

Lundblad V, B. E. (1993). An alternative pathway for yeast telomere maintenance rescues est1-senescence**.** . *Cell, 73*(2), 347-360.

Lundblad, V. (1997). The end replication problem: More than one solution. *Nature Medicine, 3*(11), 1198-1199.

M'kacher, R., Laithier, V., Valent, A., Delhommeau, F., Violot, D., Deutsch, E., Dossou, J., Beron-Gaillard, N., Girinsky, T., Bourhis, J., Carde, P., Bernheim, A., & Parmentier, C. (2003). Sensitivity to radiation and alkylating agent of peripheral lymphocytes and fibroblasts in a hoyeraal-hreidarsson syndrome patient. *Pediatr. Hematol. Oncol, 20*, 651-656.

Ma, J., Kim, E., Haber, J., & Lee, S. (2003). Yeast Mre11 and Rad1 proteins define a ku-independent mechanism to repair double-strand breaks lacking overlapping end sequences. *Molecular and Cellular Biology, 23*(23), 8820-8828.

Macdonald F and Ford CHJ (1997). Molecular Biology of Cancer. *Bios Scientific Publishers Ltd.*

Makarov, V. L., Hirose, Y., & Langmore, J. P. (1997). Long G tails at both ends of human chromosomes suggest a C strand degradation mechanism for telomere shortening. *Cell, 88*(5), 657-666.

Manguan-Garcia, C., Pintado-Berninches, L., Carrillo, J., Machado-Pinilla, R., Sastre, L., Pérez-Quilis, C., & Perona, R. (2014). Expression of the genetic suppressor element 24.2 (GSE24.2) decreases DNA damage and oxidative stress in X-linked dyskeratosis congenita cells. *PloS One, 9*(7), 1-12.

Mari, P.-O., Florea, B. I., Persengiev, S. P., Verkaik, N. S., Brüggenwirth, H. T., Modesti, M., … van Gent, D. C. (2006). Dynamic assembly of end-joining complexes requires interaction between Ku70/80 and XRCC4. *Proceedings of the National Academy of Sciences of the United States of America, 103*(49), 18597-18602.

María A Blasco, Han-Woong Lee, M.Prakash Hande, Enrique Sampe, Peter M Lansdorp, Ronald A DePinho, Carol W Greider. (1997). Telomere shortening and tumor formation by mouse cells lacking telomerase RNA *Cell, 91*(1), 25-34.

Marrone, A., Walne, A., & Dokal, I. (2005). Dyskeratosis congenita: Telomerase, telomeres and anticipation. *Current Opinion in Genetics & Development, 15*(3), 249-257.

Marrone, A., & Dokal, I. (2004). Dyskeratosis congenita: Molecular insights into telomerase function, ageing and cancer. *Expert Reviews in Molecular Medicine, 6*(26), 1-23.

McEachern MJ, H. J. (2006). Break-induced replication and recombinational telomere elongation in yeast. *Annual Review of Biochemistry, 75*, 111-135.

McIlrath J, Bouffler SD, Samper E, Cuthbert A, Wojcik A, Szumiel I, Bryant PE, Riches AC, Thompson A, Blasco MA, Newbold RF, Slijepcevic P. (2001). Telomere length abnormalities in mammalian radiosensitive cells. . *Cancer Res., 61*(3), 912-915.

McIlrath, J., Bouffler, S., Samper, E., Cuthbert, A., Wojcik, A., Szumiel, I., et al. (2001). Telomere length abnormalities in mammalian radiosensitive cells. *Cancer Research, 61*(3), 912-915.

McPherson JP, B. Lemmers, A. Hirao, A. Hakem, J. Abraham, E. Migon, E. Matysiak-Zablocki, L. Tamblyn, O. Sanchez-Sweatman, R. Khokha, J. Squire, M.P. Hande, T.W. Mak, R. Hakem. (2004). Collaboration of Brca1 and Chk2 in tumorigenesis *Genes & Development, 18*, 1144-1163.

Mitchell, J. R., Wood, E., & Collins, K. (1999). A telomerase component is defective in the human disease dyskeratosis congenita. *Nature, 402*(6761), 551-555.

Molenaar, C., Wiesmeijer, K., Verwoerd, N. P., Khazen, S., Eils, R., Tanke, H. J., & Dirks, R. W. (2003). Visualizing telomere dynamics in living mammalian cells using PNA probes. . *The EMBO Journal, 22*(24), 6631-6641.

Molgora B, Bateman R, Sweeney G, Finger D, Dimler T, Effros RB, Valenzuela HF. (2013). functional assessment of pharmacological telomerase activators in human T cells**.** . *Cells, 2*(1), 57-66.

Moyzis, R., Buckinghan, J., Cram, L., Dani, M., Deaven, L., Jones, M., et al. (1988). A highly conserved repetitive dna-sequence, (ttaggg)n, present at the telomeres of human-chromosomes. *Proceedings of the National Academy of Sciences of the United States of America, 85*(18), 6622-6626.

Mukherjee B, Kessinger C, Kobayashi J, Chen BP, Chen DJ, Chatterjee A, Burma S. (2006). Dna-pk phosphorylates histone h2ax during apoptotic dna fragmentation in mammalian cells.. *DNA Repair, 10*(5), 575-590.

Nelson, N. D., & Bertuch, A. A. (2012). Dyskeratosis congenita as a disorder of telomere maintenance. . *Mutat Res, 730*(1-2), 43-51.

Newman JP, Banerjee B, Fang W, Poonepalli A, Balakrishnan L, Low GK, Bhattacharjee RN, Akira S, Jayapal M, Melendez AJ, Baskar R, Lee HW, Hande MP. (2008) Short dysfunctional telomeres impair the repair of arsenite-induced oxidative damage in mouse cells. *J Cell Physiol.* 214(3):796-809

Nigam, A. (2011). Senescence (ageing). *Indian J Dermatol, 56*(6), 615-621.

Nishio, N., & Kojima, S. (2010). Recent progress in dyskeratosis congenita. *International Journal of Hematology, 92*(3), 419-424.

O'Driscoll, M. C., Scott, D., Orton, C. J., Kiltie, A. E., Davidson, S. E., Hunter, R. D., & West, C. M. (1998). Radiation-induced micronuclei in human fibroblasts in relation to clonogenic radiosensitivity. *British Journal of Cancer, 78*(12), 1559-1563.

O'Sullivan, R. J., & Karlseder, J. (2010). Telomeres : Protecting chromosomes against genome instability. *Nat Rev Mol Cell Biol, 11*(3), 171-181.

Obe G, D. M.,. (2010). DNA double strand breaks and chromosomal aberrations. 2010;128:8-16. *Cytogenet Genome Res, 128*(1-3), 8-16.

Oeseburg, H., de Boer, R. A., van Gilst, W. H., & van der Harst, P. (2010). Telomere biology in healthy aging and disease RID C-3828-2008. *Pflugers Archiv-European Journal of Physiology, 459*(2), 259-268.

Olovnikov AM. (1996). Telomeres, telomerase, and aging: Origin of the theory**.** . *Exp Gerontol., 31*(4), 443-448.

Olovnikov AM. (1973). A theory of marginotomy: The incomplete copying of template margin in enzymatic synthesis of polynucleotides and biological significance of the phenomenon. . *J. Theor. Biol, 41*, 181-190.

Pai, G. S., Yan, Y., DeBauche, D. M., Stanley, W. S., & Paul, S. R. (1989). Bleomycin hypersensitivity in dyskeratosis congenita fibroblasts, lymphocytes, and transformed lymphoblasts. *Cytogenetics and Cell Genetics, 52*, 186.

Parry EM, Alder JK, Lee SS, Phillips JA 3rd, Loyd JE, Duggal P, Armanios M. (2011) Decreased dyskerin levels as a mechanism of telomere shortening in X-linked dyskeratosis congenita. *J Med Genet* 48(5):327-33

Parshad R, Sanford KK, Jones GM. (1983). Chromatid damage after G2 phase x-irradiation of cells from cancer-prone individuals implicates deficiency in DNA repair. *Proc Natl Acad Sci U S A., 80*, 5612-5616.

Pellegrini, L., Yu, D., Lo, T., Anand, S., Lee, M., Blundell, T., et al. (2002). Insights into DNA recombination from the structure of a RAD51-BRCA2 complex. *Nature, 420*(6913), 287-293.

Pereboeva, L., Westin, E., Patel, T., Flaniken, I., Lamb, L., Klingelhutz, A., & Goldman, F. (. (2013). DNA damage responses and oxidative stress in dyskeratosis congenita. . *PloS One, 8*(10), 1-8.

Podhorecka, M., Skladanowski, A., & Bozko, P. (2010). H2AX phosphorylation: Its role in DNA damage response and cancer therapy. 920161. doi:10.4061/2010/920161. *Journal of Nucleic Acids, 2010*

Polychronopoulou, S and Koutroumba, P. (2004). Telomere length variation and telomerase activity expression in patients with congenital and acquired aplastic anemia. *Acta Haematol, 111*, 125-131.

Qin, Q., Niu, J., Wang, Z., Xu, W., Qiao, Z., & Gu, Y. (2012). Astragalus membranaceus inhibits inflammation via phospho-P38 mitogen-activated protein kinase (MAPK) and nuclear factor (NF)-κB pathways in advanced glycation end product-stimulated macrophages. . *International Journal of Molecular Sciences, 13*(7), 8379-8387.

Ratts RB, Weng. N. (2012). Homeostasis of lymphocytes and monocytes in frequent blood donors. *Frontiers in Immunology, 3*, 271.

Rogakou, E. P., R. Pilch, D., Orr, A. H., Ivanova, V. S., & and Bonner, W. M. (1998). DNA double-stranded breaks induce histone H2AX phosphorylation on serine 139. *The Journal of Biological Chemistry, 273*(10), 5858-5868.

Rooney S, Alt FW, Lombard D, et al. (2003). Defective DNA repair and increased genomic instability in artemis-deficient murine cells*. The Journal of Experimental Medicine, 197*(5), 553-565.

Roos WP, K. B. (2012). DNA damage-induced apoptosis: From specific DNA lesions to the DNA damage response and apoptosis**.**. *Cancer Letters,* , 1-12.

Saito Y, Fujimoto, H and Kobayashi, J (2013). Role of NBS1 in DNA damage response and its relationship with cancer development *Translational Cancer research*, 2(3), 178-189

Samper E, F.A. Goytisolo, P. Slijepcevic, P.P. van Buul, M.A. Blasco. (2000). Mammalian Ku86 protein prevents telomeric fusions independently of the length of TTAGGG repeats and the G-strand overhang *EMBO rep*, 1 (2000), 244–252

Scheel C, Karl-Ludwig Schaefer, Anna Jauch, Monika Keller, Daniel Wai, Christian Brinkschmidt, Frans van Valen, Werner Boecker, Barbara Dockhorn-Dworniczak and Christopher Poremba. (2001). Alternative lengthening of telomeres is associated with chromosomal instability in osteosarcomas *Oncogene, 20*(29), 3835-3844.

Sieron, P., Hader, C., Hatina, J., Engers, R., Wlazlinski, A., Müller, M., and Schulz, M A (2009). *DKC1* overexpression associated with prostate cancer progression *British Journal of Cancer, 101*(8), 1410-1416.

Shcherbakova, D. M., Zvereva, M. E., Shpanchenko, O. V., & Dontsova, O. A. (2006). Telomerase: Structure and properties of the enzyme, the peculiarities of the yeast telomerase. *Molecular Biology, 40*(4), 580-594.

Slijepcevic, P. (2001). Telomere length measurement by Q-fish. *Methods in Cell Science, 23*, 17-22.

Slijepcevic, P. (2006). "The role of DNA damage response proteins at telomeres--an "integrative" model." DNA Repair (Amst) 5(11): 1299-1306.

Slijepcevic, P. (2008). DNA damage response, telomere maintenance and ageing in light of the integrative model. *Mechanisms of Ageing and Development, 129*(1-2), 11-16.

Smogorzewska, A., B. van Steensel, A. Bianchi, S. Oelmann, M. R. Schaefer, G. Schnapp, and T. de Lange. (2000). Control of human telomere length by TRF1 and TRF2. . *Molecular and Cellular Biology, 20*, 1659-1668.

Stimpson, K. M., Matheny, J. E., & Sullivan, B. A. (2012). . Dicentric chromosomes: Unique models to study centromere function and inactivation., . *Chromosome Research : An International Journal on the Molecular, Supramolecular and Evolutionary Aspects of Chromosome Biology, 20*(5), 595-605.

Strong MA, Vidal-Cardenas SL, Karim B, Yu H, Guo N, Greider CW. (2011). Phenotypes in *mTERT*$^{+/-}$ and *mTERT*$^{-/-}$ mice are due to short telomeres, not telomere-independent functions of telomerase reverse transcriptase. *Molecular and Cellular Biology, 31*(12), 2369-2379.

Stucki M, Clapperton JA, Mohammad D, Yaffe MB, Smerdon SJ, Jackson SP. (2005). mdc1 directly binds phosphorylated histone h2ax to regulate cellular responses to dna double -strand breaks**.**. *Cell, 123*(7), 1213-1226.

Subba R K. (2007). Mechanisms of disease: DNA repair defects and neurological disease *Nature Clinical Practice Neurology, 3*(3), 162-172.

Takai, H., Smogorzewska, A., & de Lange, T. (2003). DNA damage foci at dysfunctional telomeres. *Current Biology, 13*(17), 1549-1556.

Tanaka H,Marc S. Mendonca, Paul S. Bradshaw, Derek J. Hoelz, Linda H. Malkas, M. Stephen Meyn, and David Gilley. (2005). DNA damage-induced phosphorylation of the human telomere-associated protein TRF2. *Proc Natl Acad Sci U S A., 102*(43), 15539-15544.

Tarsounas M, P. Munoz, A. Claas, P.G. Smiraldo, D.L. Pittman, M.A. Blasco, S.C. West. (2004). Telomere maintenance requires the RAD51D recombination/repair protein *Cell, 117*, 337-347.

Tracy M. Bryan, Anna Englezou, Luciano Dalla-Pozza, Melissa A. Dunham1 & Roger R. Reddel. (1997). Evidence for an alternative mechanism for maintaining telomere length in human tumors and tumor-derived cell lines. *Nat.Med, 3*, 1271-1274.

Van Gent DC, van der Burg M. (2007). Non-homologous end-joining, a sticky affair**.** . *Oncogene, 26*(56), 7731-7740.

Van Steensel, B., Smogorzewska, A., de Lange (1998). TRF2 protects human telomeres from end-to-end fusions. *Cell, 92*, 401-413.

Venteicher, A. S., Abreu, E. B., Meng, Z., McCann, K. E., Terns, R. M., Veenstra, T. D., et al. (2009). A human telomerase holoenzyme protein required for cajal body localization and telomere synthesis. *Science, 323*(5914), 644-648.

Venteicher, A. S., Meng, Z., Mason, P. J., Veenstra, T. D., & Artandi, S. E. (2008). Identification of ATPases pontin and reptin as telomerase components essential for holoenzyme assembly. *Cell, 132*(6), 945-957.

Vogel, C., & Marcotte, E. M. (2012). Insights into the regulation of protein abundance from proteomic and transcriptomic analyses. *Nature Reviews. Genetics, 13*(4), 227-232.

Vulliamy T, Anna Marrone, Frederick Goldman, Andrew Dearlove, Monica Bessler, Philip J. Mason & Inderjeet Dokal. (2001). The RNA component of telomerase is mutated in autosomal dominant dyskeratosis congenita *Nature, 413*, 432-435.

Vulliamy, T., Beswick, R., Kirwan, M., Marrone, A., Digweed, M., Walne, A., et al. (2008). Mutations in the telomerase component NHP2 cause the premature ageing syndrome dyskeratosis congenita. *Proceedings of the National Academy of Sciences of the United States of America, 105*(23), 8073-8078.

Wagner, H. P. (1998). Cell cycle control and cancer. *Indian J Pedlatr, 65*, 805-814.

Wang, H., Perrault, A., Takeda, Y., Qin, W., Wang, H., & Iliakis, G. (2003). Biochemical evidence for ku-independent backup pathways of NHEJ. *Nucleic Acids Research, 31*(18), 5377-5388.

Weng NP. (2002). Regulation of telomerase expression in human lymphocytes**.** *Springer Semin Immunopathol., 24*(1), 23-33.

Wlodek D., Hittelman W. N. (1987). The repair of double strand breaks correlates with radiosensitivity of L5178Y-S and L5178Y-R cells.
. *Radiat. Res., 115*, 566-575.

Wong, J. M. Y., & Collins, K. (2006). Telomerase RNA level limits telomere maintenance in X-linked dyskeratosis congenita. *Genes & Development, 20*, 2848-2858.

Wright WE, Piatyszek MA, Rainey WE, Byrd W, Shay JW. (1996). . Telomerase activity in human germline and embryonic tissues and cells. *Dev Genet, 18*, 173-179.

Wyatt, H. D. M., West, S. C., & Beattie, T. L. (2010). InTERTpreting telomerase structure and function. *Nucleic Acids Research, 38*(17), 5609-5622.

Wymana Claire, Ristic Dejan, Kanaar Roland. (2004). Homologous recombination-mediated double-strand break repair. *DNA Repair, 3*, 827-833.

Yasaei H and Slijepcevic P. (2010). Research defective artemis causes mild telomere dysfunction. *Genome Integrity, 1*(3)

Zeng, X. L., Thumati, N. R., Fleisig, H. B., Hukezalie, K. R., Savage, S. A., Giri, N., & Wong, J. M. Y. (2012). The accumulation and not the specific activity of telomerase ribonucleoprotein determines telomere maintenance deficiency in X-linked dyskeratosis congenita. *Human Molecular Genetics, 21*(4), 721-729.

Zha, S. Cristian Boboila & Frederick W Alt. (2009)**.** Mre11: Roles in DNA repair beyond homologous recombination. *Nature Structural & Molecular Biology, 16*, 798-800.